Iowa Research Online
The University of Iowa's Institutional Repository

University of Iowa
Iowa Research Online

Theses and Dissertations

Fall 2010

# Investigation of unsteady and non-uniform flow and sediment transport characteristics at culvert sites

Hao-Che Ho
*University of Iowa*

Follow this and additional works at: https://ir.uiowa.edu/etd

Part of the Civil and Environmental Engineering Commons

Copyright 2010 Hao-Che Ho

This dissertation is available at Iowa Research Online: https://ir.uiowa.edu/etd/814

## Recommended Citation

Ho, Hao-Che. "Investigation of unsteady and non-uniform flow and sediment transport characteristics at culvert sites." PhD (Doctor of Philosophy) thesis, University of Iowa, 2010.
https://doi.org/10.17077/etd.zp388rmo

Follow this and additional works at: https://ir.uiowa.edu/etd

Part of the Civil and Environmental Engineering Commons

www.manaraa.com

# INVESTIGATION OF UNSTEADY AND NON-UNIFORM FLOW AND SEDIMENT TRANSPORT CHARACTERISTICS AT CULVERT SITES

by

Hao-Che Ho

An Abstract

Of a thesis submitted in partial fulfillment
of the requirements for the Doctor of
Philosophy degree in Civil and Environmental Engineering
in the Graduate College of
The University of Iowa

December 2010

Thesis Supervisors: Associate Professor George Constantinescu
Adjunct Associate Professor Marian Muste

www.manaraa.com

# ABSTRACT

The present study is an integral part of a broader study focused on the design and implementation of self-cleaning culverts, i.e., configurations that prevent the formation of sediment deposits after culvert construction or cleaning. Sediment deposition at culverts is influenced by many factors, including the size and characteristics of material of which the channel is composed, the hydraulic characteristics generated under different hydrologic events, the culvert geometry design, channel transition design, and the vegetation around the channel. The multitude of combinations produced by this set of variables makes the investigation of practical situations challenging.

In addition to the above considerations, the field observations, and the laboratory and numerical experiments have revealed additional complexities of the flow and sediment transport through culverts that further increase the dimensions of the investigation. The flow complexities investigated in this study entail: flow non-uniformity in the areas of transition to and from the culvert, flow unsteadiness due to the flood wave propagation, and the complex correlation between the flow and sediment hydrographs produced during storm events. To date, the literature contains no systematic studies on sediment transport through multi-box culverts. Similarly, there is limited knowledge about the non-uniform, unsteady sediment transport in channels of variable geometry. Furthermore, there are few readily useable numerical models that can reliably simulate flow and sediment transport in such complex situations.

Given the current state of knowledge, the main goal of the present study is to investigate the above flow complexities in order to provide the needed insights for optimizing the culvert design. The research was phased so that field observations were conducted first to understand the culvert behavior in Iowa landscape. Modeling through complementary hydraulic model and numerical experiments was subsequently carried out to gain the practical knowledge for the development of the self-cleaning culvert designs.

www.manaraa.com

Abstract Approved: _____
Thesis Supervisor

_____
Title and Department

_____
Date

_____
Thesis Supervisor

_____
Title and Department

_____
Date

www.manaraa.com

# INVESTIGATION OF UNSTEADY AND NON-UNIFORM FLOW AND SEDIMENT TRANSPORT CHARACTERISTICS AT CULVERT SITES

by

Hao-Che Ho

A thesis submitted in partial fulfillment
of the requirements for the Doctor of
Philosophy degree in Civil and Environmental Engineering
in the Graduate College of
The University of Iowa

December 2010

Thesis Supervisors: Associate Professor George Constantinescu
Adjunct Associate Professor Marian Muste

www.manaraa.com

Copyright by

HAO-CHE HO

2010

All Rights Reserved

www.manaraa.com

Graduate College
The University of Iowa
Iowa City, Iowa

CERTIFICATE OF APPROVAL

_____

PH.D. THESIS

_____

This is to certify that the Ph.D. thesis of

Hao-Che Ho

has been approved by the Examining Committee
for the thesis requirement for the Doctor of Philosophy
degree in Civil and Environmental Engineering at the December 2010
graduation.

Thesis Committee: _____
George Constantinescu, Thesis Supervisor

_____
Marian Muste, Thesis Supervisor

_____
Robert Ettema

_____
Ching-Long Lin

_____
A. Jacob Odgaard

_____
Larry J. Weber

www.manaraa.com

To my family



www.manaraa.com

ACKNOWLEDGMENTS

It was very enjoyable for me to study in IIHR-Hydroscience & Engineering. IIHR gave me the opportunity to work with many prominent researchers in the world. I especially appreciate the valuable guidance and great patience from my advisor Dr Marian Muste and Professor Robert Ettema and Professor George Constantinescu during my research study. I also want to thank Professor Jacob Odgaard, Professor Ching-Long Lin, and Professor Larry Weber for their assistance related to my study.

The friendliness from my lab mates is fruitful and makes me feel I am not alone in IIHR. I would like to thank Dr Dongsu Kim who gave me his continuous encouragement during my research. I also thank my friends, Bo Chen, Yuwei Li, Yushi Wang, and Chi Chi Chio for many discussions related to classes and my life. There are many friends in Iowa City I wish to give them my thanks. They also helped me getting through many difficulties.

Further, I would like to share my joy with my family. My wife, Catherine Wang, always supports and takes good care of me. I do not think I could finish my thesis without her. I also give my special appreciation to my parents. They adequately finance me through my PhD degree. They also support me for any decision I made. Without their help I could not complete my thesis.

Finally, I want to thank God. He has been my shepherd and made me realize “do not worry about tomorrow; for tomorrow will care for itself. Each day has enough trouble of its own”. Thank you, God.



www.manaraa.com

ABSTRACT

The present study is an integral part of a broader study focused on the design and implementation of self-cleaning culverts, i.e., configurations that prevent the formation of sediment deposits after culvert construction or cleaning. Sediment deposition at culverts is influenced by many factors, including the size and characteristics of material of which the channel is composed, the hydraulic characteristics generated under different hydrologic events, the culvert geometry design, channel transition design, and the vegetation around the channel. The multitude of combinations produced by this set of variables makes the investigation of practical situations challenging.

In addition to the above considerations, the field observations, and the laboratory and numerical experiments have revealed additional complexities of the flow and sediment transport through culverts that further increase the dimensions of the investigation. The flow complexities investigated in this study entail: flow non-uniformity in the areas of transition to and from the culvert, flow unsteadiness due to the flood wave propagation, and the complex correlation between the flow and sediment hydrographs produced during storm events. To date, the literature contains no systematic studies on sediment transport through multi-box culverts. Similarly, there is limited knowledge about the non-uniform, unsteady sediment transport in channels of variable geometry. Furthermore, there are few readily useable numerical models that can reliably simulate flow and sediment transport in such complex situations.

Given the current state of knowledge, the main goal of the present study is to investigate the above flow complexities in order to provide the needed insights for optimizing the culvert design. The research was phased so that field observations were conducted first to understand the culvert behavior in Iowa landscape. Modeling through complementary hydraulic model and numerical experiments was subsequently carried out to gain the practical knowledge for the development of the self-cleaning culvert designs.



www.manaraa.com

TABLE OF CONTENTS

LIST OF TABLES ..... viii

LIST OF FIGURES ..... ix

LIST OF SYMBOLS ..... xvi

LIST OF ABBREVIATIONS ..... xviii

CHAPTER1 INTRODUCTION ..... 1

1.1 Overview of culvert issues ..... 1
1.2 Problem statement ..... 1
1.3 Study objectives ..... 3
1.4 Approach ..... 4
1.5 Background ..... 6
1.5.1 Iowa culverts ..... 9

CHAPTER 2 LITERATURE REVIEW ..... 11

2.1 Hydrodynamic considerations for channel ..... 11
2.1.1 Loop rating curve ..... 12
2.1.2 Sediment transport during flood events ..... 15
2.2 Hydrodynamic considerations for flows through culverts ..... 17
2.2.1 Unsteady flow at culvert ..... 17
2.2.2 Sedimentation at culverts ..... 19
2.2.3 Current culvert design considerations ..... 21
2.2.3.1 Types of flow through culverts ..... 22
2.2.3.2 Hydraulics of inlet control ..... 23
2.2.3.3 Hydraulics of outlet control ..... 24
2.2.4 Sediment mitigation culvert designs ..... 26
2.2.5 Numerical modeling of culverts and design software ..... 28
2.2.5.1 Numerical modeling ..... 28
2.2.5.2 Culvert design software ..... 29

CHAPTER 3 CONSIDERATIONS ASSOCIATED WITH SEDIMENT TRANSPORT IN UNSTEADY FLOWS ..... 31

3.1 Unsteady flow in channel ..... 33
3.1.1 Rating curves ..... 33
3.1.2 Rating curve sensitivity analysis ..... 36
3-1-3 Sediment hydrograph ..... 47
3.2 Unsteady flow at culvert ..... 51
3.3 Field observations of sediment deposition at culverts ..... 54
3.3.1 Monitoring of a culvert with high sedimentation rates ..... 54
3.3.2 Analysis of sedimentation at the culvert ..... 59

CHAPTER4 INVESTIGATION METHOD ..... 63

4.1 Experimental Facilities ..... 63
4.2 Numerical Simulations ..... 68



www.manaraa.com

4.3 Field Observations ..... 69
4.3.1 Large-Scale Particle Image Velocimetry ..... 69
4.3.2 Quantitative Mapping at Culvert/Bridge Sites ..... 71
4.3.2.1 Waterway vicinity mapping ..... 72
4.3.2.2 Flow measurement ..... 74
4.3.2.3 Assembling flow and terrain data ..... 76

CHAPTER 5 FIELD MEASUREMENT IN UNSTEADY CHANNEL FLOWS ..... 78

5.1 Introduction ..... 78
5.2 Calibration measurement ..... 83
5.2.1 Large-scale particle image velocimetry ..... 83
5.2.2 LSPIV and ADCP measurement ..... 86
5.3 Measurement of loop rating curve ..... 96
5.4 Summary ..... 100

CHAPTER 6 RESULTS FROM INVESTIGATIONS OF SEDIMENT DEPOSITION AT CULVERTS ..... 103

6.1 Overview ..... 103
6.2. Hydraulic model experiments ..... 103
6.2.1 Baseline experiments ..... 105
6.2.1.1 Test 1: Sediment mobility and deposition patterns for a range of flows ..... 105
6.2.1.2 Test 2: suspended versus bed load transport ..... 108
6.2.1.3 Test 3: Sediment accumulation rates ..... 110
6.2.1.4 Test 4 Baseline flow ..... 112
6.2.1.5 Test 5: Flow kinematics through the culvert area ..... 115
6.2.1.6 Test 6: Simulation of discrete sampled hydrograph ..... 118
6.2.2 Validation experiment ..... 124
6.2.2.1 Test 7: Qualitative evaluation of sedimentation pattern in model 1/5B ..... 125
6.2.2.2 Test 8: The mechanics of sediment deposit formation ..... 126
6.3 Numerical experiment ..... 132
6.3.1 Simulation scenarios ..... 132
6.3.2 Simulation setting ..... 133
6.3.2.1 Computational grid ..... 133
6.3.2.2 Flow modeling ..... 133
6.3.2.3 Post processing ..... 133
6.3.3 Numerical model testing ..... 134
6.3.4 Comparison of numerical and laboratory experiments ..... 137

CHAPTER 7 CULVERT STREAMLINING ..... 140

7.1 Experiments for screening the self-cleaning culvert configurations ..... 141
7.1.1 Fillet approach ..... 142
7.1.1.1 Fillet-based design A ..... 142
7.1.1.2 Fillet-based design B ..... 144
7.1.1.3 Fillet-based design C ..... 145
7.1.1.4 Fillet-based design D ..... 147
7.1.2 Vanes Approach ..... 149
7.1.2.1 Vane-based design A ..... 149
7.1.2.2 Vane-based design B ..... 150
7.2 Numerical simulation of the Fillet-based Self-Cleaning Culverts ..... 152



www.manaraa.com

7.3 Assessment of the performance of the fillet-based self-cleaning culvert .....154
7.3.1 Overview .....154
7.3.1 Test for the assessment of the performance fillet-based self-cleaning culvert .....155
7.3.2 Flow kinematics in the vicinity of the original culvert configuration.....156
7.3.3 Mitigation of sedimentation at culvert .....158

CHAPTER 8 CONCLUSION AND RECOMMENDATION .....164

8.1 Conclusions.....164
8.2 Recommendations for future studies .....168

REFERENCES .....170

APPENDIX A SURVEY OF IOWA COUNTY ENGINEERS.....174

APPENDIX B FIELD VISIT OF CULVERTS IN IOWA.....181

APPENDIX C MOBILE LARGE-SCALE PARTICLE IMAGE VELOCIMETERY .....225



www.manaraa.com

LIST OF TABLES

Table 1.1 Department of Transportation Multi-barrel Culvert Survey Result.....6

Table 3.1 Design cases for numerical simulations of unsteady flows .....38

Table 6.1 Four flow conditions tested in Test 1.....106

Table 6.2 Three flow conditions tested in Test 3.....113

Table 6.3 Three flow conditions tested in Test 6.....118

Table 6.4 Simulation case and reference model .....132

Table 7.1 Summary of fillet-based design A .....143

Table 7.2 Summary of fillet-based design B .....145

Table 7.3 Summary of fillet-based design C .....146

Table 7.4 Summary of fillet-based design D .....147

Table 7.5 Summary of vane-based design A .....150

Table 7.6 Summary of vane-based design B .....151

Table A.1 List of Survey County Engineering .....174

Table B.1 Statistics of culvert in Johnson County (Johnson county Secondary Road Department) .....182



www.manaraa.com

LIST OF FIGURES

Figure 1.1 Silted culvert: a) view upstream from the culvert, and b) view of the culvert entrance ..... 8

Figure 1.2 Typical sedimentation pattern at a culvert in Iowa ..... 8

Figure 1.3 Selected responses on culvert sedimentation from a survey of the Iowa county engineers ..... 10

Figure 1.4 Selected responses on sedimentation at culverts resulting from the Iowa survey ..... 10

Figure 2.1 Rating curve, Q = f(h), in unsteady flow based on laboratory data ..... 14

Figure 2.2 Rating curve for flood at Connecticut River ..... 14

Figure 2.3 Comparison between rating curve made by USGS and measured discharge using MLSPIV during high flows ..... 15

Figure 2.4 Evolution of suspended transport rate during a hydrograph with duration Tr=40s and Tr = 320s ..... 16

Figure 2.5 A counter-clockwise hysteresis collected at a small basin ..... 17

Figure 2.6 The measurement of the water elevation along the flume in which a two-barrel culvert was place ..... 18

Figure 2.7 Time-variation of the water level upstream and downstream the culvert model with the triangular discharge hydrograph over the culvert ..... 18

Figure 2.8 Measured rates of sediment transport versus predicted rates for several methods: particle diameter(1.33mm), bed elevation (154 mm) ..... 20

Figure 2.9 Examples of scour at entrance of culvert for 7-mm gravel (A), 16-mm angular gravel (B), 35-mm cobbles (C), and 37-mm angular rock (D) (REFERENCE) ..... 21

Figure 2.10 Types of flow regimes through culverts with inlet and outlet control; inlet control (left); outlet control (right) ..... 23

Figure 2.11 Sediment mitigation design example: (top) pre-construction condition in 1992, (bottom) post-construction in 2000 ..... 27

Figure 2.12 Design procedure flowchart used in computer codes for the culvert design ..... 30

Figure 3.1 Superposition of flow complexities in the flow through culverts; considerations include hydrograph, sediment inflow, coupling of flow depth and discharge, and passage through the transition to the culvert ..... 33



www.manaraa.com

Figure 3.2 Deviation of the unstedy rating curve from the conventional one obtained through extrapolation applied to measurements in steady flow conditions....35

Figure 3.3 Hydraulic parameters for the hydrograph corresponding to case 3....39

Figure 3.4 Analysis of the sensitivity of stage-discharge relationship with the channel slope based on comparison of cases C1,C2, and C3....40

Figure 3.5 Discharge hydrographs in cases C3, C4, and C5. The three cases correspond to flood events with different time-to-peak values....41

Figure 3.6 Effect of the total duration of the flood event on stage-discharge relationship. Results are shown for cases C3, C4, and C5....41

Figure 3.7 Discharge hydrographs for cases C3,m C6 and C7 that have the same duration of the time to peak and different durations of the time from peak flow to base flow....42

Figure 3.8 Predicted looped rating curves for cases C3, C6, and C7....43

Figure 3.9 Discharge hydrographs for cases C3 and C8. The symmetric hydrographs have different peak flows....43

Figure 3.10 Predicted looped rating curves for cases C3 and C8....44

Figure 3.11 Predicted looped rating curves for cases C6 and C9....45

Figure 3.12 The relative importance of various terms in the momentum equation for the reference test (case 3)....46

Figure 3.13 Flow and sediment hydrograph at Clear Creek (10/02/07~10/04/07)....49

Figure 3.14 Sediment-discharge rating curve at Clear Creek (10/02/07~10/04/07)....49

Figure 3.15 Flow and sediment hydrograph at Clear Creek (10/14/07~10/16/07)....50

Figure 3.16 Sediment-discharge rating curve at Clear Creek (10/14/07~10/16/07)....50

Figure 3.17 Geometry of the three-barrel culvert placed in the rectangular channel....51

Figure 3.18 Upstream and downstream rating curves at the culvert showing a hysteresis behavior....52

Figure 3.19 Hydrographs of the main hydraulic parameters upstream of the culvert....53

Figure 3.20 Looped rating curves in a rectangular channel without a culvert and with a three-box culvert....53

Figure 3.21 Culvert site in solon:a) Satellite view of the study area, and b) two-year precipitation hydrograph from the weather station (ICY03) in the neighborhood....55



www.manaraa.com

Figure 3.22 Three-box culvert and sedimentation process in Old Mill Creek in Solon, Iowa (View of the culvert entrance). It can be observed that the sediment and debris trapped in the upstream basin reduce considerably the entrance area of the culvert. ....57

Figure 3.23 Three-box culvert and sedimentation process on Old Mill Creek in Solon, Iowa. Downstream view from the culvert. ....58

Figure 3.24 Sediment cores were collected in the sedimentation upstream the culvert shown in Figure 3.22 ....60

Figure 3.25 Sediment cores were collected in the sedimentation downstream the culvert shown in Figure 3.23 ....60

Figure 3.26 Sediment core collected from the upstream sedimentation near the culvert (number 2 in Figure 3.24a): a) Photograph shows stratification, and b) Grain size analysis presents L2 and L5 were coarse particles, but L4 and L6 were fine particles ....61

Figure 3.27 Sediment core collected from the downstream sedimentation near the culvert (number 6 in Figure 3.25a): a) Photograph shows stratification, and b) Grain size analysis presents L2 were coarse particles, but L3 were fine particles ....61

Figure 3.28 Sediment core collected in the channel(number 2 in Figure 3.24a): a) Photograph shows layers separated by fine particle, and b) Grain size analysis....62

Figure 4.1 Hydraulic models: a) overview of the 1/20 flume, b) the culvert model (1/20A) without wind wall, and c) the culvert model (1/20B) with wind wall ....64

Figure 4.2 Sediment feeder ....66

Figure 4.3 Schematic view of model 1/5B: (top), and view upstream toward headbox of the model (bottom)....67

Figure 4.4 SeaTek MTA depth profiler containing 32 multiple transducer arrays....68

Figure 4.5 Computation domains :a) the three-box l culvert design, and b) self-cleaning culvert design placed in the expansion upstream the culvert ....69

Figure 4.6 MLSPIV unit: a) general view; b) mast deployed and ancillary equipment....70

Figure 4.7 River reach plan's decomposition ....72

Figure 4.8 Waterway vicinity ortho-rectification protocol: (1) identification of the planar surfaces on the images; (2) ortho-rectification of the surfaces; (3) assembling of the ortho-images of the planar surfaces to obtain the ortho-image of the landscape....75

Figure 4.9 LSPIV time-averaged velocity field for the Jordan Creek site, downstream the culvert. ....76



www.manaraa.com

Figure 4.10 Example of mapping: (left)Ortho-image of the studied area, and (right)The corresponding digital map containing selected features of the waterway and its vicinity .....77

Figure 5.1 Rating curve for USGS gaging station 05454500 on the Iowa River in Iowa City, U.S.A: a) The rating curve is based on multiple direct measurements [271 measurements were acquired between 1984 and 2006. More than 80% of them were acquired for flows less than 200 m3/s]. b) Sample of rating curve adjustment due to changes in the channel hydraulics. .....79

Figure 5.2 Deviation of the unsteady rating curve from the conventional one obtained with a one-to-one relationship applied to measurements in steady flow conditions and extrapolated for high flows .....80

Figure 5.3 Appearance of the free surface at the same river location (area of about 1,000 m2): a) foam; b) ice floes; c) ripples driven by internal turbulence; d) lack of tracers; e) ripples driven by wind (gusts).....85

Figure 5.4 Overview of the LSPIV and ADCP measurements: a) Location of the measurements; b) raw velocities measured by ADCP in one of the transects; c) averaged velocity vector field obtained from LSPIV measurements. .....88

Figure 5.5 ADCP data illustrating the effect of the bridge pier on the downstream flow: a) view of the site with raw measurements averaged over depth (all transects); b) total depth-averaged computed in 21 nodes using 5 ADCP transects averaged horizontally in a 3-m radius; c) spatially averaged (3-m averaging radius) vertical profiles for the streamwise velocity component; d) illustration of the secondary currents in the cross section using the distribution of the spanwise velocity component. .....91

Figure 5.6 Averaged total vectors obtained with LSPIV and ADCP measurements.....92

Figure 5.7 Velocity at the free surface (LSPIV) and in the vertical (ADCP) at the same location .....93

Figure 5.8 Vertical velocity distribution of the spanwise velocity components illustrating the presence of secondary currents.....95

Figure 5.9 Effect of the index-velocity value on the discharge calculation.....95

Figure 5.10 LSPIV measurements during the Iowa River flood of 2008: a) location of the measurement site .....96

Figure 5.11 Chronology of the measurements during the flood wave propagation and video frames of the recordings considered in the present analysis .....101

Figure 5.12 Rating curve measurements: a) video recordings acquired on June 10th, 2008, b) vector field, c) cross-section velocity profiles used for discharge measurements, d) LSPIV discharge estimates superposed on the rating curve of the USGS gaging station. .....102

Figure 6.1Trial flow conditions of Test 1 .....107



www.manaraa.com

Figure 6.2 Sediment accumulation upstream the culvert. The sediment patterns illustrated in photos a) to d) above illustrates the results of the simulations with steady flows set for cases A to D in Figure 6.1. .....107

Figure 6.3 Sediment deposited at the culvert: a) using suspended load (crushed walnut shells); b) with bed load (silica sand) .....109

Figure 6.4 Sediment load distribution.....111

Figure 6.5 Rate of sediment accumulation in expansion and three barrels .....111

Figure 6.6 Mound height variation from one-hour to six-hour.....112

Figure 6.7 Flow condition in baseline test 4.....113

Figure 6.8 Sediment deposited after 2 hours for case B in model B .....114

Figure 6.9 Rate of sediment accumulation in the culvert area for flow case B .....114

Figure 6.10 Surface flow field for the case B with headwater depth 0.255ft: (a) Velocity vectors, (b) Velocity vectors and velocity magnitude contour, (c) Streamlines.....116

Figure 6.11 Surface flow field for Flatbed C with headwater depth 0.382ft: (a) Velocity vectors, (b) Velocity vectors and velocity magnitude contour, (c) Streamlines.....117

Figure 6.12 Hydrological events investigated in the culvert model .....119

Figure 6.13 Consecutive simulation of hydrological events: a) case B, b) case B→ case C, c) case B→ case C→ case D, and d) case B→ case C→case D→ case B.....120

Figure 6.14 Consecutive sedimentation: case B→case C→case B .....121

Figure 6.15 Sedimentation a) simulate flow conditions: case C → case D; b) simulate flow condition case B for two hours .....122

Figure 6.16 Synthesis of various experimental approaches adopted in the laboratory study in model 1/20B.....123

Figure 6.17 Sediment deposition patterns: a) Initial condition, b) case A, c) case B, d) case C.....126

Figure 6.18 MTA measurements of sediment deposition in the vicinity of the culvert .....127

Figure 6.19 Sediment deposition in the expansion area after running the model for 12 hours: a) image of sedimentation in the expansion area (the box delineate the area measured with MTAs), b) bathymetry pattern obtained from MTAs measurements.....129

Figure 6.20 Dynamic bed form evolvement upstream the culvert: a) 3-hour running, and b) 6-hour running .....130



www.manaraa.com

Figure 6.21 Dynamic bed form evolvement upstream the culvert: a) 9-hour running, and b) 12-hour running .....131

Figure 6.22 Near surface flow field for flow case B obtained with numerical simulation: (a) streamlines, (b) streamwise velocity, (c) out of plane vorticity .....135

Figure 6.23 Sediment transport characteristics for case B obtained from numerical simulations: (a) shear velocity (b) sediment transport.....135

Figure 6.24 Surface flow field for the case B obtained in laboratory tests with LSPIV and imagery: (a) Streamline and velocity magnitude contour at the free surface, (b) streamwise velocity at the free surface, (c) vorticity at the free surface, and (d) sedimentation (Relevant comparisons: 6.22 a, b, and c with 6.24 a, b, and c, respectively and 6.22b with 6.24d.) .....136

Figure 6.25 Near surface flow field for flow case C obtained with numerical simulation: (a) streamlines,(b) streamwise velocity, (c) out of plane vorticity .....136

Figure 6.26 Surface flow field for the case C obtained in the laboratory with LSPIV: (a) Streamline and velocity magnitude contour, (b) streamwise velocity, (c) vorticity.....137

Figure 6.27 The mesh resolution: (a) the numerical model mesh, (b) the LSPIV analysis mesh .....138

Figure 6.28 Comparison of average velocities error between numerical simulations (with FLUENT) and experimental results (with LSPIV) :(a) case B, and (b) case C.....138

Figure 7.1 Sedimentation pattern compare to the baseline test result.....144

Figure 7.2 Sedimentation pattern compare to the baseline test result.....145

Figure 7.3 Sedimentation pattern compare to the baseline test result.....146

Figure 7.4 Sedimentation pattern compare to the baseline test result.....148

Figure 7.5 Sedimentation pattern compare to the baseline test result.....150

Figure 7.6 Sedimentation pattern compare to the baseline test result.....151

Figure 7.7 The fillet-based self-cleaning design geometry.....152

Figure 7.8 Near surface flow field for flow case B over the self-cleaning system obtained with numerical simulation: (a) streamlines,(b) streamwise velocity, (c) out of plane vorticity .....153

Figure 7.9 Sediment transport characteristics for case B over the self-cleaning system obtained from numerical simulations: (a) shear velocity (b) sediment transport .....153

Figure 7.10 Sediment deposition patterns: a) Initial condition, b) case A, c) case B, d) case C.....156



www.manaraa.com

Figure 7.11 Streamline in 1/5B: a) reference condition, and b) FA design model .....157

Figure 7.12 Velocity contours in 1/5B: a) reference condition, and b) FA design model .....157

Figure 7.13 MTAs deployment in culvert boxes .....158

Figure 7.14 Sedimentation map in the culvert boxes at 6-hour: a) no self-cleaning system placed upstream the culvert boxes, and b) self-cleaning system placed upstream the culvert boxes .....160

Figure 7.15 Sedimentation map in the culvert boxes at 12-hour: a) no self-cleaning system placed upstream the culvert boxes, and b) self-cleaning system placed upstream the culvert boxes .....161

Figure 7.16 Longitudinal bed profiles in the left box: a) measurements at 6-hour, and b) measurements at 12-hour.....162

Figure 7.17 Longitudinal bed profiles in the central box: a) measurements at 6-hour, and b) measurements at 12-hour.....163

Figure B.1 Iowa Map indicate the counties we visited.....181

Figure B.2 Distribution of Triple-box culverts in Johnson County.....182

Figure B.3 Marion County: Yellow markers are field visit locations, and Red markers are USGS stream stations.....203

Figure B.4 Buena Vista County Map: Yellow markers are field visit locations and Red marker is USGS stream station in this county.....216

Figure C.1 MLSPIV unit: a) general view; b) Camera and panning control equipment.....226

Figure C.2 Removal of image distortion due to recording with an oblique angle and reconstruction of the image in real coordinates. .....226

Figure C.3 Relation between CRT coordinates and physical coordinates.....229

Figure C.4 Method to create non-distorted image .....229



www.manaraa.com

LIST OF SYMBOLS

Alphabetical symbols

| | |
|---|---|
| $A$ | Full culvert cross section area; the area of the channel |
| $B$ | Width of channel |
| C | Celerity velocity |
| $c$ | Constant based on the culvert configuration |
| $C_b$ | Coefficient expressing effective width contraction |
| $D$ | Depth of the culvert; D=A/B |
| $f$ | Darcy-Weisbach friction factor |
| F | Froude number |
| $h_L$ | Head Loss |
| $h_p$,$h_s$ | Water depth of peak and base flow |
| $HW$ | Headwater depth |
| $K$ | Conveyance; Coefficients based on the culvert configuration |
| L | Length of the channel |
| $M$ | Coefficients based on the culvert configuration |
| $Q$ | Barrel discharge; channel discharge |
| $q_s$ | Sediment discharge |
| $S$, $S_0$ | Channel slope |
| $S_f$ | Friction slope |
| $T_p$, $T_b$ | Time to peak and base flow |
| $TW$ | Tailwater depth |
| $U$ | Mean velocity |
| $u_*$ | Friction velocity |
| $u_{*b}$ | Friction velocity of base flow |
| $u$, $v$, $x$, $y$ | CRT (image) coordinates |



www.manaraa.com

| | |
|---|---|
| $V_s$ | Speed of flood wave |
| Y | Constant based on the culvert configuration |
| $z$ | Water surface elevation |

Greek symbols

| | |
|---|---|
| $\delta$ | Total error in a measurement |
| $\Delta t$ | Time interval between two successive images |
| $\Delta x_{i,j}$, $\Delta y_{i,j}$ | Particle displacements at a grid point (i, j) in the x and y directions |
| $\Delta X$, $\Delta Y$ | Step size in physical coordinates |
| $\lambda$ | Unsteady parameter |
| $\Gamma$ | Unsteady parameter |
| $\tau$ | Shear stress on the wall |



www.manaraa.com

LIST OF ABBREVIATIONS

| | |
|---|---|
| ADCP | Acoustic Doppler Current Profiler |
| CAP | Culvert Analysis Program |
| CCD | Charge-coupled device |
| CRT | Cathode ray tube |
| FESWMS | Finite Element Surface Water Modeling System |
| FHWA | Federal Highway Administration |
| GRP | Ground reference point |
| HDS-5 | Hydraulic Design Series No.5 |
| HEC-RAS | Hydrologic Engineering Center – River Analysis System |
| HY-8 | Culvert Hydraulic Analysis Program |
| IA | Interrogation area |
| IIHR | Iowa Institute of Hydraulic Research |
| LSPIV | Large-Scale Particle Image Velocimetry |
| MDSHA | Maryland State Highway Administration |
| MESBOAC | Match, Extend, Set, Bury, Offset, Align, Consider |
| MLSPIV | Mobile Large-Scale Particle Image Velocimetry |
| MTA | Multiple Transducer Arrays |
| PIV | Particle Image Velocimetry |
| PTU | Pan-tilt unit |
| USGS | US Geological Survey |



www.manaraa.com

# CHAPTER1

# INTRODUCTION

## 1.1 Overview of culvert issues

Culverts are commonly used to pass roads over small streams without blocking stream flow. The sediment load conveyed by streams may at times accumulate and partially block culverts, seriously reducing their capacity to convey design flows. Multi-barrel culverts (culverts with more than one conduit) are especially prone to sediment blockage because of geometric configuration. This thesis shows how sediment blockage may readily occur at multi-barrel culverts, and indicates options for mitigating such blockage.

## 1.2 Problem statement

A culvert is a short conduit placed transversely through an embankment so as to convey stream flow from one side of the embankment to the other (e.g., Chow, 1959). Culverts are used extensively to pass flows through road embankments. The combined effects of road site layout, highly variable, non-uniform, and varying flow rates, along with sedimentation, vegetation, and debris accumulation factors at times makes culvert flows rather site-specific, three-dimensional, and unsteady. Consequently, it can be difficult to develop flow field and sediment transport formulations valid for all culverts. One flow and sediment feature is common for culverts: sediment will deposit near and in a culvert if the approach flow does not convey its sediment load continuously through the culvert.

Sediment deposition at culverts is influenced by many factors, including the size and characteristics of material of which the channel is composed, the hydraulic characteristics generated under different hydrologic events, the culvert geometry design, the channel transition design, and the presence of vegetation around the channel. The multitude of combinations produced by this set of variables makes the investigation of

www.manaraa.com

practical situation a complex undertaking. Most hydraulic manuals provide design specifications only for clear water conditions, and leave the issue of sediment management unaddressed.

This study was motivated by quite widespread problems with culvert sedimentation, notably for culverts located in rural Iowa where streams typically convey substantial sediment loads. The problems indicated the need for guidance on how culvert designs can mitigate or inhibit sediment deposition and blockage. The guidance should be applicable to new culverts and existing culverts. In regions where high rates of soil erosion occur, there is pressing need for such methods. Iowa is one such area. Its numerous multi-box culverts face chronic sediment problems.

Culvert literature reveals that little in detail is known about sedimentation at culverts. The relevant literature is scarce and lacks systematic studies of sediment transport through multi-box culverts, and how sediment deposition reduces flow through culverts. While it is accepted that sediment transport through culverts is strongly influenced by local soil and land-use conditions in the drainage area adjacent to the culvert, scant information exists on flow to and through multi-barrel culverts. Several considerations have led to the limited literature on culvert sedimentation:

1. The complexity of the flow carrying sediment through multi-barrel culverts;
2. Lack of field, experimental, and numerical simulation observations; and,
3. Simple neglect of culvert sedimentation as an engineering concern. Culverts are a common, low-cost, hydraulic structure whose performance often is taken for granted.

The present study considers three aspects of culvert flow complexity. The first complexity relates to the change in flow geometry from the undisturbed cross section of the stream (usually trapezoidal) to the geometry of the multi-barrel culvert (at least

www.manaraa.com

double the stream cross section area in the undisturbed region). This change in geometry occurs twice at the culvert sites: an expansion exists upstream the culvert, and a contraction to the original cross section shape occurs downstream the culver. The transitions at culvert produce a three-dimensional non-uniform flow behavior gradually varying in space, as the flow moves downstream. The second complexity is the unsteadiness of runoff flows from the catchments drained by a culvert. Flow unsteadiness must be studied with theoretical tools, because laboratory investigations cannot easily replicate transitions the flow and sediment transport during a large time scale as required by the propagation of a flood wave. Even simulations for the simpler cases, such as the unsteady flow through a constant section open-channel, are not yet sufficiently accurate to be applied to the practical situations. The reason for this status is the lack of field observations in unsteady flows due to the high temporal resolution requirements for the instrument and data acquisition system.

The third source of complexity arises because it is difficult to generalize information about non-uniform, unsteady sediment transport in channels of non-uniform three-dimensional geometry. Presently, there are few readily useable (and inexpensive) numerical models that can simulate flow and sediment transport in such situations. Considerable reliance must be placed on field and laboratory work. One interesting point in this regard is that limited experimental evidence suggests that the sediment transport and stream flow hydrographs are not in phase: the peak of sediment hydrograph arrives before or after the peak of discharge.

## 1.3 Study objectives

The study is structured to address two overall objectives that in turn entail a set of specific tasks. One objective is to reveal and document the flow and sediment-transport processes occurring in the unsteady, non-uniform flow field at the entrance transition to

www.manaraa.com

multi-barrel culverts. The second objective has the practical aim of developing recommendations for self-cleaning designs to substantially lessen sedimentation at multi-barrel culverts. To the term "substantially lessen," not eliminate, is used here, because complete elimination is not feasible for most culvert sites and designs.

The following specific tasks were performed in pursuit of the studies two overall objectives (in parentheses are mentioned the investigative tools used for the tasks):

1. Investigate hydraulic aspects of unsteady open channel flows (analytical, field observations, and numerical simulations);
2. Determine the hydraulic performance of the multi-barrel culvert under different flow conditions (analytical, laboratory and field observations, numerical simulations);
3. Understand the coupling between flow and the sedimentation at culverts under different flow conditions (laboratory and field observations);
4. Investigate the sediment deposition patterns at multi-barrel culverts (laboratory and field observations); and,
5. Determine and test design elements or features that inhibit sedimentation at culverts (laboratory and numerical experiments).

## 1.4 Approach

The great variability of culvert sites required that the study narrow its focus on selected specific aspects of unsteady, non-uniform, sediment-laden flow at one configuration of box culvert. The study approached these aspects in two steps employing the tasks listed above:

1. Analysis of unsteady flows in open channels of constant cross section; and,
2. Analysis of non-uniform flows and sediment transport in channel geometries typically encountered at the entrance transition to culverts.

www.manaraa.com

The first step was addressed by means of analytical and field observations. Numerical simulations were used to capture the sensitivity of the open-channel flow to the characteristics of the inflow hydrograph. Field observations during the historical flood of 2008 in Iowa River at Iowa City were acquired and analyzed. As the field observations are conducted with an image-based technology still under scrutiny, a reference experiment in Iowa River is firstly presented. The second step was carried out using field inspection and measurement,) hydraulic modeling, and numerical simulations. The methods produced the following information:

1. Field observations are aimed at understanding typical sedimentation patterns and their dependence on channel and culvert geometry and the hydrodynamic conditions during normal and extreme hydrologic events. Field monitoring were accomplished using the Digital Mapping software in conjunction with IIHR's mobile Large-Scale Particle Image Velocimetry (LSPIV) system. The software, developed at IIHR, combines LSPIV with image-based terrain survey concepts (Hauet et al., 2008.a,b).
2. Hydraulic model experiments are used for replicating the sedimentation process observed in situ for two- and three-box culverts. The major tasks for the hydraulic model study are to accurately replicate the performance curve of the culvert and the dynamics of the sediment accumulation using a set of experimental conditions. The experiments were conducted in a progressive manner adding gradually flow features in the model with the goal to eventually be able to conduct experiments with unsteady and non-uniform conditions similar with those produced during the storm events.
3. Numerical simulations enhance the understanding of the sedimentation processes and aid testing flow cases complementary to those conducted in the model reducing the number of (more expensive) tests to be conducted in the laboratory.

www.manaraa.com

The research is phased such that field observations have been conducted first, followed by modeling through complementary hydraulic model and numerical experiments. The results from each research stage are being used heuristically to design the next stage. Subsequently, observations inferred from all research phases are being compiled to provide the needed insights for implementation of practical solution to culvert sedimentation.

## 1.5 Background

Culverts may comprise multiple conduits (thereby the term *multi-barrel culvert*) or a single conduit. In general, larger flows and road embankment heights require the use of multi-barrel culverts. Usual culvert cross-sections are circular, box, elliptical, pipe-arch, and arch. Cross-section shape selection is based on construction cost, limitations on upstream water-surface elevation, road embankment height, and desired hydraulic performance. A nation-wide survey of state transportation engineers revealed that multi-barrel culverts, especially multi-box culverts, are commonly used through the United States (Table 1.1).

Table 1.1 Department of Transportation Multi-barrel Culvert Survey Result (Gary, 2008)

| State | Multiple culvert use | Circular or box | Lowered invert on barrel |
|---|---|---|---|
| Alaska, Arkansas, Colorado, Connecticut, Maine, Maryland, Michigan, Minnesota, Nebraska, Nevada, North Dakota, South Carolina | Yes | Both | Yes |
| Montana, Utah | Yes | Box | Yes |
| Georgia, Hawaii, New Mexico, Wyoming | Yes | Both | No |
| Iowa | Yes | Box | No |
| California, Idaho, Kentucky | Yes | Circular | No |
| Indiana, Ohio, Washington | No | --- | --- |

www.manaraa.com

Culverts convey a large range of flow rates and sediment loads. They customarily are designed to convey flow events having a 50-year return period, but usually convey much smaller flows, and sometimes are dry. Multi-barrel culverts usefully accommodate a large range of flow rates, and fit within typical road embankment heights. For large flows, the large flow cross-section of a multi-barrel culvert is an advantage, because a lesser upstream headwater elevation is needed compared that needed for a single-barrel culvert of lesser flow area.

The flow area of a multi-barrel culvert typically exceeds that of the stream channel along which it is located. Channel transitions merge the culvert with the stream channel upstream and downstream. The transitions comprise an expansion is needed upstream of the culvert, followed by a contraction downstream. Because culverts usually convey flows that are of lower velocity and lesser depth than the design flows, flow through the entrance transition typically is not uniformly distributed across the culvert entrance. In many situations flow concentrates in one barrel. A related consequence is that, over several years of relatively low flow, stream sediment deposits in one side of the entrance transition and in one or more barrels. Consequently, a barrel may silt-in with sediment. A view of such a situation is illustrated in Figure 1.1, where the upstream side of the culver is shown. Such sedimentation can reduce the capacity of culverts to handle the larger flow events, and pose high-water problems upstream of culverts. This problem and the costs it incurs are compounded because many culverts are small enough in area, yet also rather long, so that cleaning sediment from a partially filled culvert can be very difficult and costly. The problem is particularly severe for culverts draining small rural watersheds, as documented by (Vassilios, 1995; Andrzej el at., 2001; Charbeneau, 2002).

www.manaraa.com

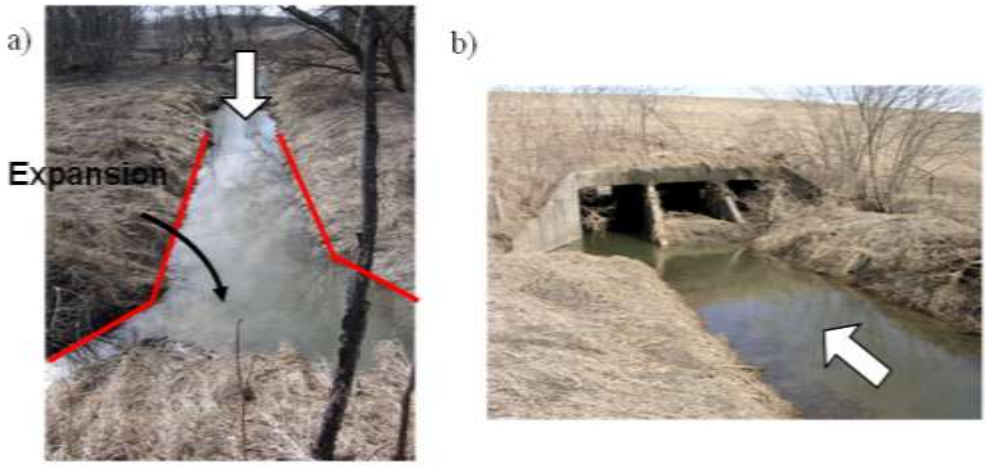


Figure 1.1 Silted culvert: a) view upstream from the culvert, and b) view of the culvert entrance

Figure 1.2 Typical sedimentation pattern at a culvert in Iowa

www.manaraa.com

### 1.5.1 Iowa culverts

During 2007, the present study assessed the extent and severity of the sedimentation at culverts in Iowa. The assessment entails a series of field visits to more than 30 culverts. Though the culverts were of diverse dimensions and shapes, they commonly had experienced extensive blockage by sediment, and had required difficult and costly cleanup operations. Silting situations, such as those illustrated in Figure 1.2, were encountered at several of the culverts. The chronic nature of the sedimentation is illustrated by the fact that some of the culverts clogged re-clogged two years after cleanup. Chapter 5 gives more details and findings from the field.

A survey of Iowa county engineers and Iowa Department of Transportation (IDOT) staff provided further insight into the scope of sedimentation at multi-barrel culverts in Iowa. The insights revealed several key aspects of the sedimentation at Iowa culverts. The full results of the survey are provided in Appendix A. The main features of the sedimentation at culverts are summarized here:

1. Multi-box culverts are commonly used in Iowa, as illustrated in Figure 1.3a.
2. Their major maintenance problems are attributable to accumulation of sediment and debris (see Figure 1.3b).
3. The main causes of culvert sedimentation are little known yet (see Figure 1.4a).
4. The design notion that the sedimentation will be always be washed away by storm events is not substantiated by experience, as captured in Figure 1.4b.
5. Experience indeed suggests that some storm events aggravate the sediment deposition.
6. About 70% of the survey respondents have not found a successful design approach to mitigate culvert sedimentation. Others presented that application of terrace or drop inlet can mitigate the sediment deposition. Maintenance usually requires that the sediment be removed from culverts as indicated by Figure 1.4c

www.manaraa.com

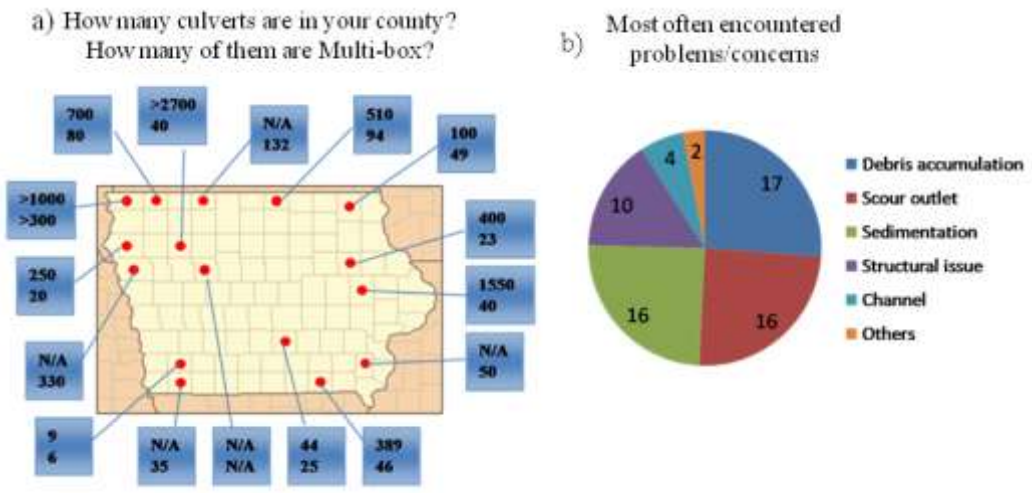


Figure 1.3 Selected responses on culvert sedimentation from a survey of the Iowa county engineers

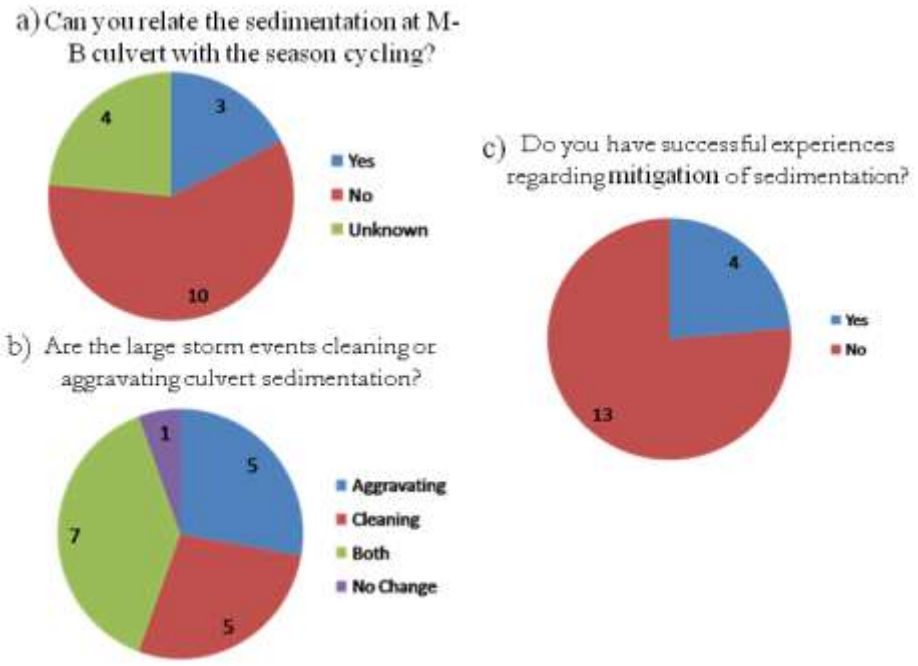


Figure 1.4 Selected responses on sedimentation at culverts resulting from the Iowa survey

www.manaraa.com

# CHAPTER 2

# LITERATURE REVIEW

Culvert presence in a stream disrupts the stream's balance of water flow and sediment transport, doing so in a continuous interplay of erosion and sedimentation. This process is accelerated during storm events when water depths and velocities are high and the flow regime is rapidly changing. Culvert design infrequently attempts to account for the disruption in the sediment transported by the streamflow to be conveyed through a culvert. Research on sedimentation at culverts is limited to date, though extensive information exists regarding sediment transport in open channels. The ensuing literature review of literature focuses primarily on culverts but also touches on sediment transport in channels.

## 2.1 Hydrodynamic considerations for channel

Culverts are designed to pass a large range of flow rates. Although they usually convey relatively small flows, they must also pass large flows occur during storm events. In accordance with the culvert's drainage role in passing storm hydrograph flows, consideration of unsteady flow is therefore required. However, research on unsteady flows through culverts is nearly nonsexist. Unsteadiness in open channel, however, will be considered instead, in the context of the variation of flow capacity to transport sediment. There are two unique relationships which would deviate from the steady flow: stage-to-discharge and sediment rate-to-discharge. The first, also called rating curve, does not reflect a one-to-one relationship, but entails a loop curve instead. The loop rating curve can theoretically be demonstrated by Saint-Venant equations (Chow 1959). The other one also departs a unique relation. However, the formation of a loop curve between sediment rate and flow rate is not promised. The review of literature of unsteadiness in open channel flow will be presented in the ensuing section.

www.manaraa.com

### 2.1.1 Loop rating curve

When a flood wave or hydrograph propagates along a channel, the wave front approaching a cross-section will experience an increase in the velocity (Henderson, 1966) that influences rate of sediment transport along a channel. After the flood peak passes the cross-section, the rear of the wave reduces the velocity at a given discharge at the cross-section. Under some conditions, these effects will be manifested as distinctive loops in the stage–discharge relationship. This phenomenon can be explained by observing the nonlinear partial differential equations for the unsteady flow in an open-channel flow, also known as St. Venant equations (Jain 2000):

$$\frac{\partial y}{\partial t} + D\frac{\partial V}{\partial x} + V\frac{\partial y}{\partial x} = 0 \tag{2.1}$$

$$\frac{1}{g}\frac{\partial V}{\partial t} + \frac{V}{g}\frac{\partial V}{\partial x} + \frac{\partial y}{\partial x} = S_0 - S_f \tag{2.2}$$

where y is water depth, D = A/B, V is velocity, $S_0$ is bed slope, and $S_f$ is friction slope

Eq (2.2) can be re-organized as below:

$$S_f = S_0 - \frac{\partial y}{\partial x} - \frac{1}{g}\frac{\partial V}{\partial t} - \frac{V}{g}\frac{\partial V}{\partial x} \tag{2.3}$$

By substitution for $S_f$ into Manning equation in terms of conveyance yields:

$$Q = K\sqrt{S_0 - \frac{\partial y}{\partial x} - \frac{1}{g}\frac{\partial V}{\partial t} - \frac{V}{g}\frac{\partial V}{\partial x}} \tag{2.4}$$

where K is conveyance coefficient

Depending on the number of terms kept in the above equation, it represents different physical meaning and uses different methods of river routing in the channel. The flood routing in the river with a gentle bed slope, for example, the last two terms in the

www.manaraa.com

radical are the acceleration terms and can be neglected in equation (2.4), which can be written as the famous Jones formula:

$$Q = K\sqrt{S_0 - \frac{\partial y}{\partial x}} \tag{2.5}$$

The above equation reveals that the bed slope and the diffusion term are the dominant factors of the flood routing in the gentle slope channel. By virtue of the energy losses associated with flow through a culvert, culvert presence influences effective bed slope of the channel in which it resides.

Although the unsteadiness can be explained and solved by the above equations, it is necessary to define reasonable parameters to characterize the effect of hydrograph. Takahashi (1969) proposed an unsteadiness parameter in order to analysis the one-dimensional equation of flood waves:

$$\lambda = \frac{V_s}{C\sin\theta} \tag{2.6}$$

where $V_s = (h_p - h_b)/T_d$ and $C = \sqrt{gh_p}$; $h_p$ and $h_s$ are the water depth of peak flow and base flow. $T_d$ is the duration of flood wave

Suszka (1987) introduced a similar parameter $\Gamma$ to characterize the unsteadiness for open channels flows:

$$\Gamma = \frac{1}{u_{*b}}\frac{\Delta h}{\Delta T} \tag{2.7}$$

where $u_{*b}$ is friction velocity of the base flow, $\Delta h$ is the difference of water level between base flow and the maximum, and $\Delta T$ is the duration of the hydrograph

Tu (1992) followed by Song (1994) experimentally showed that the larger value of the above parameter, the more pronounced is the loop. The corresponding loop rating curve result is shown in Figure 2.1.

www.manaraa.com

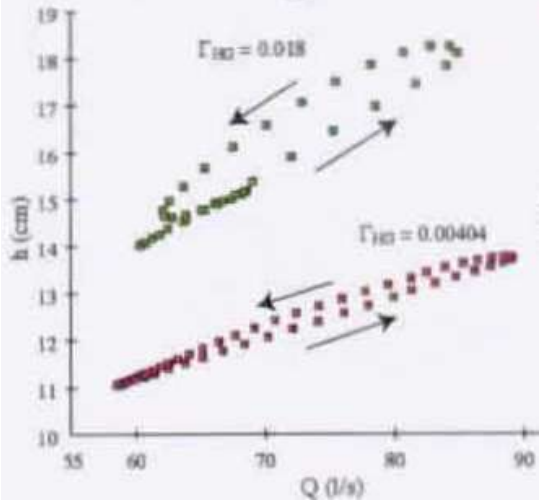


Figure 2.1 Rating curve, Q = f(h), in unsteady flow based on laboratory data (Qu 2003)

Field data has been measured in Connecticut River at Hartford, Connecticut shows the loop rating in Figure 2.2 (Jansen et al., 1979). During the field measurement, two flood events occurred. A small flood (curve A) preceding the main flood (curve B) can be observed to on the rating curve constructed for the field study.

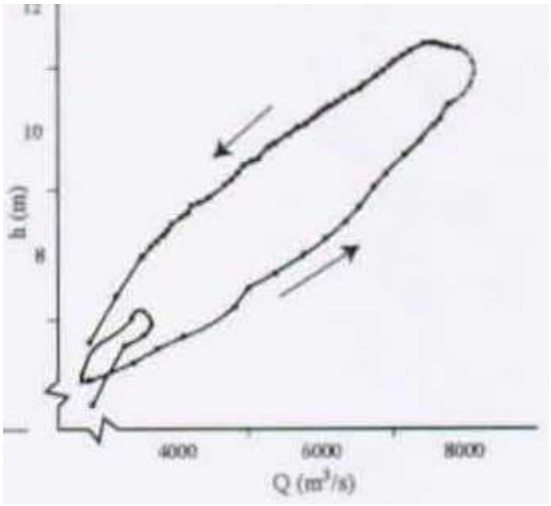


Figure 2.2 Rating curve for flood at Connecticut River (Jansen et al., 1979)

www.manaraa.com

Kim (2006) collected discharge data during flood wave propagation at Clear Creek, Coralville, Iowa during a storm in the winter of 2005. The direct discharge measurements collected during the storm showed that the discharge peaked at a stage that was 3.4 % larger than the one estimated discharge from the single-value rating curve made by USGS.

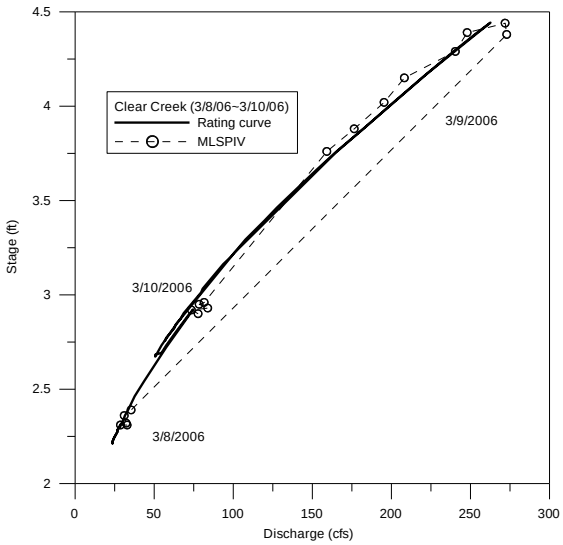


Figure 2.3 Comparison between rating curve made by USGS and measured discharge using MLSPIV during high flows (Kim, 2006)

### 2.1.2 Sediment transport during flood events

According to the aforementioned loop rating curve, the average velocity in the channel will reach its peak before the maximum discharge. Moreover, Graf and Qu (2003) demonstrated that the friction velocity also reached its maximum value before the maximum discharge with the average velocity expressed by a logarithmic law; this finding relates directly to the fact that the flow is shallower for the same discharge on the

www.manaraa.com

rising limb of the loop. The sediment discharge rate, however, is unclear when its peak will arrive.

The sediment discharge rate, $q_s$, may not immediately respond to the corresponding variation of velocity. Shutter and Verhoeven (2001) simulated sediment transport during flood events with laboratory and field experiments. Both laboratory and field result presented that suspended sediment transport rate is higher in the rising limb than in the falling limb for the same flow rate (see Figure 2.4). The difference behavior of the sediment rate in the rising limb and the falling limb compromises the use of a traditional sediment transport formula, where discharge and sediment concentration are related in a unique relation.

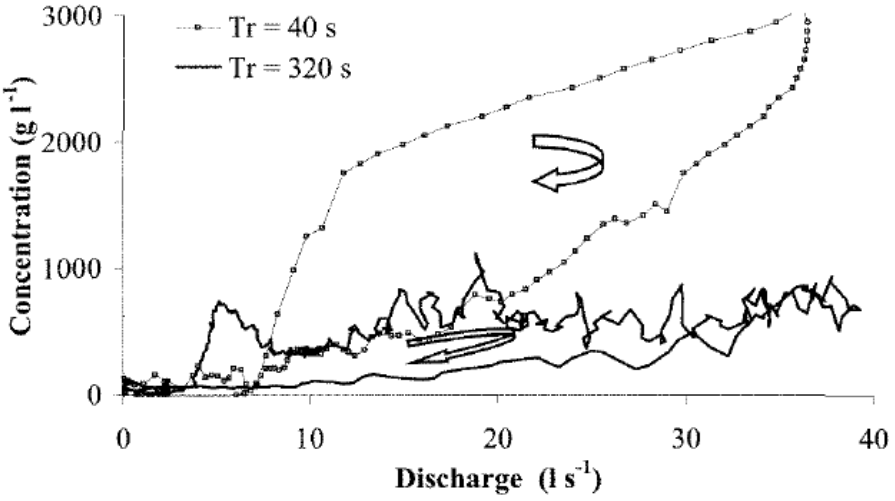


Figure 2.4 Evolution of suspended transport rate during a hydrograph with duration $T_r$=40s and $T_r$ = 320s (Shutter and Verhoeven, 2001)

Klein (1984) pointed out the importance of the location of sediment sources which may cause a counter-clockwise hysteresis between suspended transport rate and discharge. Figure 2.5 presents his field measurement during storm events in a small basin.

www.manaraa.com

Lenzi and Marchi (2000) analyzed suspended load during floods in a small stream in northeastern Italy. Clockwise and counter-clockwise hysteresis loops were both observed in different floods. The above results show an important conclusion. The common clockwise hysteresis occurs when sediment source contributing area is channel itself. On the other hand when sediment source are form the basin's slopes, a counter-clockwise hysteresis occurs.

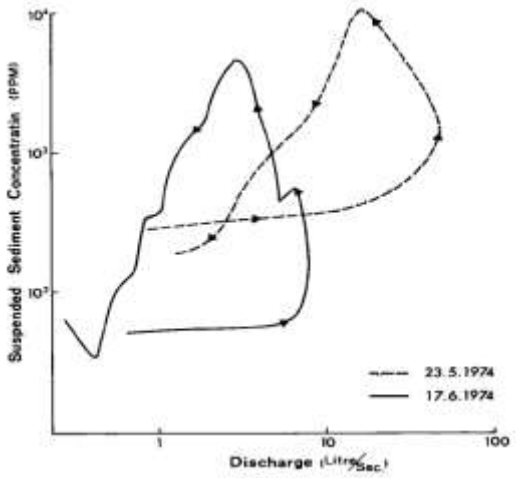


Figure 2.5 A counter-clockwise hysteresis collected at a small basin (Klein 1984)

## 2.2 Hydrodynamic considerations for flows through culverts

### 2.2.1 Unsteady flow at culvert

The forgoing discussion of looped rating curves for flow and sediment bear closely on a culvert's capacity to pass flow and sediment. Meselhe and Hebert (2007) measured the head water depth evolution with the passage of a flow hydrograph through a culvert. The culvert model was a low weir with two circular barrels (Figure 2.6). In their experiment, as the flow increased, the culvert barrels slowly transitioned from

www.manaraa.com

partially full to full. During the falling limb, the culvert barrel continued to flow full with a lower discharge than during rising limb. In Figure 2.7it shows that the maximum value of water level arrived later than the maximum value of the discharge.

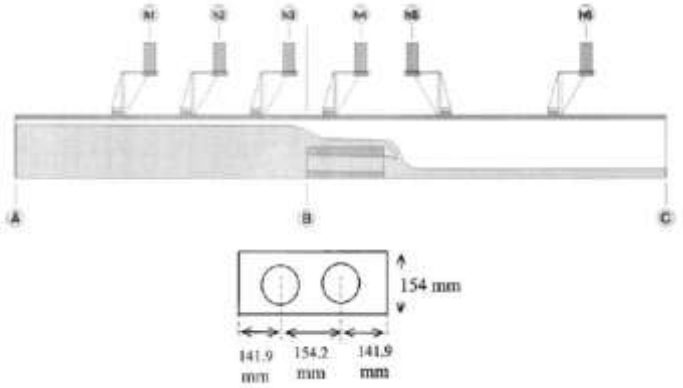


Figure 2.6 The measurement of the water elevation along the flume in which a two-barrel culvert was place (Meselhe and Hebert, 2007)

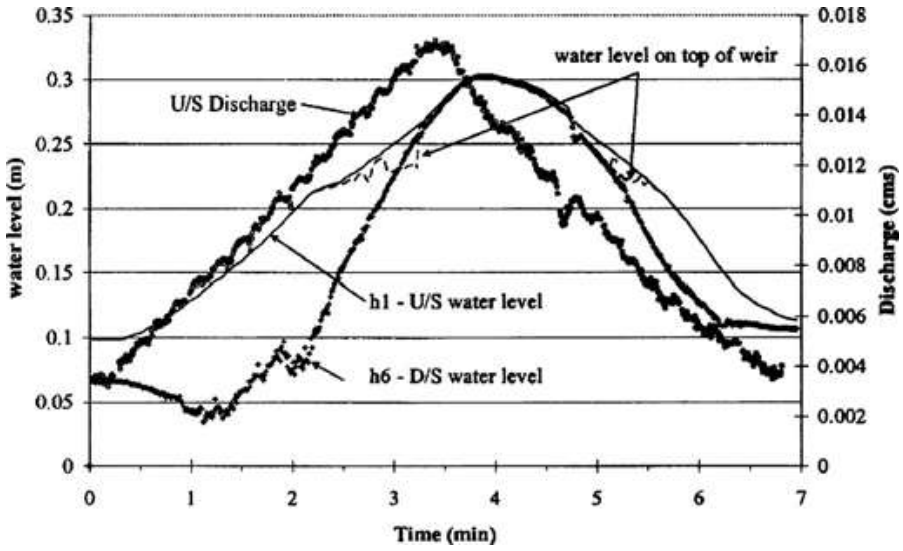


Figure 2.7 Time-variation of the water level upstream and downstream the culvert model with the triangular discharge hydrograph over the culvert (Meselhe and Hebert, 2007)

www.manaraa.com

### 2.2.2 Sedimentation at culverts

Culverts are usually constructed on relative mild channel slopes to avoid supercritical flow upstream the entrance. However, a relatively mild slope potentially increases the probability of sediment deposition near culverts ,even during storm events. Sediment building up near and through a culvert decreases the culvert's flow capacity, possibly causing the culvert not to pass its design discharge. Sediment deposition is especially an issue for multi-barrel culverts, because inadequacies in approach flow distribution cause one or more barrel typically is more susceptible to sediment deposition.

Sediment deposition at culverts is influenced by many factors, including the size and characteristics of the channel's bed and bank material, the hydraulic characteristics generated under different hydrology events, the culvert geometry design, channel transition design, and the vegetation around the channel. Culvert sites reflect numerous combinations of these variables, thereby complicating general investigation of culvert performance. Most design guides provide design specifications only for the clear water conditions. The customary design assumption is that sediment might deposit at normal flow condition and then be flushed out during storm events prevails. Practical experience, however, suggests otherwise. Moreover, in many situations the quick growth of vegetation on the fertile sediment deposits in the culvert area stabilizes sediment deposits, which then may grow in size.

Many prior studies (Vassillios 1995, Charbeneau et al. 2002, and Rigby et al. 2002), however, show that significant sediment problems occur at multi-barrel culvert sites:sediment buildup in the barrels, and clogging of the barrels with debris; and erosion at the inlet and outlet. Despite these reports of problems,, current culvert design guides give little attention to the effects of the interactions between the stream and the culvert, and to the sedimentation problems.

Because of the unsteady nature of sediment deposition at culverts, laboratory and numerical investigation are difficult to perform, with the result that there are few studies

www.manaraa.com

on this subject. Most studies comprise field observations. In one of these studies, Vassilios (1995) reports events at a reinforced concrete box culvert During a major rains storm the culvert was entirely blocked with sediment, causing substantial local flooding..

Goodridge (2009) investigated the behavior of bed load transport in the culvert with a hydraulic model which was a single pipeline culvert. Incipient motion and critical shear stresses were investigated with the culvert model. The Engelund and Hansen, Meyer-Peter Mőller, Shields, Toffaleti, Schoklitsch, DuBoys, Yang, and Rottner methods are investigated to the application into culvert sediment transport. The flow condition in the barrel is under full and partial full. Figure 2.8 shows the result for the culvert under partial full flow regime. Given each model's deviation, the empirical coefficients were then recalibrated.

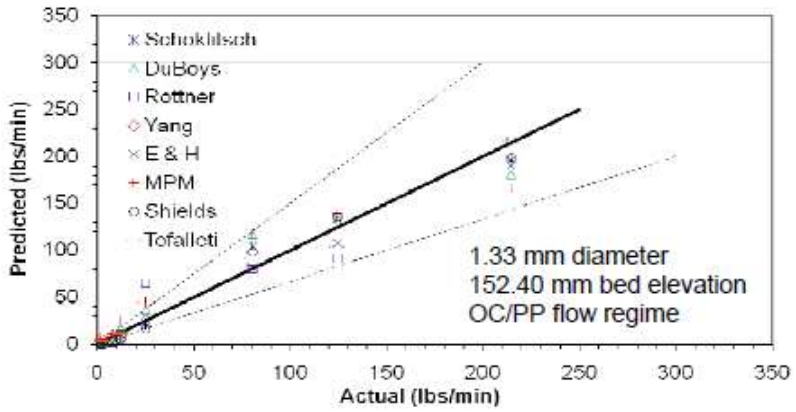


Figure 2.8 Measured rates of sediment transport versus predicted rates for several methods: particle diameter(1.33mm), bed elevation (154 mm) (Goodridge, 2009)

Besides investigating sediment deposition at culvert sites, studies also have focused on scour at t culvert inlets and outlets, and on ways to improve culvert design to enhance local ecology. In this regard, bottomless and buried invert culvert designs are of

www.manaraa.com

interest because they facilitate fish migration through culverts (Kerenyi et al. 2003, Crookston and Tullis 2008). The resulting scour at the entrance along the foundation and outlet was measured (Figure 2.9). Predictive equations for estimating scour depth were developed and compared to Maryland State Highway Administration (MDSHA) methodology. The prevention of scour at culvert inlet and outlet is the main concern of these studies.

Figure 2.9 Examples of scour at entrance of culvert for 7-mm gravel (A), 16-mm angular gravel (B), 35-mm cobbles (C), and 37-mm angular rock (D) (REFERENCE)

Few studies examine culvert sedimentation,, although the literature on sediment transport in open channels and close conduits is abundant. Sediment transport through culverts subject to unsteady and non-uniform flow have still to be conducted. Some effort has been made to develop culvert designs that inhibit sediment deposition.

### 2.2.3 Current culvert design considerations

Culvert design fundamentally involves the optimal selection of the barrel cross-section that passes a given design discharge. Hydrologic and hydraulic analyses are required for designing culverts. Hydrologic analysis yields an estimate of the design discharge. Hydraulic analysis is then used to size the culvert. Accurate estimation of design runoff rates in the watershed is the key aspect to be considered in the design. Not

www.manaraa.com

to be overlooked are the rates of sediment transport a culvert must pass. These aspects are especially important as some watersheds are subject to land use change.

The magnitude of the design peak flow depends on the selection of a flood frequency which is decided in conjunction with the importance of the roadway. A complete theoretical analysis of the hydraulics of a particular culvert is difficult to conduct, because flow conditions vary significantly from culvert to culvert and flow conditions can vary over time at a given culvert. The traditional design methods are however diverse and lengthy. Therefore, the variety of flows are defined and classified in a simplified manner that only partially captures the different considerations involved in the flow at culverts. As a consequence, in many cases post-construction intervention is needed. The following sections discuss previous research associated with culvert hydraulics and current design protocols in order to set the stage of the present research. Similar efforts at estimating sediment yields from watersheds exist, but are highly approximate.

2.2.3.1 Types of flow through culverts

As precursor to preparing the laboratory and numerical studies conducted for the present study, it is useful to review briefly the types of flow condition that may occur at culverts. Bodhaine (1982) usefully classified culvert flows into six types on the basis of the location of the control section and the relative height of the headwater and tailwater elevations. Normann (1985) distinguished between flows controlled at the inlet and at the outlet sections of the culvert. The later classification is included in FHWA Hydraulic Design Series No.5 (HDS-5). This classification and its analytical treatment are widely used throughout most states in the US. Culverts with outlet control have subcritical flow in the barrels with the control section situated close to the downstream end of the culvert. Figure 2.10 illustrates examples of flow through culverts with inlet and outlet controls.

www.manaraa.com

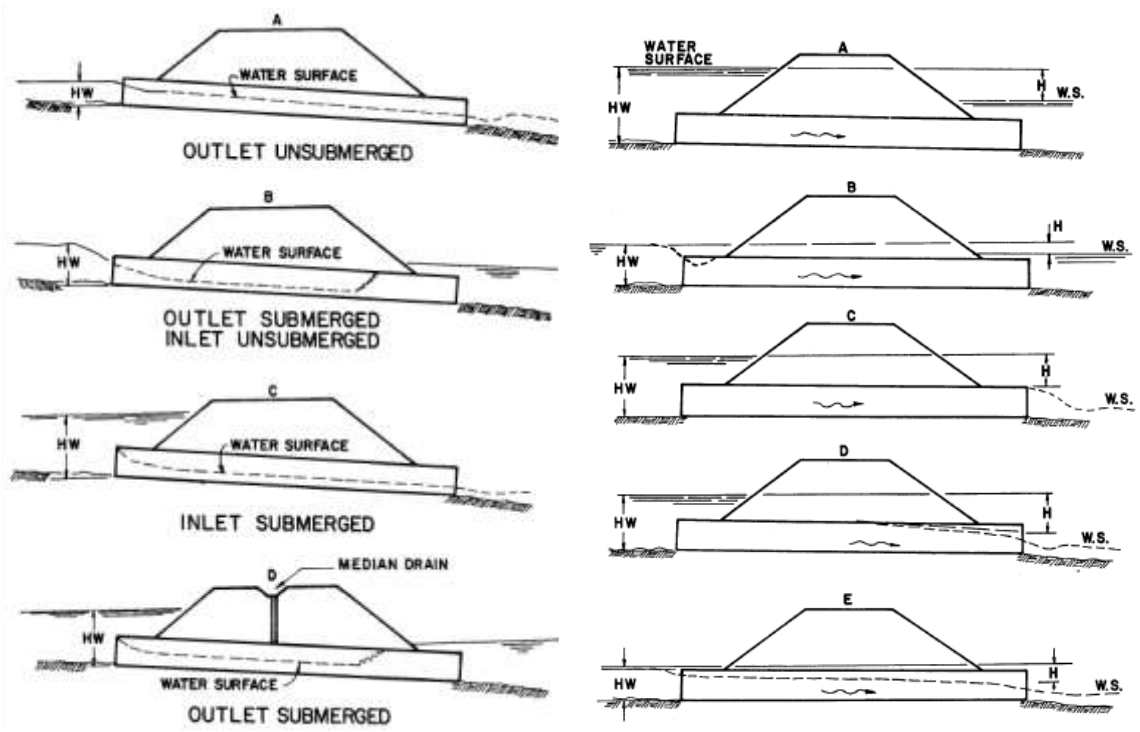


Figure 2.10 Types of flow regimes through culverts with inlet and outlet control (HDS-5, 1985); inlet control (left); outlet control (right)

2.2.3.2 Hydraulics of inlet control

Inlet control is a common design criterion. A culvert with inlet control performs as a weir when the inlet is unsubmerged and as an orifice when the inlet is submerged. If the entrance is unsubmerged, the inlet control section is near the entrance of the culvert. The two (energy) equations used in HDS-5 for the case of an unsubmerged inlet control are:

$$\frac{HW}{D} = \frac{E_c}{D} + Kg^{M/2}\left[\frac{Q}{A\sqrt{gD}}\right]^M - 0.5S \tag{2.8}$$

$$\frac{HW}{D} = Kg^{M/2}\left[\frac{Q}{A\sqrt{gD}}\right]^M \tag{2.9}$$

www.manaraa.com

where *A*=full culvert cross section area (*A*=*BD* for a box culvert), *Q*= barrel discharge, and S=slope of the culvert, *K* and *M* are the coefficients based on the culvert configuration.

Charbeneau (2006) assumed $V_c = Q/(C_b B y_c)$, where $C_b$ = coefficient expressing effective width contraction associated with the culvert entrance edge conditions. Neglecting the head loss, a simplified energy equation is obtained:

$$\frac{HW}{D} = \frac{3}{2}\left(\frac{1}{C_b}\right)^{2/3}\left(\frac{Q}{A\sqrt{gD}}\right)^{2/3} \tag{2.10}$$

When the culvert inlet is submerged, it performs as either an orifice or as a sluice gate. Based on studies of Normann (1985), the equation used in HDS-5 for submerged inlet control performance is:

$$\frac{HW}{D} = Y + cg\left[\frac{Q}{A\sqrt{gD}}\right]^2 - 0.5S \tag{2.11}$$

where *Y*, *c* are the constants based on the culvert configuration.

Charbeneau (2006) applied energy equation and rearranged (2.11) in the dimensionless performance equation:

$$\frac{HW}{D} = \frac{1}{2(C_b C_c)^2}\left(\frac{Q}{A\sqrt{gD}}\right)^2 + C_c \tag{2.12}$$

2.2.3.3 Hydraulics of outlet control

If both the upstream and the downstream ends of the culvert are unsubmerged, a free-surface flow will develop in the culvert if the channel slope is mild. The control section for this case occurs at the outlet section of the culvert, or further downstream. The flow is partly full in the culvert and can be described by the following energy equation:

www.manaraa.com

$$HW = y_c + \frac{1}{C_d^2}\frac{V_3^2}{2g} + \frac{LQ^2}{K_2 K_3} - S_0 L \tag{2.13}$$

If the control section is further downstream, Jain (2000) assumed head loss $h_L = \left(1/C_d^2 - 1\right)V_3^2/2g$ due to entrance, and the above equation (2.13) is

$$HW = TW + \frac{1}{C_d^2}\frac{V_3^2}{2g} + \frac{LQ^2}{K_2 K_3} - S_0 L \tag{2.14}$$

Full flow is a typical type of culvert outlet control. According to Jain (2000), $h_L = \left[\left(1/C_d^2\right) - 1\right]\left(V_3^2/2g\right)$ and $h_{ex} = \left[\left(V_3^2/2g\right) - \left(V_4^2/2g\right)\right]$, where $C_d$ is discharge coefficient. Based on Manning discharge formula, $h_{2-3}$ could be written into $n^2 L V_3^2 \big/ R_0^{4/3}$. An expression of energy equation can be modified as

$$\frac{HW}{D} = \frac{TW}{D} + \frac{n^2 Lg}{R_0^{4/3}}\left(\frac{Q}{A\sqrt{gD}}\right)^2 + \frac{1}{2C_d^2}\left(\frac{Q}{A\sqrt{gD}}\right)^2 - \frac{L}{D}S_0 \tag{2.15}$$

where , $R_0$ is hydraulic radius in the barrel, and *n* is Manning coefficient.

For the full flow culvert condition, the equation for outlet control (seeHDS-5 REFERENCE?) is expressed as

$$HW_0 + \frac{V_1^2}{2g} = TW + \frac{V_4^2}{2g} + H_{loss} \tag{2.16}$$

By neglecting the approach and exit velocities, Equation (2.16) becomes

$$HW_0 = TW + H_{loss} \tag{2.17}$$

where $H_{loss}$ is total loss: i.e.,

$$H_{loss} = \left(1 + K_e + \frac{2gn^2 L}{R_0^{4/3}}\right)\frac{V^2}{2g} \tag{2.18}$$

In equation (2.18), $K_e$ is a coefficient varying with inlet configuration, and *V* is velocity in the barrel.

www.manaraa.com

The case of culverts with inlet control is relatively simple to handle. By contrast, deducing the relationship between the headwater elevation and discharge for the case of culverts with outlet control is more difficult and depends on more variables. For example, equation (2.15) would be affected by the geometry of the culvert entrance, *TW*, and the roughness in the barrel.

### 2.2.4 Sediment mitigation culvert designs

Conventional culvert design normally does not consider explicitly sediment transport through a culvert. Attempts to include such consideration have been made, but they are mostly limited to practical recommendations with little or no analytical considerations.

The Maryland State Highway Administration (MDSHA) introduced new design guidelines to construct a stable culvert system (Kosicki and Davis 2001). The design approach is intuitive and it aims at maintaining the stability of the stream at the passage through the culvert by avoiding scouring or aggradation. Elements of this approach include maintaining the consistency of dimension, pattern, and profile of the stream with particular attention given to maintaining bankfull width. Flood plain culverts are appropriately located on the sides to relieve the extra flow for the main channel. Figure 2.11b shows a reconstructed culvert based on these guidelines. In 1992, MDSHA engineers replaced an existing culvert (Figure 2.11a) with a pipe arch in the main channel to avoid sediment deposition in the culvert and scour at the outlet. The central barrel of this culvert accommodates flows up to the bankful flow condition and has its invert buried 0.6 m below the streambed to provide for fish passage. As for the side barrels, the inverts of the flanking pipe arch and 3-m round structural plate pipes were placed at the bankfull elevation, approximately 0.6 m above the streambed to convey the out-of-bank flows. The construction was finished in 1994. Figure 2.11b shows the culvert vicinity after six years. During this time interval, the new design displayed no scouring

www.manaraa.com

downstream, no sediment deposit upstream, and a well-defined thalweg aligned with the stream centerline. Similar design guidelines were proposed by Minnesota Department of Transportation (Hansen et al. 2009). The approach, named MESBOAC (Match, Extend, Set, Bury, Offset, Align, Consider) method, aims to match the culvert width with natural stream dimensions while maintaining sediment balance. Both alternative culvert designs have essentially the same construction principle: burying the central culvert, matching bankfull width and offsetting multiple culvert barrels. The study case presented by MDSHA illustrates that, as expected, the sedimentation problem was solved. However, the potential uncertainties in the estimation of bankfull width and offsetting elevation may have negative impacts in the safety of traffic during high flows. This implementation example illustrates the importance of accurate estimation of hydrograph in the watershed and its implications on the design methodology.

Figure 2.11 Sediment mitigation design example: (top) pre-construction condition in 1992, (bottom) post-construction in 2000

www.manaraa.com

## 2.2.5 Numerical modeling of culverts and design software

### 2.2.5.1 Numerical modeling

Several numerical models simulate flow through culverts. However, so far, simulations of culverts with considerations of the three-dimensional aspects of the flow, flow unsteadiness and non-uniform geometry of the culvert area have not been attempted, according to the present researcher knowledge. The few numerical simulations of steady flow through culverts that have been reported in the literature are reviewed below.

Ferguson and Deak (1994) found that the area upstream of a culvert acts as a reservoir, which retains incoming runoff while earlier runoff is passing through the culvert. Their model assimilates the culvert entrance to an orifice characterized by an orifice equation ($C_d$ = 0.8). Using this approach they tested the model for various storm hydrographs of different flows and peak rates to predict the culvert performance over a wide range of upstream stages and conveyed flow volumes.

Vassilios (1995) used the HEC-6 model (US Army Corps of Engineers, 1991) to simulate the transport of sediment through culverts. The culvert was simulated as open channel, since HEC-6 does not have the capability to compute the pressurized flows. Two hydrological flow conditions were simulated and both of them showed that the culvert traps a major portion of the incoming sediment.

Charbeneau (2002) performed a culvert numerical simulation using the Finite Element Surface Water Modeling System (FESWMS) code (http://water.usgs.gov/software/FESWMS-2DH/ ). First, the numerical model was calibrated using the hydraulic modeling experimental data. Then the calibrated model was used to simulate flow in different channel configurations and to evaluate potential remedies for existing culvert systems. In the evaluation of potential remedies for existing culverts, it was found that changing the expansion ratio had little effect on flow characteristics downstream of the expansion. The most effective remedy identified during

www.manaraa.com

the experimental and numerical modeling program was to place rock gabions upstream of the culvert entrance.

Finally, the culvert equations used in HDS-5 can be utilized within HEC-RAS (HEC, 1998). Once the shape, size, material type, and location of the culvert system within the cross section are specified, users can use HEC-RAS to calculate sediment transport through the culvert and predict sediment transport load under different flow conditions.

2.2.5.2 Culvert design software

Culvert design typically entails a combination of hand calculations, charts and nomographs. In the HDS-5 manual, the dimensionless performance equations are used for calculations of culvert flow with inlet control (e.g., equations (2.2), (2.3) and (2.5)), and with outflow control (e.g., equations (2.11) and (2.12)). The values of the design variables are obtained through an iterative procedure in which inlet control and outlet control calculations are repeated several times for a given design discharge. The general culvert design procedure is summarized in Figure 2.12

Given the complexity of the analysis and the multitude of variables involved, it is desirable to automate the design process. Such an attempt is the goal of computer programs for culvert design such as CAP (Culvert Analysis Program), HY-8 (Culvert Hydraulic Analysis Program), Culvert Master, and Iowa Culvert Hydraulics. For example, Jones (2005) developed the a software package called the Iowa Culvert Hydraulics which incorporates three methods for computing design discharges and then sizing culvert geometry for inlet and outlet control. Within this application, the performance of a culvert under various design discharges can be calculated to determine the main parameters defining the geometry of the culvert. The analytical methods

www.manaraa.com

implemented in these codes require experienced users who can make decisions which take into consideration structure safety, hydraulic efficiency, and the construction cost.

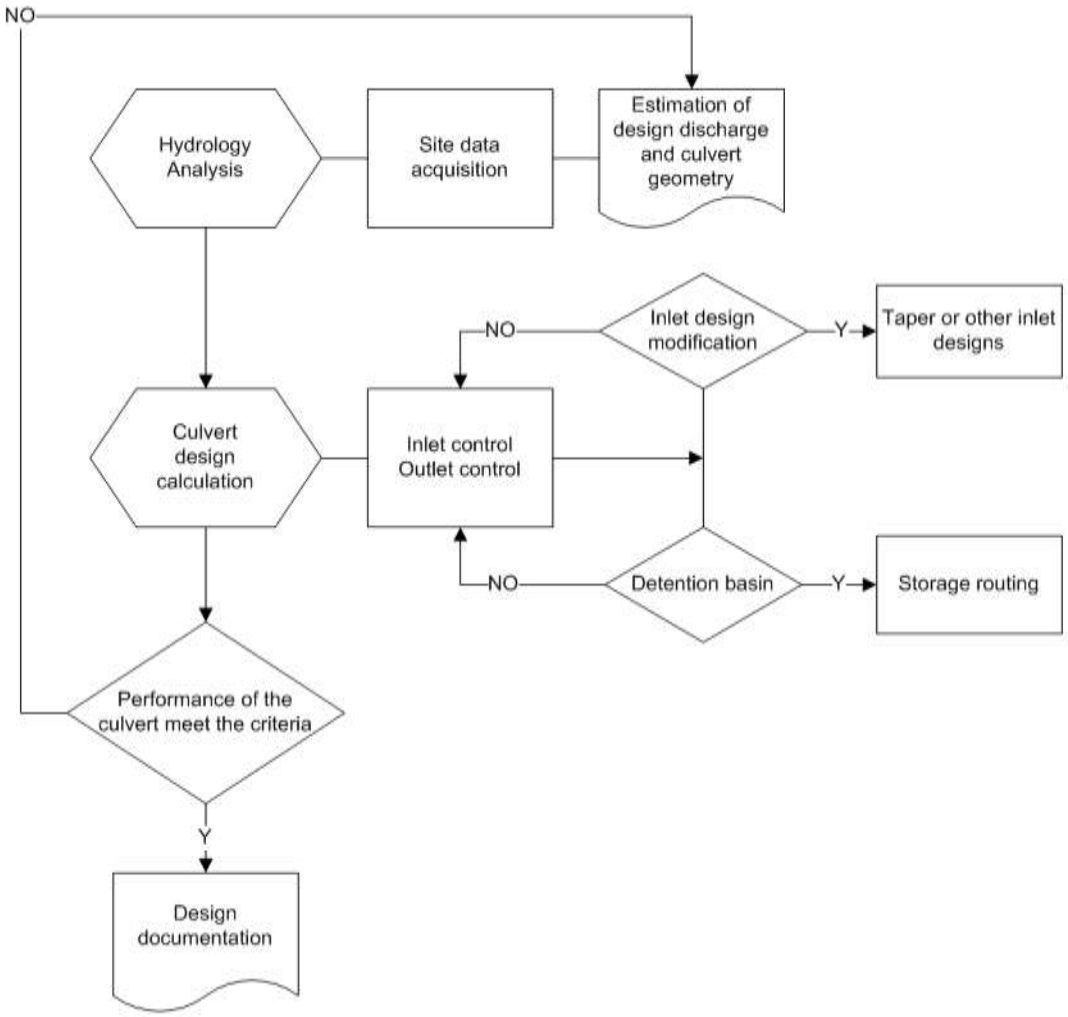


Figure 2.12 Design procedure flowchart used in computer codes for the culvert design

www.manaraa.com

# CHAPTER 3

# CONSIDERATIONS ASSOCIATED WITH SEDIMENT TRANSPORT IN UNSTEADY FLOWS

Given the complexity of the flow at culverts, most of the design considerations and guidelines described in the previous chapter use a simplified approach entailing steady flow based on a peak-flow estimate. However, flows through culverts commonly are highly unsteady. Little attention has been given to the effect of the unsteady flow propagating through the channel and culverts, and the fate of sediment transport (see Figure 3.1). For multi-barrel culverts the issue of flow non-steadiness and non-uniformity are particularly important, because the flow must transition from the approach stream channel to the several barrels. The transition may not lead flown equally to each barrel, and it can be especially prone to sediment deposition. This chapter is an overview of the main considerations associated with unsteady sediment transport through culverts. It leads to the design of the study's laboratory and numerical experiments. Include here is a sensitivity analysis of a flow rating curve to changes in the precipitation and channel characteristics. This task is done by applying the HEC-RAS applied to hypothetical channel.

Of interest in the present investigation are tare the unsteady flow features associated with storm events. Storms are associated with surges of flow and sediment through the hydraulic structure during the first (raising) phase, followed by the recession of water and sediment in the second (falling) phase. While closely coupled, the unsteady flow and sediment transport during storms do not develop the same gradients and do not attain their peak (maximum values) at the same time. These characteristics are intricately related to the precipitation intensity and duration, as well as to the soil, land-use coverage, and topography of the culvert drainage area. The storm is basically producing

www.manaraa.com

a closed-loop unsteady flow (the flood wave) that propagates as a non-uniform flow through the culvert and its transitions from and back to the natural channel.

As discussed in Chapter 2, numerous studies of unsteady flow in channels are available in the literature. However, the sensitivity of the impact factors on the unsteady flow and specifically the effect of the culvert on the flow unsteadiness in the channel where it is situated have yet to be studied. For a comprehensive understanding, preliminary considerations on the main relevant processes at culverts are presented separately in the following order:

1. Flood wave propagation through a constant-section open channel for various inflow hydrographs
2. Water and sediment hydrograph in channel flows
3. Flood wave propagation through culverts
4. Field observation of sedimentation at the culvert site

These processes are considered separately to elucidate their individual effects, as their coupling complicates interpretation of their combined effects. The discussion highlights potential implications for flow at culverts and the additional considerations required in the methodologies to design culverts.

www.manaraa.com

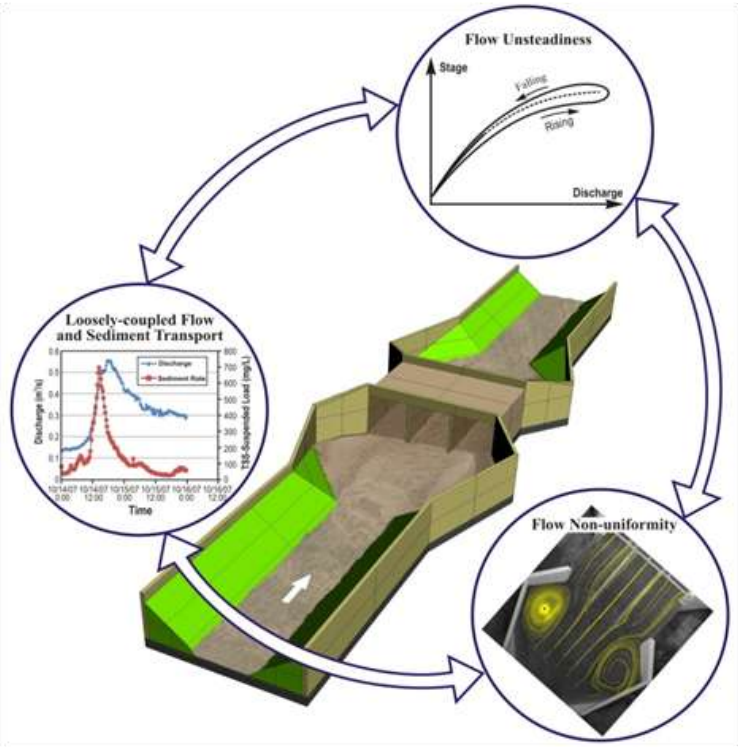


Figure 3.1 Superposition of flow complexities in the flow through culverts; considerations include hydrograph, sediment inflow, coupling of flow depth and discharge, and passage through the transition to the culvert.

## 3.1 Unsteady flow in channel

### 3.1.1 Rating curves

The most common method used by monitoring agencies to report flow rates in streams is based on an empirically derived stage-discharge rating curve developed for steady flows. The methodologies for obtaining rating curves are well established, widely applied, and relatively simple and reliable for the range of flows for which they are developed (Buchanan and Somers, 1969). For the case of uniform steady flow, a one-to-one relationship between the discharge and water stage in the channel can be constructed by concomitantly measuring discharges and stages. These direct discharge measurements are plotted in a stage-discharge plot. Generally, discharges are plotted on the abscissa and

www.manaraa.com

stages are plotted on the ordinate, as illustrated in Figure 3.2. The regression curve which fits these points is called the rating curve. The curve is labeled in the figure as Steady Flow Rating Curve (SFRC). SFRC depends on the characteristics of the channel including cross-section area, roughness, and slope of the free surface; hence the relationship is unique for each gaging site Morphological changes of the channel, changes in roughness, and the occurrence of a flood which changes the water surface slope can cause significant deviations from the aforementioned standard rating curve.

It is well known that the steady rating curves are not suitable for reporting measurements during unsteady flows (Henderson, 1966). During unsteady flows, such as storm events, the rating curve displays a relationship described by a loop also called hysteresis as illustrated in Figure 3.2. It can be seen from the plot that for unsteady flow event the maximum water discharge and maximum water stage do not necessarily arrive at the same time as in the case of SFRC. The maximum velocity arrives first subsequently followed by the maximum discharge.Use of SFRC for steady and unsteady flow situations introduces significant errors that have been recognized for a long time (Fenton and Keller, 2001, Jain and Chalisgaonkar, 2000, Aschwanden et al., 2009). Given that the construction of ratings curves to accommodate the wide range of unsteady flows that might occur in rivers due to natural or man-induced causes is a challenging task from many perspectives, the one-to-one stage-discharge rating curves is widely used for steady and apparently unsteady flows. The most challenging aspect is that there is need for direct measurements to capture the loop curve shape for each individual unsteady event, as usually they are not identical. Until new procedures are set in place, the monitoring agencies continue to use conventional procedures for estimating the discharge for both steady and apparently unsteady flows despite that detailed studies showed that during floods the use of steady rating curves may lead to errors up to 8.3%, as documented by (Westphal et al., 1999) at gaging stations along the Mississippi River during the flood of 1993.

www.manaraa.com

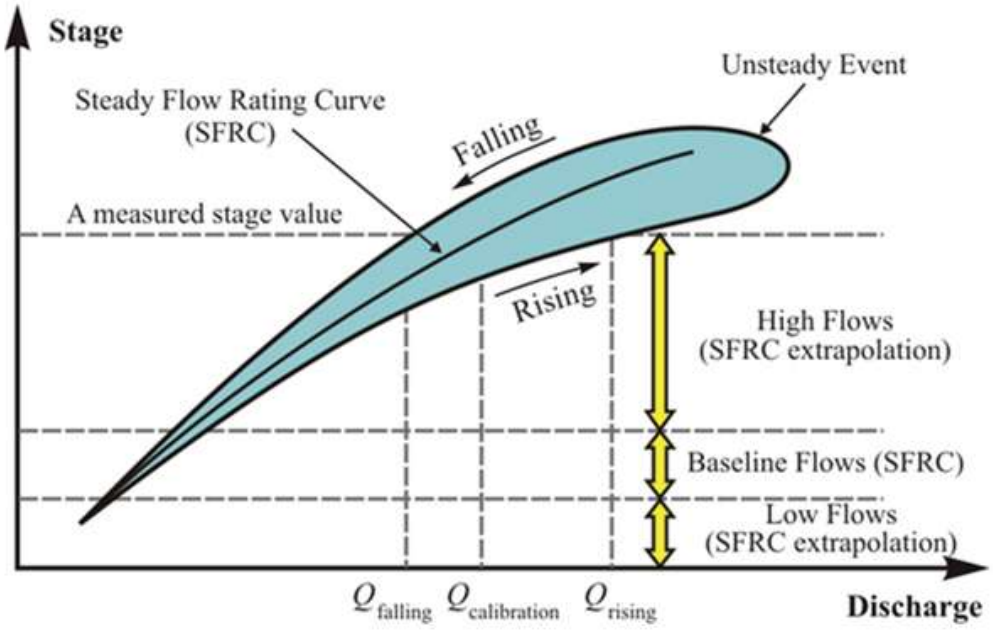


Figure 3.2 Deviation of the unstedy rating curve from the conventional one obtained through extrapolation applied to measurements in steady flow conditions

Accurate estimation of flood flows is of critical importance in order to obtain the necessary quantities for sizing channels such as culverts. The use of a one-to-one stage-discharge relation to approximate the dynamics of flood waves has adverse consequences for flood forecasting, as forecasting models use the rating curve information as input. The outcomes of the warning systems are also biased when using the one-to-one rating relationship in their estimation. This consequence arises because the one-to-one stage-discharge relationship shows flow rates on the rising limb that are greater than those for the same stage during flood recession, as illustrated in Figure 3.2. The differences are magnified at high flows and are directly related to the precipitation duration and intensity of the storm event. In order to highlight the sensitivity of the rating curves to various

www.manaraa.com

types of hydrographs conveyed through rivers,the next section considers the nature of the stage-discharge hysteresis using the HEC-RAS numerical model.

### 3.1.2 Rating curve sensitivity analysis

The sensitivity of the rating curve to changes in the precipitation and channel characteristics are briefly considered here by applying the HEC-RAS applied to hypothetical channel. The model is capable of simulating the one-dimensional (section averaged) unsteady flow in open channels using the dynamic wave method. It is based on the continuity and momentum equations that can be written as:

$$\frac{\partial A_T}{\partial t} + \frac{\partial Q}{\partial x} = 0 \tag{3.1}$$

$$\frac{\partial Q}{\partial t} + \frac{\partial QV}{\partial x} + gA\left(\frac{\partial z}{\partial x} + S_f\right) = 0 \tag{3.2}$$

where the water surface slope is $\frac{\partial z}{\partial x} = \frac{\partial y}{\partial x} + \frac{\partial z_0}{\partial x}$, y is the flow depth, and $z_0$ is the bed elevation.

The unsteady rating curves for a given hydrograph can be obtained by solving the above equations which are equivalent to the 1-D St. Venant equations (2.1) and (2.2) in Chapter 2. The hydraulic variables which affect the characteristics of the closed-loop rating curve are evaluated below. Two unsteady parameters presented in Chapter 2 were also investigated for their capabilities to describe the looped rating curve. The first parameter defined by Takahashi (1969) is λ. It was used to characterize the unsteadiness in the one-dimensional governing equations. This parameter is related to the ratio of the speed of the rising water surface to the vertical component of the celerity of long waves. The other parameter, $\Gamma$, was proposed by Suszka (1987). It is defined as the ratio of the

www.manaraa.com

rising speed of flood waves to the friction velocity of the base flow before the passage of the discharge hydrograph.

A rectangular channel with a width of 100 ft and a depth of 35 ft was considered in all the test cases examined here. Six discharge hydrographs were designed to pass through this constant cross-section channel, and three different gentle slopes were considered. For the first symmetric hydrograph the peak flow was $Q_p$ = 10,000 $ft^3/s$, the duration of the time to peak was $T_p$ = 24hr, and the duration of the time to base flow was $T_b$ = 24hr. The three bed slopes were S = 0.0008, S = 0.0001, and S = 0.00001. These three cases, labeled as C1, C2, and C3, allowed investigating the effect of the bed slope. Additionally, two symmetric hydrographs with the same peak flow but with different total durations ($T_p$= $T_b$ = 72hr, and $T_p$ = $T_b$ = 12hr) were created and calculations were performed with a bed slope S = 0.0001. These two cases (labeled as C4, and C5) together with the reference case (C3) were used to study the effect of the total duration. Another two cases (labeled as C6, and C7) were considered for which the duration of the time to base was $T_p$ = 24hr, $T_b$ = 12hr and $T_p$ =24hr, $T_b$ = 72hr, respectively. These two cases were again compared to reference case C3 to understand the effect of the duration of the time to base. Case C8 was similar to the reference case except that the peak flow was 20,000$ft^3/s$. The last case (labeled as C9) was used to investigate the effect of varying the value of the unsteady parameter for a hydrograph with the same total duration but different values of $T_p$ and $T_b$. The main parameters defining these cases which attempt to reproduce typical hydraulic conditions in channels are summarized in Table 3.1.

www.manaraa.com

Table 3.1 Design cases for numerical simulations of unsteady flows

| | $Q_p$ ($ft^3/s$) | S ($10^{-4}$) | $T_p$ (hr) | $T_b$ (hr) | $\Delta h$ (ft) | $\tau$ | U (ft/s) | Q ($ft^3/s$) | C | $\lambda$ | $\Gamma$ ($10^{-4}$) |
|---|---|---|---|---|---|---|---|---|---|---|---|
| C1 | 10000 | 8 | 24 | 24 | 14.05 | 0.03 ~0.2 | 0.95 ~3.68 | 100 ~9937 | 22.16 | 0.0045 | 0.246 |
| C2 | | 0.1 | 24 | 24 | 33.81 | 0.0042 ~0.074 | 0.47 ~2.79 | 100 ~9934 | 35.38 | 0.5531 | 1.495 |
| C3 | | 1 | 24 | 24 | 33.58 | 0.0078 ~0.007 | 0.60 ~2.85 | 100 ~9934 | 34.97 | 0.0556 | 1.018 |
| C4 | | | 72 | 72 | 34.11 | 0.0085 ~0.073 | 0.62 ~2.80 | 100 ~9992 | 35.21 | 0.0187 | 0.374 |
| C5 | | | 12 | 12 | 32.12 | 0.0049 ~0.103 | 0.52 ~2.99 | 100 ~9768 | 34.29 | 0.1084 | 2.783 |
| C6 | | | 24 | 12 | 33.35 | 0.0032 ~0.078 | 0.43 ~2.85 | 100 ~9934 | 34.86 | 0.0738 | 2.383 |
| C7 | | | 24 | 72 | 33.89 | 0.0085 ~0.078 | 0.62 ~2.85 | 100 ~9937 | 35.11 | 0.0279 | 0.557 |
| C8 | 20000 | | 24 | 24 | 60.43 | 0.0071 ~0.095 | 0.6 ~3.32 | 100 ~19867 | 45.64 | 0.0765 | 2.169 |
| C9 | 10000 | | 12 | 24 | 26.75 | 0.0094 ~0.127 | 0.65 ~3.61 | 100 ~9822 | 31.64 | 0.0652 | 1.115 |

*Note:*

*S = bed slope, $T_p$ = time to peak, $T_b$ = time to base flow, $\Delta h$ = water depth difference between peak and base flow, $\tau$ = shear stress in channel, U = average velocity, Q = discharge, F = Froude number, C = celerity =* $\sqrt{gh_p}$ ,

$\lambda$ = *unsteadiness parameter* = $\dfrac{\Delta h/(T_p+T_b)}{C\times\sin\theta} \equiv \dfrac{\Delta h/(T_p+T_b)}{C\times S}$

$\Gamma$ = *unsteadiness parameter* = $\dfrac{1}{u_b^*}\dfrac{\Delta h}{T_p+T_b}$, $u_b^*$ =*friction velocity of the base flow*

For a typical unsteady flow event, the hydraulic parameters, Q(t), h(t), and U(t), generally should reach their maximum values in the following order: $U_{max}$, $Q_{max}$, and $h_{max}$. Figure 3.3 shows that the peak velocity, discharge and stage in case 3(C3) follow this trend. More precisely, results show that $U_{max}$ is reached after 1270 minutes, $Q_{max}$ after 1450 minutes, and $h_{max}$ after 1480 minutes. The variations of the main variables in

www.manaraa.com

case C3 is typical for unsteady flow events in channels and can be used as the reference case.

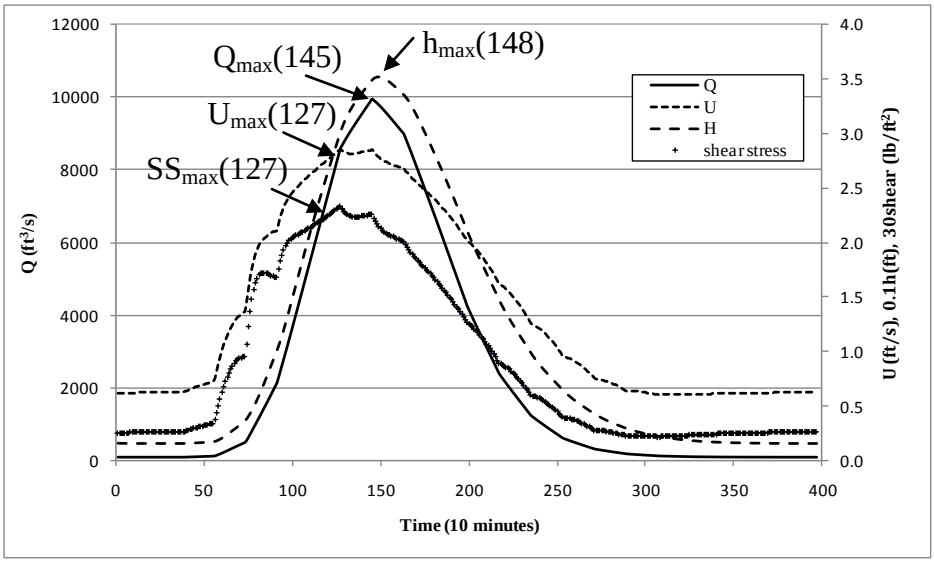


Figure 3.3 Hydraulic parameters for the hydrograph corresponding to case 3

Comparison of cases C1, C2 and C3 in Figure 3.4 shows that the bed slope value affects the looped rating curve. The loop created by the relatively steep bed slope was quite different from the other two loops. The value of the unsteady parameter $\lambda$ changed by close to two orders of magnitude, from 0.0045 to 0.5531. This means the parameter is sensitive to the value of the bed slope, at least over the range of bed slopes limited by the C1 and C2 values. However, the parameter $\lambda$ is not appropriate to characterize the unsteadiness in the channel, because the results in Figure 3.4 show that the curves for C2 and C3 are similar even though their bed slopes are significantly different. The other parameter $\Gamma$ increased its value from $0.246\times10^{-4}$ to $1.018\times10^{-4}$ as the bed slope decreased from S = 0.0008 to S = 0.0001. However, the trend did not continue as the bed slope decreased from S = 0.0001 to S = 0.00001. Still, the parameter $\Gamma$ showed a larger sensitivity among the three cases, and will be used as the main indicator of the

www.manaraa.com

unsteadiness in channel in the following sensitivity analysis. The result of Figure 3.4 shows the bed slope is a main variable affecting the hysteresis over the range of bed slopes defined by C1 and C2. When the bed slope becomes relatively small, the effect of the bed slope is minor as seen from the comparison of the loops in cases C2 and C3.

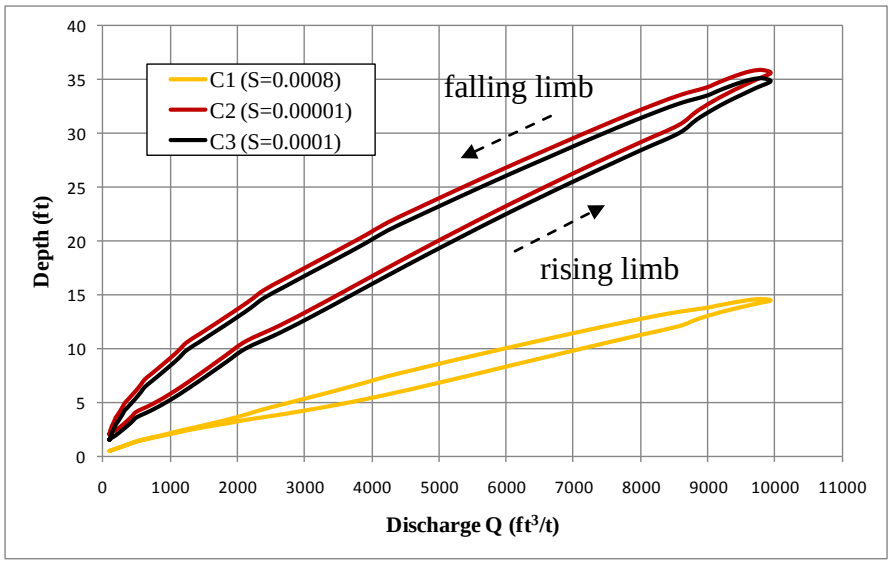


Figure 3.4 Analysis of the sensitivity of stage-discharge relationship with the channel slope based on comparison of cases C1,C2, and C3

The hysteresis loops predicted by the symmetric hydrographs in cases C3, C4, and C5 are shown in Figure 3.5. The duration of the flood was 48hr (24hr+24hr), 148hr (72hr+72hr), and 24hr (12hr+12hr), respectively. Figure 3.6 shows that the rising speed of the flood wave significantly affected the unsteadiness in the channel. The unsteady parameter $\Gamma$ varied from $0.374\times10^{-4}$ to $2.783\times10^{-4}$. For C4, which has the longest flood wave duration, the maximum difference between the discharge on the rising and the falling limbs was less than 500ft$^3$/s. The maximum difference between the discharge on the rising and the falling limb was close to 2,800ft$^3$/s in case C5, when calculated for the same water elevation. The differences between water elevations calculated at the same

www.manaraa.com

discharge were up to 10ft. The result demonstrates that if the channel encounters a spike-like discharge hydrograph, the deviation from the one-to-one relation rating curve will be significant.

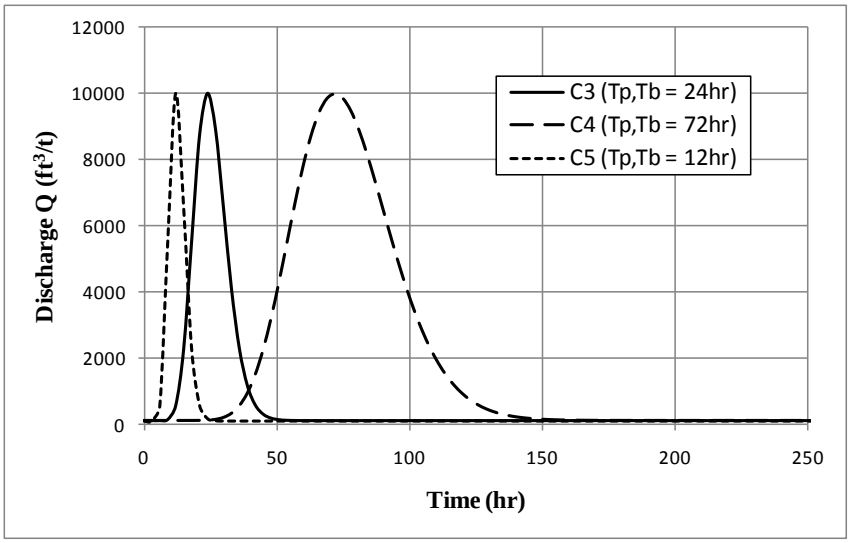


Figure 3.5 Discharge hydrographs in cases C3, C4, and C5. The three cases correspond to flood events with different time-to-peak values.

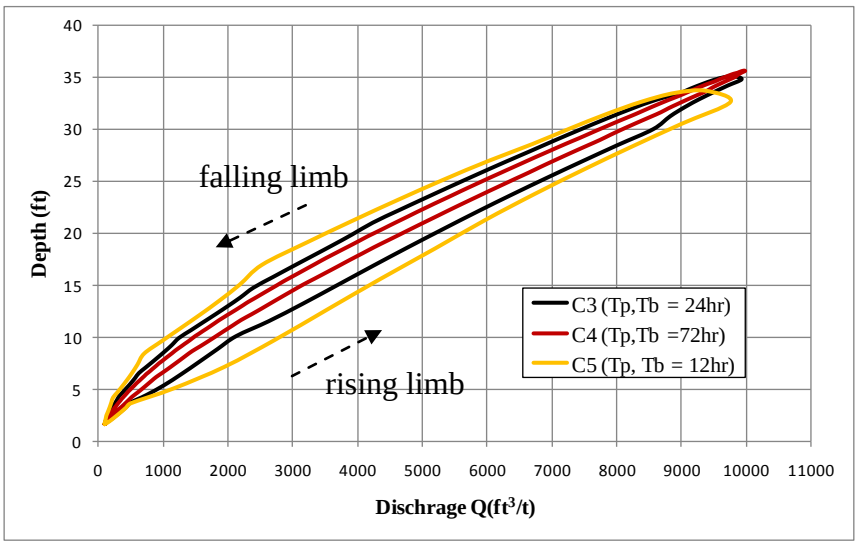


Figure 3.6 Effect of the total duration of the flood event on stage-discharge relationship. Results are shown for cases C3, C4, and C5.

www.manaraa.com

The effect of the falling speed of the flood wave was investigated by changing the time from the peak flow to the base flow with respect to the hydrograph considered in the base case, C3. Figure 3.7 presents three hydrographs with the same duration from the base flow to the peak but with different durations from the peak to the base flow. The values for cases C3, C6 and C7 are $T_b$ = 24hr, $T_b$ = 12hr, and $T_b$ = 72hr, respectively. The rating curves for the three cases are shown in Figure 3.8. The rising limb is similar in all the loops. As the falling speed of the flood wave increased, large deviations from the steady flow were observed during the falling limb. The value of the unsteady parameter $\Gamma$ increased rapidly due to the changing duration of the peak to base flow (see Table 3.1). These results imply that a large change of the rising or falling speed of the flood wave biases the rating curve away from the steady-flow rating curve.

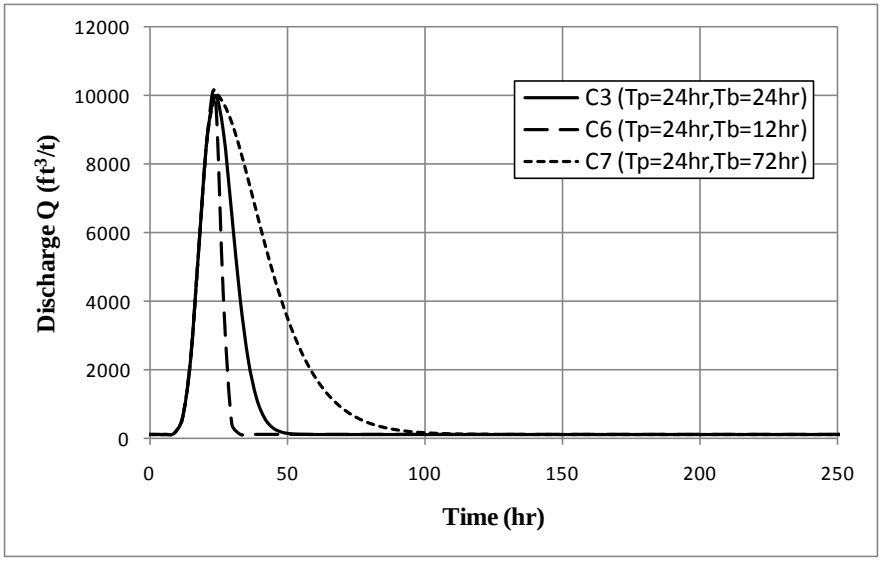


Figure 3.7 Discharge hydrographs for cases C3,m C6 and C7 that have the same duration of the time to peak and different durations of the time from peak flow to base flow.

www.manaraa.com

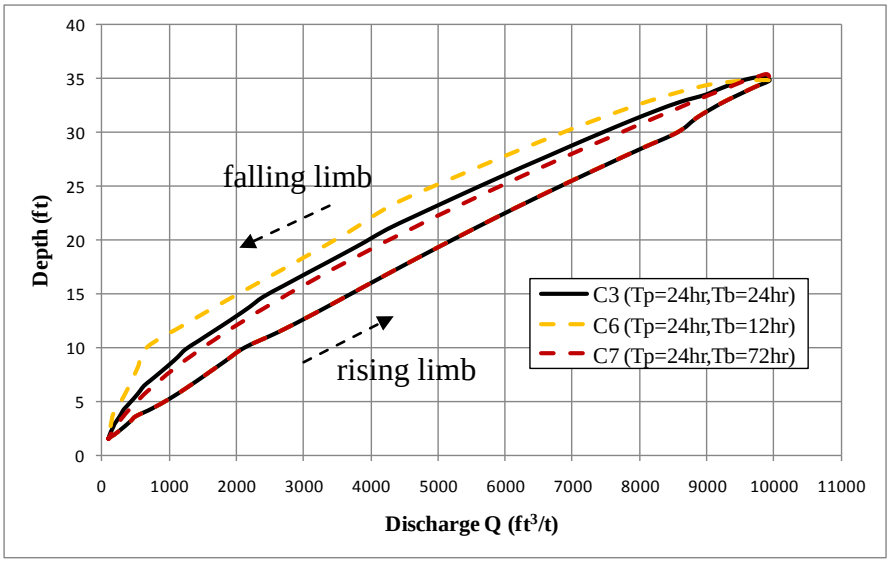


Figure 3.8 Predicted looped rating curves for cases C3, C6, and C7

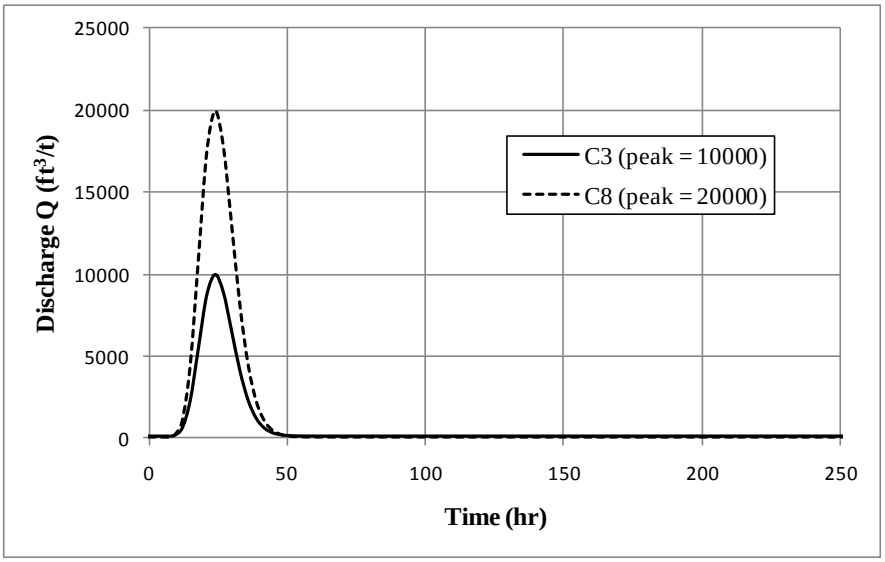


Figure 3.9 Discharge hydrographs for cases C3 and C8. The symmetric hydrographs have different peak flows

The peak flow was increased to 20,000ft$^3$/s in case C8 to examine the effect of peak flow with respect to the base case C3 for which the peak flow is 10,000ft$^3$/s. Figure 3.9 shows the input hydrograph for the two cases. The value of the unsteady parameter Γ

www.manaraa.com

for C8 increased by about 100% compared to case C3, which is consistent with the increase in the peak discharge between the two cases (see Figure 3.10). This finding suggests $\Gamma$ is a reasonable indicator of the unsteadiness in the channel for hydrographs in which the main difference is the peak discharge.

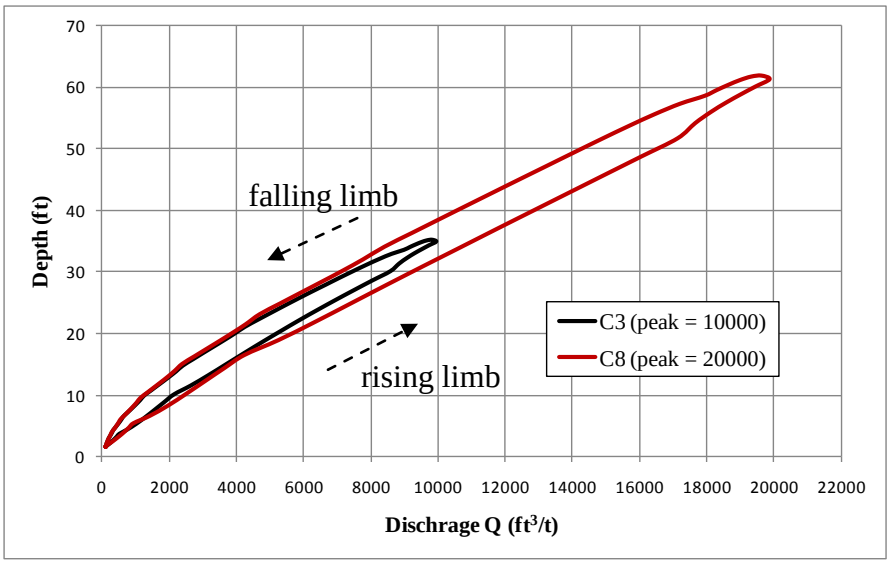


Figure 3.10 Predicted looped rating curves for cases C3 and C8

The parameter $\Gamma$ is sensitive to both the duration of the time to peak and the time to base. The last test case (C9) was designed to investigate the sensitivity of the unsteady parameter $\Gamma$ between hydrographs with different values of the time to base but with the same total duration of 36h ($T_p$ = 24hr, $T_b$ = 12hr for C6 and $T_p$ = 12hr, $T_b$ = 24hr for C9). The values of the peak discharge for both hydrographs are the same. The values of $\Gamma$ are $2.383\times10^{-4}$ for case C6 and $1.115\times10^{-4}$ for case C9. Accordingly, $\Gamma$ is sensitive to the value of the time to base. Figure 3.11 show important differences are present between the looped rating curves in cases C6 and C9. Overall, the use of the parameter $\Gamma$ to characterize the unsteadiness in the channel appears to be a reasonable choice.

www.manaraa.com

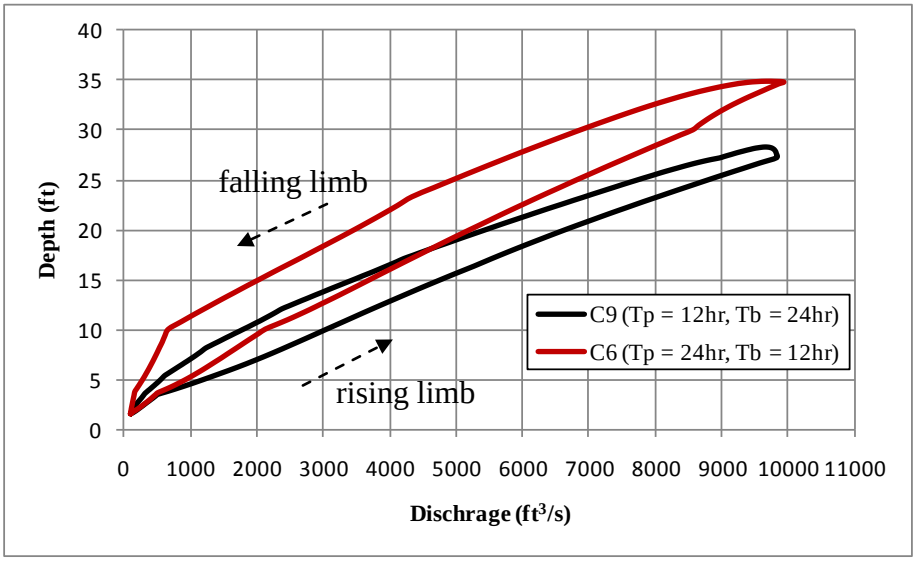


Figure 3.11 Predicted looped rating curves for cases C6 and C9

The effects of each momentum term in equation (2.3) shown below need to be considered.

$$S_f = S_0 - \frac{\partial y}{\partial x} - \frac{1}{g}\frac{\partial V}{\partial t} - \frac{V}{g}\frac{\partial V}{\partial x} \tag{3.3}$$

If a term is small compared to slope $S_0$, the momentum equation can be simplified by neglecting that term. The discharge and bed slope are related through $Q = K\sqrt{S_0}$ (Jain, 2000). Figure 3.12 presents the time variation of the terms in equation (3.3) for the reference case, C3. Channel slope $S_0$ is 0.0001 and the unsteady parameter $\Gamma$ is 1.018×10-4 (see Table 3.1). The result shows that the acceleration term can be neglected through the whole flood event as it is much smaller than the value of the channel slope. The $\partial y/\partial x$ term cannot be neglected, because this term has a value comparable (~57.2%) to that of S0 when flood event starts.

The present analysis was conducted based on results obtained in channels of simplified geometry and for simplified shapes of the discharge hydrograph. that the analysis leads to the following findings:

www.manaraa.com

1. In unsteady channel flows produced by a typical hydrograph, the peak velocity will be reached first, the peak discharge will follow and the peak water stage will be reached last;
2. For the same hydrograph, the unsteadiness in the channel is larger if the channel slope is relatively small;
3. The parameter $\Gamma$ is a better choice than $\lambda$ to characterize the unsteadiness in the channel; and,
4. The term $\partial y/\partial x$ is the most important term in the momentum equation, its variation is controlled by the propagation of the flood wave.

More sophisticated experiments and numerical analysis are required in order to understand what variables should be used to characterize the unsteadiness in channels of more complex shapes subject to flood events with hydrographs of more realistic shapes.

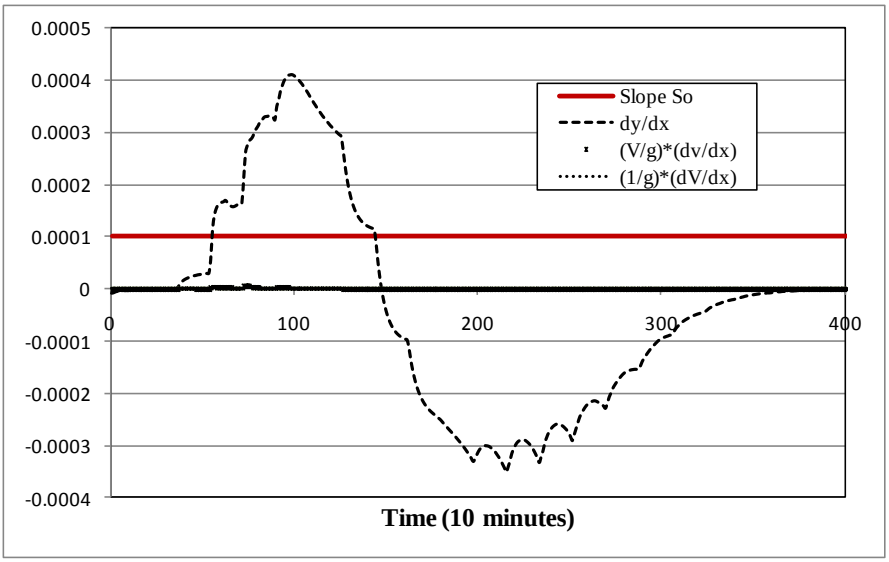


Figure 3.12 The relative importance of various terms in the momentum equation for the reference test (case 3)

www.manaraa.com

### 3-1-3 Sediment hydrograph

The first primary objective of this study is developing an understanding of the transport of sediment through culverts. In this regard, the basic question to address is what fraction of the total sediment entering a culvert deposits near or within a culvert of given geometry. Total sediment discharge comprises bed load and the suspended bed material load component. This study does not consider washload.

Bed load transport is defined as the part of the load moving on, or near, the bed by rolling, saltation, or sliding. Suspended load transport is defined as the sediment that moves in suspension with the flow. Generally, the bed load transport mode is dominant when the flow velocity is relatively low, while the suspended load transport mode is dominant when the velocity is relatively high. The mechanics of bed load and suspended sediment load transport are different. In most cases both components of the sediment transport are non-negligible. Particles of sediment that initially moved with the suspended sediment can continue their movement as part of the bed load and vice versa. If the bed load transport component increases, the resisting force acting on the flow will increase. The effect of increasing the suspended sediment load component on the mean flow is less clear.

The time lag between the peak values of the discharge and the stage discussed in the previous section is not the only complexity associated with the propagation of a flood wave in a channel. Similar time lags also occur between the peak flow discharge and the sediment transport rates. It is common knowledge that sediment transport rates increase when the stream flow velocity increases. What is less discussed in the literature is that for the same flow velocity in a closed-loop unsteady flow, the sediment transport rate is non-unique, as it assumes different values on the falling and rising limbs or the sediment hydrograph. The difference takes the form of a hysteresis in the relationship between sediment transport rates and flow rates, as is illustrated below in the field observations made by Loperfido (2007). The suspended sediment concentrations in Figures 3.13 and

www.manaraa.com

3.15 are obtained from turbidity measurements through calibrated correlations. The suspended sediment rate measurements were continuously and simultaneously obtained through a long-term experimental program conducted in the Clear creek watershed in Iowa.

Moreover, the results in Figures 3.13 and 3.15 demonstrate that the peak sediment transport rate does not coincide with the occurrence of the maximum stream discharge. The peak of sediment hydrograph occurs before the peak flow discharge. Figure 3.14 and 3.16 reveal that the sediment transport rate for a given discharge is larger in the rising limb compared to the falling limb.

Based on the considerations presented in the previous section, the hysteresis of the stage–discharge curve for unsteady flow conditions can be explained by setting $\partial Q/\partial t = 0$. For example, the following equation stems from the continuity equation:

$$\frac{\partial Q}{\partial t} = A\frac{\partial V}{\partial t} + V\frac{\partial A}{\partial t} = 0 \tag{3.4}$$

It can be observed from equation (3.4) that, if the water stage increases, the term $\partial A/\partial t$ is positive, and $\partial V/\partial t$ becomes negative. This indicates that the velocity reaches the maximum value before the occurrence of the peak discharge. The maximum water stage occurs after the peak discharge. However, the hysteresis of the sediment-discharge hydrograph is much more complicated to explain. In literature, the clockwise loop was explained based on early suspended sediment depletion or the cessation of the rainfall (Peart and Walling, 1988). Moreover, the clockwise loop is not the only form of hysteresis in the flow-sediment rates relationship. Depending on the local conditions, the occurrence of a counter-clockwise hysteresis loop is also possible. Based on the interplay between the characteristics of the precipitation and those of the soil, it is possible to use the hysteresis direction as an indicator on the source of the sediment, i.e., from within the channel or from the soil surface of the drainage area.

www.manaraa.com

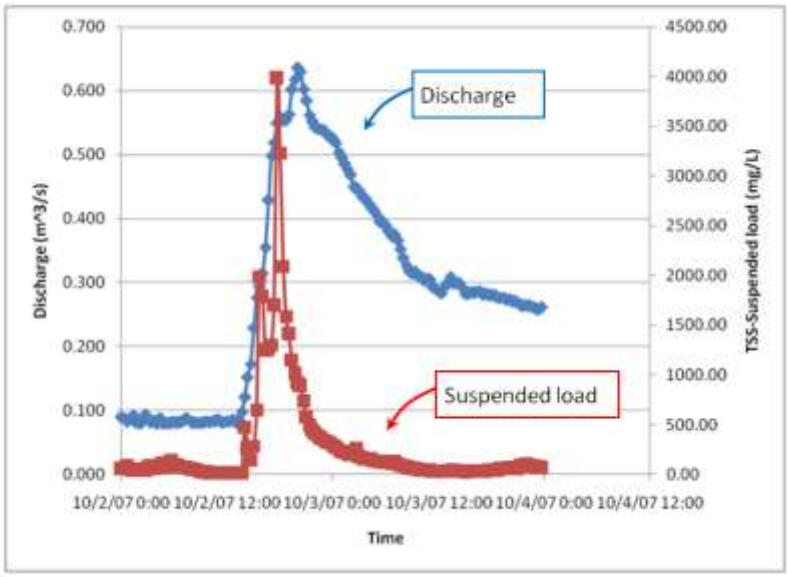


Figure 3.13 Flow and sediment hydrograph at Clear Creek (10/02/07~10/04/07)

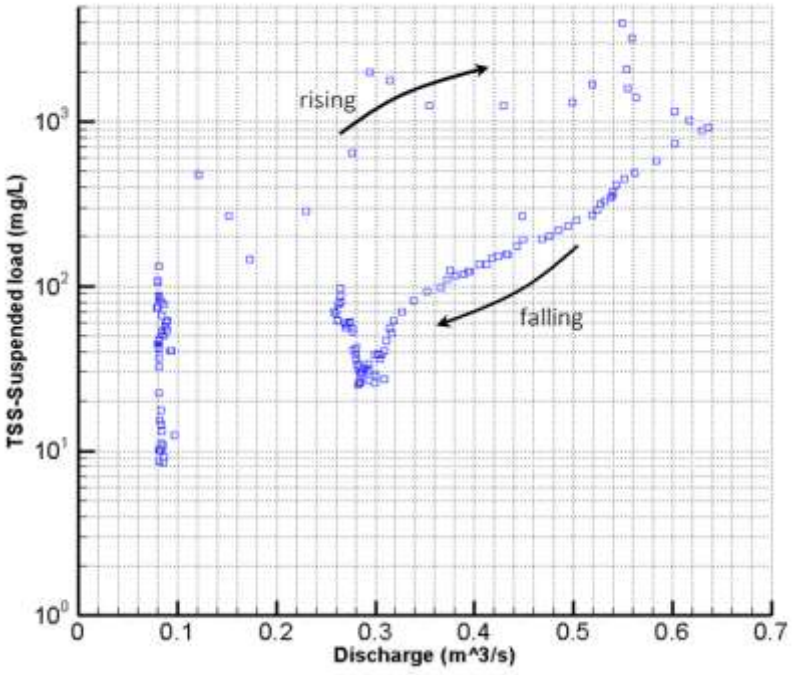


Figure 3.14 Sediment-discharge rating curve at Clear Creek (10/02/07~10/04/07)

www.manaraa.com

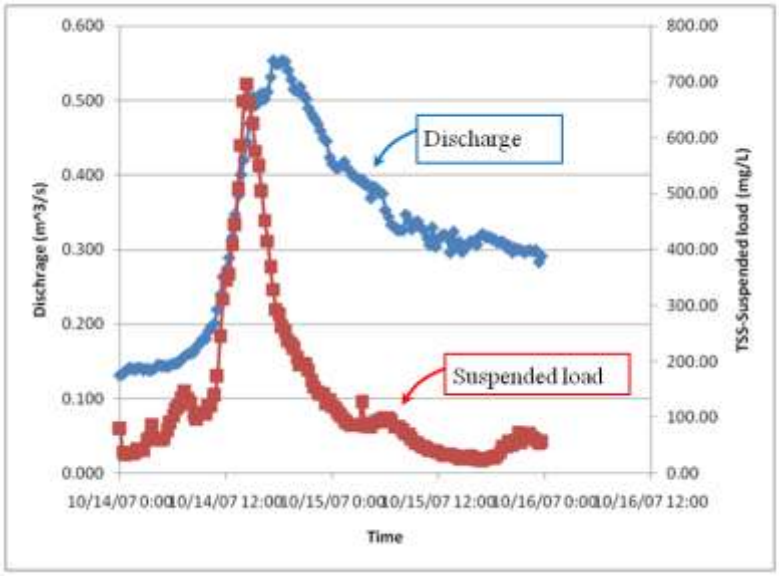


Figure 3.15 Flow and sediment hydrograph at Clear Creek (10/14/07~10/16/07)

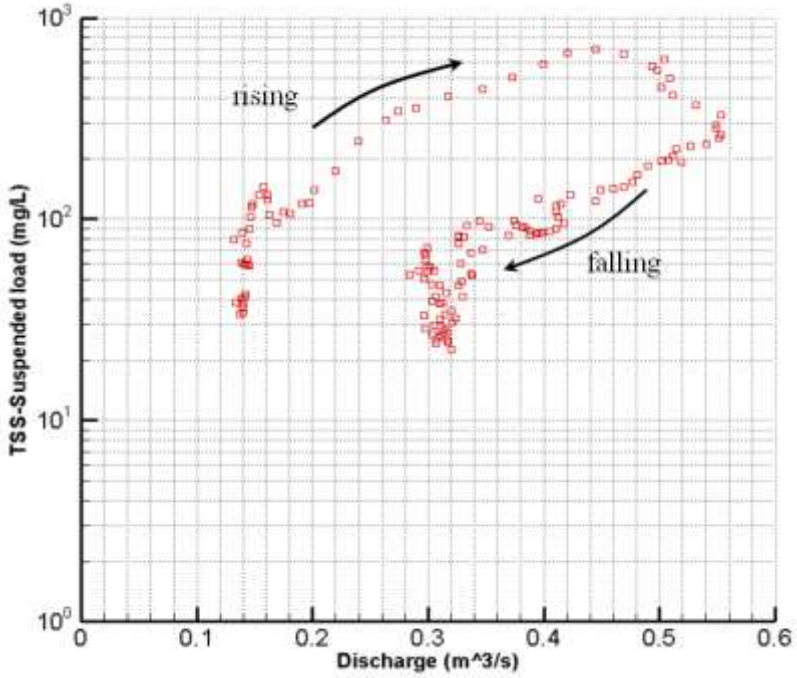


Figure 3.16 Sediment-discharge rating curve at Clear Creek (10/14/07~10/16/07)

www.manaraa.com

## 3.2 Unsteady flow at culvert

Current design methodologies for culverts are mainly based on the peak flow of the design discharge without much attention given to the effect of the unsteady flow propagating through the channel. The previous sections showed that the unsteady flow induces a time lag between the peaks in the hydraulic parameters and sediment transport in the channel. The purpose of this section is to derive the rating curve at a culvert when a flood wave propagates in a channel containing a culvert. The analysis of the unsteady flow at the culvert is performed using HEC-RAS. The channel is considered to have a rectangular section. A three-box culvert is placed in the middle of the section. Figure 3.17 shows the geometry of the three-box culvert (each box is 20ft wide and 20ft height). A symmetric hydrograph with a peak flow $Q_p$ = 10,000 $ft^3/s$ for which the duration of the time to peak was $T_p$ = 24hr and the duration of the time to base flow was $T_b$ = 24hr was considered.

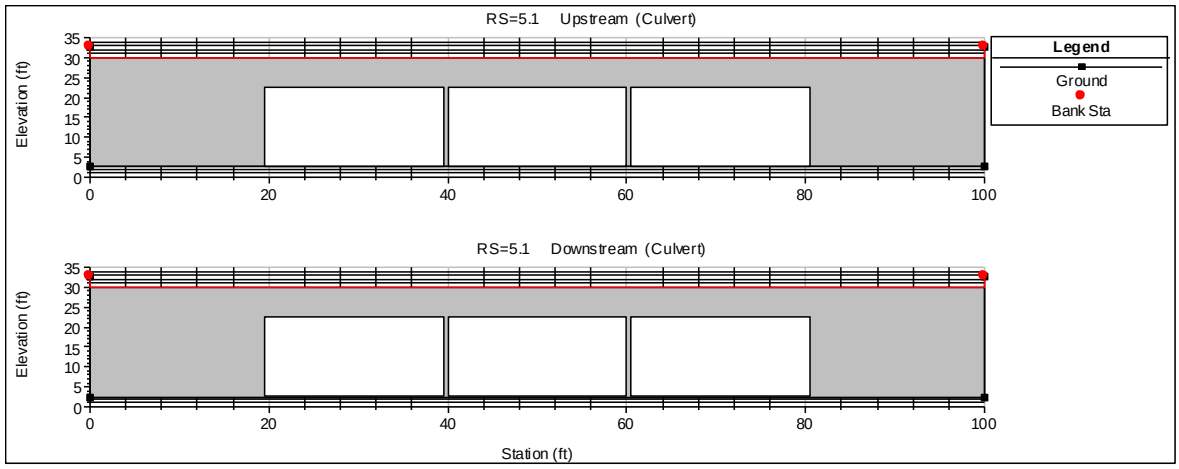


Figure 3.17 Geometry of the three-barrel culvert placed in the rectangular channel

Figure 3.18 shows the upstream and downstream limps of the rating curves at the culvert. Looped rating curves were observed on both sides of the culvert. Figure 3.19 allows inferring the time lag between the peak values of the main hydraulic parameters,

www.manaraa.com

Q(t), HW(t), and $V_u(t)$, where HW is the head water depth in the culvert and $V_u$ is the velocity upstream of the culvert. These three parameters reach their peak values in the following order: $V_{umax}(137)$, $Q_{max}(148)$, and $HW_{max}(150)$. The significant time lag among the peak times for these variables shows that unsteady flow effects through the culvert indeed are important.

The rating curves for the reference case (C3) in which the culvert is not present and for the same channel with the culvert are compared in Figure 3.20. Because of the culvert, the unsteadiness was reduced. The value of the unsteadiness parameter $\Gamma$ decreased from $1.018\times10^{-4}$ in case C3 to $0.858\times10^{-4}$ in the simulation with the culvert. However, unsteady flow effects cannot be neglected in the channel even when the three-box culvert is present.

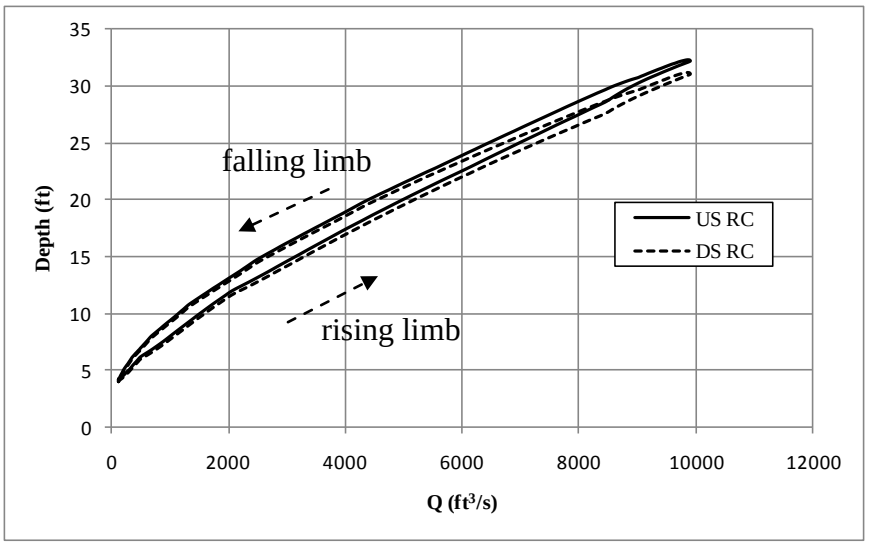


Figure 3.18 Upstream and downstream rating curves at the culvert showing a hysteresis behavior

www.manaraa.com

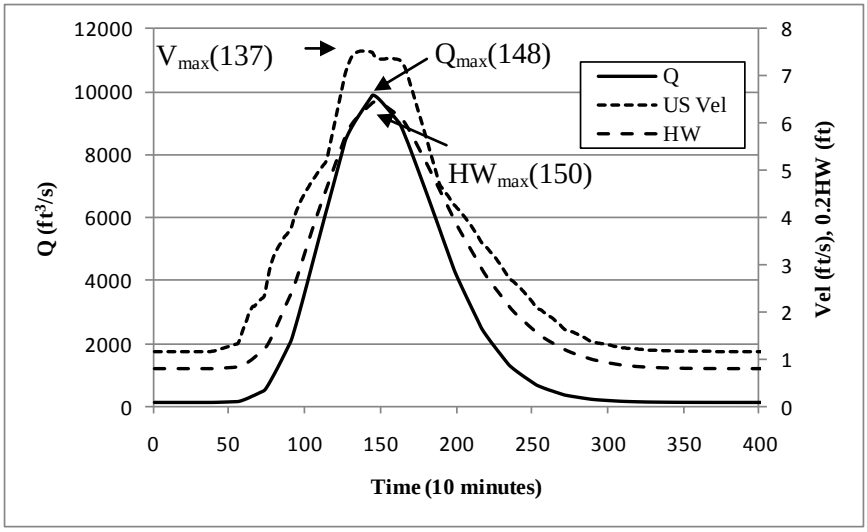


Figure 3.19 Hydrographs of the main hydraulic parameters upstream of the culvert

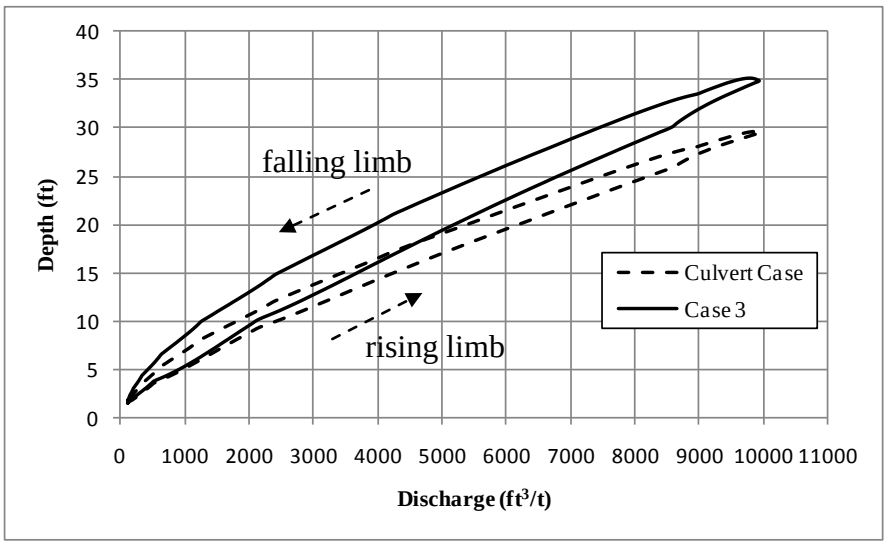


Figure 3.20 Looped rating curves in a rectangular channel without a culvert and with a three-box culvert

The numerical analysis of the unsteady flow at the culvert based on HEC-RAS indicates that significant unsteadiness effects occur at the culvert site during the time the

www.manaraa.com

flood wave is passing. However, the unsteadiness in the channel will be mitigated by the presence of the culvert.

The following sections of this chapter will extend this analysis to more complex cases. The unsteady flow in the Iowa River induced by the propagation of the measured 2008 flood wave will be analyzed (Chapter 5). The sediment transport, sediment deposition, and the flow distribution through the culvert for different peak flows will be analyzed using hydraulic modeling in the laboratory, numerical and field studies (Chapter 6).

## 3.3 Field observations of sediment deposition at culverts

Several factors can affect sediment transport through the model culvert, including the material and characteristics of which the channel is composed, hydraulic characteristics generated under different flow conditions, sediment particle distribution, and the geometry of the culvert. Generally speaking, sediment will deposit in the culvert if the sediment discharge in the approaching channel is larger than through the culvert. Various formulas exist for predicting sediment discharge for steady flow conditions in a fluvial channel. Two major difficulties complicate estimation of sediment deposition at a culvert:

1. The flow to the culvert is unsteady; and,
2. The sources of sedimentation are transported as bed load and suspended load.

The significant research concerning sediment transport through the culvert is limited, and does not address these difficulties. Therefore, this chapter focused on its field observations to provide insights.

### 3.3.1 Monitoring of a culvert with high sedimentation rates

The field visits conducted in three Iowa counties entailed sites that where known for serious sediment deposition problems. During 2007, more than 30 culverts were

www.manaraa.com

investigated in Johnson, Marion, and Buena Vista counties in the state of Iowa. A short report for each site visit is presented in Appendix B. While diverse in many respects, the visited culverts showed the common feature: they were partially silted, requiring difficult and costly cleanup operation. In general, the use of multi-box culvert is widespread although some various culvert type and materials are used. The field investigation contributed to the knowledge of the construction of the hydraulic models in the laboratory. Several field investigations still continue to provide the information needed for this study and to confirm theoretical and laboratory results related to the sedimentation process.

The selection site is the three-box culvert located on Old Mill Creek near Solon, Iowa. The study area is shown in Figure 3.21a. Moreover, it experienced several storm events and dynamic sediment transport in two years. At this location Old Mill Creek is about 10 ft wide and flows approaching to a three-box culvert. Figure 3.22 and 3.23 present the sediment deposition process upstream and downstream the culvert. The culvert was cleaned before our first visit on March 17$^{th}$ 2007, and sediment noticeably deposited through the culvert on July 10$^{th}$ 2008.

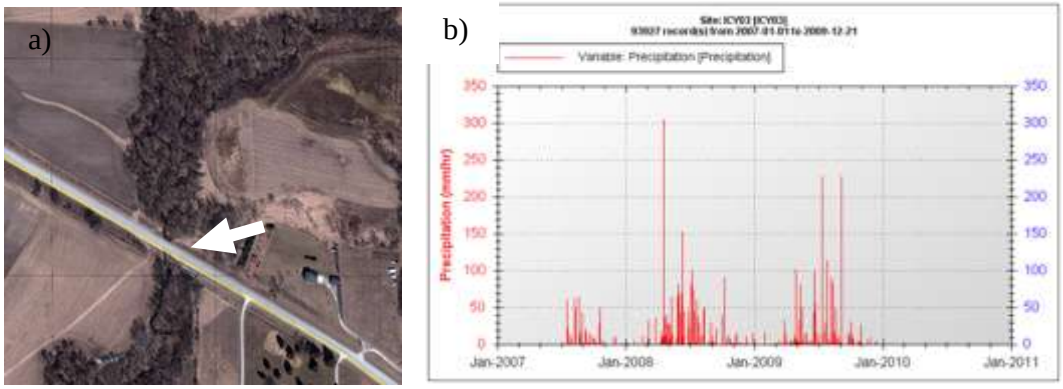


Figure 3.21 Culvert site in solon:a) Satellite view of the study area, and b) two-year precipitation hydrograph from the weather station (ICY03) in the neighborhood

www.manaraa.com

Usually sedimentation is a relatively slow process that requires a long-term monitoring program. During the conduct of the field observation effort, the site was continuously monitoring and found to undergo a dynamic rate of sedimentation accumulation The sediment deposition observed between the visits demonstrated that the culvert experienced at least one significant storm event for which the sediment discharge through the culvert area was large. However, there is no USGS gaging station in the vicinity of the culvert to record the hydrological evolution. As a substitute, several weather stations in the culvert neighborhood are used as our surrogates for providing the precipitation, and indirectly, an indication of the inflow hydrograph passing through the culvert. The associated precipitation hyetograph, collected from a weather station 5 miles south of the culvert site, shows that the intensity was 304 mm/hr on 04/16 2008 (Figure 3.21b). The rainfall was the largest storm during the visits. Such storm can trigger sediment erosion upstream the culvert and convey large runoff sediment ending in the culvert detention basin.

www.manaraa.com

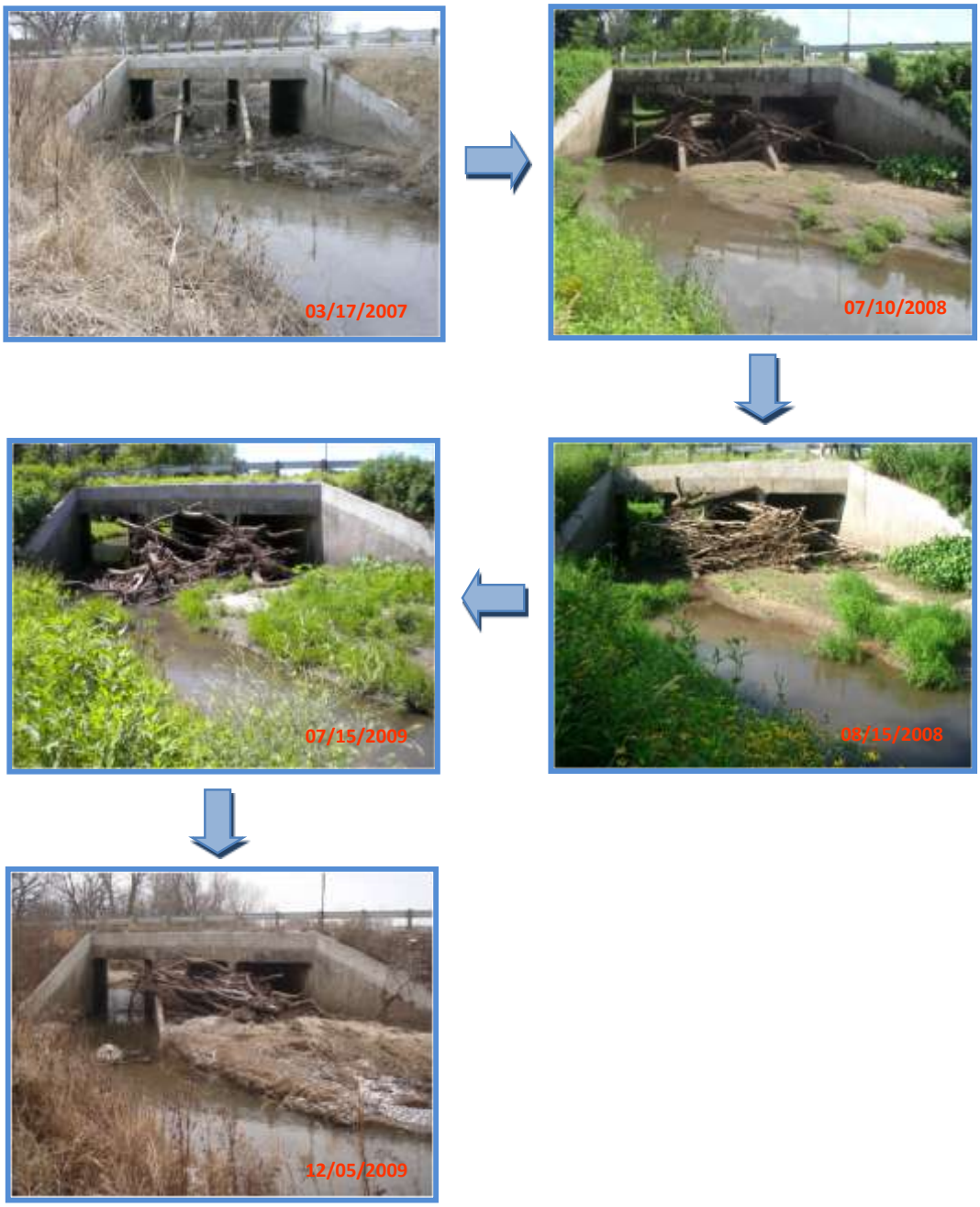


Figure 3.22 Three-box culvert and sedimentation process in Old Mill Creek in Solon, Iowa (View of the culvert entrance). It can be observed that the sediment and debris trapped in the upstream basin reduce considerably the entrance area of the culvert.

www.manaraa.com

Figure 3.23 Three-box culvert and sedimentation process on Old Mill Creek in Solon, Iowa. Downstream view from the culvert.

www.manaraa.com

### 3.3.2 Analysis of sedimentation at the culvert

During recent decades, sedimentary petrographers have attempted to relate grain size distribution and depositional processes responsible for their formation. This method is a useful way to understand the sediment transport and depositional process. An alternative method, use of chemical property as the tracer, is much more difficulty. Soil samples at the culvert were analyzed to recognize the sediment source of the sedimentation. By knowing the sediment source, the study was better able to diagnose the sediment deposition observed at the culvert site.

Seven cores with 8cm diameter were collected upstream and downstream on the third visit (Aug 15$^{th}$, 2008) as indicated in Figure 3.24a and 3.25a. The cores were split lengthwise, one half was archived and the other was sampled for grain size distribution analysis. The collecting depth of all cores is about 1.5 ft. The strata were shown in Figure 3.24b and 3.25b.

Figure 3.26, 3.27, and 3.28 illustrate the stratification of sedimentation collected upstream, downstream the culvert, and in the channel. Sediment deposits were investigated with core inspection and grain size analysis. The cores reveal that the sediment layers are interlaced. The analysis near the culvert shows that particles are group into two different sizes. However, no clear interlaced layers were observed in the channel. These indicate that the sediment deposition layers were made by different storm events, and thereby different flow events. The closet precipitation hydrograph (Figure 3.21b) also implied that there were two major storm events between visits. Therefore, every major storm event induced large sediment discharge and made a pair of strata: one is made of courser grain, the other is finer.

Although other methods are widely applied to determine the sediment source in a watershed (e.g., Peart and Walling, 1988; Slattery et al., 1995; Walling and Woodward, 1992; Ritchie et al, 2008), the method of sedimentary petrography applied in for the

www.manaraa.com

present culvert site can effortlessly provided useful information on sediment deposition during storm events at the site.

Figure 3.24 Sediment cores were collected in the sedimentation upstream the culvert shown in Figure 3.22

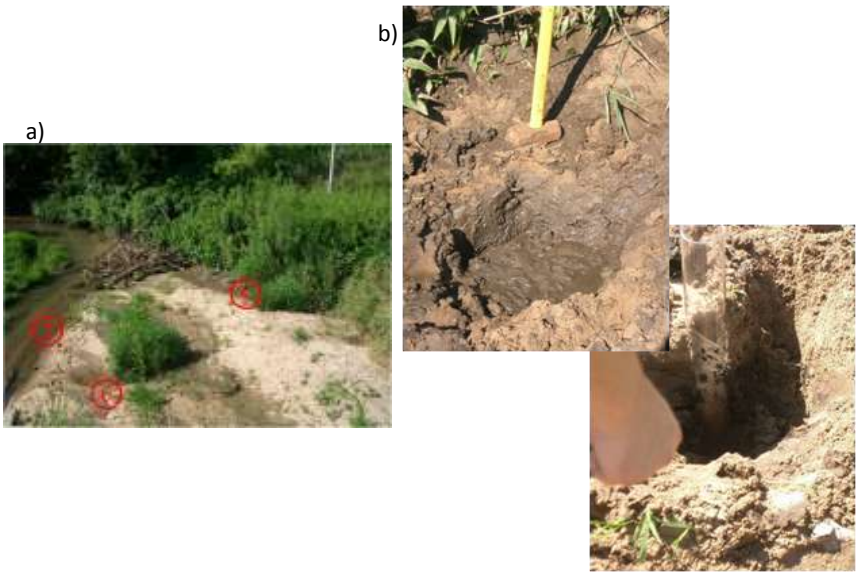


Figure 3.25 Sediment cores were collected in the sedimentation downstream the culvert shown in Figure 3.23

www.manaraa.com

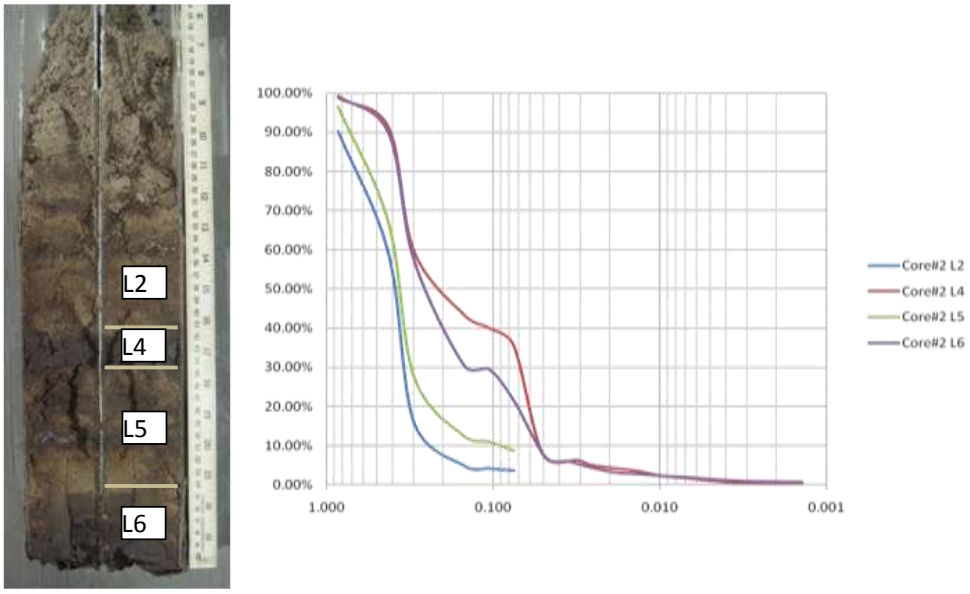


Figure 3.26 Sediment core collected from the upstream sedimentation near the culvert (number 2 in Figure 3.24a): a) Photograph shows stratification, and b) Grain size analysis presents L2 and L5 were coarse particles, but L4 and L6 were fine particles

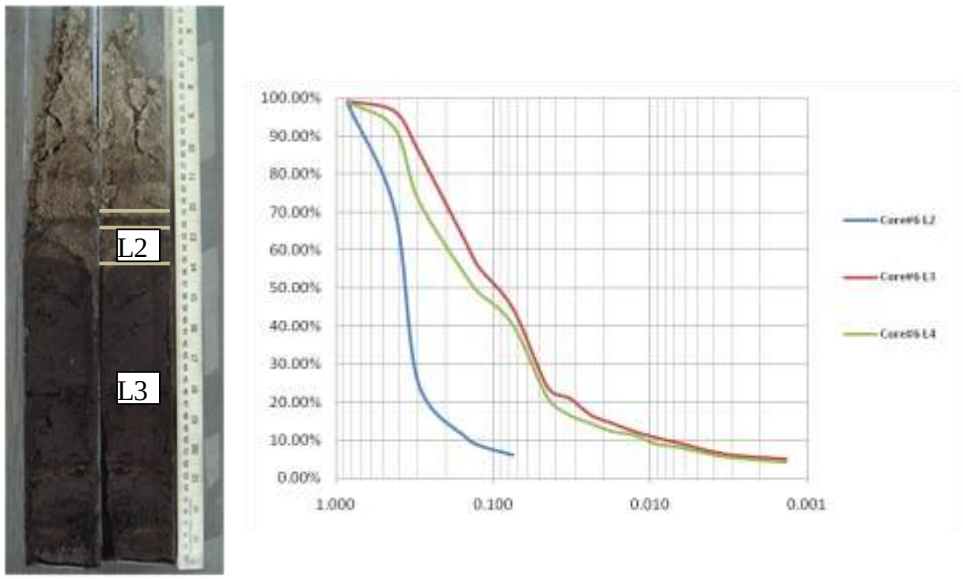


Figure 3.27 Sediment core collected from the downstream sedimentation near the culvert (number 6 in Figure 3.25a): a) Photograph shows stratification, and b) Grain size analysis presents L2 were coarse particles, but L3 were fine particles

www.manaraa.com

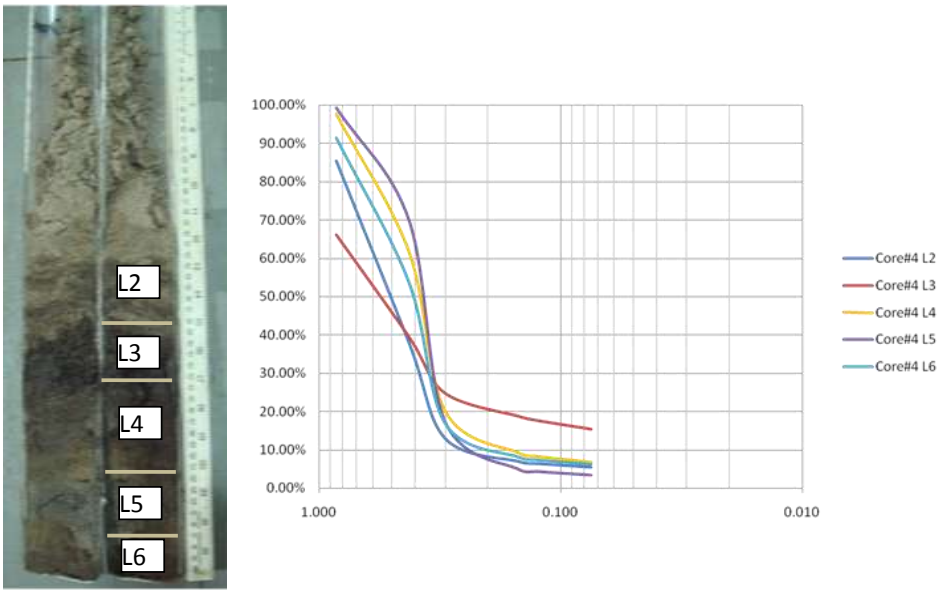


Figure 3.28 Sediment core collected in the channel(number 2 in Figure 3.24a): a) Photograph shows layers separated by fine particle, and b) Grain size analysis

www.manaraa.com

# CHAPTER4

# INVESTIGATION METHOD

This chapter presents the laboratory flumes, numerical modeling software and field survey approach used collectively as the method to investigate flow and sediment transport performance of multi-barrel culverts with an approach expansion linking the approach stream to the culvert. In line with the study's second primary objective, the methods focus on improved design of the transition expansion between the approach stream and the multi-barrel culvert.

## 4.1 Experimental Facilities

A basic layout of hydraulic model replicated a three-box culvert connected to a channel expansion upstream and channel contraction downstream. Three hydraulic models of this culvert design were used. They were built in IIHR's Model Annex, at the University of Iowa. Two models were small-scale culvert models with fixed boundary. They were constructed in the same flume (shown in Figure 4.1a). The length scale of both models was 1:20 from a prototype culvert. Figure 4.1a provides the layout of the flume. The plan form of the flume included four major parts: inlet, channel, culvert model, and outlet. The model's design provided the flexibility in dealing different geometries of the stream-culvert system. The first geometry, labeled model 1/20A, was a 1/20 scale, three-box culvert model without a wingwall connection to the expansion and the rectangular stream channel. Model 1/20B was also a 1/20 scale culvert model, but with wingwall connection and a compound stream channel (see Figure 4.1b). Model 1/20A had a simplified geometry retaining the essential features of the stream-culvert system. It was decided to more accurately replicate the details of the channel and culvert geometry. The second model 1/20B was built based on the design dimensions provided

www.manaraa.com

by Iowa Department of Transportation. The geometry of this configuration is given in Figure 4.1c.

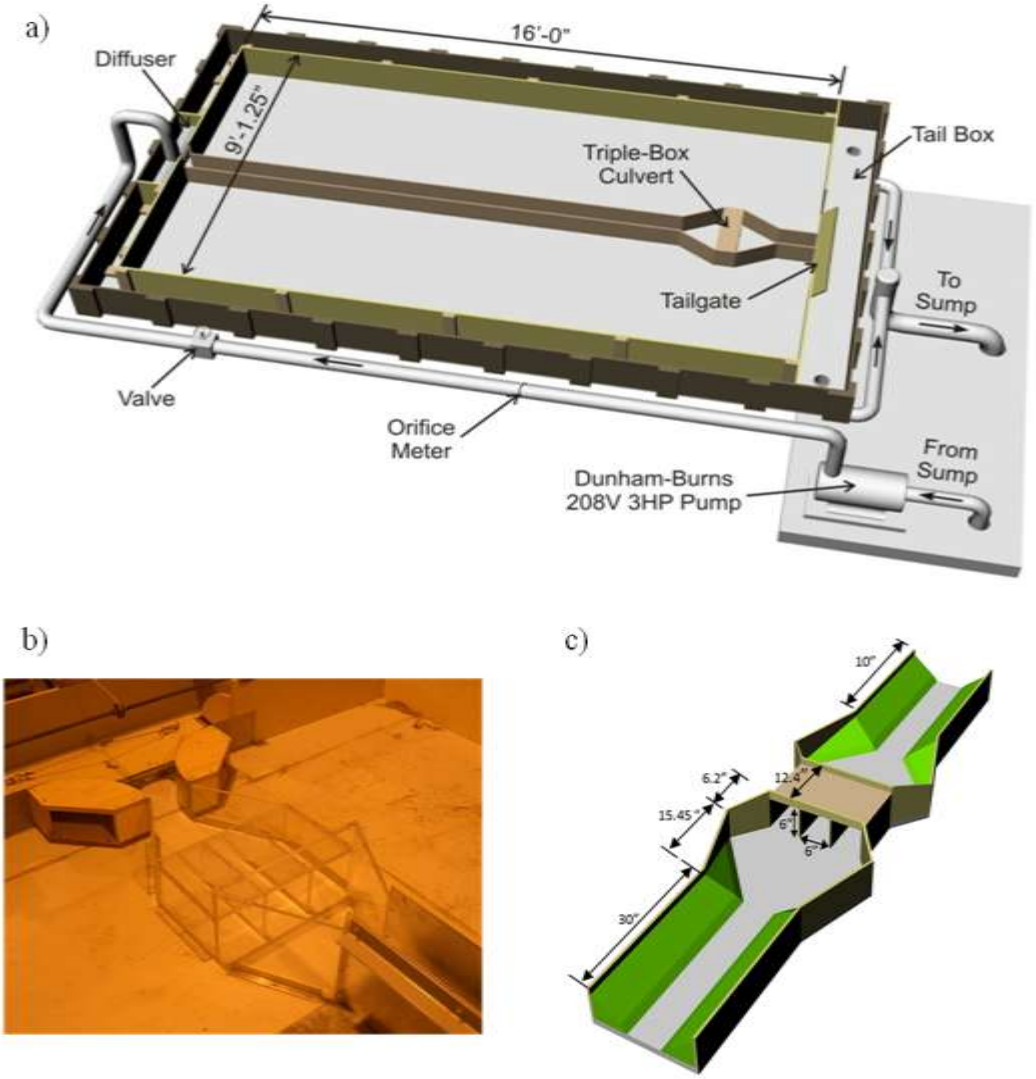


Figure 4.1 Hydraulic models: a) overview of the 1/20 flume, b) the culvert model (1/20A) without wind wall, and c) the culvert model (1/20B) with wind wall

The water flows for models 1/20A and 1/20B were pumped from an underground reservoir by means of a 3hp pump. A valve positioned before the diffuser was used to

www.manaraa.com

control flow rate. A diffuser and flow straighteners were installed in the headbox to stabilize the flow before entering the flume channel. Eight holes uniformly located in the diffuser were facilitated the flow. Trial-and-error adjustments were made to equalize water flow among the holes in order to keep the flow uniform in the channel.

Another important aspect of the experiments was the simulation of sediment movement to and through the culverts. Sediment was added into the channel by a sediment-feed device (Figure 4.2). A number of perforations were drilled into a cylinder to allow the sand to pass through. A variable speed motor was used to control the amount of sediment added into the channel. Special attention was given to ensure a good circulation of sediment in the channel. The flow conditions needed to ensure sediment movement were tested iteratively until the sediment mobility was uniform throughout the channel. Provision was made to trap all the released sediment in order to accurately quantify the sediment transport during the tests.

The measurements obtained from models 1/20A and 1/20B were water depth, discharge, velocity distribution, and the volume of sedimentation fed into the approach flow. Water depth was measured with the point gauge. This device is a pointer that can measure the elevation of water surface. Discharge was measured by the difference of hydraulic head and calculated using the following calibration equation:

$$Q = C_d \times \sqrt{\Delta h} \tag{4.1}$$

where $C_d$ is the calibration coefficient

Velocity measurements of the free surface were done by image-based technique. Large-Scale Particle Image Velocimetry (LSPIV) was used to measure the velocity distribution around the culvert. The velocities near the culvert were measured

www.manaraa.com

simultaneously in two-dimensions. The details of this technique are presented in Appendix C.

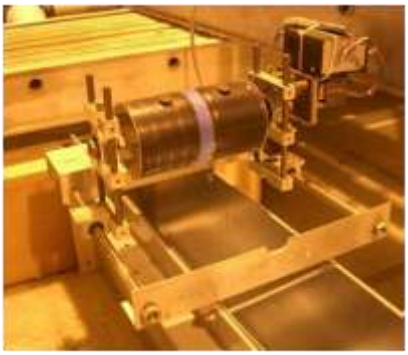

Figure 4.2 Sediment feeder

The second model was considerably larger, having a 1/5 length-scale ratio. It had the capability to recirculate the sediment. A flume, 65.7ft long, 9.3ft wide and 2ft deep, was modified to accommodate the model, which is shown in Figure 4.3.. The model had three distinct sections. The first section is a compound channel comprising a trapezoidal main channel connected to a floodplain. The compound channel has an erodible sand bed. The main channel side slope was set at 1:1, and that of the flood plain is 4:3. Next section contains the culvert proceeded by an expansion and a contraction downstream. The modeled culvert had three barrels. The expansion and contraction parts were fitted with erodible bed, while the culvert invert was made of plywood. The last model section was a short erodible channel leading to the tailgate. Water and sediment from the tailgate were returned to the headbox by means of two pumps.

The measurements made from model 1/5B were discharge, velocity, and bathymetry. The discharge and velocity measurements were essentially the same as for models 1/20A and 1/20B. The bathymetry measurements were made using a SeaTek MTA. It captured the bed form topography using high frequency sound wave technology.

www.manaraa.com

The travel time principle is at the basis of MTA operation. Specifically, sound waves are transmitted toward the bed where the waves are partially reflected back to the sensor. The sensor records the time for the sound waves to travel from the sensor to the object and back to the sensor, whereby the distance (i.e., bathymetry in instrument coordinate system) from the sensor to the reflective object is estimated. An ultrasonic depth probe, comprising 32 arrays of transducers, was employed for the measurements (see Figure 4.4). Each transducer is spaced 3 cm apart, and the maximum range is approximately 100 cm. The instrument has the capacity to measure small scale of bed forms (Friedrich et al., 2005). The measurement accuracy of the system is 1mm of vertical resolution, and 2cm of the horizontal resolution.

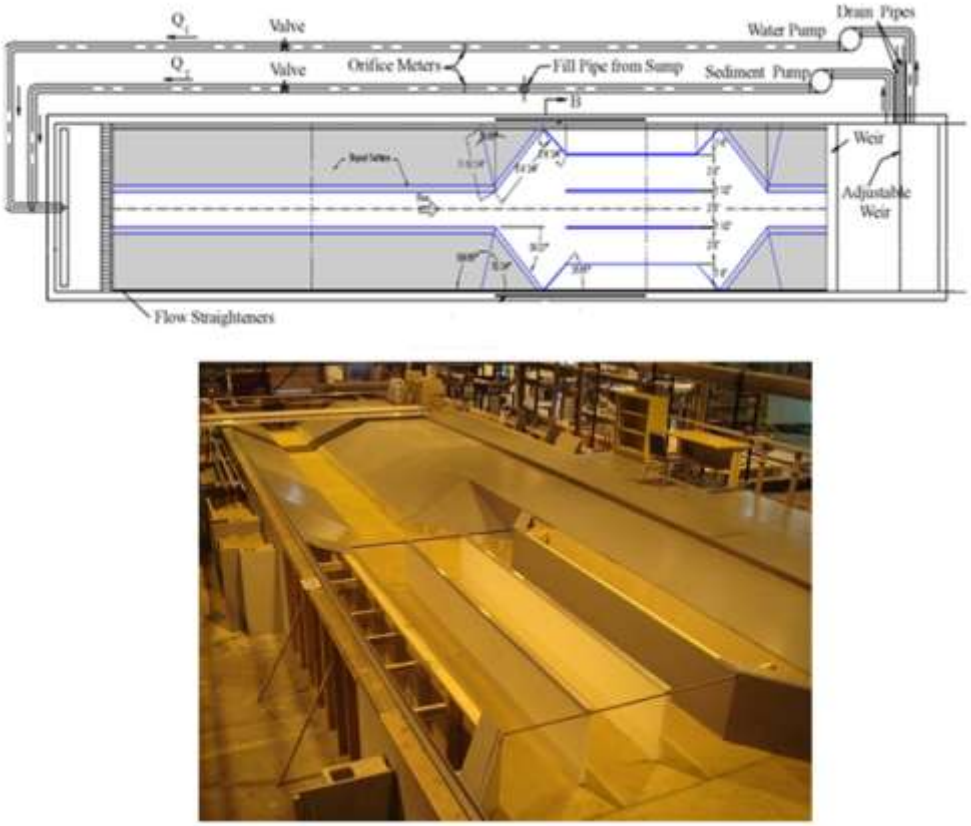


Figure 4.3 Schematic view of model 1/5B: (top), and view upstream toward headbox of the model (bottom)

www.manaraa.com

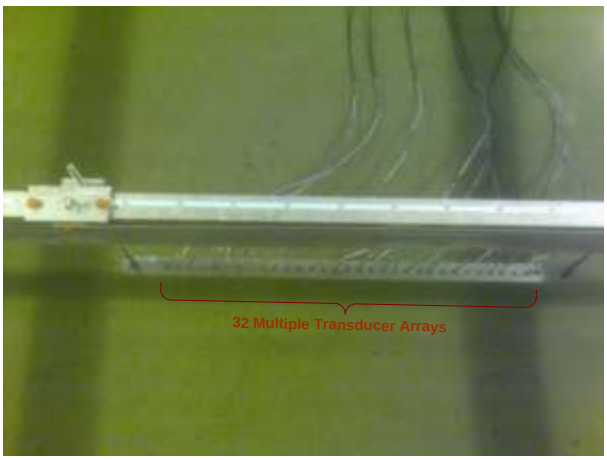


Figure 4.4 SeaTek MTA depth profiler containing 32 multiple transducer arrays

The models were operated using similitude of sediment particle entrainment and movement. This similitude requirement was met by using the Shields diagram to determine flow velocities and discharges in the model. The resulting model-scale velocities were of sufficient magnitude that Reynolds number (viscosity) effects were negligible.

## 4.2 Numerical Simulations

The numerical simulations were performed to obtain flow field information associated with the sedimentation observed in the model culverts. HEC-RAS was used. It is a widely used one dimensional open channel flow model, having the capability of analyzing culvert performance within the framework of one-dimensional flow calculations using the energy and momentum equations. HEC-RAS was used especially to investigate the time dependant variation of flow in the channel leading to the culvert.

The commercial software FLUENT was used to simulate and analyze the non-uniform flow through the culvert model. The calculation domains for numerical simulations were developed for two different culvert designs, illustrated in Figure 4.5. One domain was developed for hydraulic model 1/20B described in Section 4.1. The

www.manaraa.com

simulation examined the hydrodynamics of water flow for the conventional culvert design. The other model configuration was developed to investigate the effect of the different self-cleaning systems placed in the culvert area. The calibration of the numerical model used the data collected from the hydraulic models.

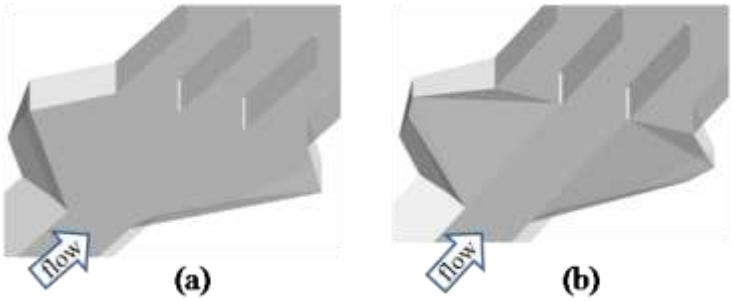


Figure 4.5 Computation domains :a) the three-box l culvert design, and b) self-cleaning culvert design placed in the expansion upstream the culvert

## 4.3 Field Observations

The study used an innovative approach for mapping the geomorphic and hydraulic features at the field sites monitored. The approach was used as a way to overcome the complexity of conditions at the sites. It was first developed to facilitate the monitoring of waterway characteristics at bridge sites (Hauet el at., 2009), and uses techniques from Large-Scale Particle Image Velocimetry (LSPIV) and close-range Photogrammetry, which will be introduced in the following sections.

### 4.3.1 Large-Scale Particle Image Velocimetry

The quantitative mapping method proposed herein is based on an imaging technique developed at IIHR in 1995 (Muste et al., 2004). The original technique and

www.manaraa.com

methodologies were developed for characterizing features derived from free-surface flow velocities in streams over large scale areas (Fujita et al., 1998). The method, dubbed Large-Scale Particle Image Velocimetry (LSPIV), was successfully used in laboratory and field conditions for mapping of the free-surface flow characteristics such as streamlines, large-scale vortices, and velocity gradients. It has been expanded to measure free-surface velocities in cross sections and channel discharges under field conditions (Muste et al., 2004). Currently, IIHR has assembled a mobile (truck-based) LSPIV unit, labeled the Mobile Large-Scale Particle Image Velocimetry (MLSPIV) to enable convenient measurements at field location of interest (see Appendix C).

MLSPIV was developed for measuring stream's free-surfaces velocities. The unit, illustrated in Figure 4.6, essentially comprises an imaging device set on a telescopic mast. The light weight aluminum, hydraulically operated mast allows for setting the camera from 15 ft to 50 ft above the ground level to accommodate imaging of various stream widths. Camera positioning and panning control are remotely conducted using a notebook computer located in the truck cabin. The MLSPIV truck is equipped with a power generator, additional batteries, and an uninterrupted power supply (UPS) that provides power for all equipments, a notebook computer, a pan-tilt unit, and a digital camera (Figure 4.6). Three guy wires are used after positioning to secure the mast against wind-induced or accidental vibrations.

Figure 4.6 MLSPIV unit: a) general view; b) mast deployed and ancillary equipment

www.manaraa.com

### 4.3.2 Quantitative Mapping at Culvert/Bridge Sites

The technique used for the study was developed to facilitate the monitoring of waterways characteristics at culvert/bridge sites. The existing analytical, experimental, and numerical simulation prediction of typical sediment deposition patterns at culvert sites are not clear and well documented to date. The continuous monitoring at culverts is of great importance to understand the sedimentation process and map the deposition pattern. The methodology of digital mapping described herein is applicable to waterway bridge monitoring in general, but is especially well suited for monitoring of culverts and small bridges (defined as those that cross waterways with watersheds encompassing less than 300 $km^2$ ) that are typical for Iowa and surrounding states. The key facets of this monitoring methodology are as described below:

1. To provide accurate quantitative mapping of the waterway characteristics (i.e., information about flow distribution and velocity magnitude, channel and bank characteristics, including vegetation presence) in the culvert vicinity;
2. To record waterway changes upstream and downstream of the culvert with an emphasis on quantifying changes in sediment deposition pattern, channel pattern, shape, and elevation. The data must be recorded in a digital format, readily available for tracking aforementioned changes over short or long time periods;
3. To reduce the effort, time, and cost associated with current monitoring methods; and,
4. To improve the safety of culvert/bridge inspections conducted during normal and extreme hydrological events.

The newly developed technique assembles several innovative processes to accomplish the above tasks. It was carried out in 3 steps:

1. Water vicinity mapping: Images of a river reach taken from several angles are ortho-rectified and assembled to obtain a panoramic distortion free image of the

www.manaraa.com

area;

2. Flow measurement: Image pairs of the river free-surface flow are analyzed using LSPIV to obtain the surface velocity field;
3. Assembling of flow and terrain data: The information obtained in steps 1 and 2 is assembled, stored and analyzed. Characteristics elements of the waterway are identified and localized in the ortho-rectified image, which leads to the creation of a digital map stored in electronic format.

The technique's main algorithms are described subsequently in conjunction with images acquired in-situ at a culvert site on Jordan Creek near Solon, Iowa.

Figure 4.7 River reach plan's decomposition

4.3.2.1 Waterway vicinity mapping

A river reach can be broadly described using quasi-planar surfaces (Figure 4.7); i.e. having at least two floodplains, two sloping banks and water flow surface. More quasi-planar surface can be used to describe complex 3D river reach geometry.

The images containing these planar surfaces need to be ortho-rectified, or mapped into a new and free of distortion image where the image coordinate system (in pixel) is linearly related to the actual coordinate system (in meter for example). The ortho-

www.manaraa.com

rectification is carried out using an 8-parameter, plan-to-plan transformation (Mikhail et al. [2001]):

$$X = \frac{a_1 i + a_2 j + a_3}{a_7 i + a_8 j + 1} \tag{4.2}$$

$$Y = \frac{a_4 i + a_5 j + a_6}{a_7 i + a_8 j + 1} \tag{4.3}$$

where [i, j] are the coordinates of a point in the image coordinates system (in pixels), [X, Y ] are the coordinates of the same point in the actual coordinates system (in meters) and $a_i$ are the projective transformation parameters.

Determination of the transformation parameter is accomplished using an implicit method (Wei, 1994) based on a set of GRPs, i.e. points of known coordinates in the actual coordinate system and in the image coordinate system. At least 4 GRPs are needed to solve for the $a_i$ parameters, and a least square fit is applied if more than 4 GRPs are available. The ortho-rectification of the waterway vicinity is accomplished with a graphical user interface and encompasses three steps, as illustrated in Figure 4.8:

1. Identification of the different planar surfaces on the images;
2. Ortho-rectification of the planar surface using Equation (4.1) and (4.2); and,
3. Assembling of the ortho-images of the planar surfaces to obtain the ortho-image of the waterway vicinity.

The result of the above processing steps is a color ortho-image of the area of interest that is a scaled replica of the actual vicinity of the waterway.

www.manaraa.com

4.3.2.2 Flow measurement

LSPIV has been successfully implemented to measure free-surface velocities and discharges in various streams [e.g., Bradley et al., 2002, Creutin et al., 2003, Fujita, 1994, Fujita et al., 1998, Hauet et al., 2008, in press]). The technique is the extension of the conventional PIV applied in fluid mechanics [Adrian, 1991]. Estimation of free-surface velocities with LSPIV is based on the same concept as human vision. Specifically, the technique "guesses" using special pattern-recognition algorithms where small particles floating on the free-surface are moving in consecutive images, separated at a known time interval. A classical cross-correlation algorithm is used to determine the movement of flow tracers. In this study, a PIV algorithm for large scale applications with low resolution images, developed by Fincham and Spedding [1997], is used.

The advantage of this algorithm is that it decreases the mean bias and root mean square errors [Piirto et al., 2005]. It calculates the correlation between the interrogation area (IA) centered on a point $a_{ij}$ in the first image (image A) and the IA centered at point $b_{ij}$ in the second image (image B) recorded with a time interval of $\delta_t$ seconds. The correlation coefficient R(aij , bij ) is a similarity index for the gray-scale intensity of a group of pixels contained in the two compared IAs, expressed as:

$$R(a_{ij}, b_{ij}) = \frac{\sum_{i=}^{Mi}\sum_{j=1}^{Mj}[(A_{ij} - \overline{A_{ij}})(B_{ij} - \overline{B_{ij}})]}{[\sum_{i=1}^{Mi}\sum_{j=1}^{Mj}(A_{ij} - \overline{A_{ij}})^2 \sum_{i=1}^{Mi}\sum_{j=1}^{Mj}(B_{ij} - \overline{B_{ij}})^2]^{1/2}} \qquad (4.4)$$

where $M_i$ , $M_j$ are the sizes of the interrogation areas (in pixels), and $A_{ij}$ and $B_{ij}$ are the distributions of the grey-level intensities in the two interrogation areas.

www.manaraa.com

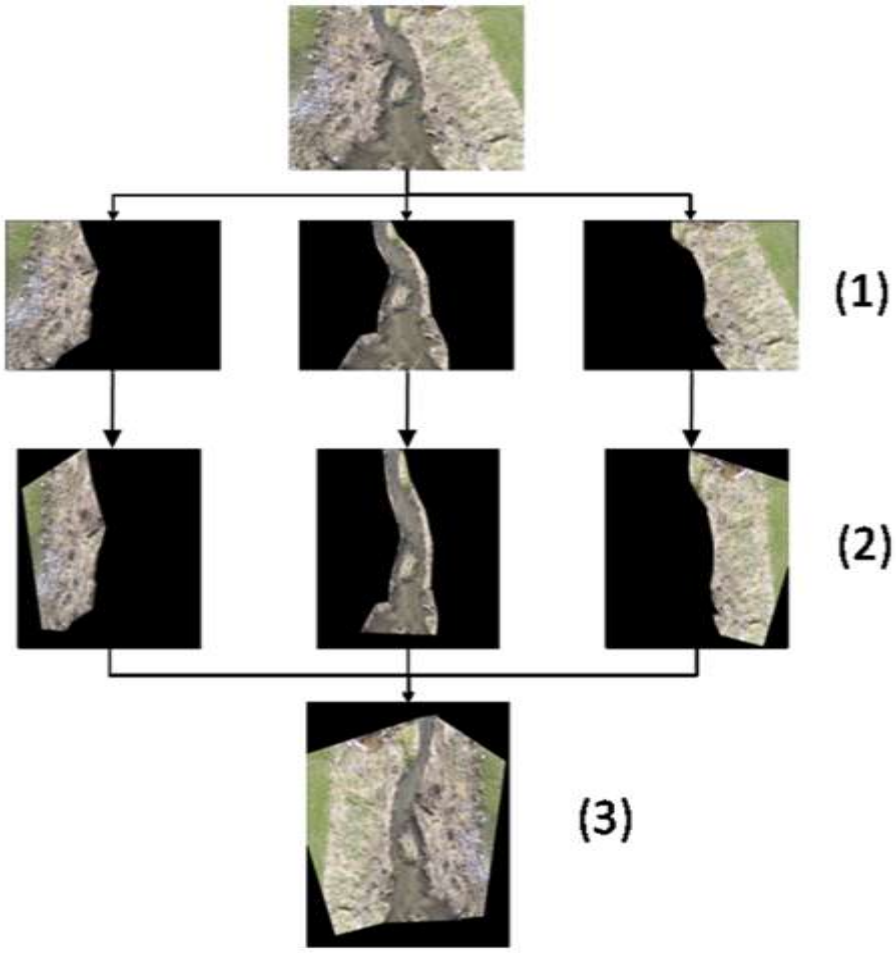


Figure 4.8 Waterway vicinity ortho-rectification protocol: (1) identification of the planar surfaces on the images; (2) ortho-rectification of the surfaces; (3) assembling of the ortho-images of the planar surfaces to obtain the ortho-image of the landscape.

The correlation coefficients are only computed for points within a pre-defined searching area (SA). The SA size is selected so that the displacement of tracer patterns from the first image is contained within the SA of the second image, commensurate with the expected range of velocities of the river. For rivers with small cross-stream velocities, the SA should be asymmetric, elongated in the direction of the flow. The algorithm assumes that the most probable displacement of the fluid from point $a_{ij}$ during the period $\delta_t$ is the one corresponding to the maximum correlation coefficient. Sub-pixel

www.manaraa.com

displacement accuracy is reached using a parabolic fit [Fujita and Komura, 1992]. Velocity vectors are derived from these displacements by dividing them by $\delta_t$. The process is iteratively conducted over the entire image using a computational grid. An example of LSPIV surface velocity field for the Jordan Creek site, downstream the culvert, is shown in Figure 4.9.

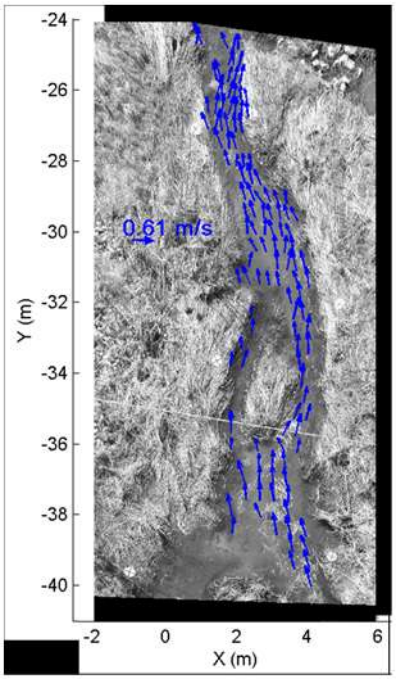


Figure 4.9 LSPIV time-averaged velocity field for the Jordan Creek site, downstream the culvert.

4.3.2.3 Assembling flow and terrain data

In this step, the ortho-rectified dry land in the vicinity of the water way and the velocity of free-surface are assembled in one map for further analysis. In general, the waterway encompasses the bridged stream or river bed along with its banks, abutments, and any other local obstructions that significantly impact flow velocity, flow alignment, and scour depth. Software allows identifying, selecting and extracting features of

www.manaraa.com

importance for customized analysis. These operations are conveniently carried out by scrawling the mouse over assembled ortho-rectified image of the site. Each feature is labeled with a code name and its coordinates are saved so that a map of the waterway characteristics can be created. For example, the colored ortho-image in Figure 4.10 allows easy identification of:

1. The intersection between the banks and the river surface waterline defining the shape and the angle of attack of the stream;
2. Islands, debris, deposits or other obstacle in the channel;
3. Floodplain characteristics, including land cover (rocks, mud, vegetation), the presence of side ditches, vegetation, debris or other obstacles.

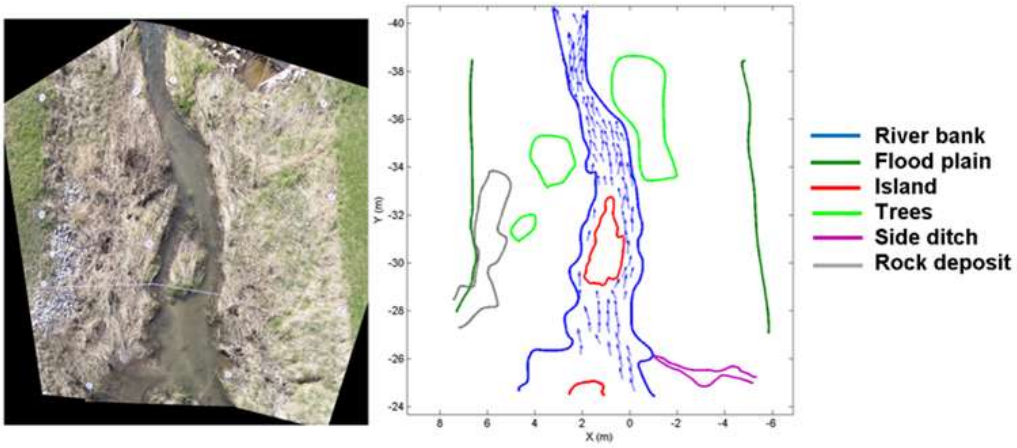


Figure 4.10 Example of mapping: (left)Ortho-image of the studied area, and (right)The corresponding digital map containing selected features of the waterway and its vicinity

www.manaraa.com

# CHAPTER 5

# FIELD MEASUREMENT IN UNSTEADY CHANNEL FLOWS

## 5.1 Introduction

This chapter investigates the capability of the non contact image based technique to capture the hydrodynamics of rivers subjected to unsteady flow such as the flood wave propagation following storms. In the first part of the chapter, the image based technique is compared with a well established acoustic instrument to validate its performance. Subsequently, the image based technique is employed for obtaining direct discharge measurement in Iowa River during the 2008 flood.

Monitoring could not rely on single-value rating curves. Such curves are valid as long as the channel is stable and the flow within the whole channel is steady, but this was not reliably the case for the culvert sites. To capture changes in the hydraulics of the gaging station, the rating curve was verified by comparison with direct discharge measurements about eight times per year (Hirsch and Costa, 2004). This high frequency of taking calibration measurements was required because changes in the river cross sections might alter the stage/discharge relation. Significant changes can occur due to scour or deposition of sediment in various parts of the cannel or to changes in streambed and bank roughness. Such changes are particularly prevalent during flood events. Occasionally, changes are so severe as to require adjustments to the stage-discharge rating. The adjustments can create large differences in the area of the extrapolated portion of the curve, such as the one illustrated in Figure 5.1b for the flood of the Iowa River that occurred during 2008 in Iowa City. During this flood, the river discharge peaked at 1,163 $m^3/s$, leading to differences in stage of about 2 m between the before-the-flood stage-discharge curve and the one determined after the flood occurred (see Figure 5.1).

Direct measurement of the stream discharge needed to obtain the rating curves is an elaborate process where velocity measurements are the most complex and laborious

www.manaraa.com

activity. Velocity measurements across the channel cross section can be obtained with different instruments. In the last three decades, the conventional mechanical instruments used for acquiring velocities have been increasingly replaced by a new generation of acoustic instruments. These instruments considerably improve the efficiency and the frequency at which the velocity measurements needed for establishing rating curves can be acquired. The conventional, as well as the newer acoustic instruments, used to collect direct discharge measurements needed to obtain the rating curves are typically deployed from boats. The high operational hazards involved with the deployments of boats and equipment during extreme flows (e.g., floods) leave no choice but to extrapolate the available direct flow measurements for higher flows using a one-to-one stage-discharge relationship, labeled SRFC in Figure 5.2.

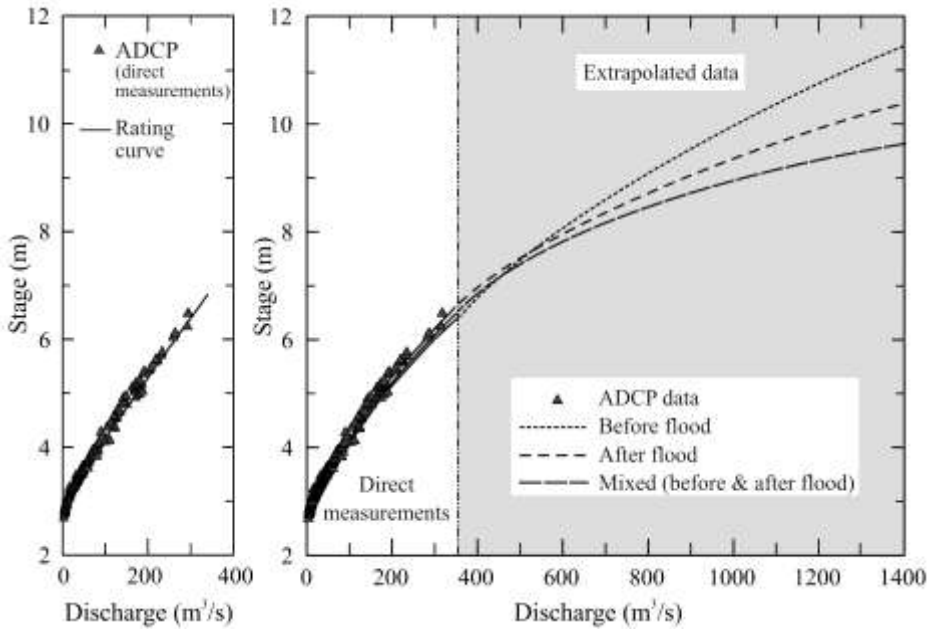


Figure 5.1 Rating curve for USGS gaging station 05454500 on the Iowa River in Iowa City, U.S.A: a) The rating curve is based on multiple direct measurements [271 measurements were acquired between 1984 and 2006. More than 80% of them were acquired for flows less than 200 $m^3/s$]. b) Sample of rating curve adjustment due to changes in the channel hydraulics.

www.manaraa.com

As noted in Chapter 2, it has been recognized for a long time that there are problems associated with the one-to-one rating curves. This is especially the case for unsteady flows, such as those developing during floods. In these situations, unknown uncertainties in the rating curves occur because of several factors. One significant source of uncertainty is due to the fact that most of the calibration measurements for the rating curves are obtained during quasi-steady flow conditions occurring in normal flows. This region, labeled baseline flows in Figure 5.2, typically accounts only for a small fraction of the total flow range (up to four times for the data displayed in Figure 5.1). The extrapolated portion of the rating curve in the region of high flows is prone to errors given that the extrapolation is based on a limited sample of direct measurements in the baseline flows area. An even larger source of uncertainty for high flows is due to the fact that the extrapolation of the rating curves does not account for flood-wave propagation effects. A flood wave passing through a river site is described in the stage-discharge space by a double-sided loop rating curve, as illustrated by the UFRC curve in Figure 5.2. The loop curve (a.k.a. hysteresis effect) is the result of the unsteady flow associated with the flood wave propagation.

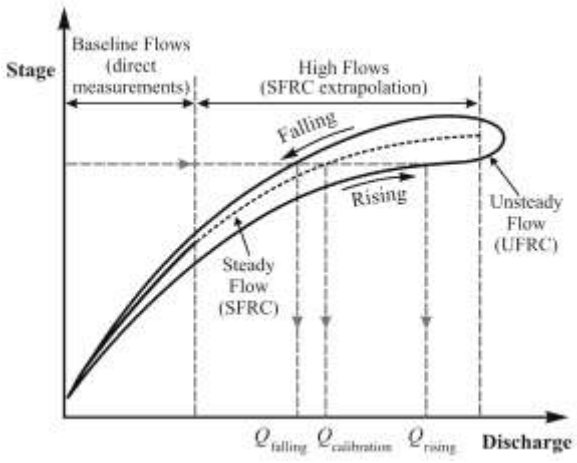


Figure 5.2 Deviation of the unsteady rating curve from the conventional one obtained with a one-to-one relationship applied to measurements in steady flow conditions and extrapolated for high flows

www.manaraa.com

When a flood wave propagates in a river, the wave front approaching a cross-section will experience an increase in velocity (Henderson, 1966). After the flood peak passes the cross-section, the rear of the wave reduces the velocity. This acceleration-deceleration sequence of the flow produces a loop in the stage–discharge relationship that is distinct from the one-to-one relationship (see Figure 5.2). Details on the physical background of the hysteresis phenomenon, and in-depth discussions on the equations that govern unsteady flow can be found in Chapter 3.

The important practical implications of neglecting the hysteresis effect in determining the rating curves are: a) the maximum water discharge and maximum water stage do not arrive at the same time at a given river location; b) for the same stage, the discharge is higher during the time the water level is rising than during the time the water level is falling; and c) even if calibration measurements exist for the area affected by the hysteresis, the deviation from the single-valued rating curves are associated with the measurement uncertainty rather than the hydraulic process. Moreover, the shapes of the loop curves are not unique, i.e., the loop curve varies from event to event. The shape and extent of the loop curve is determined by the discharge hydrograph which is the combined effect of hydro-geological (e.g., soil characteristics and moisture content) and meteorological variables (e.g. rain intensity and duration). It is obvious from the above considerations that the use of single-valued rating curves for estimating high flows is subject to large errors.

Rating curves are routinely used for flow monitoring and forecasting during normal and extreme flows, such as floods. Flood forecasting is a data-driven process, with streamflow being the most important input data. Accurate and reliable flood forecasts require both real-time streamflow information for model initialization and historical streamflow records for calibration. The accuracy of the discharge estimates obtained with current-meters and stage meters is 5 to 10% (Hirsch and Costa, 2004). While use of the new acoustic instruments has improved the measurement accuracy, the

www.manaraa.com

conventional methods for estimating discharge are outdated and of limited accuracy. For high flows the accuracy is not even known, due to a lack of calibration measurements. The considerations presented above reveal the role and importance of direct discharge measurements and the need for a large number of such measurements to provide continuous and accurate stream-flow estimates. These estimates are important for many water management purposes, but they are critically important for preventing the detrimental societal and economic impacts associated with floods.

Development of new instruments for acquiring direct discharge measurements over the entire range of flows in a stream will provide the detailed data needed for several purposes:

1. Identification of flow transients in channel flows produced by active controls (etc., locks, dams, industrial effluents), vessel traffic, and floods;
2. Improvements in the accuracy and reliability of flood forecast and monitoring;
3. Testing of scientific hypothesis on river processes; and,
4. Design of procedures for the estimation of streamflow at ungaged sites.

These purposes encompass the measurement needs for the present study. To get the measurement method sufficiently developed for the study, an additional investigation was carried out using flows readily observed in the Iowa River in Iowa City. This chapter now specifically describes the measurements acquired with a video based measurement technique during normal flows and high flows (floods), notably the LSPIV technique utilized in the study is introduced. . In the first campaign, LSPIV measurements were carried out in parallel with measurements acquired with Acoustic Doppler Current Profilers (ADCP). In the second campaign, LSPIV measurements were acquired in the

www.manaraa.com

Iowa River before and after the arrival of the peak flow in Iowa City during the historic flood of 2008. The one-dimensional unsteady numerical simulation results of the flow in the Iowa River during the 2008 flood also are presented. They are compared to the LSPIV measurements.

## 5.2 Calibration measurement

### 5.2.1 Large-scale particle image velocimetry

The fast-paced developments in optics, lasers, electronics, and computer hardware and software over the last four decades have triggered a considerable increase in the use of image-based techniques for flow visualization and quantitative measurements. This new generation of instruments, conventionally grouped under the generic name of Particle Image Velocimetry (PIV), has greatly improved our capabilities to measure instantaneous velocity vector fields in a variety of laboratory-scale flows (e.g., Raffel et al., 1998). In the last decade, conventional PIV has been extended to large-scale flows, such as those encountered in hydraulic applications (Fujita et al., 1998). The technique, dubbed LSPIV, uses conventional PIV image- and data-processing algorithms. Areas as large as hundreds of $m^2$ have been non-intrusively mapped using LSPIV to provide velocity vector fields (Fujita et al., 1998; Bradley et al., 2002; Creutin et al., 2003). This capability cannot be matched by any alternative instruments. Since its inception, LSPIV has matured considerably and become increasingly used in hydrometry (Muste et al., 2008).

It is assumed herein that the reader is familiar with LSPIV techniques, principles, and configurations. Details about LSPIV can be found in Appendix C. With this consideration in mind, only those LSPIV aspects that are central to the present measurements will be discussed herein. The raw LSPIV result is a velocity vector field estimated for the entire imaged area. Velocity-derived quantities (flow patterns, vorticity, strain) at the free surface are readily available using the LSPIV raw results. LSPIV

www.manaraa.com

velocity measurements in conjunction with river bathymetry and stage measurements in a cross section provide flow discharges. While bathymetry requires an additional instrument, stage measurements can be obtained from LSPIV images using scaling considerations. Use of images instead of other types of transducer outputs makes LSPIV based techniques relatively simple and user-friendly. LSPIV is a fully digital technique, does not require calibration, and allows reprocessing of raw information with variable spatial and temporal resolutions.

In general, PIV components are strongly interrelated, such that the selection of one approach for a component imposes the types of devices or approaches available for the remaining components. Moreover, the selection of specific components and their integrated operation is driven by rules of thumb that relate the concentration of patterns in the image and their size with the image processing parameters and the expected particle displacement in the series of images (Adrian, 1991). Use of these rules is common practice for PIV measurements in the laboratory environment. Unfortunately, except possibly in the case of sufficiently small channels and streams, less than desirable laboratory recording conditions require procedural adjustments when LSPIV is implemented in field conditions.

The most challenging problem in field measurements, and a central issue for the LSPIV measurements discussed in this study, is attaining a good visualization of the stream free surface. A river site can display very distinct appearances, as illustrated in Figure 5.3 by images of the Iowa River captured at various times. One favorable LSPIV measurement situation occurs when the free surface is visualized by naturally occurring tracers/patterns floating at the free surface. Such examples are foam or ice floes traveling with the free surface (see Figure 5.3a and b, respectively). These tracers, however, are not always available or do not exist in sufficient quantities in natural streams. Another favorable situation is when specular reflection formed by incident light interacting with the free-surface deformations can be used as a seeding surrogate (see Figure 5.3c). In this

www.manaraa.com

case, the free-surface waviness is generated by large-scale turbulence structures approaching the free surface or by the wind turbulence. Using the light intensity variation associated with the waviness as a tracer substitute, researchers were able to obtain accurate LSPIV measurements (e.g., Creutin et al., 2002; Fujita & Hino, 2003). Unfavorable situations are considered those when the free surface is mirror-like (see Figure 5.3d) or wind gusts are moving above the stream producing non-uniform movement of the ripples propagating at the free surface (see Figure 5.3e). When these types of unfavorable situations are encountered, the addition of free surface tracers is necessary for reliably visualizing the free surface.

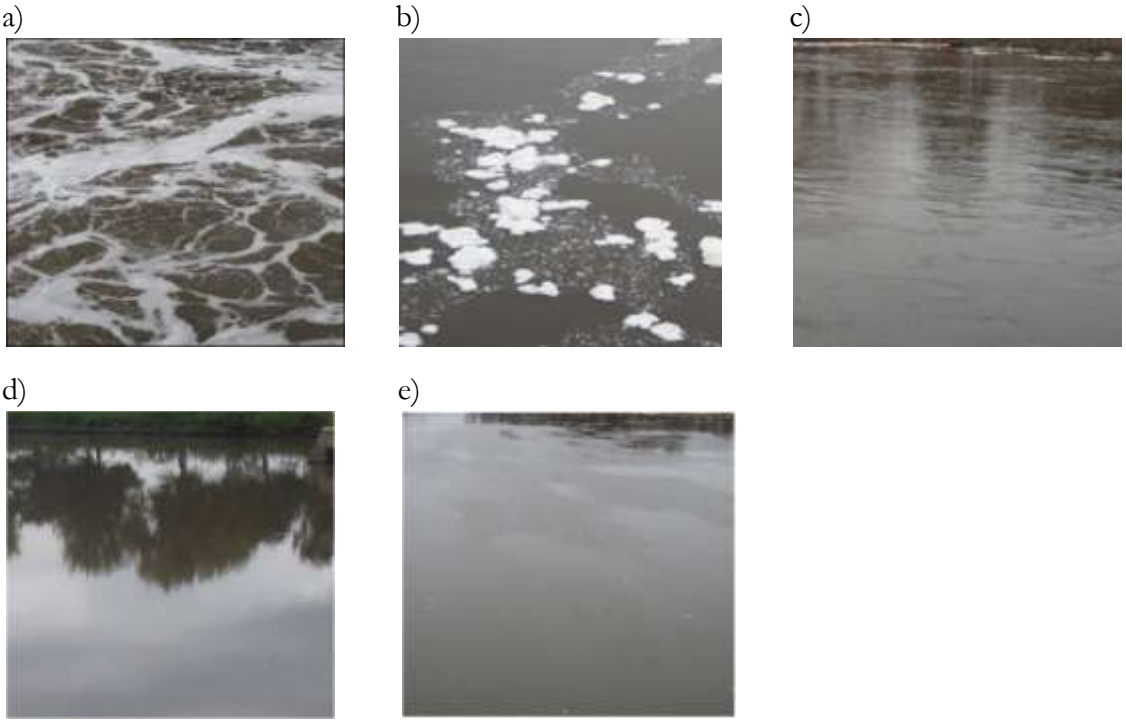


Figure 5.3 Appearance of the free surface at the same river location (area of about 1,000 $m^2$): a) foam; b) ice floes; c) ripples driven by internal turbulence; d) lack of tracers; e) ripples driven by wind (gusts)

www.manaraa.com

For both "naturally-occurring" and artificial (added) tracers, the key requirement is that they have to accurately follow local flow movements. Tracer inertia and submergence are primary factors determining the suitability and accuracy of the flow visualization. Adverse factors for floating tracers can be strong winds at the free surface or aggregation of the seeding particles induced by particle-to-particle attraction forces. The measurements presented in this section used exclusively the turbulence-driven ripples boiling at the free surface. The assumption is made herein that the ripples are conveyed downstream at the free surface velocity. The results presented below will provide some insights into their effectiveness and utility as well as associated issues that need further consideration.

### 5.2.2 LSPIV and ADCP measurement

The calibration measurements were obtained from concurrent measurements with LSPIV and ADCP. Measurements were acquired from a bridge located approximately 1 km downstream of USGS gaging station #05454500 on the Iowa River in Iowa City (IA). The ADCP measurements followed the operational guides recommended by USGS (2002). The LSPIV images were taken using a commercial HD camera (Sony HDR-HC1) positioned at about 10 m above free surface level from a mast anchored on the left river bank. The data acquired in the campaign can be grouped as follows (see Figure 5.4a):

1. ADCP transects acquired about 35 m downstream the bridge (five consecutive transect of about 1.5 minutes each);
2. zig-zaged ADCP measurements across the river covering a river stretch of about 115 m downstream from the repeated transects location (survey duration 32 minutes); and,
3. LSPIV measurements covering two adjacent field of views (the upstream view was recorded simultaneously with the ADCP transects).

www.manaraa.com

A general comment about the measurements illustrated in Figure 5.4 concerns ADCP and LSPIV productivity. The vector fields at the surface and in the verticals across the stream were acquired with a relatively small amount of effort, in less than an hour. The LSPIV measurements were collected remotely from the bank without the need to deploy a boat and personnel in the river. Video images were recorded for 25 minutes, a longer than usual recording time, to allow for several analyses. Both instruments were equipped with data acquisition software that allowed for data quality checks in real time, such that if they would have been found affected by obviously large errors, new measurements could have been taken immediately.

The main target of these calibration measurements was to compare the discharge estimates provided by the LSPIV with those inferred from ADCP measurements and the discharge estimate provided by the neighboring USGS gaging station. A similar experiment was carried out by Creutin et al. (2003) in the vicinity of the same USGS gaging station several years before. The tracing of the free surface movement was, however, dramatically different for these two experiments. In the measurements performed by Creutin et al., the tracing was accomplished by foam generated by a weir located just upstream from the LSPIV measurement site. At this location the foam is present throughout the year (see Figure 5.3a). The discharge measurements were made within a 20-day period, for discharges ranging from 50 to 300$m^3$/s. The PIV measurements were then compared to 215 current-meter measurements made at this site by the USGS. The measurements were consistent with the current meter estimates over the whole measurement range, with a 4% overall underestimation of the discharge (Creutin et al, 2003). For the present calibration measurement, the average discharge predicted based on the data collected at the five ADCP transects was 6.3% higher than the USGS rating curve-based value of the average discharge. Our less than optimum LSPIV measurements taken simultaneously with the ADCP data were found to be 4.3% lower than the USGS discharge obtained using rating curves. There are many reasons that

www.manaraa.com

can potentially explain the approximately 10% difference between the ADCP and LSPIV predictions. Some of these reasons are discussed below.

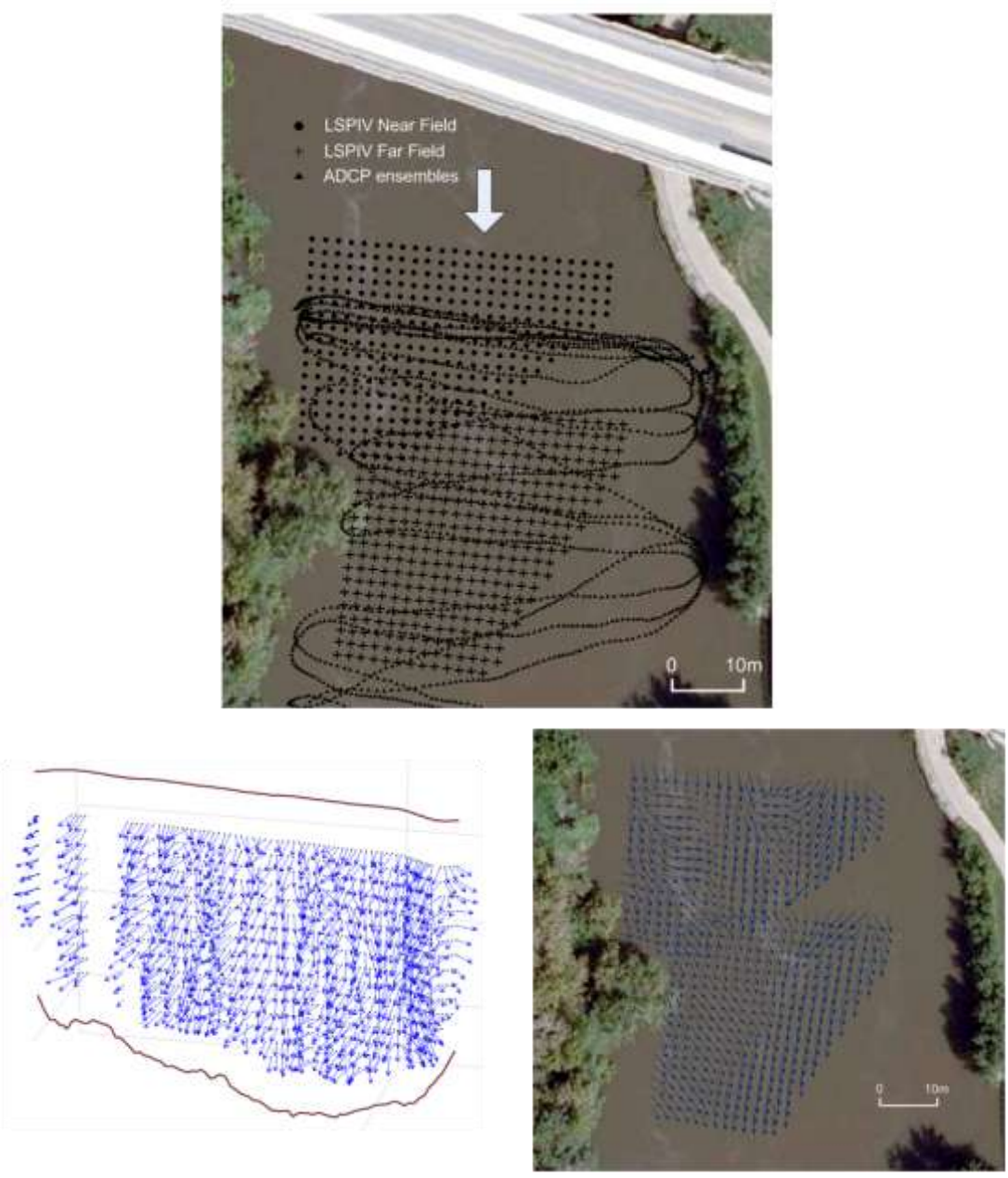


Figure 5.4 Overview of the LSPIV and ADCP measurements: a) Location of the measurements; b) raw velocities measured by ADCP in one of the transects; c) averaged velocity vector field obtained from LSPIV measurements.

www.manaraa.com

While the measurement environment for ADCP was adequate, the LSPIV measurements were challenged by several factors. The first factor was the tracing of the free surface used in the measurement campaign. Tracing was provided by naturally-occurring ripples at the free surface, similar to the ones shown in Figure 5.3c. While in some instances this visualization means suffices, it is obviously less efficient and accurate than a particle-based tracing alternative. The second, and major, factor was related to difficulties caused by strong wind at the measurement site and throughout the data acquisition time period. The major wind-related detrimental aspect was the gustiness of the wind sweeping the free surface. The gusts triggered wind-driven waves that were non-uniformly distributed across the river width. At times, the gusts were so strong that the resulting free-surface waves apparently traveled upstream (especially on the right side of the river, near the bank). Visual observation, similar to LSPIV processing, perceives the movement of the wind-driven waves using specular reflection, which is a materialization of the incident light interaction with the free-surface deformations. In the absence of the wind, specular reflection can be successfully used as seeding surrogate for tracking the movement of flow (Creutin et al., 2002). It is expected that the action of strong winds interferes with the underlying channel flow in the upper layers of the depth. The magnitude of these changes is not easily quantified in the absence of local wind measurements or without using analytical inferences in conjunction with the measurements.

An additional wind-driven effect existing during our measurements was the vibrations induced to the mast supporting the video camera. This effect is mentioned here just as a cautionary note, as it can be easily overcome with a judicious selection and deployment of the camera support.

difficulty further factor, less apparent during the acquisition of the measurements, was the effect of the bridge structural elements on the flow distribution in the measurement section, as illustrated in Figure 5.5. The bridge piers generate foam trails

www.manaraa.com

(labeled I, II, and III) that travel downstream through the openings between the piers. The foam is generated upstream by the weir as described above. In between the trails there are regions of three-dimensional flows developed in the wake of the piers. The velocity distributions shown in Figure 5.5a, b, and c support well these visual observations. Figure 5.5a displays the depth-averaged velocity at 21 nodes obtained along the cross-section A-B. Each node defines a point where averaging was applied to ADCP pings (vertical velocity profiles) collected in 3 m radius areas around the point. The averaging is dubbed as spatial averaging and was applied to data acquired from the five transects. Vector components are represented in a river-attached coordinate system with the streamline direction defined by the mean direction of all the vectors acquired in the five repeated transects. This is a procedure previously suggested by ADCP users (e.g., Dinehardt and Burau 2005). Given that the sampling frequency of the ADCP used in these measurements was 1 Hz, the samples used for spatial averaging are equivalent to a temporal averaging of 45 seconds.

Figure 5.5b shows vertical velocity profiles obtained with the spatial averaging described above. Detailed inspection of these profiles allowed us to observe that the velocity profiles in regions I, II and III were 10-15% larger than the profiles between the regions, corresponding to the pier wakes. Figure 5.5c displays the span wise distribution of the spatially averaged vector field. The three averaged vector fields clearly indicate the presence of the piers to correspond to the “dents” in the horizontal velocity distribution (Figure 5.5b), the non-typical vertical distributions (Figure 5.5c), and the presence of the secondary currents in the cross section (Figure 5.5d).

www.manaraa.com

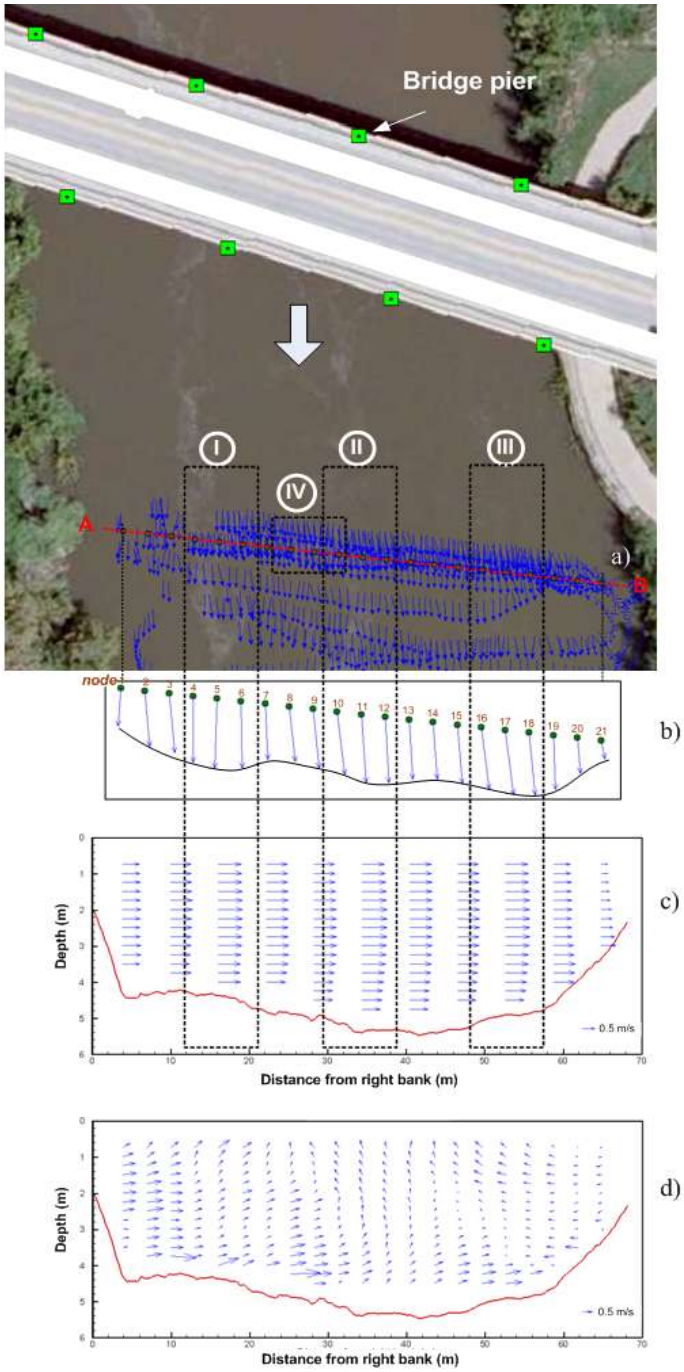


Figure 5.5 ADCP data illustrating the effect of the bridge pier on the downstream flow: a) view of the site with raw measurements averaged over depth (all transects); b) total depth-averaged computed in 21 nodes using 5 ADCP transects averaged horizontally in a 3-m radius; c) spatially averaged (3-m averaging radius) vertical profiles for the streamwise velocity component; d) illustration of the secondary currents in the cross section using the distribution of the spanwise velocity component.

www.manaraa.com

The ADCP measurements discussed above were used as reference for LSPIV data. In general, a direct ADCP–LSPIV data comparison is not possible, as the ADCP cannot measure at the free surface. The first measurement point in the ADCP velocity vertical was located at 0.76 m from the surface. The ADCP vectors used for comparison represent spatially averaged data from the five repeated transects in a radius of 3 m centered on the grid nodes and also depth averaged (double spatial averaging). The LSPIV vectors were obtained after several post-processing tests were applied to the recorded images to eliminate the effect of mast vibration and to limit the effect of the wind effect on the processed data. These post-processing tests included averaging over increasing time periods of contiguous recordings (from 2 seconds to 5 minutes for consecutive image pairs) and using different sampling strategies (continuous versus randomized with variable sampling times). The LSPIV vector field provided in Figure 5.5a, for example, was obtained by using video segments (amounting at 5 minutes) selected randomly from the total of 15 minutes recording.

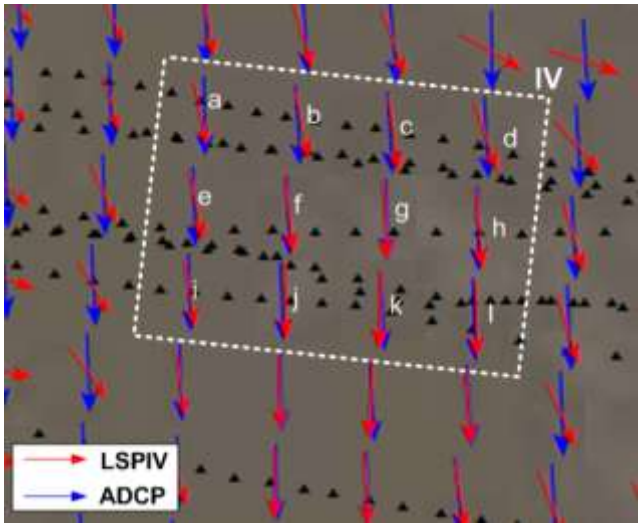


Figure 5.6 Averaged total vectors obtained with LSPIV and ADCP measurements

www.manaraa.com

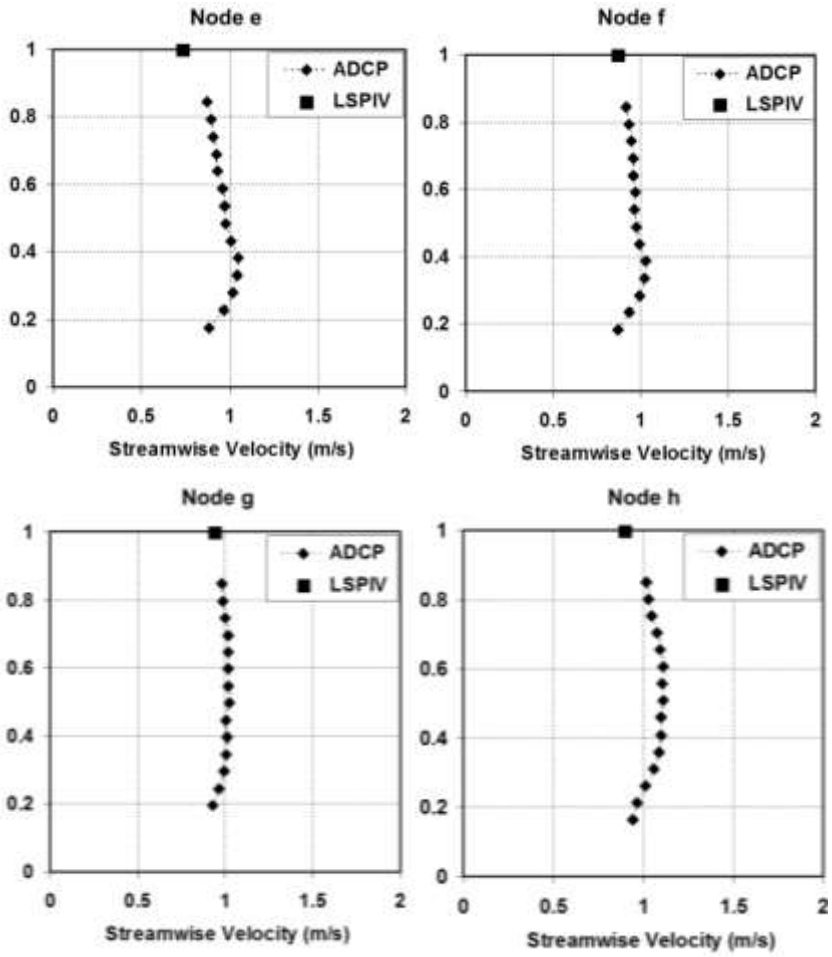


Figure 5.7 Velocity at the free surface (LSPIV) and in the vertical (ADCP) at the same location

Figure 5.6 displays ADCP and LSPIV velocity vector fields on an area of about 100 $m^2$, labeled IV in Figure 5.5a. Comparison of the vector fields collected with ADCP and LSPIV suggests that the measurements with the two instruments are in good agreement. Consequently, it can be hypothesized that the wind was not disturbing the LSPIV measurements for the area subjected to analysis. Vertical velocity profiles at nodes e, f, g, h (in the central area of the analysis) show that the LSPIV velocity measurements at the free surface are biased low (Figure 5.7). Slightly lower velocity in the upper layers of the depth for the ADCP measurements can be attributed to the bias

www.manaraa.com

associated with the near-transducer errors (Muste et al., 2010). The "dipping' of the velocity at the free surface is a finding that was reported by several previous studies in both laboratory (Yang et al., 2004) and field conditions (Dinehardt and Burau, 2005; Nezu et al., 1993). A potential contributor to this lower velocity is the presence of secondary currents in the channel. The plots shown in Figures 5.7 and 5.8 suggest, indeed, that in the absence of the wind effect, the deviation of the velocity from the standard logarithmic velocity profile can be most probably related to the presence of secondary currents in the cross-section (see Figure 5.5d). A good illustration of the presence of the secondary currents is shown in Figure 5.8, where the vertical profiles of the spanwise velocity component are plotted. They indicate a clear left-right flow movement at the top and an even larger right-left movement near the bed.

The implications of the existence of a velocity bias for the LSPIV streamwise velocity component are multiple, especially for estimation of the discharges. The routine procedure to estimate discharge measurements from LSPIV data is to assign an index-velocity for relating the free-surface velocity measured by LSPIV to the channel depth-averaged velocity. A value of k = 0.85 is generally accepted for river flows and used in conjunction with other measurement techniques (Costa et al., 2000). The value of the index-velocity coefficient is based on the assumption that the vertical velocity distribution is logarithmic. A low bias at the free surface, which is related to the presence of secondary currents in the cross-section, will considerably affect the discharge estimation. Figure 5.9 illustrates the sensitivity of discharge estimation for different values for the index velocity. Discharges from ADCP are computed for flow volume enclosed in cylinders of 3 m radius centered on computational nodes. The sensitivity of discharge estimation shows that the index value for relating surface velocity and average velocity will be larger than the general value (k=0.85) because of the presence of the secondary current in the channel.

www.manaraa.com

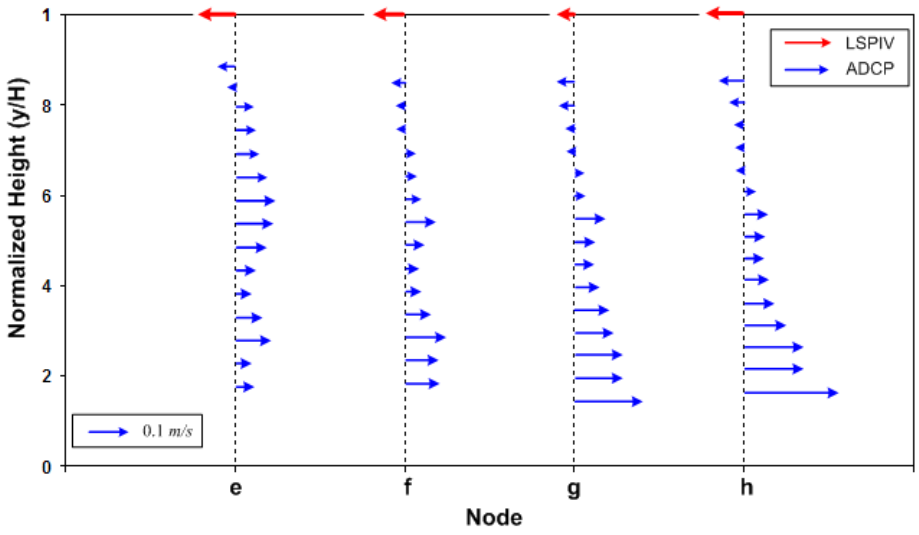


Figure 5.8 Vertical velocity distribution of the spanwise velocity components illustrating the presence of secondary currents

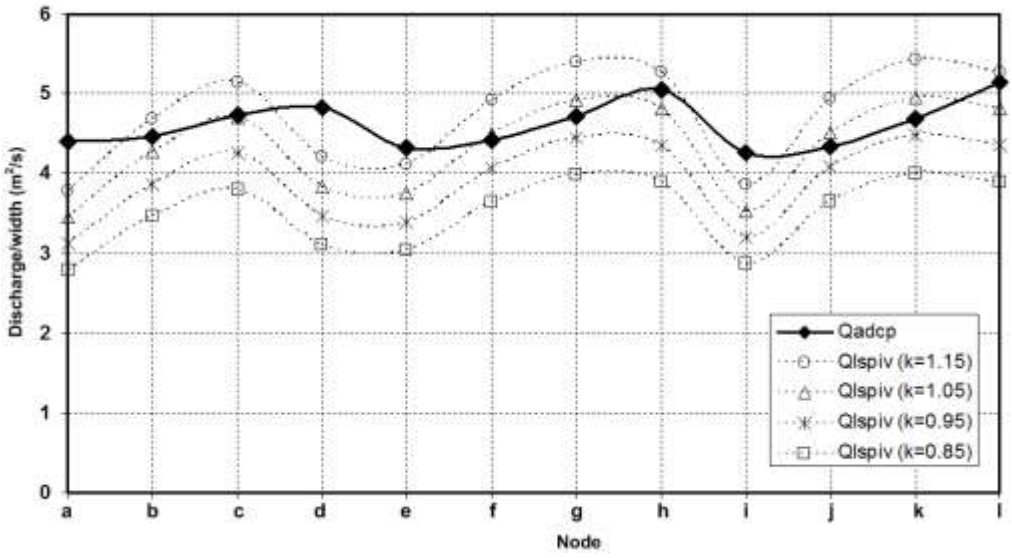


Figure 5.9 Effect of the index-velocity value on the discharge calculation.

www.manaraa.com

## 5.3 Measurement of loop rating curve

LSPIV measurements were conducted in the Iowa River in Iowa City, several days before and after the historic flood of 2008 reached its peak on June 15. The LSPIV measurement site was situated about 250 m upstream from USGS gaging station #05454500 (the same one used for the calibration measurement reported in the previous section). Aerial photos of the measurement site and the area used for acquiring the LSPIV measurements are shown in Figure 5.10. The images were taken using a commercial HD camera (Sony HDR-HC1) positioned on a pedestrian bridge, as shown in Figure 5.10. While not optimal, this bridge site offered the safety needed to take measurements during these critical flood conditions. Previous measurements at this site benefitted from considerably better viewing positions (Creutin et al., 2003, Kim, 2006). Those positions cood not be used for LSPIV measurements during the 2008 flood due to traffic restrictions and power failure. Nevertheless, the proof-of-concept results presented in this section underline the capabilities of the LSPIV to provide acceptable accuracy in a difficult environment..

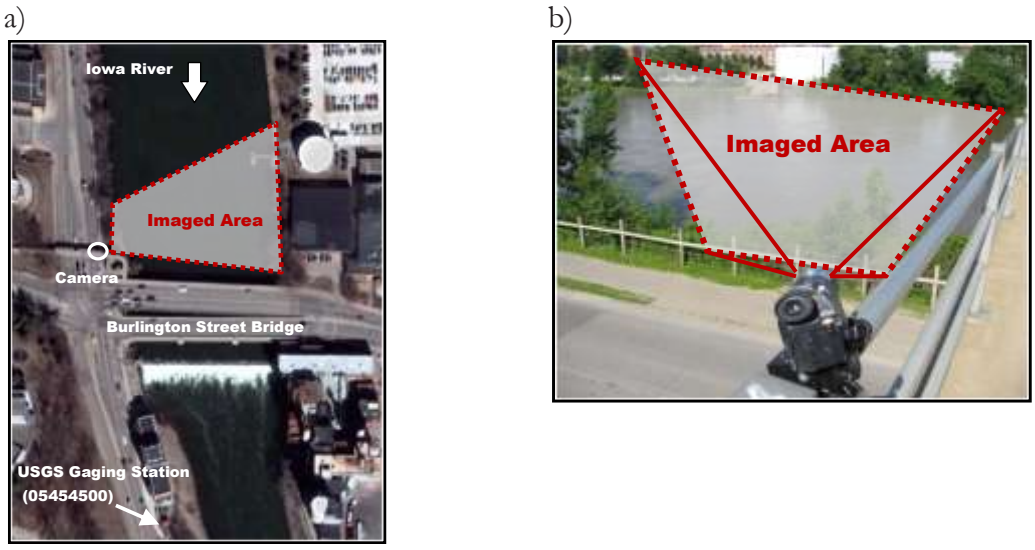


Figure 5.10 LSPIV measurements during the Iowa River flood of 2008: a) location of the measurement site

www.manaraa.com

Figure 5.11 shows the chronology of the LSPIV measurements and photos of the river during the image acquisition period. The peak flow during the flood is considered here as the reference time scale to facilitate the identification of the rising ("-") and falling ("+") limbs of the rating curve (see Figure 5.2). The images reveal the presence of ripples at the free surface. This enabled application of the LSPIV software without the need of additional tracers. The high velocities and turbulence during the flood wave propagation precluded acquisition of measurements with conventional instruments due to the danger posed to the boat and equipment that would have to be deployed in the river during the flood. Also noticeable in the sequence of photos is the variation of the river stage during the flood wave propagation. During normal flow conditions, the free surface at this location is very quiet, as illustrated in Figure 5.3d.

LSPIV measurements reported next were acquired five, four, and two days prior to the flood peak on June 15 and two, three, five, and nine days after the flood peak. The hydrograph of the site shown in Figure 5.11 indicates that for this time period the flood wave overtopped the spillway of the Coralville Reservoir Dam located 13.2 km upstream from the measurement site. During normal flows, the discharge in the river reach downstream of the dam is controlled by a sluice gate located at the bottom of the dam. The dam overtopping created a good context for this study, as it provided a flow situation in the Iowa River where the flood wave propagation was minimally obstructed by the presence of the controlling structure. During the flood propagation, the Iowa River did not reach the bankfull stage at the measurement location.

Figure 5.12 summarizes the LSPIV results for this measurement campaign. Figure 5.12a replicates video frames acquired at the site on June 10$^{th}$, 2008. Figure 5.12b shows the velocity distribution at the free surface superposed on the ortho-rectified video recording. The vector field was obtained using 100 images recorded over 10 seconds. Observe that the velocity vectors are missing near both river banks. A small area along the bank is hidden in the near field, as the bank on this side is steep. In the far field, the

www.manaraa.com

image resolution is poor because of the large distance and the reflections of nearby buildings on the river free surface (see Figure 5.11). These effects are also visible in the cross-section velocity profiles shown in Figure 5.12b. The cross-section velocity profiles maintain their shape but shift up and down during the flood wave transition, with the maximum velocity varying between 1 m/s and 2 m/s.

The discharges for the seven LSPIV measurements acquired during the dam overtopping are plotted in Figure 5.12d against the rating curve at the USGS station. The velocity-area method was used to calculate the discharge based on the velocity profiles shown in Figure 5.12c and the cross section and river stage at the site. The bathymetry data were acquired after the flood using a multi-beam sounder (Reson Seabat 7125). The river stage was established using recorded video images, in conjunction with additional scaling applied to the water intake located in the river. The seven LSPIV discharges fall on the extrapolated area of the rating curve (dotted line in Figure 5.12d). The need for using extrapolation is because there are no other direct measurements taken during the flood at this location. The extrapolated portion of the curve is based on the direct measurement taken at low flows (continuous line in Figure 5.12d). The rating curve at this site is produced by USGS and adjusted occasionally to verify if the cross-section is stable. There are no indications that the bathymetry has changed over time in the area where the LSPIV measurements were taken (Goodrich 2008, personal communication).

The plot displayed in Figure 5.12d indicates that the seven LSPIV measurements do not coincide with the rating curve obtained with conventional methods. The LSPIV discharges follow the overall trend of the USGS rating curve, but they do not collapse on a unique curve for the rising and falling limbs of the flood wave propagation. The results suggest a relationship between stage and discharge similar to the conceptual rating curve shown in Figure 5.2. The loop curve inferred based on the LSPIV measurements shows stage differences of up to 0.5 m for the same discharge value, depending if the measurements were taken on the rising or falling limbs of the flood wave propagation.

www.manaraa.com

Such differences are critical when the data are used for monitoring and warning systems or as input for flood forecast models.

The results presented in this section contribute new measurements to the continuously growing number of field applications of LSPIV. The innovative aspects of this study consisted in exploring the reliability of the traceless LSPIV method and its application to acquire velocity measurements during extreme floods. It is known that the free surface appearance is function of stream bulk velocity, bed roughness, flow depth and channel geometry (Polatel, 2005). The traceless LSPIV method was successfully tested in alpine and subalpine streams (Creutin et al., 2002; Fujita and Hino, 2003; and Hauet, 2006). There are, however, less traceless LSPIV measurements available for flat relief rivers, such as those typically encountered in the U.S. Midwest (e.g., the Iowa River). In these cases, traceless LSPIV measurements are not possible during normal flows in the river (up to 400 $m^3/s$), as the free surface has a mirror-like appearance. Another innovative feature of the measurements described in this section is the capturing of the rising and falling stages of the flood wave propagation through a site. The measurements proved that LSPIV is a reliable and cost-effective remote measurement technique that can be used to accurately measure discharge during large floods. For such extreme conditions, use of other instruments to provide estimation of the discharge in the river is not possible. The only generally available source of streamflow information for the 2008 flood event is based on the extrapolation of data in the USGS rating curve at the same location. Using this rating curve, the National Whether System overpredicted the peak stage by 0.54 m (1.5 ft) and predicted the flood peak stage will arrive in Iowa City two days after it actually occurred during the flood event. The fact that forecasting is inherently related to historical and current streamflow information derived directly from available rating curves emphasizes the relevance and the importance of the research issue considered in the present chapter.

www.manaraa.com

The societal and economic implications of inaccurate flood forecasting are obvious. As previously described, there is an immediate need for new methodological and measurement approaches to improve the accuracy of the existing rating curves, especially in their extrapolated area. The need is even more pressing as the use of analytical or numerical simulation results attempted so far has not led to a commonly accepted procedure (Perumal et al, 2004). Data collection during major floods is not only important for forecasting purposes but also because it enables testing scientific hypotheses on river processes and supports regional analysis and estimation of streamflow information at ungaged sites.

## 5.4 Summary

The results of the LSPIV measurement technique applied to flow in the Iowa River established that the technique is adequately reliable for use in addressing the study's principal topic of sedimentation at multi-barrel intakes. LSPIV is shown to yield detailed velocity vector fields revealing flow distributions in field situations. The ensuing chapters of the thesis document the technique's use in field and laboratory application.

www.manaraa.com

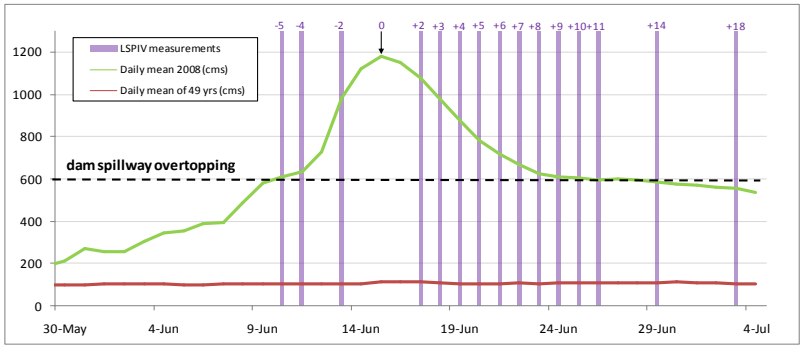

Figure 5.11 Chronology of the measurements during the flood wave propagation and video frames of the recordings considered in the present analysis



www.manaraa.com

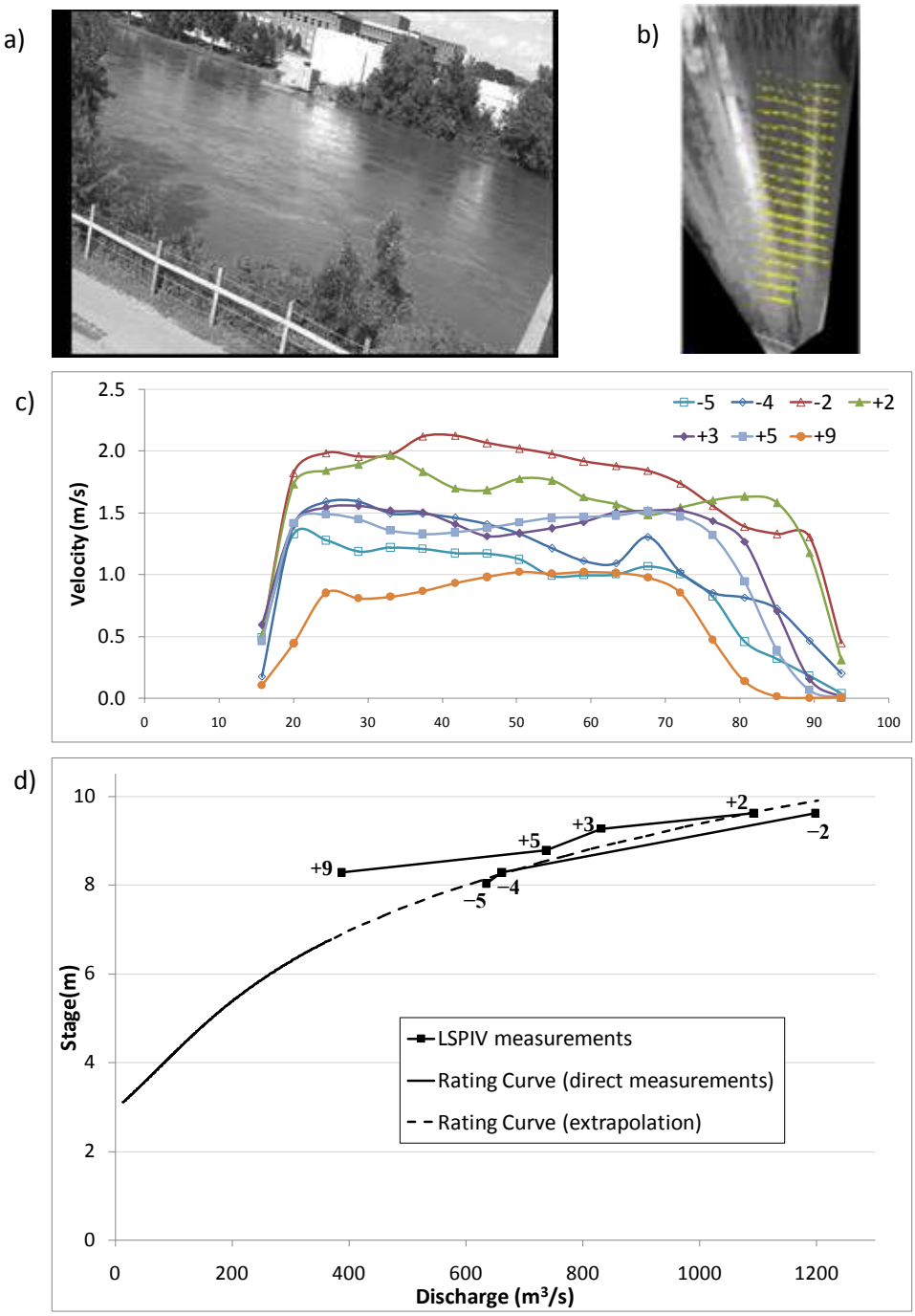


Figure 5.12 Rating curve measurements: a) video recordings acquired on June 10th, 2008, b) vector field, c) cross-section velocity profiles used for discharge measurements, d) LSPIV discharge estimates superposed on the rating curve of the USGS gaging station.

www.manaraa.com

# CHAPTER 6
# RESULTS FROM INVESTIGATIONS OF SEDIMENT DEPOSITION AT CULVERTS

## 6.1 Overview

This chapter presents the results obtained from the field, laboratory, and numerical investigations of sediment deposition at the culvert geometries described in Chapter 4. The experiments were phased so that field observations were conducted first (and afterwards whenever was considered necessary from the monitoring point of view). Subsequently, the modeling through complementary hydraulic model and numerical experiments was carried out. Inferences from each research stage were translated to the next stage. Finally observations inferred from all research phases were compiled in a unique framework to provide the needed insights for further practical action, such as the culvert streamlining discussed in Chapter 7.

## 6.2. Hydraulic model experiments

The laboratory investigation in this section to supports work toward attaining the study's objective of identifying the propensity and location of sediment deposition and accumulation at a representative culvert entrance. A series of, the flow features were added into the experiments to be able to distinguish among the flow features contributing to the observed sediment deposition at culverts.

A three-box culvert design was used, because it is typical of box culverts in Iowa, and the U.S. generally, and because field observations are available for such culverts. The field observations benefitted the conduct of the laboratory experiments. It is noted here, that two-box culverts have the same sedimentation problems, but they were not simulated for the experiments; the problems may not be as severe as at three-barrel culverts.

www.manaraa.com

A simple geometry is used as the basis for the study: i.e., a channel approaching the culvert at normal angle, typical culvert geometry with wing walls and expansion area. Channel transitions involving expansion and contraction were included in all models, because they are enhancing the non-uniform nature of the flow in the culvert area. These expansions were also included in the prior studies (Charbeneau 2006). From the hydraulic point of view, the designed experiments entailed both clear-water as well as live-bed experiments. The former experiments were conducted using a 1:20 scale model; the latter experiments were conducted using a 1:5 scale model. Both models and the flumes containing them are described in Chapter 4.

A simplifying assumption made for the experiments is that sedimentation at culverts is mainly associated with bed load transport. While it is expected that the suspended-sediment transport worsens culvert sedimentation, it is assumed that bedload transport is the major cause of sedimentation. The finer particles in suspension would pass with flow through a culvert. The field observations supported this assumption. Therefore, by employing the bed load experiments was deemed to be sufficient in order to track the overall sedimentation process and to develop design approaches for sedimentation mitigation.

The experiment approach entailed qualitative, or visual, evaluation of sediment deposition. Quantitative evaluation of deposition rate and sediment discharge concentration was not needed for these early experiments. The program of experiments comprises baseline, validation, screening, and performance series of experiments. The baseline experiments used two hydraulic models (scale ratio 1/20, labeled as model 1/20A and 1/20B) with fixed boundary to obtain a qualitative evaluation of sediment accumulation at traditional culverts. The validation experiment used the relatively large hydraulic model (scale ratio 1/5, labeled as 1/5B). Model 1/5B is with loose boundary to validate the tests performed with model 1/20B. The screening experiments, presented in the next section, were operated with model 1/20A. The cross section of model 1/20A

www.manaraa.com

makes tests convenient for quickly checking the possible effectiveness of self-cleaning concepts, and eliminating concepts found not to hold good promise for being effective. The performance experiments, presented in Chapter 7, investigated the performance of the self-cleaning culvert system with model 1/5B.

### 6.2.1 Baseline experiments

The baseline experiment conducted with the model 1/20A and 1/20B simulated different hydrological conditions in which the culvert model kept in the un-submerged situation. The velocity distribution in the approaching channel was maintained uniform in all experiments. The baseline experiments included six tests. The first two tests, however, can be considered preliminary as they were only aimed at checking the impact of the operating conditions and of the modeling assumptions used in the hydraulic modeling, hence their subsequent use in the study.

The first test investigated the regions in which sediment particles are deposited in the model under four different flow conditions. The second test verified if the deposition patterns provided by suspended sediment load are the same as those provided by the bead load. The third test was extended the operation time for the case which made the most serious deposition. The fourth test was similar to the previous tests but operated in the model 1/20B. The fifth test was to measure velocity distribution in the interested area around the culvert model by using LSPIV. The last test simulated sediment transported with the “stepped” hydrograph.

#### 6.2.1.1 Test 1: Sediment mobility and deposition patterns for a range of flows

To examine sediment mobility through the model culvert, four flow conditions were tested (see Table 6.1 and Figure 6.1). Flow velocities in the approach channel were varied from 1.32 ft/s to 0.92ft/s, with a constant sediment load added into the channel by

www.manaraa.com

the cylinder. The sediment served essentially as a tracer to delineate the potential region of sediment accumulation. The investigated areas were focused in the expansion and culvert barrels. If sediment accumulated in the channel, the velocity was not sufficient to transport sediment and not be considered for the following tests. Observations from the four cases are presented in Figure 6.2. All modeled flow conditions were with the un-submerged control situation for which flow depth did not exceed culvert height.

Cases A and B had flow velocities 1.36 ft/s and 1.28 ft/s in the approach channel. Sediment did not accumulate, but constantly moved in the channel for both flow conditions, even though dunes developed in it. Local sediment accumulation was observed in the expansion at the channel inlet. Figure 6.2 (a) and (b) show the results of case A and, respectively, B that ran for one hour. It was observed that sediment was prone to deposit and accumulate in the right and left region.

Table 6.1 Four flow conditions tested in Test 1

| Case | Discharge ($ft^3/s$) | Headwater (ft) |
|---|---|---|
| A | 0.150 | 0.220 |
| B | 0.163 | 0.250 |
| C | 0.172 | 0.300 |
| D | 0.180 | 0.392 |

www.manaraa.com

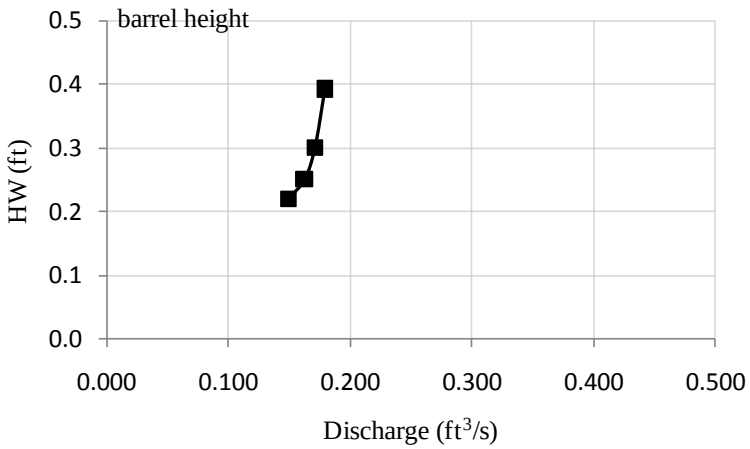


Figure 6.1Trial flow conditions of Test 1

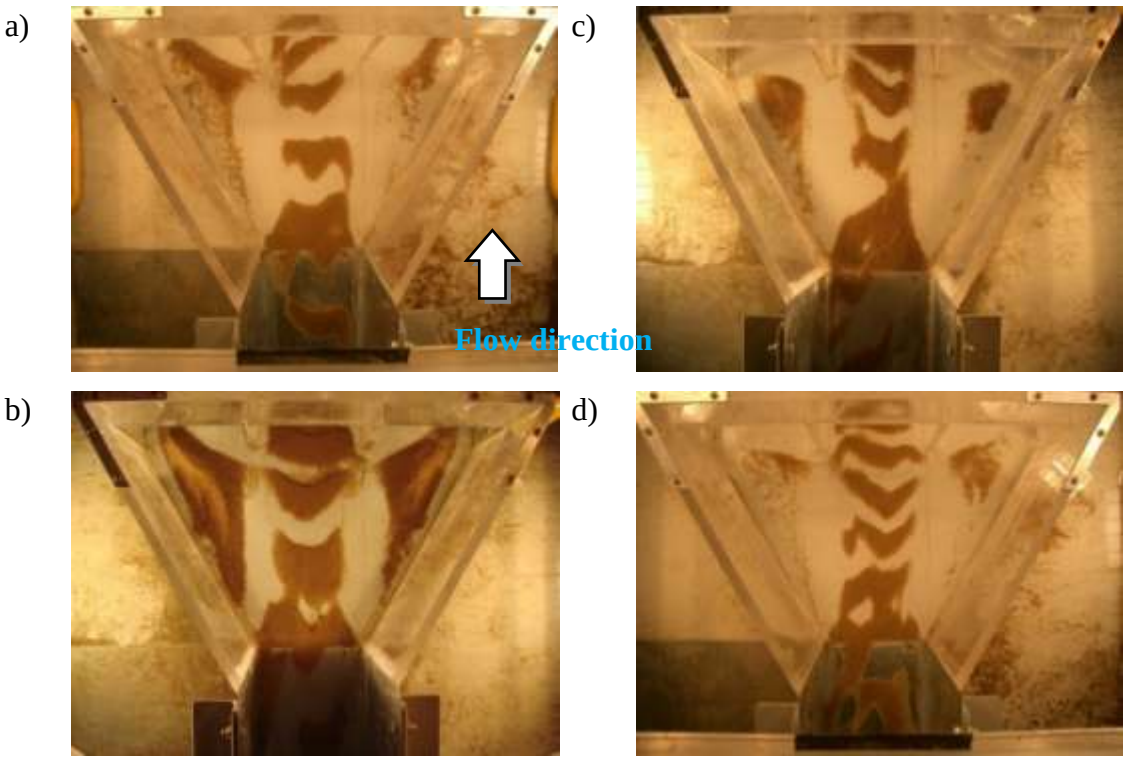


Figure 6.2 Sediment accumulation upstream the culvert. The sediment patterns illustrated in photos a) to d) above illustrates the results of the simulations with steady flows set for cases A to D in Figure 6.1.

www.manaraa.com

Figures 6.2c and d show the results for both cases C and, respectively, D, after one hour operation. Sedimentation in the expansion seemed milder in the expansion because sediment accumulated in the channel. The flows for cases C and D had average velocities 1.15 ft/s and 0.92 ft/s respectively in the approach channel. Sediment mobility in the channel was lower compared to previous two cases. Sediment accumulated in the channel and less sediment load was transported into the culvert model section. Therefore, both flow conditions were not used in subsequent tests.

6.2.1.2 Test 2: suspended versus bed load transport

The assumption that bed-load transport is mainly responsible for the sediment deposits in the culvert entrance required assessment. For this purpose, an experiment where only suspended sediment was fed in the facility was designed for a flow that was tested before with bed load. The selected flow condition is case B. Sediment was supplied above at the free surface using the rolling sediment feeder in the same section where the sediment was released as bed load in previous experiments. Crushed nut shell was served as the model suspended sediment particle for this test, instead of silica sand. The transport rate was kept below the transport capacity in order to avoid bed forms developing in the channel. Figure 6.3 shows the result of sediment deposition around the culvert.

The sediment particles moved as suspended load without deposition in the channel. The dunes were formed in the expansion, and sediment deposited in the barrels. The secondary current reduced the transport capacity in the sides of the expansion, but not in the central region of the expansion. The deposition patterns developed upstream the culvert were similar to those formed in the experiments with bed load as illustrated in Figure 6.3b. The experiment enforced the assumption that the low flow areas are the culvert regions where it is expected to encounter sediment deposits. The combination of

www.manaraa.com

the sediment transport fraction would accelerate the rates of sediment buildup. A further inference to be drawn is that bed load experiments are adequate to track the overall sedimentation process and then to develop approaches for sedimentation mitigation. Although the mechanisms between bed load and suspended load are different, we can assume that the approach worked for bed load can also succeed to suspended load for the similar deposition pattern.

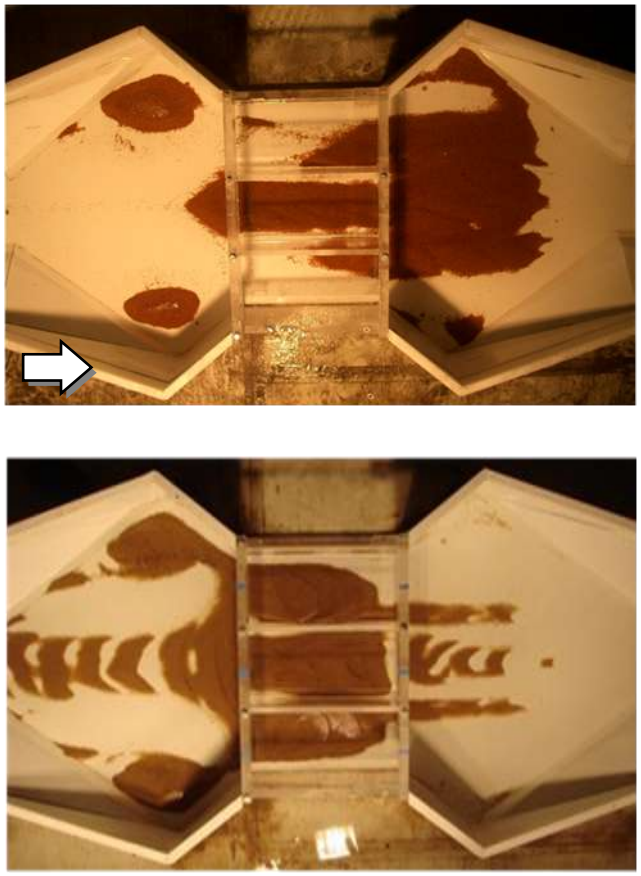

Figure 6.3 Sediment deposited at the culvert: a) using suspended load (crushed walnut shells); b) with bed load (silica sand)

www.manaraa.com

6.2.1.3 Test 3: Sediment accumulation rates

The objective of this test was to record the sediment deposition patterns occurring in the expansion and the culvert barrels at different time. Model 1/20A, described in the above section, was used for this purpose. The test was only conducted for a specific flow condition (case B), and the operating time was from one to six hours.

Overall, the six images which were taken every hour showed that sediment accumulated in the sides of the expansion, but did not in the central region. Sediment accumulation is not easy to detect from the images taken from the top view. To evaluate the sediment accumulation, the sediment load in the expansion, and three barrels were separately collected (Figure 6.4). The elevations of dunes formed by sediment accumulated were also quantitatively recorded. Figure 6.5 shows sediment load accumulated in different zones with different running times, and Figure 6.6 shows the change in the elevation of dunes with time at the highest deposition point. The result reveals that sediment deposition in the central barrel was constant, but sediment gradually accumulated in the right and left barrels. In Figure 6.5, the accumulation in the expansion increased from the first hour to the fourth hour, and then became constant. The analogous result was confirmed by determining the variation of dune height in right and left parts in the expansion in Figure 6.6. The test led to the following observations:

1. Flow has the capacity to transport sediment in the center barrel;
2. Sedimentation in the side barrels increased and reduced the culvert's capacity to convey flow (sedimentation led to an increase of water stage); and,
3. Sediment accumulation in the expansion grew until attaining an equilibrium size.

www.manaraa.com

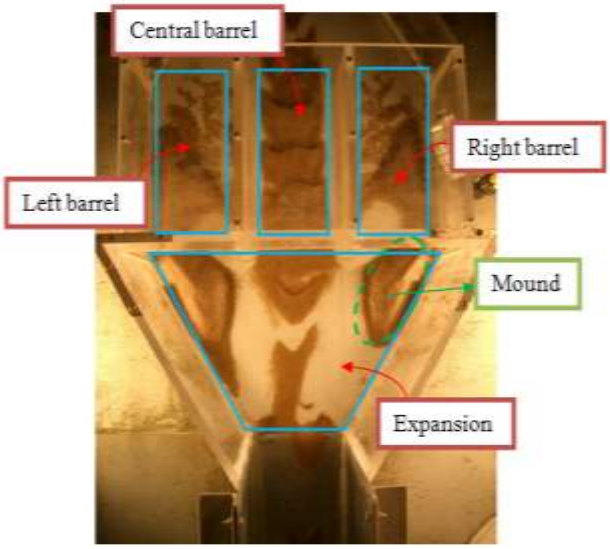


Figure 6.4 Sediment load distribution

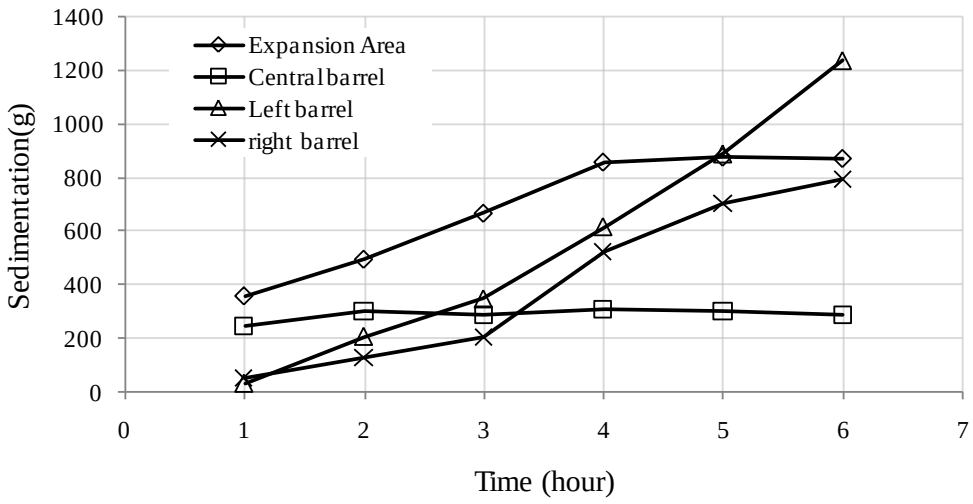


Figure 6.5 Rate of sediment accumulation in expansion and three barrels

www.manaraa.com

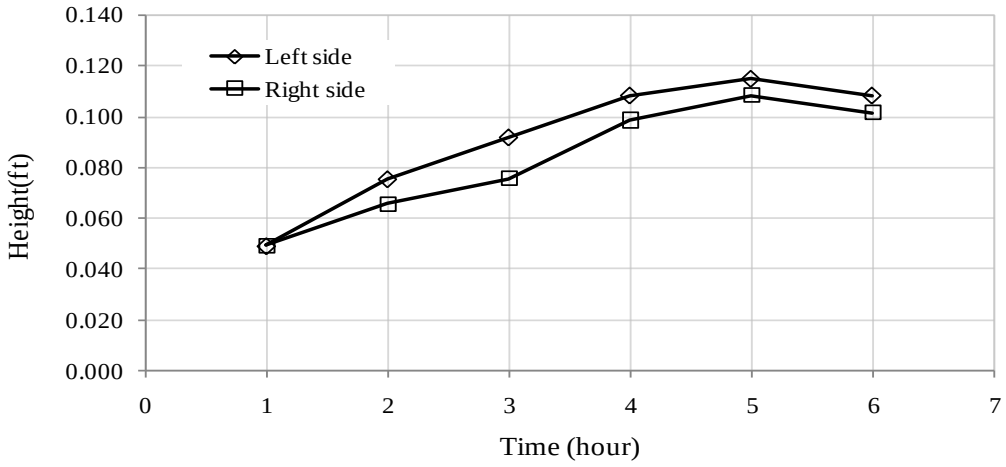


Figure 6.6 Mound height variation from one-hour to six-hour

6.2.1.4 Test 4 Baseline flow

The tests described in Sections 6.2.1.1 and 6.2.1.3 were aimed at determining the propensity of sediment to move hrough the culvert. Uneven sediment accumulation in the barrels reflected the nonuniformity of flow distribution through the barrels . Baseline test 4 was conducted to better understand sediment deposition in expansion and culvert barrels. A different culvert model (1/20B) was designed and implemented to include the culvert wingwalls that are associated with the standard box-culvert designed by Iowa Department of Transport (IDOT). The model channel geometry consisted of two trapezoidal cross sections with a 1:1 slope for the walls of main channel and a 4:3 slope for the flood channel. Wingwalls are connected to the edge of culvert barrels. Figure 4.1b shows the layout of the model. The first part of the test was conducted under three hydrological conditions. All the modeled flows were with the culvert in an un-submerged control situation, and with water flowing through the culvert's three barrels(Figure 6.7).

www.manaraa.com

Table 6.2 Three flow conditions tested in Test 3

| Case | Discharge ($ft^3/s$) | Headwater (ft) |
|---|---|---|
| A | 0.065 | 0.125 |
| B | 0.240 | 0.250 |
| C | 0.368 | 0.382 |

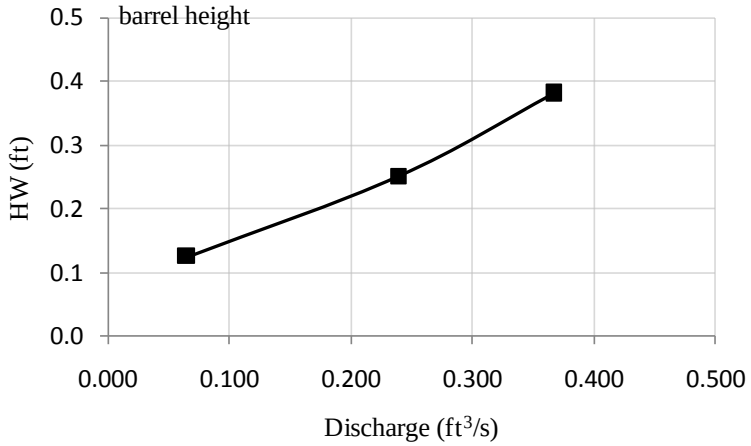


Figure 6.7 Flow condition in baseline test 4

The depth of the culvert was 0.5ft in the model, corresponding to 10ft in the prototype. Three water depths were investigated. The design discharges based on the water depth were calculated with the equation (2.9). Three cases were used to present three hydrological events from small to large. Case A was with flow depth at a quarter of the culvert height (HW/D=0.25), case B was half depth of it (HW/D=0.5), and case C was with depth at three-quarters of culvert height (HW/D=0.75).

A subsequent part of this test examined bed-sediment movement through the culvert over an extended time interval of six hours. This experiment was only done for case B, which produced the greatest sediment deposition around the culvert. The sediment deposition pattern was photographed for all the cases.

www.manaraa.com

Overall, sediment gradually deposited and accumulated in the right and left regions of the culvert approach. The desposit gradually encroached across the central region of the approach. Figure 6.8, for example, shows the result of sediment deposition after two hours. The amount of sediment accumulated in the different zones was measured as described in Section 6.2.1.3. Figure 6.9 shows that sediment deposition in the central barrel was constant and least. Sediment accumulated in the expansion grew quite rapidly, and it grew slowly in the side barrels.

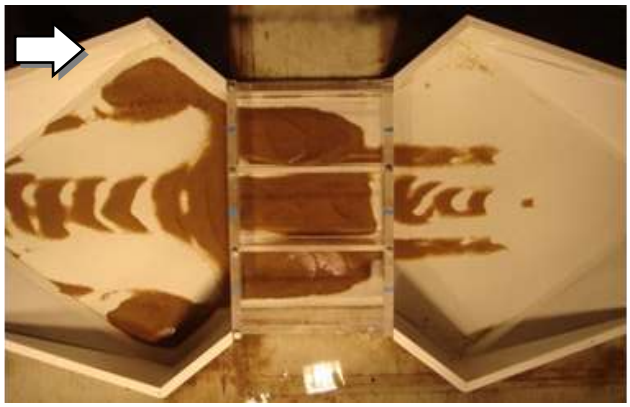

Figure 6.8 Sediment deposited after 2 hours for case B in model B

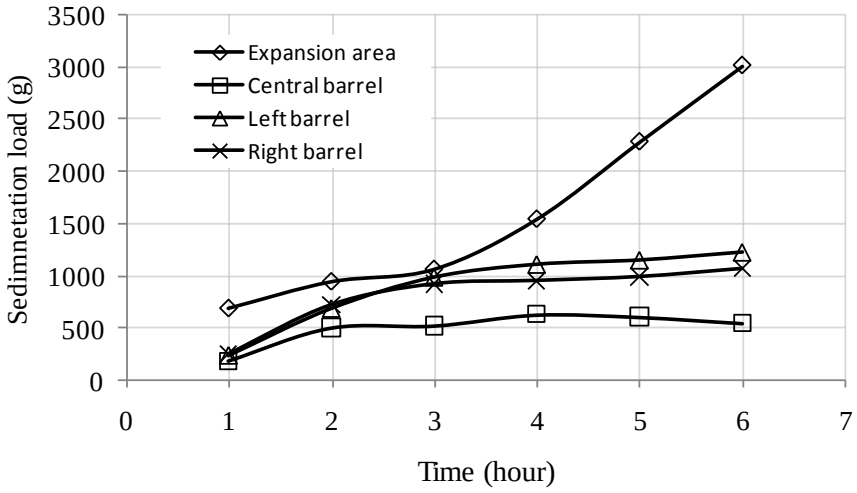


Figure 6.9 Rate of sediment accumulation in the culvert area for flow case B

www.manaraa.com

6.2.1.5 Test 5: Flow kinematics through the culvert area

The Large-Scale Particle Image Velocimetry (LSPIV) technique was used to obtain surface velocity distribution in the approach expansion. A digital camcorder (Sony HDR-HC1) was used to record successive images (30 fps) and in-house developed software was used to analyze the velocity field. The results are presented in three forms to delineate the secondary current on the water surface: average velocity vector distribution, average velocity contour, and streamlines. The measurements with LSPIV confirmed that the velocity distribution was slightly asymmetric though without significant implication for the modeling conclusions.

Figure 6.10 shows the Baseline Test result from case B, and Figure 6.11 from case C. The flow distributions on the water surface for both cases were similar. The velocity distribution in the expansion was not uniform. Flow entering the expansion acted like a jet. Secondary circulation was observed in the sides of the expansion which denotes that sediment particles would deposit in these zones. Moreover, the result shows that velocity was much greater in the central barrel than in the side barrels. This observation meant that the discharge through the central barrel is much greater than through the other barrels, an undesirable performance in terms of culvert design. The design performance of a multi-barrel culvert assumes uniform discharge distribution among all barrels.

www.manaraa.com

a)

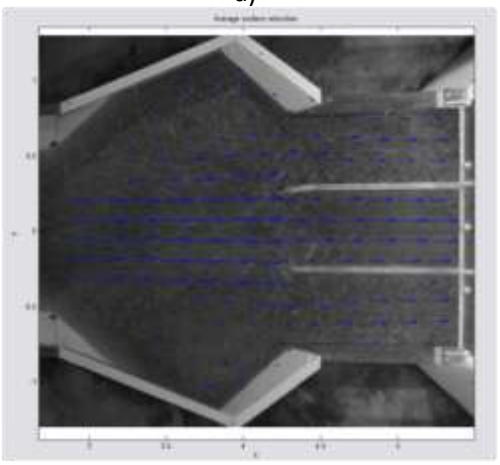

b)

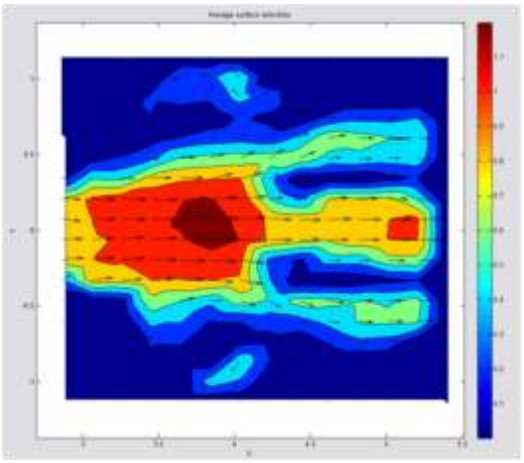

c)

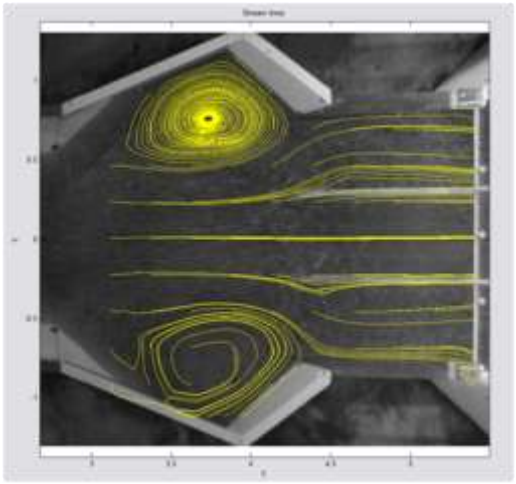

Figure 6.10 Surface flow field for the case B with headwater depth 0.255ft: (a) Velocity vectors, (b) Velocity vectors and velocity magnitude contour, (c) Streamlines

www.manaraa.com

a)

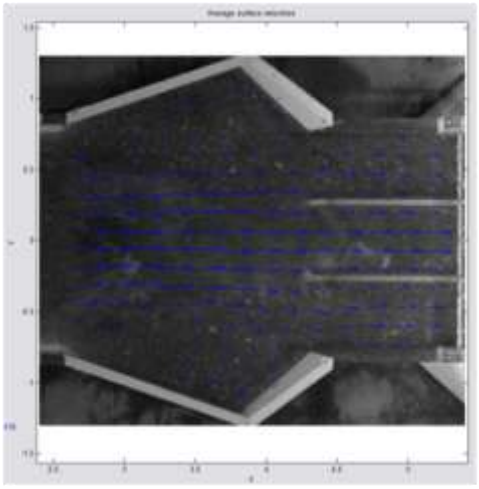

b)

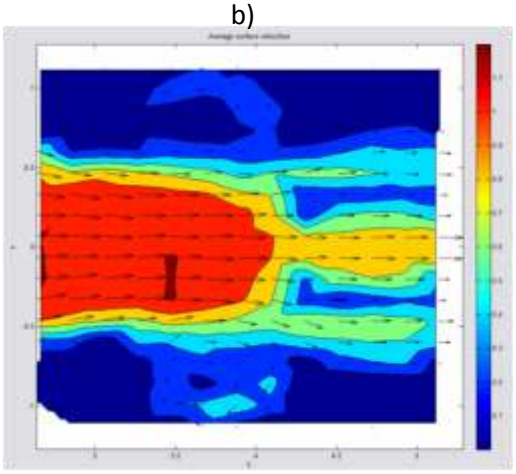

c)

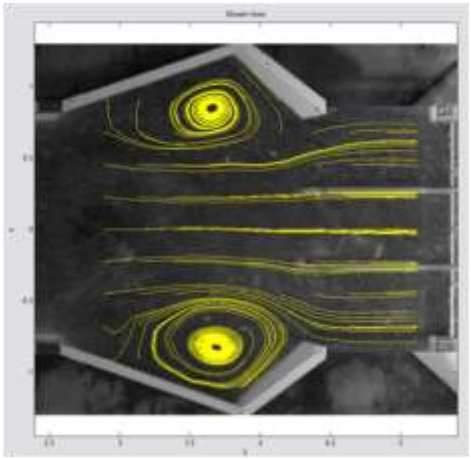

Figure 6.11 Surface flow field for Flatbed C with headwater depth 0.382ft: (a) Velocity vectors, (b) Velocity vectors and velocity magnitude contour, (c) Streamlines

www.manaraa.com

6.2.1.6 Test 6: Simulation of discrete sampled hydrograph

The model culvert uses a standard culvert design, and does not pre-suppose a rating curve for flow variation during the passage of a flow hydrograph. Therefore, no specific discharge-stage curve could be provided a priori for the model. In the absence of such information the sediment and flow combination were kept constant for each flow condition at pre-established water and sediment rates. The simulation of flow hydrograph events was approached using a "stepped" approach, whereby one flow was ran for a given period to reach and run for an established time under equilibrium. Subsequently, the resulting sediment deposition pattern was photographed after the operation was stopped. The flow was then set at the next set of operating points and run for an established time under equilibrium and subsequently stopped to allow a new photo documentation of the sedimentation patterns.

The first experiment in this series used three flow conditions that follow the conventional culvert design curve described by the equation (2.9). The adjustable rotating cylinder (Figure 4.2) was used to supply sediment into at constant rate into the channel for all three flow conditions. All the modeled flows were modeled for the culvert operating in an un-submerged situation (Figure 6.12). Three cases were used to present three hydrological events: case B was half depth of the culvert (HW/D=0.5), case C was 3/4 depth of the culvert (HW/D=0.75), and case D was close to the depth of culvert (HW/D=0.95).

Table 6.3 Three flow conditions tested in Test 6

| Case | Discharge ($ft^3/s$) | Headwater (ft) |
|---|---|---|
| B | 0.240 | 0.250 |
| C | 0.368 | 0.382 |
| D | 0.466 | 0.470 |

www.manaraa.com

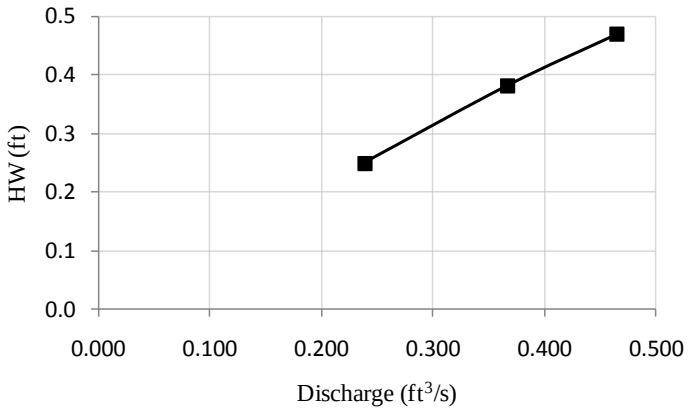


Figure 6.12 Hydrological events investigated in the culvert model

The stream power in the approaching channel based was calculated assuming that the power is the product of force and velocity in the channel:

$$\text{Power=Force} \times \text{velocity} = (\tau A) \times U = \tau \times Q \tag{6.1}$$

$$\tau = \gamma R S_E \tag{6.2}$$

The results respectively are 0.0026 (ft-lb/s), 0.0025(ft-lb/s), and 0.0022(ft-lb/s) for three cases. Accordingly, the stream power for all flow conditions in the channel is approximately constant. Therefore, it can be inferred that if the sediment was added constantly from the beginning of the approaching channel and no pile of sediment deposits in the channel was formed, the sediment load in the channel can be assumed the same in all flow conditions. The modeling was conducted in steps from the lower flow condition to higher flow condition, and back to the lower flow, i.e., case B→case C→case D→case B. Figure 6.13 shows the result of sedimentation around the culvert model. The photographs reveal that the sediment does not deposit within the culvert model under higher flow conditions approaching the culvert's flow capacity. Another modeling scenario was conducted in steps connecting the following flow conditions: case

www.manaraa.com

B→case C→case B (see Figure 6.14). The resemblance of sedimentation pattern between Figure 6.13d and Figure 6.14 led to the conclusion that sediment does not excessively deposit under higher flow conditions. Therefore it is concluded that a self-cleaning process is already partially in place for high flows passing through the culvert during storm events.

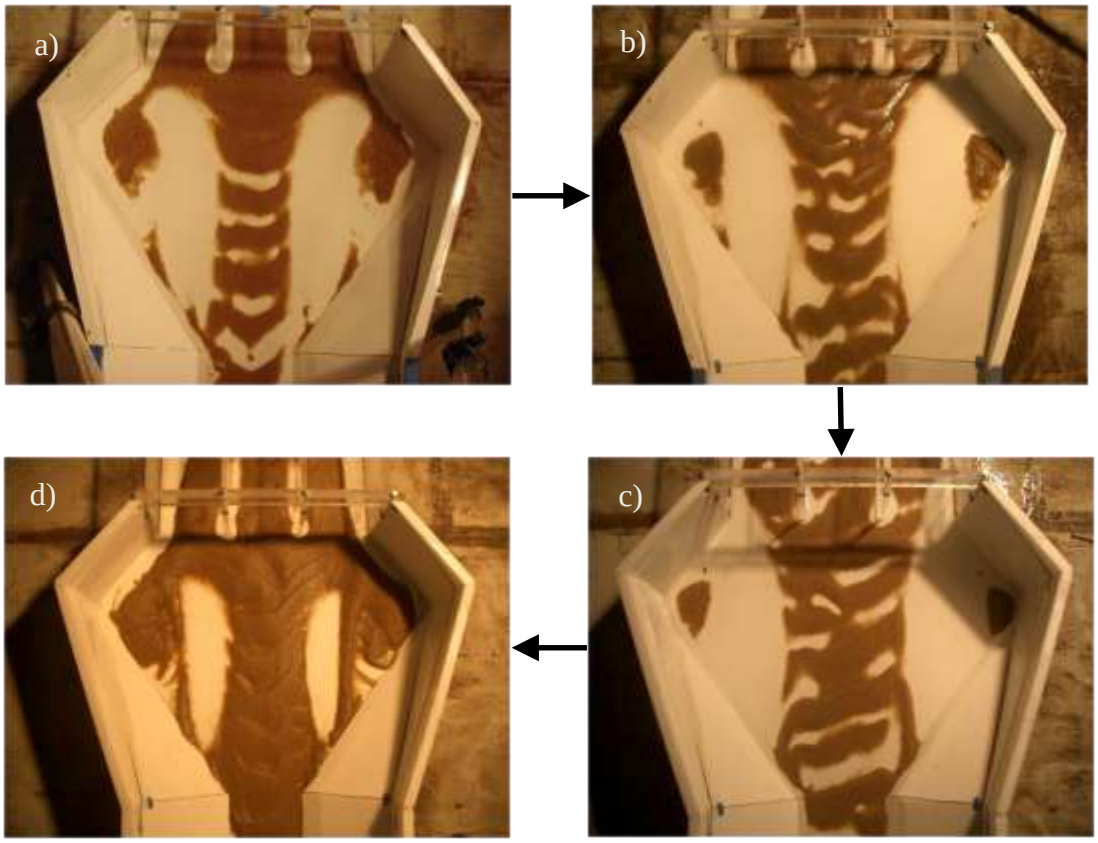


Figure 6.13 Consecutive simulation of hydrological events: a) case B, b) case B→ case C, c) case B→ case C→ case D, and d) case B→ case C→case D→ case B

www.manaraa.com

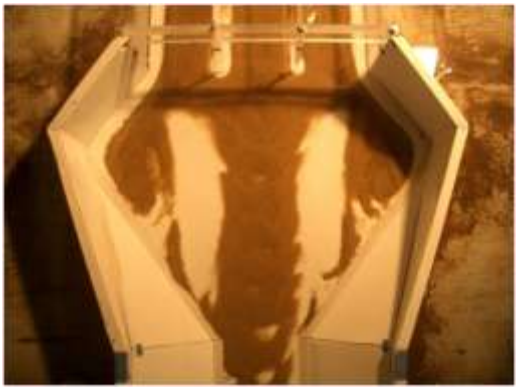

Figure 6.14 Consecutive sedimentation: case B→case C→case B

The following two experiment cases present the sedimentation patterns resulting by modeling high and low flow conditions. The first case aimed at investigating the sedimentation patterns developed by stepping from case C to case D. The result (see Figure 6.15a) confirmed the aforementioned situation. Sediment deposition pattern after operating case B for two hours was also investigated and shown in Figure 6.15b. The resemblance to the photogrammetric results depicted in Figures 6.14 and 6.13 leads to the conclusion that sediment deposits are formed under specific flow conditions (in the tested scenario corresponding to case B), but do not accumulate in the vicinity of the culvert if a storm event passes through. This conclusion is reinforced by a comparison of results from case B, case C, and case D whereby the relatively low flow of case B led to more sediment accumulations than the "stepped" simulation of a typical storm event.

This last series of tests pose new issues for the culvert design specifications. Specifically, while the culvert opening area is dictated by the maximum flow, usually a 50-year return flood event, it is this large cross-section area that leads to the situation where during the low flows (present mostly throughout the year) sediment deposits are formed, therefore reducing the available cross section. Under favorable conditions, these deposits can be removed by high storm events as shown in our laboratory tests. In field conditions, however, the deposits are strengthened by the vegetation growing between

www.manaraa.com

storm events (as the soil in the deposits is fertile) therefore the self-cleaning process cannot take place.

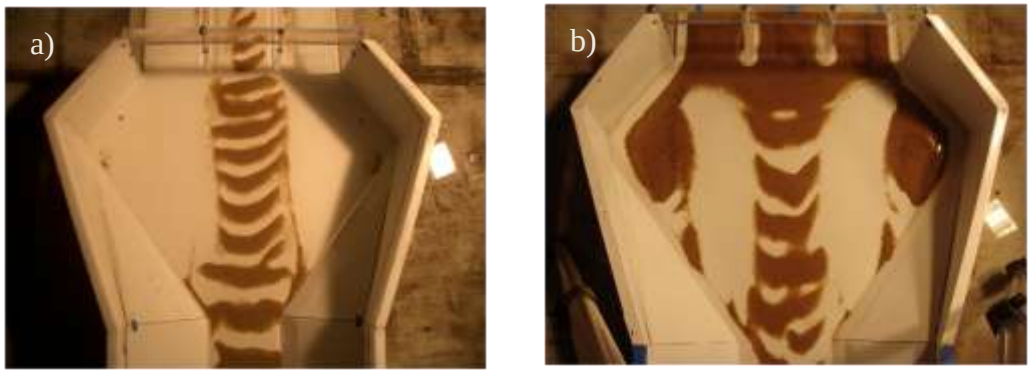


Figure 6.15 Sedimentation a) simulate flow conditions: case C → case D; b) simulate flow condition case B for two hours

The uncoupled nature of the relationship between sediment transport and flow rates was documented with field observations in Chapter 3.1.2. The experiment described herein was conducted to investigate the sediment deposition patterns when the peak sediment discharge is delivered before the flow discharge. Flow conditions B and C (as described above) were selected to represent low and, respectively, high flow conditions. Three sediment discharge rates were used. The "stepped" approach used above was applied for both flow and sediment discharges. Each test case was run 10 min to reach equilibrium for water and sediment supply. The flow and sediment discharges were uncoupled, i.e., flow and sediment were changed following the uncoupled hydrographs shown in Figure 6.16d. The resulting sediment deposition pattern is shown in Figure 6.16d. The obtained results show that the lab tests conducted so far are quasi-equivalent.

www.manaraa.com

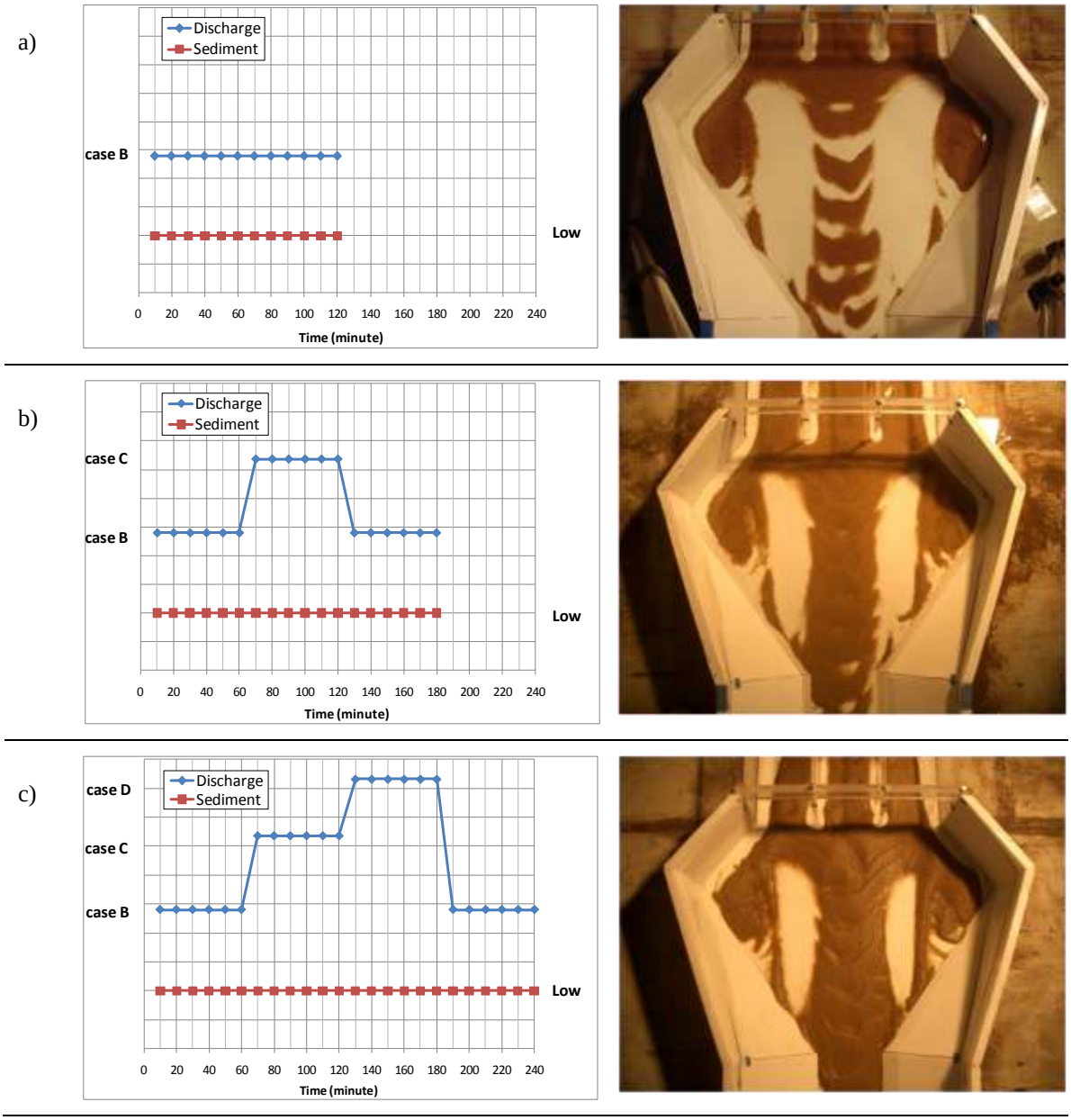


Figure 6.16 Synthesis of various experimental approaches adopted in the laboratory study in model 1/20B

www.manaraa.com

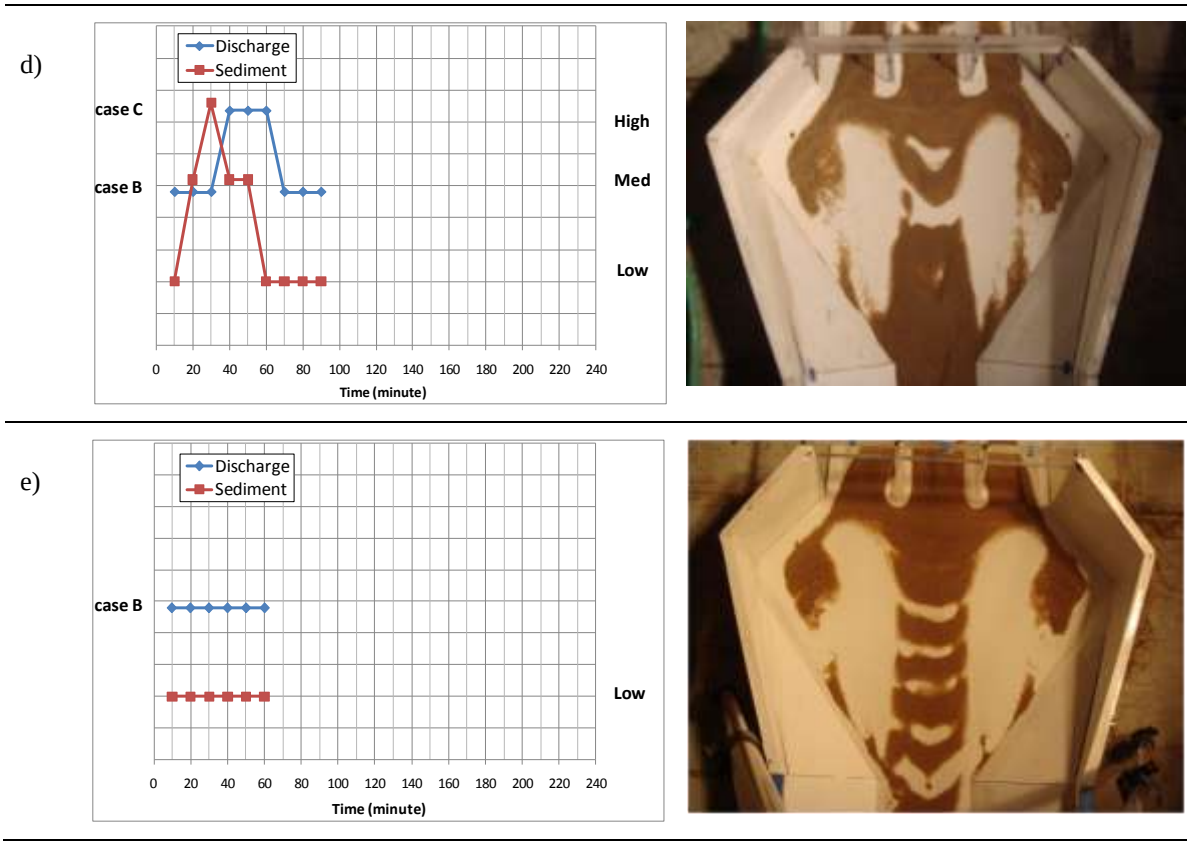


Figure 6.16 Synthesis of various experimental approaches adopted in the laboratory study in model 1/20B (Figure 6.16 continued)

### 6.2.2 Validation experiment

The tests in this section were conducted to validate the sediment deposition patterns obtained from the tests conducted in scaled model 1/20B. The larger-scale model 1/5B is used for validation of the sediment deposition patterns. It is assumed that flow and sediment transport at the scale of this model is sufficiently close to full scale. The geometry of the culvert-channel system in model 1/5B was the same as that in the tests conducted in model 1/20B. Three flow conditions denoted A, B, and C which scaled from baseline test 4 were considered and used to investigate sediment accumulation in the

www.manaraa.com

expansion. Two methods were utilized to qualitatively and quantitatively evaluate the variable patterns of sediment accumulation compared to the conditions corresponding to baseline test 4.

6.2.2.1 Test 7: Qualitative evaluation of sedimentation pattern in model 1/5B

A qualitative method was used to evaluate sediment transport and deposition in the expansion area. The method was simple and quick, being based on the imaging of a pole set horizontally in the model at a critical cross section, as shown in Figure 6.17. The pole was set in position after each test, so as to keep all the imaging conditions the same. The overall intensity of the light in the recorded images was kept the same by using the same bulbs for the illumination of the model area. The images were taken at the end of each test from the same position and the same distance, at an oblique angle. Images taken from an oblique angle are generally distorted due to the inherent geometrical distortion.

The flow condition in case B led to the largest amount of sediment deposition in the expansion. Sediment did not accumulate for the reduced discharge considered in case A. Dunes were not observed to regularly form in the expansion for case A. The increased discharge considered in the case C caused the expansion to deepen in the central part of the region. In addition, the dunes forming on the side of the expansion reached the same elevation as in case B, but were shifted toward the wall. Observations of flow and sediment movement at the various cross-sections in the expansion lead to the following findings:

1. The storm event did not clean sediment out of the culvert structure, but increased bed-sediment deposition in the expansion,
2. Sediment was prone to deposit in the side of the expansion because of the secondary current. The central barrel carried the main portion of the discharge

www.manaraa.com

and,

3. Increasing discharge could cause a scour hole upstream the culvert entrance, and therefore block the stream flow during low flow condition.

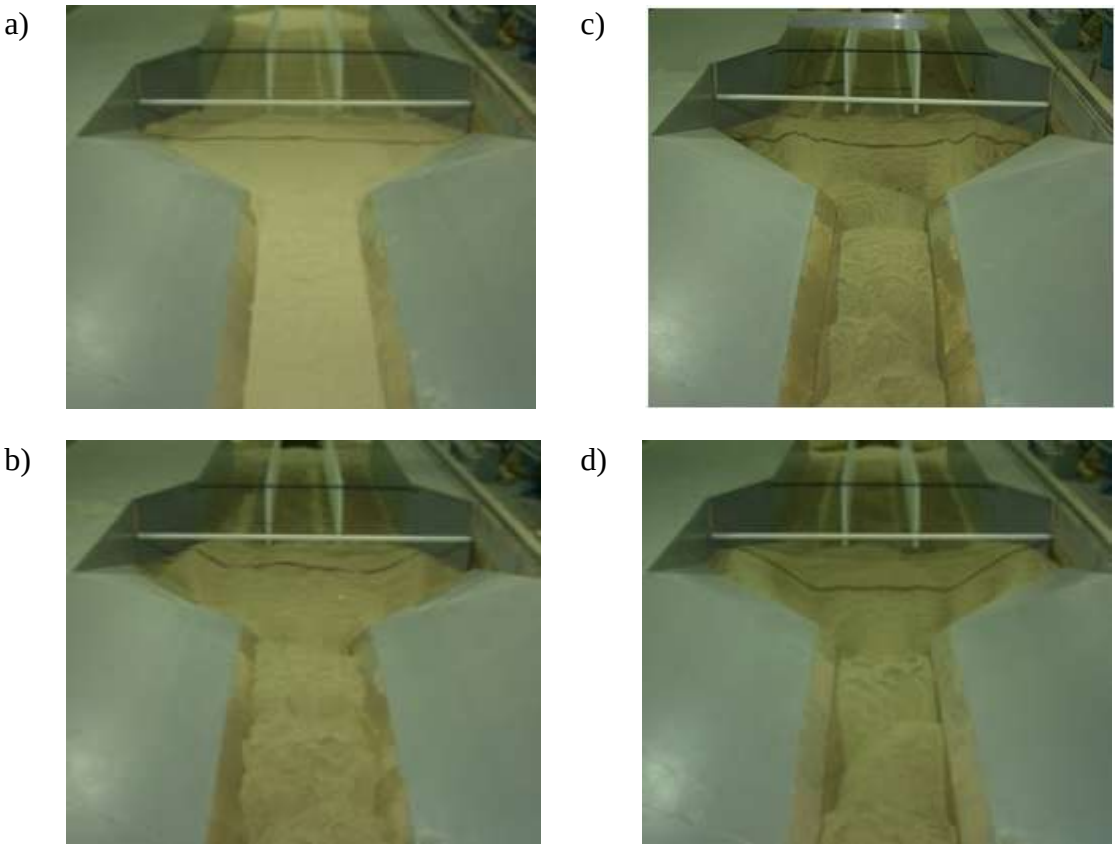


Figure 6.17 Sediment deposition patterns: a) Initial condition, b) case A, c) case B, d) case C

6.2.2.2 Test 8: The mechanics of sediment deposit formation

The tests conducted with the 1/5 Model to study sediment transport through the culvert showed that the sediment is prone to deposit in the region situated upstream of the culvert. To understand the mechanics of sediment deposition in that region, measurements were needed to reveal the spatial and temporal migration of deposition

www.manaraa.com

patterns through the culvert. An ultrasonic depth probe (MTA) comprising 32 arrays of transducers was employed to obtain spatial and temporal measurements of the bathymetry and associated bed-form migration (see Figure 4.4).

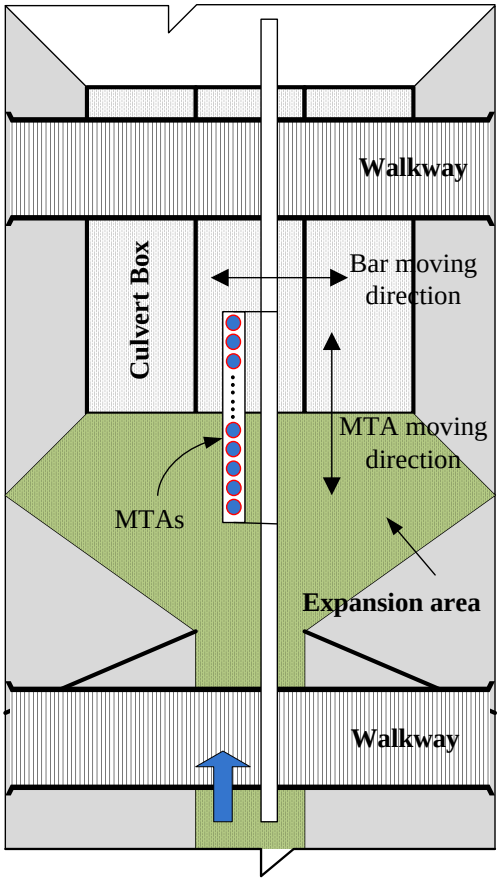


Figure 6.18 MTA measurements of sediment deposition in the vicinity of the culvert

The test was conducted in model 1/5B, with the experiment deployment as illustrated in Figure 6.18. The MTAs were deployed to survey the development of the bed forms in the expansion area and within the three culvert barrels. The MTAs were aligned parallel to the bar which moved across the flume to gather time series of the bed profiles with each of the transducers. Profiles were continuously collected for 30 seconds.

www.manaraa.com

Assuming that bed bathymetry change over 30 seconds can be neglected with respect to the dominant scales of the sediment transport process, each profile was obtained by averaging 30 sets of data to represent the bathymetry around and within the culvert. 28 profiles were measured in the expansion area and the culvert boxes. The development of the bed forms inside the culvert barrels will be discussed in Chapter 7 which assesses the performance of the self-cleaning system. The flow condition for this test was case B which led to the greatest sediment deposition. The test duration was 12 hours. The sediment evolution upstream of the culvert was measured every half hour using the MTAs. Figure 6.19 shows the sediment deposition pattern after operating the flume for 12 hours (end of the test). Figure6.19a shows a photo taken after draining out the flume. Figure 6.19b shows the bathymetry measured in the expansion area with MTAs after the test was run for 12 hours. The comparison shows that the MTAs measurements can successfully delineate the sedimentation pattern.

Figures 6.20 and 6.21 show the bathymetry contours in the expansion area at various times during the test. The initial bed elevation is zero. After operating the flume for three hours sediment particles deposit on the sides. The maximum height of the deposit is 11.09cm, about 18% of the culvert opening (the culvert opening is 2ft = 61cm). Scour holes, shown as dark blue regions in Figure 6.20a, can be detected. After six hours, scour holes are still present next to deposit (see Figure 6.20b). Sediment particles continuously deposit on the side and accumulate such that the maximum level of the deposit after six hours is 13.36cm.

The sediment deposition patterns measured after 9 hours and 12 hours from the start of the test are presented in Figure 6.21. They show the similar patterns compared to those in Figure 6.20. Sediment particles continue to gradually deposit on the sides. The maximum height of the deposit after 12 hours is 17.89cm. The main region of sediment deposition migrates into the expansion area. Thus, during the initial stages of the test sediment rapidly deposits at the right and left sides of the channel upstream of the culvert.

www.manaraa.com

The height of the deposit attains up to 25% of the culvert opening at the end of the experiment. The outline of deposition pattern and the location of dunes approach equilibrium after 6 hours. The large deposition observed at the expansion's sides means that the flow did not have enough capacity to transport sediment. Therefore sediment tended to deposit in the left and right barrels. Nevertheless, no sediment particles accumulated in the central streamwise direction during the 12 hours test. Sediment particles were continuously transported in the streamwise direction, which means the flow had the required capacity to transport sediment through the central barrel.

a)

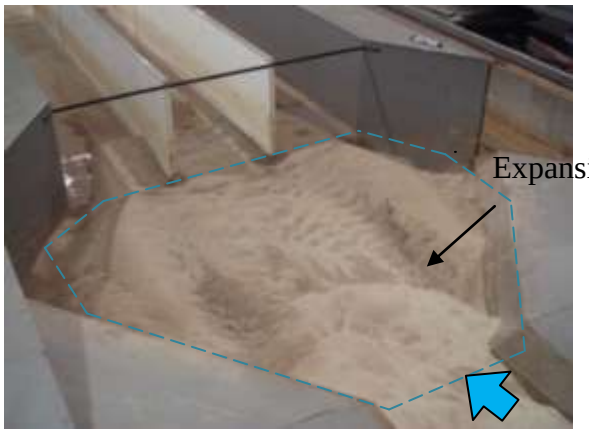


b)

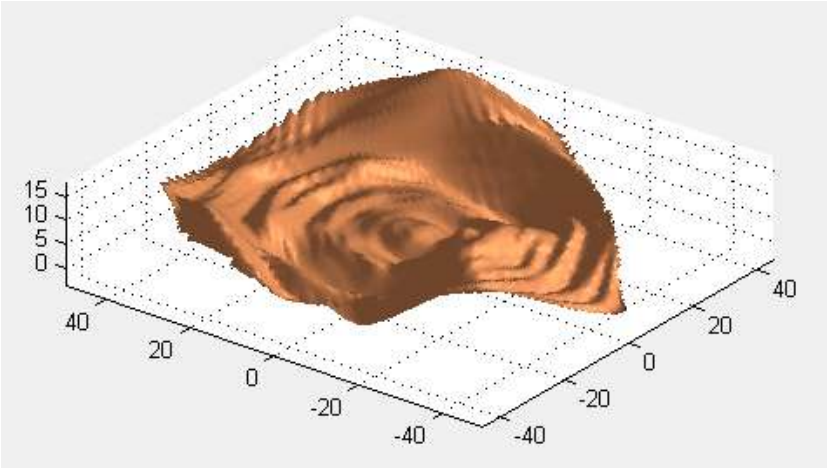


Figure 6.19 Sediment deposition in the expansion area after running the model for 12 hours: a) image of sedimentation in the expansion area (the box delineate the area measured with MTAs), b) bathymetry pattern obtained from MTAs measurements

www.manaraa.com

a)

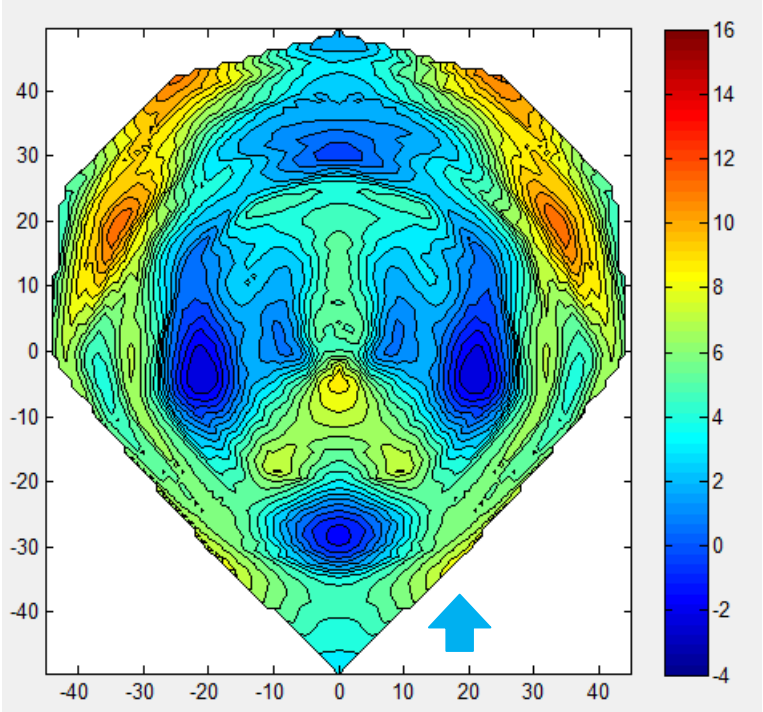


b)

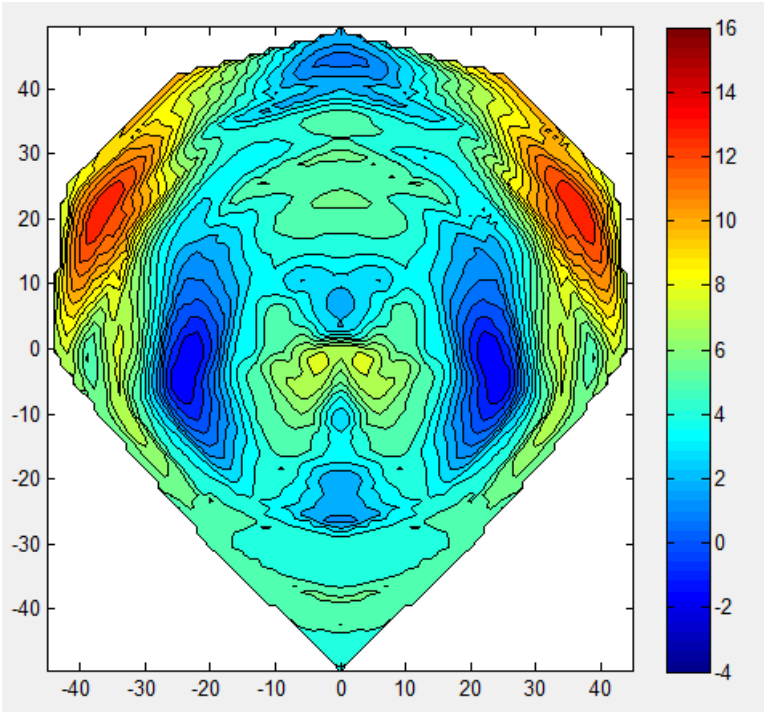


Figure 6.20 Dynamic bed form evolvement upstream the culvert: a) 3-hour running, and b) 6-hour running

www.manaraa.com

a)

b)

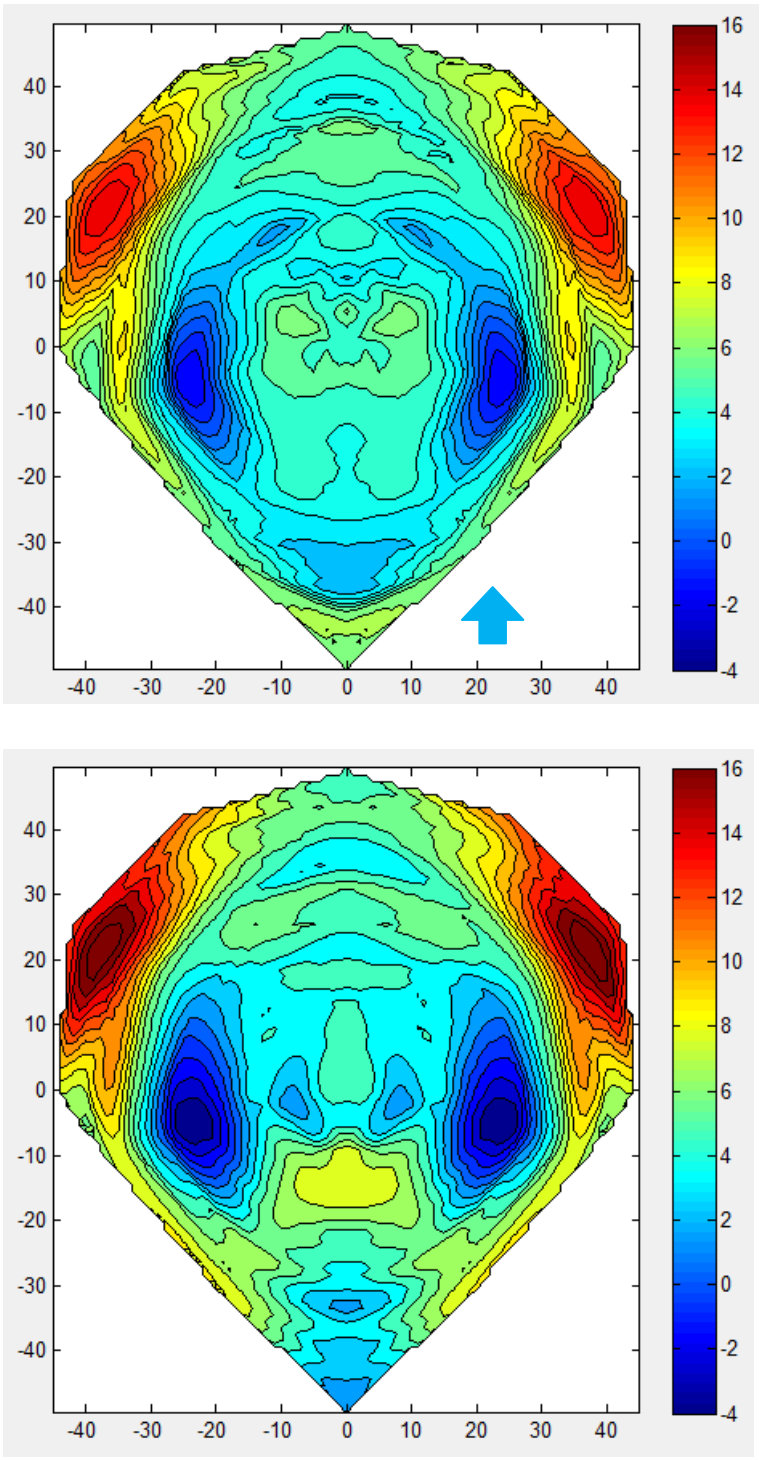


Figure 6.21 Dynamic bed form evolvement upstream the culvert: a) 9-hour running, and b) 12-hour running

www.manaraa.com

## 6.3 Numerical experiment

The numerical simulations illuminated the flow processes causing sedimentation at the model culvert. The commercial software FLUENT was used to analyze culvert configurations tested in hydraulic modeling experiments. The software was used with the domain developed from the model 1/20B, as described in Chapter 4.

### 6.3.1 Simulation scenarios

The calculation domains for numerical simulation were developed for two different culvert designs (see Figure 4.5). One domain was developed from the model 1/20B, as described in the aforementioned baseline tests. Modeling replicated the flow field at the culvertwithout self-cleaning system. The other model configuration investigated the effect of the self-cleaning system placed in the expansion, as described in Chapter 7. Two tapered fillets were added in the side parts of the expansion to increase the power of flow which could flush sediment out (see Figure 4.5b). Validation and verification of the numerical modeling was made by comparing the output of simulation with the free-surface velocity distributions obtained in the laboratory experiments with LSPIV measurements. The numerical simulations and laboratory experiments were conducted for the cases summarized in Table 6.4.

Table 6.4 Simulation case and reference model

| Case(HW/D) | Numerical experiment | Hydraulic model experiment |
|---|---|---|
| A (0.25) | 1/20B | 1/20B |
| B (0.50) | 1/20B | 1/20B |
| C (0.75) | 1/20B | 1/20B |
| A+FA (0.25) | 1/20B | 1/5B |
| B+FA (0.50) | 1/20B | 1/5B |
| C+FA (0.75) | 1/20B | 1/5B |

Note: HW = water depth, D = depth of the culvert, FA = fillet-based self-cleaning system set in the expansion, A,B,C = flow condition for case A,B,C see baseline test 4 and performance test in hydraulic modeling experiments

www.manaraa.com

### 6.3.2 Simulation setting

#### 6.3.2.1 Computational grid

The commercial software Gridgen was used to generate the calculation grids. Calculation grids were generated so that the total number of nodes will be about 2 million.

#### 6.3.2.2 Flow modeling

FLUENT required as input data on flow rates entering the system, the outflow setting at the downstream end, channel bad, bank, and piers as the wall, and water surface defined as symmetry. A turbulence model component was used to calibrate FLUENT to the three-dimension flow at the culvert. The important turbulence parameters κ and ω were evaluated to test this turbulence model component. Once the numerical model was able to reproduce the flow field data obtained from LSPIV, the FLUENT model was applied it to self-cleaning system for culverts to get reasonable results that would take much longer to obtain in the laboratory.

#### 6.3.2.3 Post processing

The Particle Tracking function in FLUENT was used to predict the paths of sediments around culverts. In order to investigate the sedimentation around culverts, shear velocity was estimated as follows:

$$u^*_n = \sqrt{\frac{\tau_n}{\rho_n}} = \sqrt{\frac{1}{\rho_n}\mu_n \frac{du_n}{dz_n}} = \sqrt{\nu_n \frac{|u_{n,horizontal,z=0.002}|}{0.002}} \quad (6.3)$$

www.manaraa.com

### 6.3.3 Numerical model testing

To compare the results of numerical simulations with those of the experiments; flow characteristics, 2D streamlines, streamwise velocity contours, and out of plane vorticity contours on the horizontal plane close to the free surface were obtained for each case. These data reveal significant aspects about how the flow conveys sediment and deposits it at the culvert inlet, and within the culvert. Two laboratory experiment data, collected from Baseline test 5, were used for numerical model validation. The numerical results were compared to measurements conducted with LSPIV in laboratory tests for homologous geometry. Comparison of average velocity in the expansion between the laboratory and the numerical model shows minor differences near the culvert piers and expansion entrance.

The Particle Tracking function in FLUENT was used to predict the paths of sediments around culverts with the following parameters: Particle number = 20, Particle location = close to the bottom and half way of the incoming channel, Gravitational acceleration = - 5.25, Particle velocity = local velocity (obtain from the solution), Particle size = $6.44 \times 10^{-3}$ (= 0.5mm=sediment size used in the experiment), and Particle density = 2.65. Figure 6.22 and 6.23 show the near-surface flow field, shear velocity contours, and sediment paths obtained from the numerical model for the flow the case B (HW/D=0.5). Figure 6.24 shows the near-surface flow field obtained with LSPIV and sedimentation documented in the laboratory experiment. Figure 6.25 shows the near-surface flow field, shear velocity contours, and sediment paths for the numerical model applied to the case C (HW/D= 0.75). Figure 6.26 shows the comparable values from the laboratory experiment obtained with LSPIV. The comparison is discussed in the following section.

www.manaraa.com

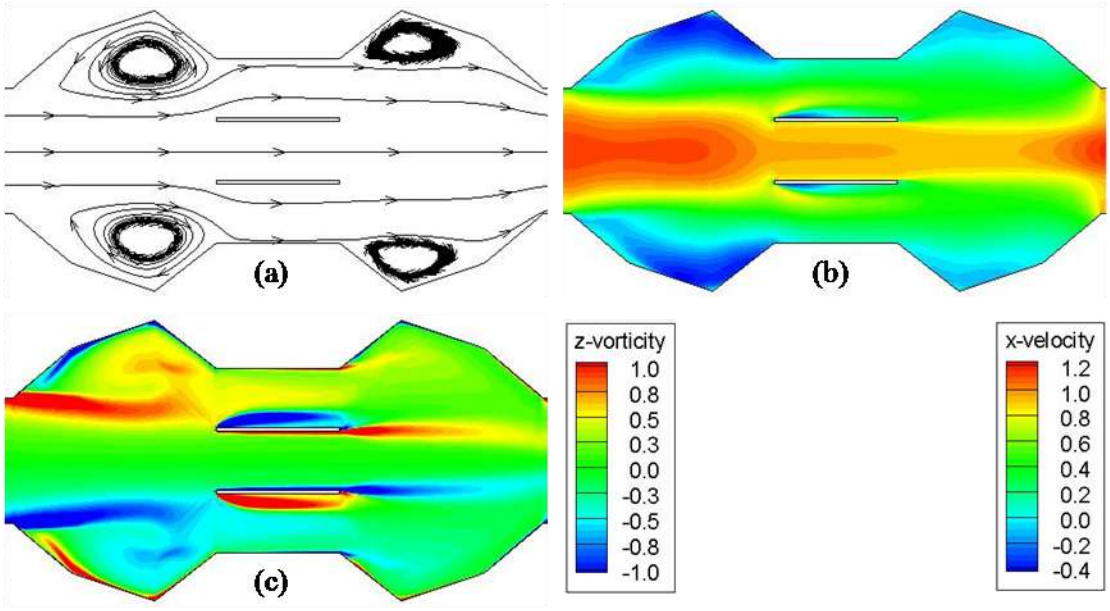


Figure 6.22 Near surface flow field for flow case B obtained with numerical simulation: (a) streamlines, (b) streamwise velocity, (c) out of plane vorticity

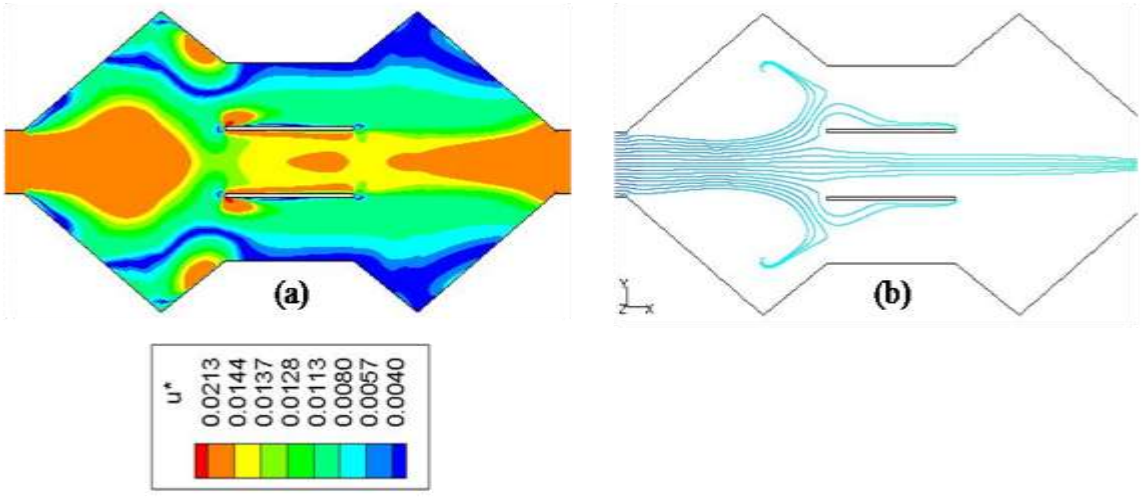


Figure 6.23 Sediment transport characteristics for case B obtained from numerical simulations: (a) shear velocity (b) sediment transport

www.manaraa.com

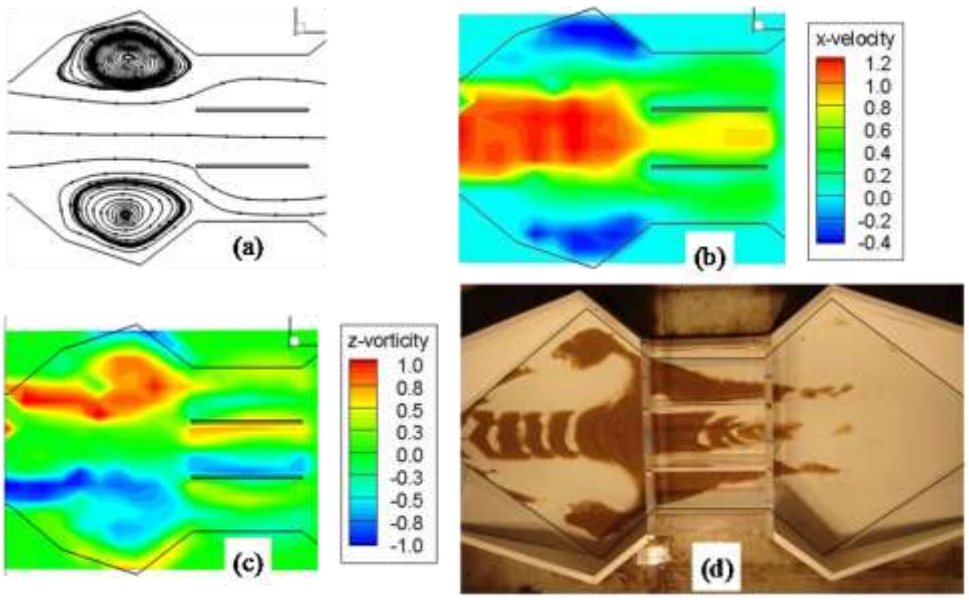


Figure 6.24 Surface flow field for the case B obtained in laboratory tests with LSPIV and imagery: (a) Streamline and velocity magnitude contour at the free surface, (b) streamwise velocity at the free surface, (c) vorticity at the free surface, and (d) sedimentation (Relevant comparisons: 6.22 a, b, and c with 6.24 a, b, and c, respectively and 6.22b with 6.24d.)

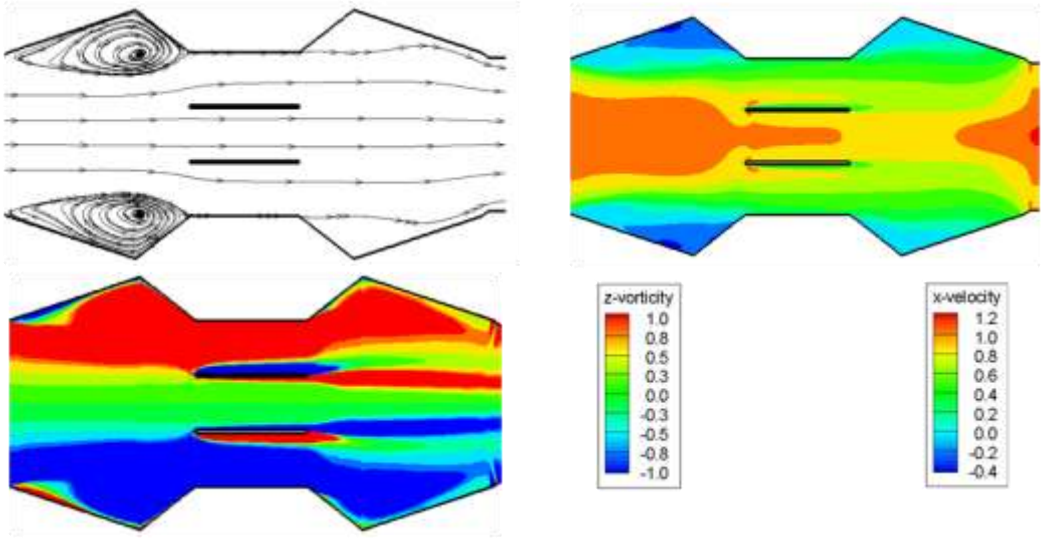


Figure 6.25 Near surface flow field for flow case C obtained with numerical simulation: (a) streamlines,(b) streamwise velocity, (c) out of plane vorticity

www.manaraa.com

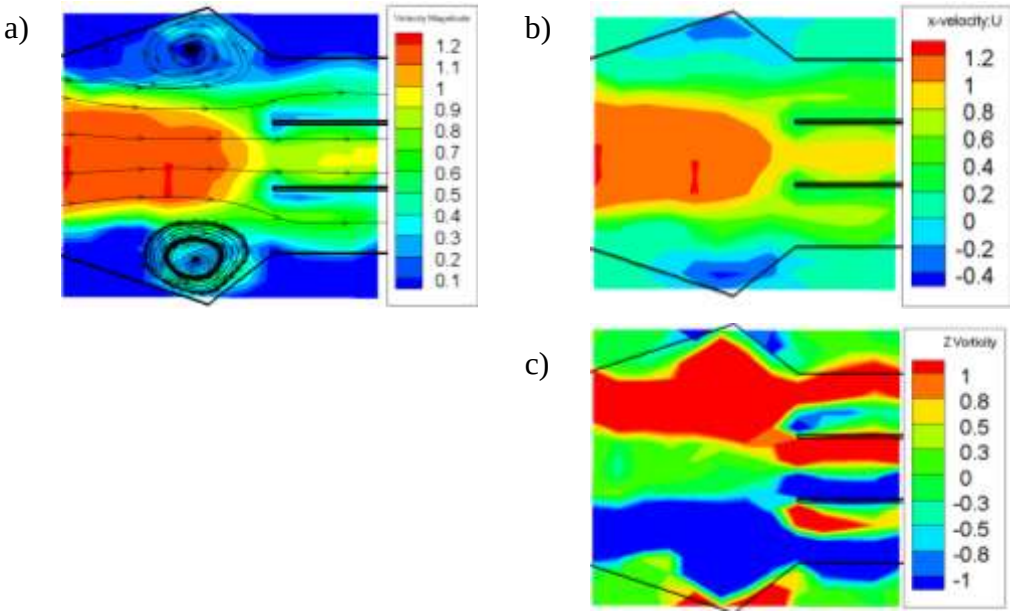


Figure 6.26 Surface flow field for the case C obtained in the laboratory with LSPIV: (a) Streamline and velocity magnitude contour, (b) streamwise velocity, (c) vorticity

### 6.3.4 Comparison of numerical and laboratory experiments

Comparison of velocity magnitudes obtained from the numerical model and the LSPIV can be affected by the computational and measurement mesh structure used for each method, respectively. The mesh resolution of the numerical model and the LSPIV mesh was different. The mesh for numerical model was much denser than it for LSPIV analysis (Figure 6.27). The results of the numerical simulation were interpolated linearly into the LSPIV mesh for the comparison purpose. Figures 6.28a and b present the difference between the numerical simulation and the laboratory experiment for the case B and C. The error is defined as:

$$error = \left| \frac{EFD - CFD}{EFD} \right| \tag{6.4}$$

www.manaraa.com

where EFD and CFD represent the average velocities at the same grid for LSPIV and numerical simulation.

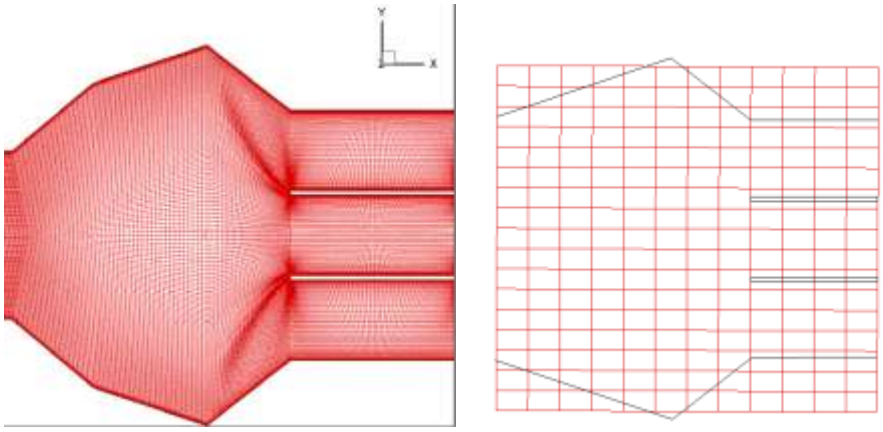

Figure 6.27 The mesh resolution: (a) the numerical model mesh, (b) the LSPIV analysis mesh

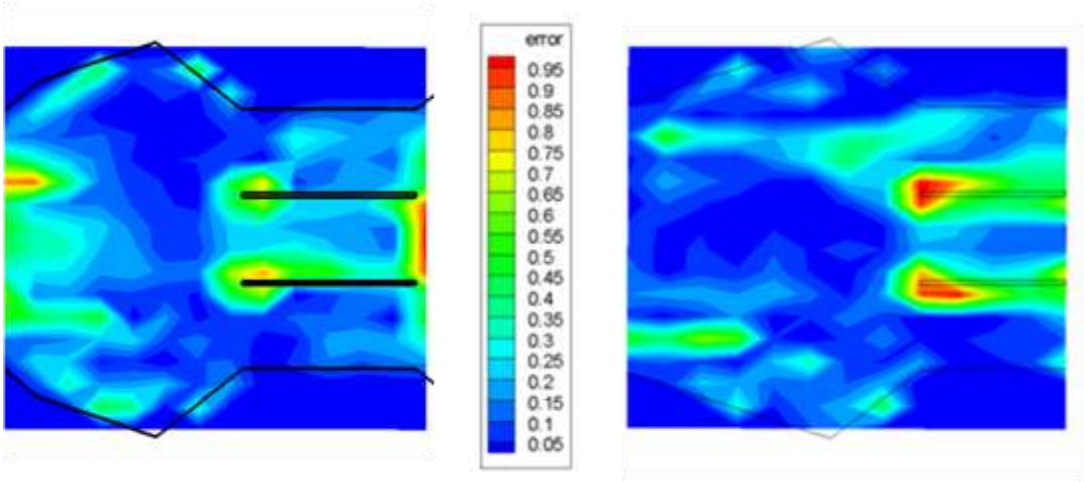


Figure 6.28 Comparison of average velocities error between numerical simulations (with FLUENT) and experimental results (with LSPIV) :(a) case B, and (b) case C

www.manaraa.com

As can be observed in Figure 6.28, the agreement between the flow fields obtained from numerical simulations and experimental results is good. Differences can be observed in the immediate vicinity of abrupt geometry changes; i.e., at corners and in front of the walls dividing the barrels. Overall, the comparison is adequate for the purpose of the present study, and confirms that the numerical model is an adequate representation of the hydraulic model. This conclusion holds because the velocities agree in the primary interested zone in the middle of the expansion region ahead of the inlet, and as the errors were under 0.20.

www.manaraa.com

# CHAPTER 7

# CULVERT STREAMLINING

The three-dimensional and unsteady character of the flow through culverts somewhat complicates the establishment of design guidelines for sedimentation-free culverts, or the implementation control measures back-fitted to prevent sedimentation. In the absence of a full understanding of the processes involved, designers and managers have had to rely on experience with existing culverts, and methods that only approximately, and with considerable uncertainty, address the range of conditions associated with culvert flows. Typically such methods comprise information gathered, in largely ad-hoc ways, from laboratory and/or small-scale field measurement, and/or from (very few) studies involving empirically-based simulation models. This chapter discusses geometric enhancement of the expansion approach to a three-barrel culvert so that flow passes smoothly to each barrel without the formation of zones of relatively quiescent water where sediment may tend to deposit.

Sedimentation at multi-box culverts is practically unavoidable. The transition of the cross section geometry from channel to culvert in the upstream expansion area produces a change in the flow distribution. The change in flow distribution does not pose problems for conveying the design flow through the culvert. The transition is, however, critical for sediment transport as the process is driven by local velocity, which is quite uneven over the cross section. So, the actual problem is not to completely eliminate sedimentation, but to minimize it and to direct the sediment such that does not substantially reduce the culvert's capacity to convey water and sediment.

The basic principals needed for a self-cleaning culvert are to increase the flow velocities, possibly increase general turbulence, and to minimize large eddies at zones of relatively quiescent water near the culvert entrance. The driving criterion for designing the self-cleaning culvert geometry was to make modifications in the upstream area of the

www.manaraa.com

culvert that would restore the shape and functionality of the original (undisturbed) stream. Consequently, one approach to the design of self-cleaning culverts is to modify the bed in the expansion and the culvert invert– simplest – in order to streamline flow in the culvert-associated area. For this purpose, various solutions were tested as subsequently discussed in this chapter. Eventually the acceptable solution from both cleaning-efficiency and practical considerations was a fillet-based configuration. With this approach the lateral areas of the expansion leading to the culvert were filled in with sloping volumes of material to both reduce the depth and to direct the flow and sediment toward the central barrel, where the original stream was located prior to the culvert construction.

## 7.1 Experiments for screening the self-cleaning culvert configurations

The experiments were conducted so as to meet the study's second primary objective, to develop and evaluate the performance of several self-cleaning systems for the culvert model, and then to decide upon the best effective self-cleaning culvert design.

The baseline tests indicated that sediment deposited unevenly in the streamwise direction and in the cross section because of the uneven velocity distribution. The channel expansion led to the culvert inducing a significant secondary current, which is the flow feature exacerbating sediment deposition. A number of self-cleaning systems were investigated to their ability to inhibit the sediment deposition. The strategy in designing the self-cleaning system was to implement a geometry that redistributed the velocity in the expansion such that forces the water and sediment to the central region. Practically, the design tried to mimic the shape of the pre-construction bed of the stream, which was limited to one (typically trapezoidal) channel. As a consequence, the self-cleaning designs increased the carrying capacity of the flow in the expansion area facilitating the

www.manaraa.com

transport of the incoming sediment downstream the culvert. Two conceptual design concepts were tested:

1. Fillets set in the expansion and/or the culvert barrels; and,
2. Guiding vanes set in the expansion.

The configuration and actions of the two design approaches were designed such that the approaches can be retrofitted the culverts, rather than being design concepts that can be only implemented at the time the culvert is constructed. All screening tests were conducted at the flow condition that caused the most serious sediment deposition in baseline tests. The corresponding situation is case B, for which the headwater elevation is half of the culvert height (HW/D=0.5), and the discharge can be obtained from the performance equation in Chapter 2.

### 7.1.1 Fillet approach

This method required placing a fillet in the expansion or culvert barrels so as to increase flow velocity. The construction of the fillet elevated the bed. The conveyance power of flow then was increased by tapering slope bed and reducing of the cross-section of flow. Four designs based on the fillet approach were used to test the performance for mitigating the sedimentation problem. The first design fitted the tapered fillet in the expansion. The subsequent designs placed the fillets though the culvert barrels on the sides where the sediment deposited because of the secondary current.

#### 7.1.1.1 Fillet-based design A

The main goal of this self-cleaning system was to streamline the bathymetry of expansion, and then direct sediment toward the main channel by the tapered bed in the expansion (see Table 7.1). The design does not affect the culvert cross section which is

www.manaraa.com

easy to retrofit and cost-effective. A summary of the configurations is given in Table 7.1.The sediment deposition compared to the traditional culvert model is represented in Figure 7.1. The change of the culvert is only in the expansion region, not the culvert barrels. Sediment deposition in the expansion was noticeably mitigated. However, sediment deposited downstream the culvert model. The sediment conveyance capacity of flow was locally increased by this design, which flushed sediment out from the expansion and the culvert barrels. Sediment, though deposited downstream.

Table 7.1 Summary of fillet-based design A

| **Fillet-based design A** | **Characteristics** |
|---|---|
| 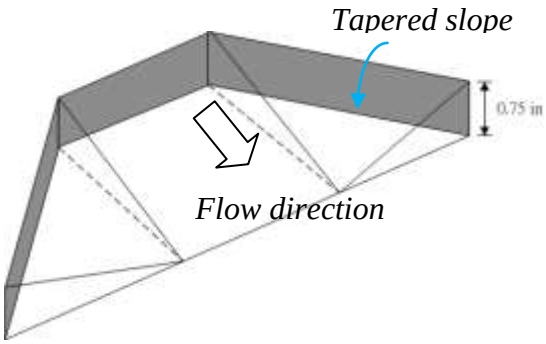 | - **Goal:** streamlining the expansion area<br>- **Geometry:** change only in the expansion area aimed at:<br>• bringing the cross section closer to its original shape<br>• - directing the sediment in the expansion to the main channel<br>- Design does not affect the culvert cross section |

www.manaraa.com

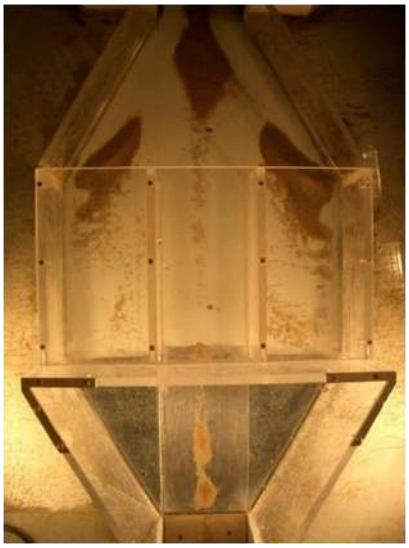

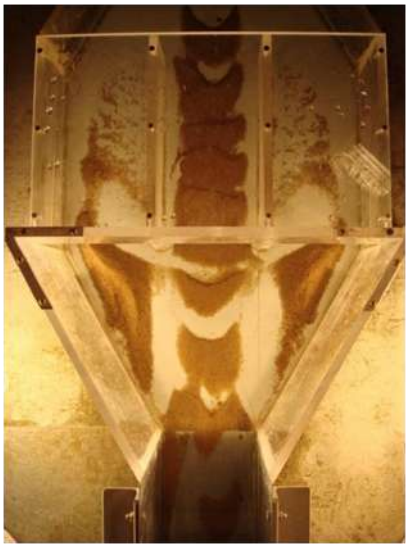

Figure 7.1 Sedimentation pattern compare to the baseline test result

7.1.1.2 Fillet-based design B

The fillet-based design B uses tapered fillet in central expansion area and elevated inverts throughout the culvert, expansion, and contraction areas. It would affect the culvert cross-section. The result shows that sediment is redistributed; no serious sedimentation occurred at sides, and sediment mostly deposits in the main channel downstream the culvert.

The summary of the fillet-based design B is given in Table 7.2. The resulting sediment deposition compared to the traditional culvert model is represented in Figure 7.2. The fillets throughout the culvert barrels reduced the culvert cross-section to increase velocities. The test showed that sediment was redistributed. No significant sedimentation occurred at the sides, and sediment mostly deposited in the channel downstream the culvert. Sediment was concentrated in the central area of the contraction and did not accumulate in barrels. No blockage of the culvert cross section and easy access to deposits for removal are favorable outcomes.

www.manaraa.com

Table 7.2 Summary of fillet-based design B

| Fillet-based design B | Characteristics |
|---|---|
| 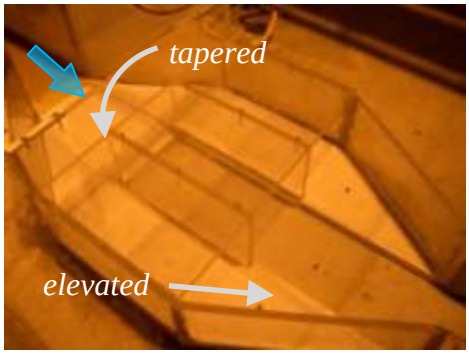 | - **Goal:** To "push" further downstream the sediment deposits formed by Design FA<br>- **Geometry:** Tapered fillet in central expansion area & elevated inverts throughout the culvert, expansion, and contraction areas<br>- Design affects the culvert cross-section |

Figure 7.2 Sedimentation pattern compare to the baseline test result

7.1.1.3 Fillet-based design C

The only difference between designs C and B is the downstream fillet. Because the previous design was observed sediment in the contraction, the objective of this design modification was to eliminate completely sediment deposition in the expansion, the

www.manaraa.com

culvert barrels, and the contraction. A summary of the configurations is given in Table 7.3. The resulting sediment deposition compared to the traditional culvert model is represented in Figure 7.3. It shows that the fillet added in contraction performed like a barrier; sediment was trapped in the central barrel. Sediment started to accumulate in the expansion after the central barrel was filled. The design did not perform well, and would be expensive to build in the field.

Table 7.3 Summary of fillet-based design C

| Fillet-based design C | Characteristics |
|---|---|
| 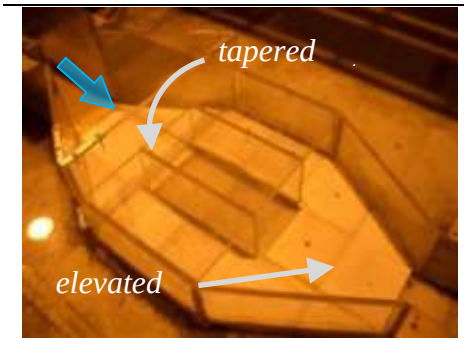 | - **Goal:** eliminate completely the sand from the expansion, culvert, and contraction areas<br>- **Geometry:** fillet added in the contraction aligned with the central barrel area<br>- Design affects culvert cross-section |

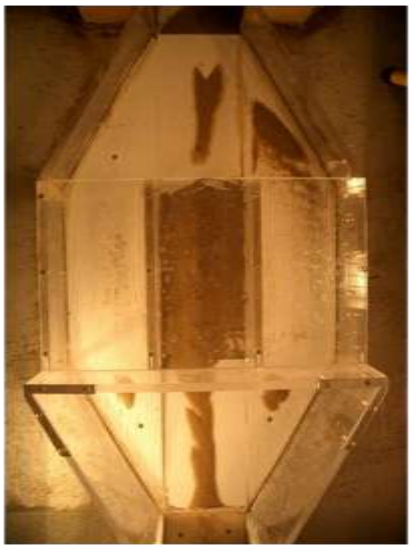

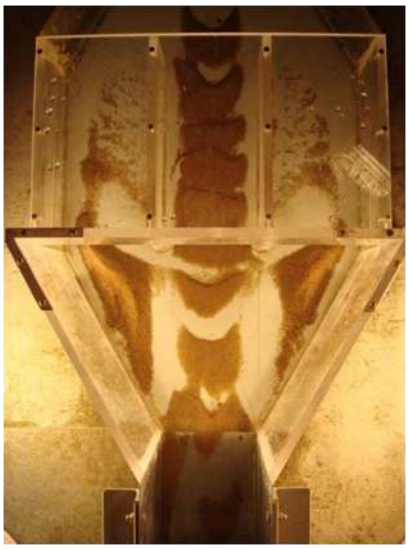

Figure 7.3 Sedimentation pattern compare to the baseline test result

www.manaraa.com

7.1.1.4 Fillet-based design D

The difference of this design compared to design B was no tapered fillet in the central pathway. The design adjustment shaped the cross-section of the culvert model similar to the connecting stream channel. The cross-section of culvert was built as close as the compound channel. A summary of the configurations is given in Table 7.4. The resulting sediment deposition compared to the traditional culvert model is represented in Figure 7.4. Sediment accumulation in side barrels did not occur, because of the effect of the elevated fillets. This design encouraged sediment to flow in the central; sedimentation in the central could be flushed out if encounter larger discharge.

Table 7.4 Summary of fillet-based design D

| Fillet-based design D | Characteristics |
|---|---|
| | - **Goal:** getting the culvert as close as possible to the original channel<br>- **Geometry:** central model area not modified: culvert side areas elevated throughout the expansion, culvert and contraction areas<br>- Design affects culvert cross-section |

www.manaraa.com

Figure 7.4 Sedimentation pattern compare to the baseline test result

The series of tests conducted with progressive alternation of the original fillet-based designs led to the conclusion that the optimal geometry for the self-cleaning design was FA, for which:

1. Sediment transport was driven downstream through the culvert;
2. Sediment deposition in the expansion area was minimum; and,
3. Sediment was equally deposited in the three boxes, but at a low overall total volume

The selected fillet-based geometry requires less field-implementation effort because the existing deposited sand in the culvert area can be used to build the fillet base. The fillet surface can be protected with riprap, and possibly grouted. An FA-based self-cleaning design will be discussed in the following section and it will be further tested in the numerical model and the performance experiments.

www.manaraa.com

### 7.1.2 Vanes Approach

Vanes are small, often cost-effective, patented structures for sediment management in rivers (Odgaard, 2009). The first known attempts to develop a theoretical design basis of vanes were by Odgaard and Kennedy (1983) and Odgaard and Spoljaric (1986). The vanes were originally designed to protect stream banks from erosion, maintain navigation depth and flood-flow capacity in rivers, and control sediment at diversions and water intakes. Appropriate installation of vanes can modify the near-bed flow pattern and redistribute flow and sediment transport by vane-generated secondary currents. The vanes used for the present tests were installed upstream the culvert structure so that the vane-generated secondary current can eliminate the channel expansion induced secondary current which causes sediment to deposit.

#### 7.1.2.1 Vane-based design A

The goal of the present design using vanes in expansion was to prevent sediment deposition in the side regions of the expansion. Four inclined vanes (10 degrees to flow direction) were laid in the expansion area, without any other modifications. Table 7.5 summarized the vane configuration and setting while Figure 7.5 shows that sediment did not accumulate in the side regions of the expansion, and that sediment was forced into the central zone. The secondary current otherwise present in the expansion was diminished by the action of the vanes.

www.manaraa.com

Table 7.5 Summary of vane-based design A

| Vane-based design A | Characteristics |
|---|---|
| 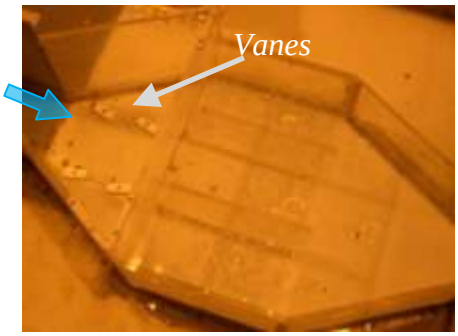 | - **Goal:** to direct the sediment to the central barrel<br>- **Geometry:** 4 inclined vanes (10 degrees, square 0.75“ , 2” long - model) in the expansion area; no other modifications<br>- Design does not affect the cross-section |

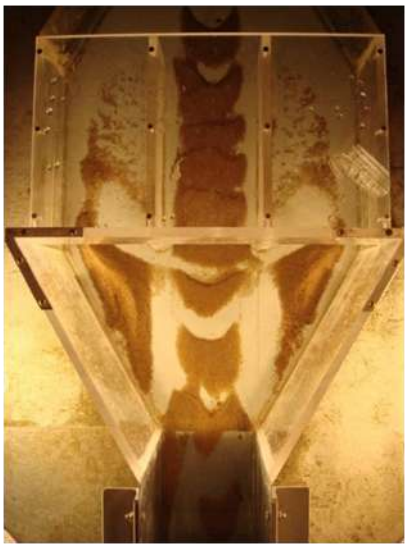

Figure 7.5 Sedimentation pattern compare to the baseline test result

7.1.2.2 Vane-based design B

Another vane approach was the previous vane-based design A plus fillets added in the left and right culvert barrels. Table 7.6 summarized the vane configuration and setting while Figure 7.6 shows the sedimentation pattern. The patterns were similar to the

www.manaraa.com

previous design, but more sediment deposition was observed to deposit in the central zone.

Table 7.6 Summary of vane-based design B

| Vane-based design B | Characteristics |
|---|---|
| 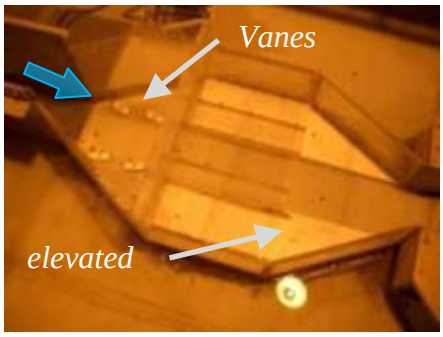 | - **Goal:** to direct the sediment to the central barrel<br>- **Geometry:** vanes as for Design VA in the expansion area & fillets in the culvert side barrels and contraction sides<br>- Design does not affect the cross-section |

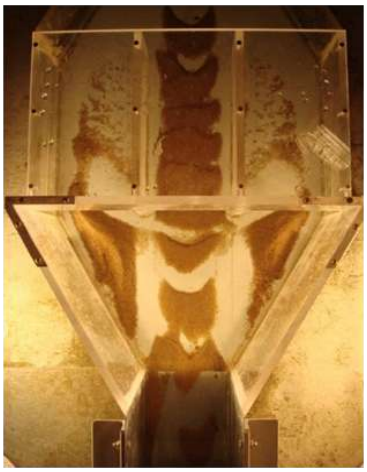

Figure 7.6 Sedimentation pattern compare to the baseline test result

www.manaraa.com

## 7.2 Numerical simulation of the Fillet-based Self-Cleaning Culverts

The fillet-based self-cleaning design tested in the numerical simulations is presented in Figure 7.7. The performance of the system will be tested. Once the numerical model was validated against its hydraulic model pair, simulations were applied with confidence to test the self-cleaning designs fitted to the culverts. Numerical simulations were computed under three hydrological conditions previously tested in the laboratory experiments, respectively cases A, B and C (see Table 6.2). Figure 7.8 and 7.9 illustrate the effect of the fillets type FA set in the culvert expansion area. The results in these figures display hydrodynamic characteristics for the flow with fillets in the case B, the reference case studied in the screening tests. It is reminded that this flow cases produced a serious sedimentation condition in the expansion. The particle tracking was conducted to simulate the sediment movement around the culvert. Figure 7.9b clearly shows that the fillets inserted in the side areas of the expansion upstream the culvert, forced the sediment movement into the central pathway. This finding confirms that the use of fillets presents a possible self-cleaning design capable to concentrate sediment towards the central zone and make use of the flow power to flush the sediment through the culvert.

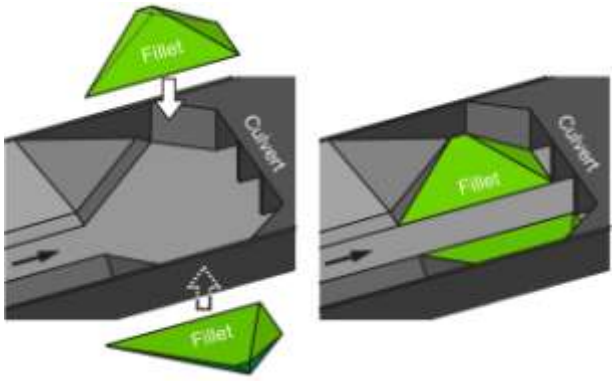


Figure 7.7 The fillet-based self-cleaning design geometry

www.manaraa.com

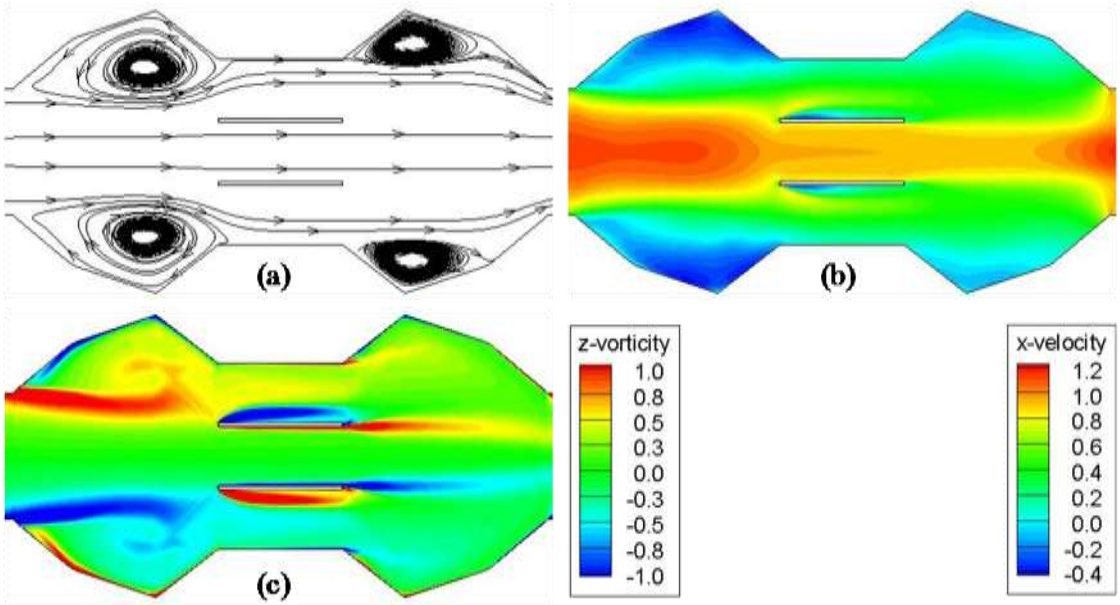


Figure 7.8 Near surface flow field for flow case B over the self-cleaning system obtained with numerical simulation: (a) streamlines,(b) streamwise velocity, (c) out of plane vorticity

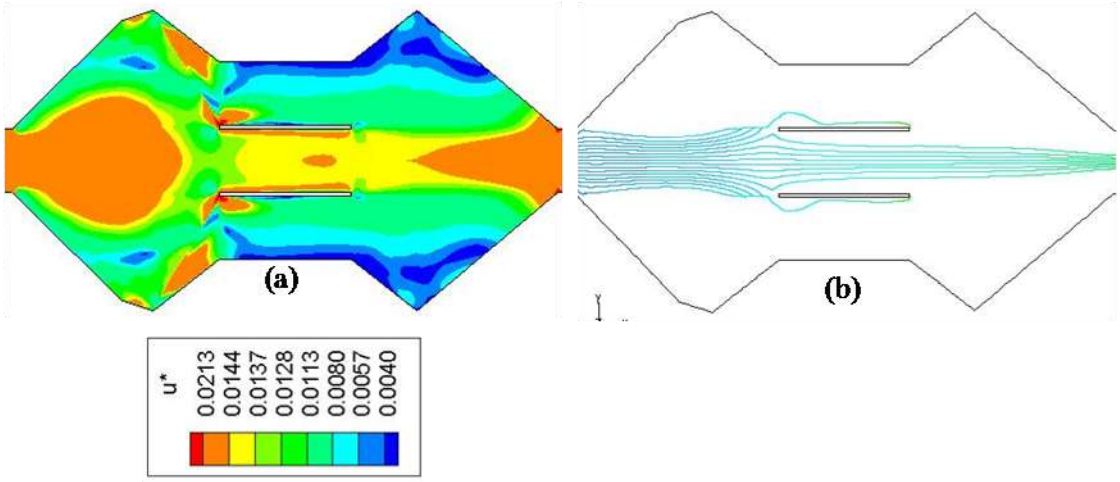


Figure 7.9 Sediment transport characteristics for case B over the self-cleaning system obtained from numerical simulations: (a) shear velocity (b) sediment transport

www.manaraa.com

## 7.3 Assessment of the performance of the fillet-based self-cleaning culvert

### 7.3.1 Overview

The purpose of the performance tests discussed in this section is to investigate the capability of the self-cleaning system compared to tests 7 and 8 (see Chapter 6). All the performance tests were conducted using the self-cleaning system that was fitted in model 1/5B. Model 1/5B is divided into three main sections. The upstream channel leading to the head box is a compound channel with erodible bed. The culvert section contains a three-barrel culvert, the expansion, and the contraction. The culvert barrel was fitted with a fixed wooden bed. The bed was erodible in the contraction and expansion regions of the culvert. The self-cleaning system was placed in the expansion region. The downstream channel is a short erodible channel connecting to the tailgate. As the slope of the flume was equal to zero, the hydraulic gradient of the flow in the performance tests was controlled by the difference in water surface elevations between the head box and the tail box. The patterns of sediment accumulation at culvert sites with a self-cleaning system in place were simulated for the three flow conditions considered in test 7. Two types of tests were performed to qualitatively and quantitatively evaluate the self-cleaning system:

1. Qualitative performance test: evaluate the performance of self-cleaning system based on the photos of a pole set horizontally in the model at the cross section corresponding to the test 7 in Chapter 6.
2. Quantitative performance test: measure the velocity distribution in the expansion and the sediment deposition in culvert barrels with the self-cleaning system placed upstream the culvert. Results were compared to measurements without the self-cleaning system upstream the culvert.

www.manaraa.com

### 7.3.1 Test for the assessment of the performance fillet-based self-cleaning culvert

The configuration of the filled-based cleaning design is shown in Figure 7.8. The results obtained in cases A, B, and C are shown in Figure 7.10. The efficiency of the self-cleaning designs was established using the empirical approach described in Chapter 6. Visual inspection of the sequence of images that tracks the development of the sediment deposit shows that the self-cleaning fillets produce the following effects:

1. Direct sediment through the central barrel of the multi-box culvert;
2. Maintain their effectiveness over a range of flows;
3. Do not obstruct the sediment transport within the culvert boxes; and,
4. Sediment deposition within the culvert boxes does not significantly change in comparison with the reference conditions indicating that most of the sediment is passed through the culvert

www.manaraa.com

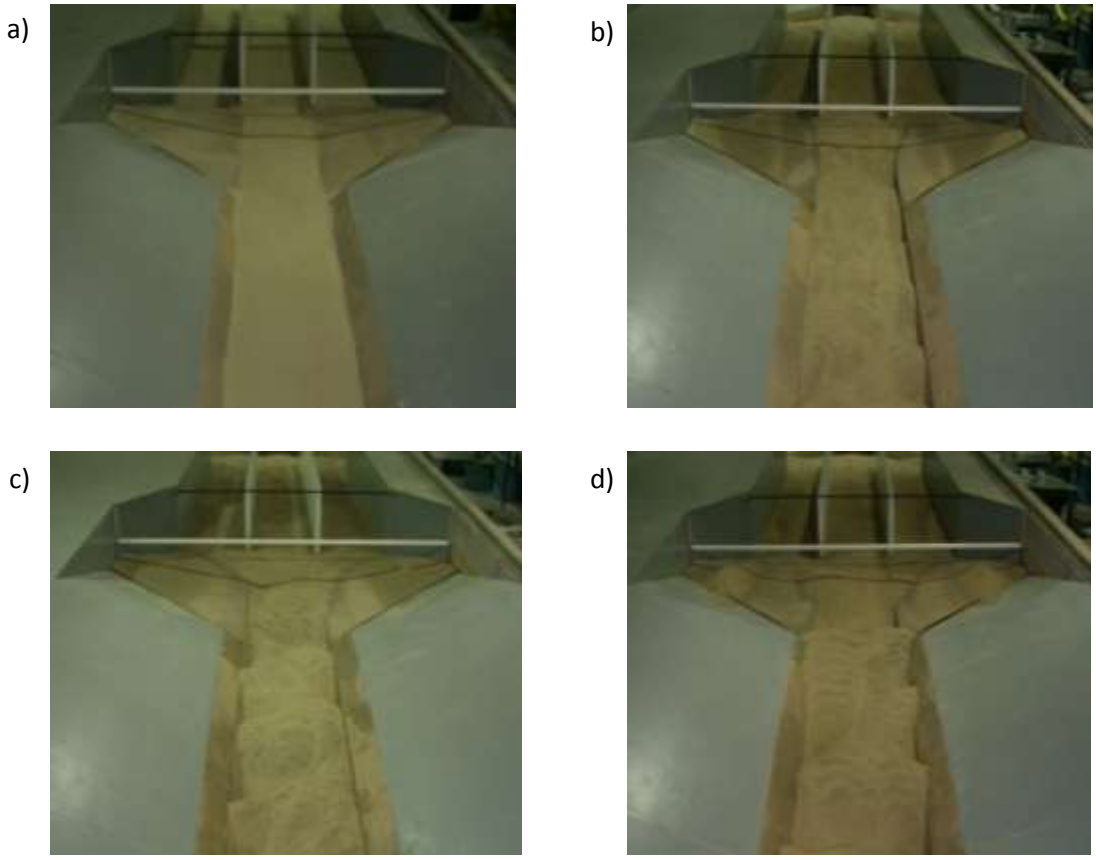


Figure 7.10 Sediment deposition patterns: a) Initial condition, b) case A, c) case B, d) case C

### 7.3.2 Flow kinematics in the vicinity of the original culvert configuration

LSPIV was used to measure velocity distribution for the reference culvert model and for the FA self-cleaning culvert design for conditions corresponding to case B. Figure 7.11a and b show the streamline for the reference culvert model and FA design culvert model, respectively. It can be noted that the FA design considerably weakened the secondary currents formed in the corners of the expansion region. Moreover, the iso-velocity contours plotted in Figure 7.12 show that the velocity magnitude was considerably increased throughout the central area of the expansion. This led to increased flow power that enhanced the transport of the incoming sediment toward the culvert.

www.manaraa.com

The LSPIV measurements demonstrate that water and sediment are forced toward the central culvert box when the self-cleaning fillets are set in the expansion. The conclusions provided by the measurements are congruent with the long-term tests conducted to monitor the sedimentation process. Figure 7.14, provided in the next section, illustrates that the sediment did not accumulate in the expansion in the tests with the fillets set in the lateral expansion areas. Both series of tests complementary validate the efficiency of the self-cleaning design conceived as part of the present study. The design is simple to implement in any stage of the culvert lifetime and it can be mostly constructed with local material, i.e., sediment deposited at the culvert prior to the culvert conditioning.

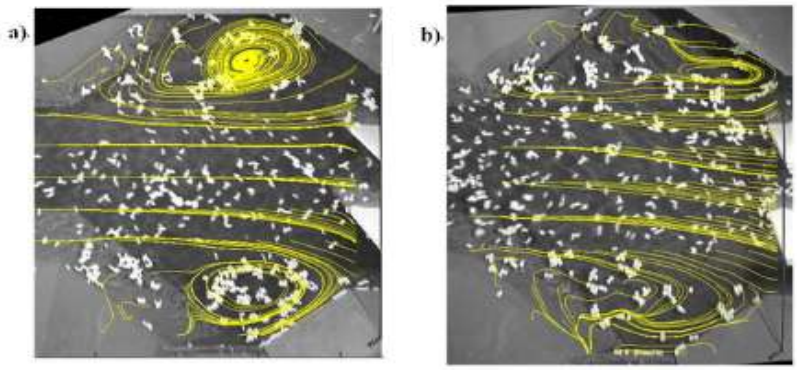


Figure 7.11 Streamline in 1/5B: a) reference condition, and b) FA design model

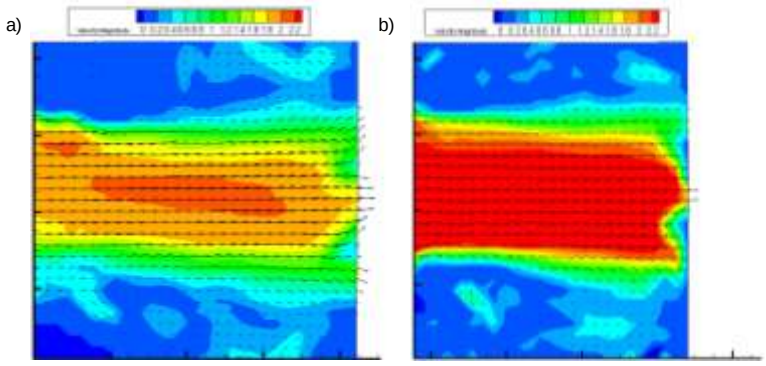


Figure 7.12 Velocity contours in 1/5B: a) reference condition, and b) FA design model

www.manaraa.com

### 7.3.3 Mitigation of sedimentation at culvert

A test was performed in model 1/5B to investigate the capability of the self-cleaning system to mitigation sedimentation. The experiment is illustrated in Figure 7.13. The MTAs were deployed to survey the development of the bed forms in the culvert boxes. Measurements were performed at 18 sections in the left and central boxes. Measurements in each section were continuously collected for 30 seconds. Assuming that the bed movement over 30 seconds is negligible with respect to the dominant scales of the sediment transport process, each bed profile in the box was obtained by averaging 30 sets of data.

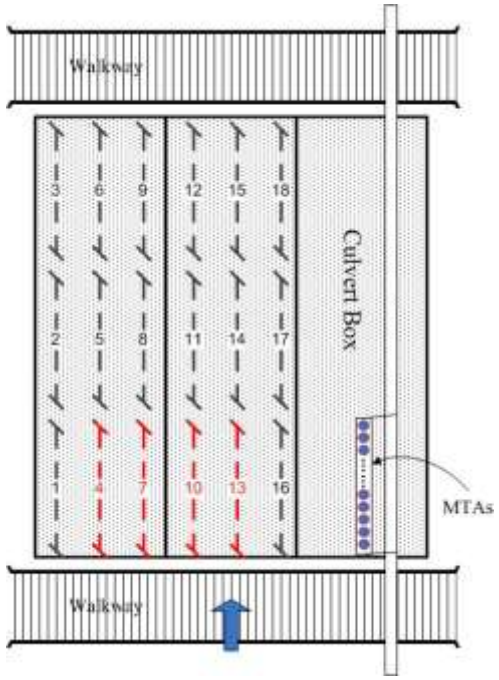


Figure 7.13 MTAs deployment in culvert boxes

The sedimentation maps inside the culvert boxes are shown in Figures 7.14 and 7.15. The results were measured after running the test for 6 hours and for 12 hours, respectively. Figures 7.14a and b show the results with and without the self-cleaning system placed upstream of the culvert, respectively. The comparison of the sediment

www.manaraa.com

deposits shows that the self-cleaning system was able to mitigate the sediment deposition in the left box. The large sediment deposition present in the left box for the case of the standard design was avoided when the self-cleaning system was installed in the culvert. The self-cleaning system was able to reduce the amount of deposited sediment in the left box by more than 70%. Figures 7.16 and 7.17 compare the bathymetry profiles for the case without and with the self-cleaning system. The red and yellow solid lines correspond to the case without the self-cleaning system placed in the expansion. The blue and green solid lines correspond to the case with the self-cleaning system in place. The results presented in Figure 7.16 show that the self-cleaning system dramatically reduced the sediment deposit in section 4 and 7 of the left box. Although a small amount of sediment deposition was observed at section 7, the self-cleaning system was able to force most of the sediment particles into the central box of the culvert.

Figure 7.17 shows the bathymetry profiles in section 10 and section 13 of the central box. After 6 hours from the start of the test. In both cases no sediment accumulated in the central box after 6 hours from the start of the test. This result implies that the flow conditions in the center part of the culvert can transport the sediment particles without significant deposition. Comparison of the bathymetry profiles in the two cases at 12 hours from the start of the tests show that bed elevation in the central part of the culvert with the self-cleaning system is larger than the culvert without self-cleaning system. It implied that more sediment particles were delivered in the center. The performance tests conducted to evaluate the self-cleaning system provide the following conclusions:

1. The self-cleaning system removes or substantially reduces the size of the recirculation areas where sediment tends to deposit;
2. The self-cleaning system strengthens the convection of sediment directly into the central box; and,

www.manaraa.com

3. The self-cleaning system amplifies the turbulence at the entrance into the side boxes and mitigates the sediment deposition inside them.

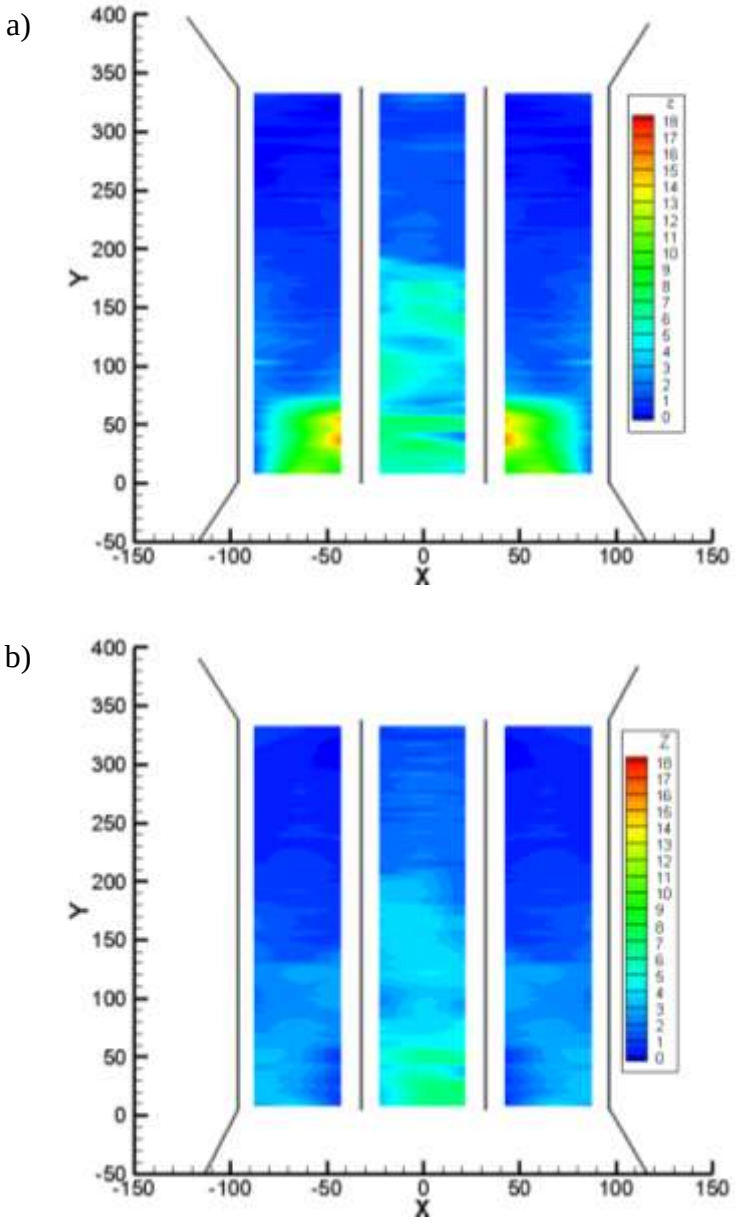


Figure 7.14 Sedimentation map in the culvert boxes at 6-hour: a) no self-cleaning system placed upstream the culvert boxes, and b) self-cleaning system placed upstream the culvert boxes

www.manaraa.com

a)

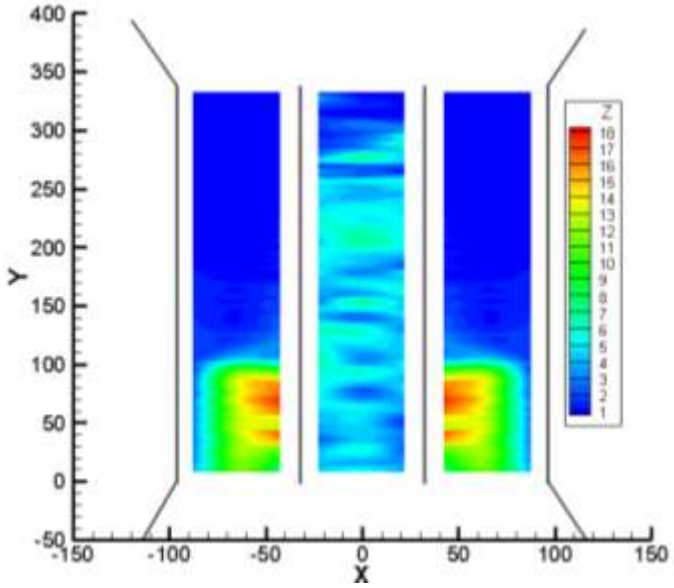


b)

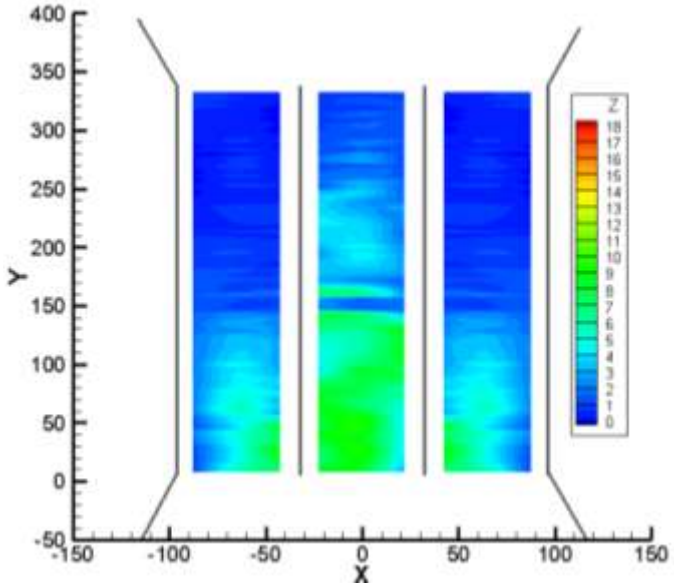


Figure 7.15 Sedimentation map in the culvert boxes at 12-hour: a) no self-cleaning system placed upstream the culvert boxes, and b) self-cleaning system placed upstream the culvert boxes

www.manaraa.com

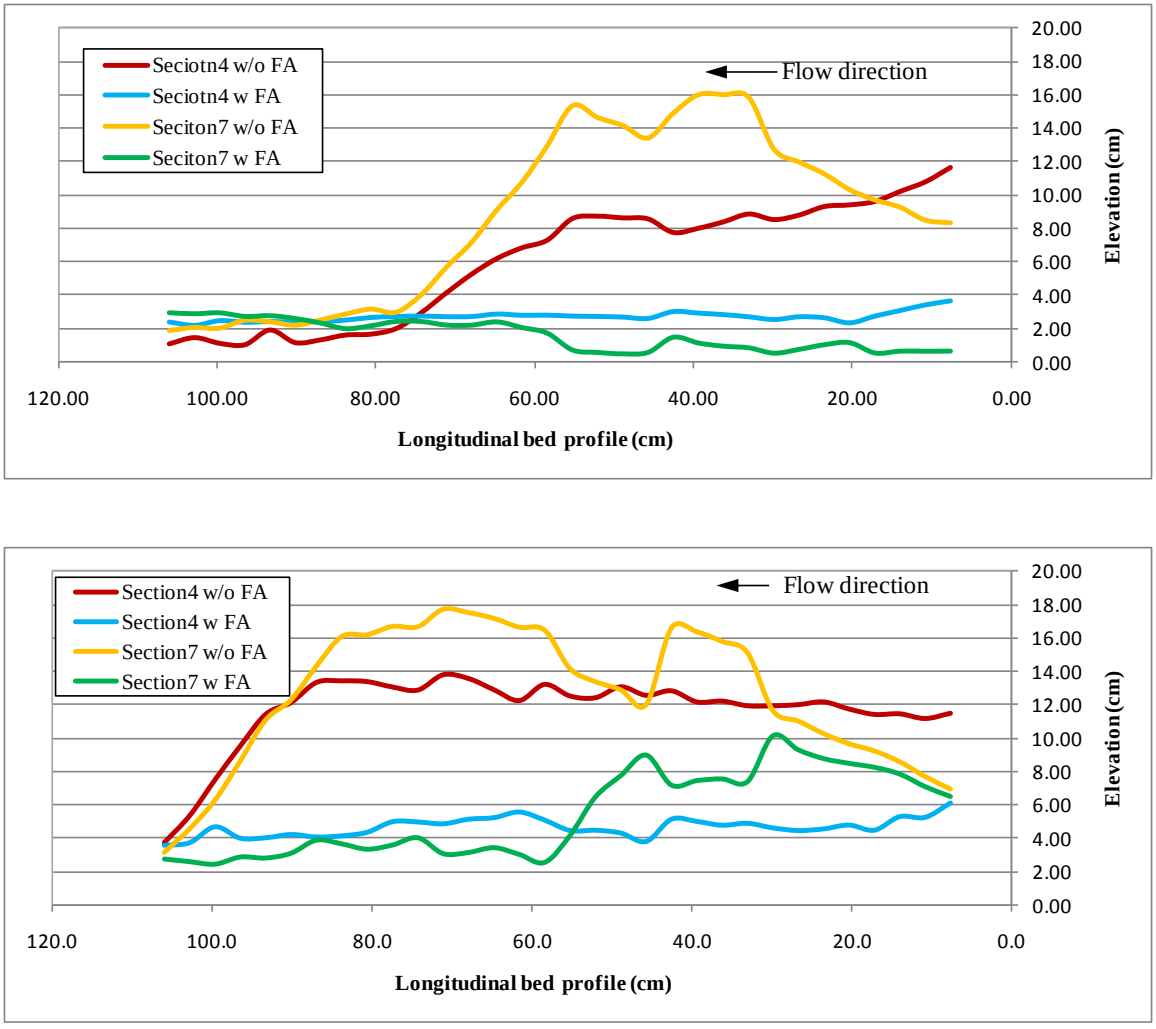


Figure 7.16 Longitudinal bed profiles in the left box: a) measurements at 6-hour, and b) measurements at 12-hour

www.manaraa.com

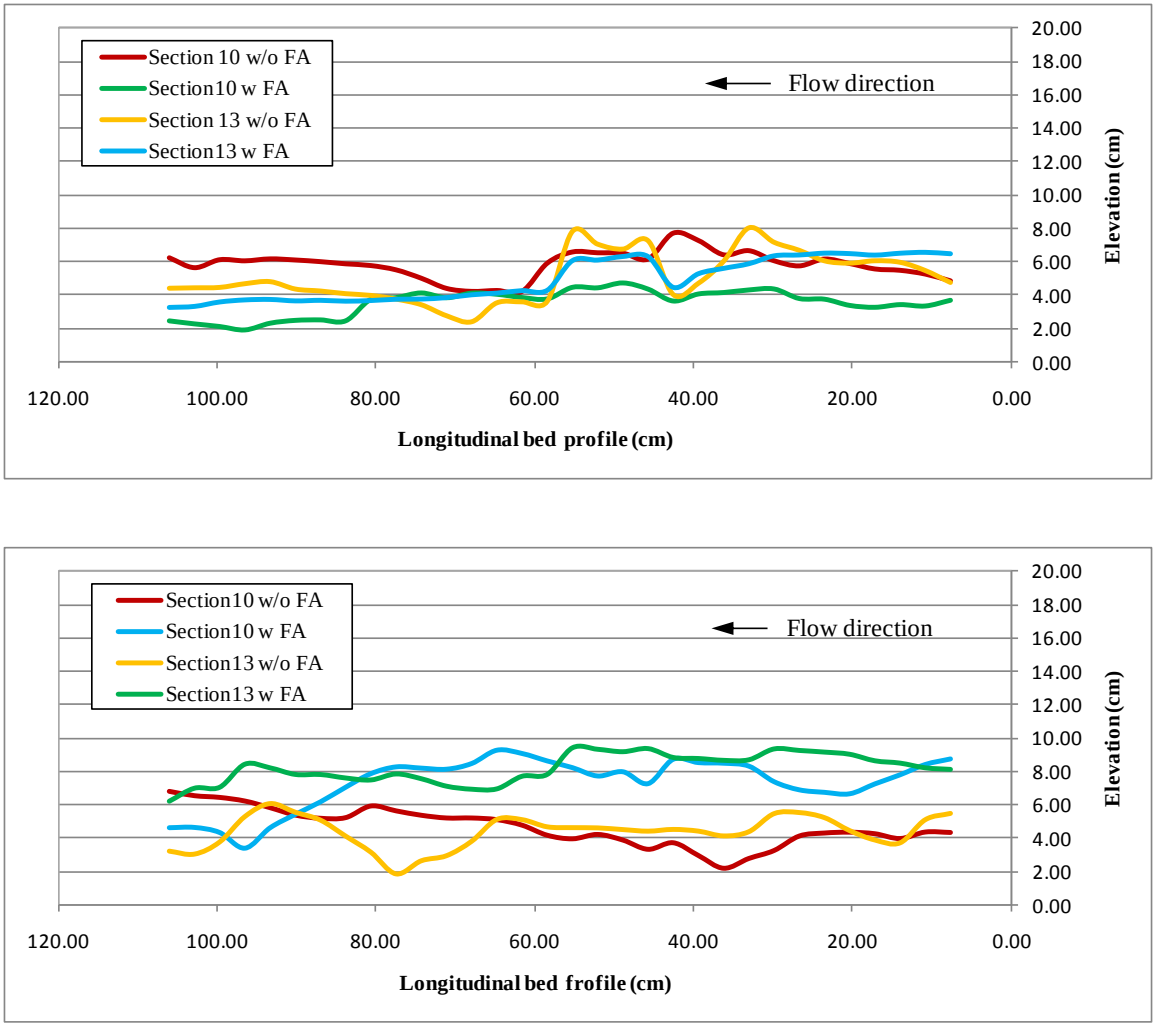


Figure 7.17 Longitudinal bed profiles in the central box: a) measurements at 6-hour, and b) measurements at 12-hour

www.manaraa.com

# CHAPTER 8 CONCLUSION AND RECOMMENDATION

## 8.1 Conclusions

The present study set out to determine as its first primary objective, how sediment accumulates at multi-barrel culverts. Its second primary objective was to indentify design adjustments that would substantially reduce sediment accumulation at such culverts. The problem of sediment accumulation leading to culvert blockage plagues numerous culverts, especially those in rural Iowa.

The main contributions of the present research entails advancements in a) technological means to comprehensively investigate flow at culverts in field and laboratory conditions, and b) understanding and prioritization of the flow and sediment transport complexities at culverts. The first category includes the development of DigiMap (tool to document hydrodynamic and morphological characteristics in the vicinity of culvert sites), design of a reliable measurement protocol for capturing the dynamics of the streambed evolution in time and space, and evaluation of the capabilities of various numerical models to describe individual processes interacting in the flow through culverts. The complementary use of these tools enabled to design the experimental investigation commensurate with the time and resources available for the research.

The second category of contributions includes new insights in the dynamics of the flood wave propagation acquired with a coupled experimental-numerical investigative approach. It was shown that the loop curve characteristics are dependent on the nature of the input hydrograph, characteristics of the channel and the control imposed by structures in the channel. Monitoring of Iowa streams led to the conclusion that the main source of sediment is bank erosion that consequently is deposited at culverts through suspended load transport. Finally, the main practical outcome of the study is that it identified weaknesses of the current methodology to design multi-barrel culverts.

www.manaraa.com

The field, laboratory, and numerical experiments performed as part of the present study have illustrated the complexity of the flow and sediment transport processes at multi-barrel culverts. The flow complexity is partially due to change of channel geometry in the vicinity of the culvert. An expansion region upstream of the culvert followed by a contraction region downstream of the culvert are used to transition the typical (e.g., trapezoidal) channel cross section to that of a multi-box culvert (where the cross section is larger). The presence of this transition at culverts creates a non-uniform, three-dimensional flow that further leads to the creation of the sediment deposits in the vicinity of culverts. In addition to the flow field complexities associated with culvert site geometry, other complexities make analysis of culvert performance difficult:

1. Flow unsteadiness caused by the flood wave propagation in the channel is another factor responsible for the increase of the flow complexity at culvert sites draining water produced by runoff flow hydrographs. In the present study flow unsteadiness effects were studied using numerical modeling, because hydraulic model studies cannot easily replicate the unsteadiness of the flow and sediment transport during a large time period, needed to accurately account for the propagation of a flood wave in a channel.
2. A significant difficulty faced is the lack of accurate field measurements of flow fields and sediment transport patterns during unsteady flows events due to the high temporal resolution requirements for the instrument and data acquisition system.
3. Sediment and flow hydrographs in rivers usually are not in phase: the peak in the sediment hydrograph arrives before or after the peak in the discharge hydrograph.

Given that the available literature contains neither a systematic study of sediment transport through multi-box culverts, nor on how sediment deposition adversely affects the flow through culverts this study attempted to separately investigate the effect of each

www.manaraa.com

of the above complexities in order to provide practical information to design sediment-free culverts using a self-cleaning approach.

Numerical simulations conducted using HEC-RAS were first used to elucidate the unsteady flow in channels of constant cross section containing a culvert structure. For a given flood-wave propagation event, the channel bed slope was found to be the major factor controlling the flow unsteadiness in the channel. The numerical simulations were also used to illustrate the effect of other parameters involved in shaping the loop curve: shape of the input hydrograph, terms involved in the governing equations. The initial numerical simulations also showed that a multi-box culvert placed in the channel reduced the flow unsteadiness effects but did not fully eliminate them.

A pair of focused field observations was integral part of the initial investigations. A long-term monitoring program conducted at a three-box culvert located in Iowa entailed repeated observations over three years to capture the dynamics of sediment deposits formation produced by a series of storms and seasonal changes in the morphology of the culvert vicinity. The analyses associated with these observations revealed that the formation of the deposits is a dynamic process commensurate with the hydrology of the basin. The sediment deposition patterns and their nature demonstrated that the main contribution to the accumulation of sediment at the culvert was the bank erosion and the rapid growth of vegetation that stabilizes the deposits between storms and seasons.

Another major field campaign was concentrated on a major storm event, the epic flood of 2008 developed in the Iowa River basin. This campaign was conducted to further develop and confirm new measurement protocols and methodologies to be used in addressing the problem of sedimentation at culverts. A preliminary calibration experiment conducted with Acoustic-Doppler Current Profilers (the typical tool used by monitoring agencies to obtain direct discharge measurements) and Large-Scale Particle Image Velocimetry –LSPIV (a new approach developed by an IIHR research group)

www.manaraa.com

showed differences from the stage-discharge measurements developed by USGS. More specific, the averaged ADCP discharge was 6.3% higher than the value inferred from the USGS rating curve, while LSPIV measurements collected simultaneously with ADCP were 4.3% lower. The major reasons for this difference were the fact that that the wind gust influenced the tracer used by LSPIV. The remarkable advantage of using LSPIV was demonstrated through the measurements conducted during the 2008 Iowa Flood. As LSPIV does not require deployment of equipment in the river, a sufficient number of direct measurements were acquired to appropriately capture the flood wave propagation. The looped hydrograph curve deduced based on the LSPIV direct measurement displayed a maximum stage difference of 0.5 m compared to the standard discharge hydrograph build with USGS current stream gaging methodologies.

Laboratory experiments conducted with hydraulic models were conducted with the aid of numerical simulations with the three-dimensional flow code FLUENT to understand the mechanics of the sedimentation processes developing culverts. The experiments entailed use of a three-barrel culvert, a culvert geometry commonly used for road crossings of small streams in Iowa. Two scales of hydraulic model were used: 1:20 and 1:5. The main finding of the 1: 20 scale hydraulic model was that the customary culvert design assumption of flow uniformity in the expansion region leading to the culvert is not correct. This assumption is the typical one currently made in standard culvert design. For example, the assumption that the discharge through the side barrels is equal to the central one is clearly violated.

Numerical simulations were used to provide detailed information on the flow around and within the culvert and on the sedimentation patterns and their location for a series of flow conditions. The performance curve of an as built and modified self-cleaning design were tested and assessed through a series of phased combined laboratory and numerical experiments. The use of numerical simulations hastened confirmation of

www.manaraa.com

the recommended design for the self-cleaning culvert by providing quick assessments of various modeling scenarios, that otherwise would have to be tested in the laboratory.

The driving criterion for design of the self-cleaning culvert geometry was to make modifications in the region situated upstream of the culvert that would restore the shape and functionality of the original (undisturbed) stream. For this purpose, the lateral expansion areas were filled with sloping volumes of material to reduce the depth (and consequently increase locally the flow velocity) and to direct the flow and sediment toward the central barrel, where the original stream was located prior to the culvert construction. This geometric changes implemented upstream of the culvert were shown to diminish the strength of the secondary currents developing at the entrance into the expansion and to maintain the flow and sediment flux closer to their original (no culvert in the channel) values.

The combined investigative approaches led to a self-cleaning design configuration that was then tested in performance experiments. Most of these tests were conducted in the live bed, 1:5 scale hydraulic model. The results confirmed the reliability and mitigation effect of the fillet-based self-cleaning design. The fillet-based self-cleaning culvert design can mitigate the sediment deposition in the side barrels and direct sediment particles toward the central barrel. The design is simple to implement in any stage of the culvert lifetime; i.e., at the time of construction or later on by retrofitting the area in the vicinity of the structure at the time of a cleanup.

## 8.2 Recommendations for future studies

The extensive investigation conducted for this study lead to several recommendations for further research:

www.manaraa.com

1. Prioritization and parameterization of the study findings and their incorporation in practical design guidelines for multi-barrel culverts. In order to substantiate the guidelines.
2. More field investigation is needed to confirm sedimentation causes at culverts. The field studies demonstrated that the driving forces for the initiation of sediment deposits at culverts can be widely different (see Appendix B).
3. Extension of the present investigations to other culvert geometries (one, two, and four- box culverts) and for various combination of culvert entrance conditions (angle of the approach flow and geometry of the wing walls).
4. Conduct of numerical simulations that consider depth-averaged, two-dimensional St. Venant equation for unsteady and non-uniform flow.

www.manaraa.com

# REFERENCES

Andrzej J. K., and Stanley R. D., (2001) "Consideration of Stream Morphology in Culvert and Bridge Design" J. of Transportation Research Board, Vol. 1743, pp 57-59

Aschwanden, C., Reed S., and Cepero K. (2009), Inundation Mapping Using Hydraulic Models and GIS: Case Studies of Steady and Unsteady Models on the Tar River, NC, ASCE Conf. Proc. 342, 297, DOI:10.1061/41036(342)297

Bodhain, G.L., (1982) "Measurement of Peak Discharge at Culvert by Indirect Method." Techniques of Water-Resource Investigations of the United States Geological Survey, Chapter A3

Bradley, A.A., Kruger, A., Meselhe, E, and Muste, M**.** (2002). "Flow Measurement in Streams Using Video Imagery," Water Resources Research, 38(12), p. 1315

Buchanan, T.J. and Sommers, W.P. (1969). "Discharge Measurements at Gaging stations," Techniques of Water Resources Investigations of the U.S. Geological Suyrvey, Book 3, Chapter A8, U.S. Government Printing Office, Washington, D.C.

Charbeneau, R. J., Henderson A. D., and Sherman L. C., (2006) "Hydraulic Performance Curve for Highway Culverts." J. Hydraulic Engineering, Vol. 132, No. 5.

Charbeneau, R. J., Henderson A. D., Murdock R. C., Sherman L. C., (2002) "Hydraulics of Channel Expansions Leading to Low-Head Culverts" Research Rep. 2109-1, Center for Transportation Research, Univ. of Texas at Austin, Austin, Tex

Chow, V. T., (1959) "Open-Channel Hydraulics" McGraw-Hill Book Company, INC., New York

Creutin, J.D., Muste, M., Bradley, A.A., Kim, S.C. and Kruger, A. (2003). "River Gauging Using PIV Technique: Proof of Concept Experiment on the Iowa River, J. Hydrol. , 277(3-4), pp. 182 – 194.

Crookston B. M., and Tullis B. P.(2008). "Scour and Riprap Protection in a Bottomless Arch Culvert.", ASCE Conf. Proc. 316, 230 ,DOI:10.1061/40976(316)230

Fenton, J.D. and Keller, R.J. (2001). " The Calculation of Steamflow from Measurement of Stage," Technical report Cooperative Research Centre for Catchment Hydrolgy and Centre for Environmental Applied Hydrology, Department of Civil and Environmental Engineering, The University of Melbourne, Australia

Ferguson, B.K. and Deak, T. (1994): Role of Urban Storm-flow Volume in Local Drainage Problems, Journal of Water Resources Planning and Management, Vol. 120, No. 4, pp. 523-530.

Fincham, A. M., and G. R. Spedding. (1997), "Low cost, high resolution DPIV for measurement of turbulent fluid flow." Experiments in Fluids 23, pp. 449–462.

Fujita, I., and Komura, S. (1992) "On the accuracy of the correlation method." 6th International Symposium on Flow Visualization, pp. 858–862.

www.manaraa.com

Fujita, I., Muste, M., Kruger, A. (1998), "Large-Scale Particle Image Velocimetry for Flow Analysis in Hydraulic Applications." J. Hydr. Res., 36(3), pp. 397-414.

Gary M. H., and Blake P. T., (2008) "Hydraulics of Multibarrel Culverts under Inlet Control." J. Irrigation and Drainage Engineering, Vol. 134, No. 4.

Goodridge, W. H. (2009). "Sediment Transport Impacts Upon Culvert Hydraulics." Graduate Theses and Dissertations, Utah State Univ., Salt Lake, Utah

Graf W. H., and Qu Z. (2003) "Flood Hydrographs in Open Channel" Water Management Issue 157 p45-52

Hansen, B., Nieber, J., and Lenhart C. (2009) "Cost Analysis of Alternative Culvert Installation Practices in Minnesota" Minnesota Department of Transportation, Final Report, MN/RC 2009-20

Hauet, A., A. Kruger, W. Krajewski, A. Bradley, M. Muste, J.-D. Creutin, and M. Wilson (2008b), Experimental system for real-time discharge estimation using an image-based method, J. Hydrol. Eng., 13(2), 105–110, doi:10.1061/(ASCE)1084-0699[2008]13:2(105).

Hauet, A., J.-D. Creutin, and P. Belleudy (2008a), Sensitivity study of large-scale particle image velocimetry measurement of river discharge using numerical simulations, J. Hydrol., 349(1–2), 178–190, doi:10.1016/ j.jhydrol.2007.10.062.

HEC (1998). "Hydrologic Engineering Center – River Analysis System (HEC-RAS), U.S. Army Corps of Engineers, Hydrologic Engineering Center, Davis, CA

Henderson F. M. (1966) "Open Channel Flow" Macmillan Company, INC, New-York

Jain S. C. (2000) " Open Channel Flow" John Wiley & Sons, INC, New York

Jansen P. Ph, Bendegom L. van, Berg J. van den, Vries M de, and Zanen A. (1979) "Principles of River Engineering" Pitman, INC, London

Jones L., (2005) "Extensions to the Iowa Culvert Hydraulics Software", Technical Report 504, Iowa Department of Transportation

Kerenyi, K.J. Jones, S., and Stein, S. (2003). "Bottomless Culvert Scour Study: Phase I Laboratory Report." Federal Highway Administration, Report Number FHWA-RD-02-078, McLean, VA, November 2003.

Kim, Y. (2006), Uncertainty analysis for non-intrusive measurement of river discharge using image velocimetry, Ph.D. thesis, Univ. of Iowa, Iowa City.

Klein M (1984) "Anti Clockwise Hysteresis in Suspended Sediment Concentration during Individual Storms" Catena 11:251 – 257

Kosicki, A. J., and Davis, S. R. (2001) "Consideration of stream morphology in culvert and bridge design" Transportation research record, Issue Number: 1743

Lenzi M., and Marchi L. (2000) "Suspended sediment load during floods in a small stream of the Dolomites (northeastern Italy) "Catena **39**: 267-282

www.manaraa.com

Loperfido, J.V. (2007) "High-frequency sensing of Clear Creek water quality: mechanisms of dissolved oxygen and turbidity dynamics , and nutrient transport", PhD. Thesis, Univ. of Iowa, Iowa City

Meselhe E. A., and Hebert K. (2007). "Laboratory Measurements of Flow through Culverts." J. Hydraulic Engr., Vol. 133, No. 8, pp 973-976

Mikhail, E. M., Bethel, J.S., and McGlone, J.C. (2001), "Introduction to Modern Photogrammetry", John Wiley & Sons, Inc., New York, NY

Muste, M., Z. Xiong, J., Schöne, Z. Li (2004). "Flow Diagnostic in Hydraulic Modeling Using Image Velocimetry," J. Hydr. Engrg, 130(3), pp. 175-185.

Normann, J. M., Houghtalen, R. J., and Johnson, W. J., (1985) "Hydraulic Design of Highway Culverts." Hydraulic Design Series No. 5, 2nd Ed., Federal Highway Administration, Washington, D.C.

Odgaard, A. J., and Kennedy, J.F. (1983). "River-bend bank protection by submerged vanes." J. Hydr. Engrg., ASCE, 109(8), 1161-1173.

Odgaard, A. J., and Spoljaric, A. (1986). "Sediment control by submerged vanes." J. Hydr. Engrg., ASCE, 112(12), 1164-1181.

Odgaard, A.J. (2009). "River Training and Sediment Management with Submerged Vanes", ASCE Press

Peart, M.R. and Walling D.E. (1988) " Techniques for establishing suspended sediment sources in tow drainage basins in Devon, UK : a comparative assessment", IAHS Publ. 174:269-279

Piirto, M., Eloranta, H., Saarenrinne, P., and Karvinen, R. (2005). "A comparative study of five different piv interrogation algorithms." Experiments in Fluids, 39:571–588, 2005. doi: DOI 10.1007/s00348-005-0992-6.

Richards, D. L., and Zeller, M. E., (1996) "Estimating Sediment Conveyance Capacity and Deposition Potential in Cuvlerts." North American Water and Environment Congress & Destructive Water, New York, NA: ASCE, 0-7844-0166-7.

Rigby E. H., Boyd M. J., Roso S., Silveri P., and Davis A. (2002) "Causes and Effects of Culvert Blockage during Large Storms" ASCE Conf. Proc. Vol 112, 298

Saleh, R.S. and Hwang, R. (1992): Analytical Hydraulic Modeling of Road Culverts, Water Resources Planning and Management: Proceedings of the 1992 National Conference, ASCE, New York, pp. 798-803.

Shutter R. D. and Verhoeven R. (2001) " Simulation of Sediment Transport during Flood Events: Laboratory Work and Field Experiments" Hydrological Sciences Journal, Volume 46, Issue 4 August 2001 , p599 – 610

Song, T. (1994) "Velocity and turbulence distribution in non-uniform and unsteady open-channel flow." PhD Thesis, EPF Lausanne, Switzerland

Suszka L. (1987) "Sediment Transport at Steady and Unsteady Flow: a Laboratory Study" PhD Thesis, No 704, EPF Lausanne, Switzerland

www.manaraa.com

Takahashi, H. (1969) “Theory of one-dimensional unsteady flows in a prismatic open channel.” Ann. Dis. Prev. Res. Inst., Kyoto University

Tu, H. and Graf, W. H. (1992) Velocity distribution in unsteady open-channel flow over gravel beds.. J. Hydrosci. Hydraul. Engng 10 , pp. 11-25.

Vassilios (1995) “Effects of sediment on Drainage Culvert Serviceability” J. Performance of Constructed Facility, Vol 9, No3

Wei, S. D., and G. Q. Ma. (1994). “Implicit and explicit camera calibration: Theory and experiments.” IEEE Transactions on Pattern Analysis and Machine Intelligence, 16(5), pp. 469-480.

Westphal, A., Thompson, D.B., Stevens, G.T., and Strauser, C.N. (1999). “Stage-Discharge Realtionships on the Middle Mississippi River,” J Water Resources Planning and Management, 125(1), ASCE, pp. 48-53.

www.manaraa.com

# APPENDIX A

## SURVEY OF IOWA COUNTY ENGINEERS

Table A.1 List of Survey County Engineering

| No | County | Name | e-mail address |
|---|---|---|---|
| 1 | Buchanan | Brian Keierleber | bcengineer@trxinc.com |
| 2 | Buena Vista | Jon Ites | jites@co.buena-vista.ia.us |
| 3 | Davis | David Grove | daviseng@netins.net |
| 4 | Emmet | Roger R. Patocka | emmeteng@ncn.net |
| 5 | Linn | Steve Gannon | Steve.Gannon@linncounty.org |
| 6 | Marion | Roger Schletzbaum | rschletzbaum@co.marion.ia.us |
| 7 | Monona | David Carney | mocoeng@longlines.com |
| 8 | Montgomery | Brad Skinner | bsmontengr@iowatelecom.net |
| 9 | Osceola | Thomas Snyder | tsnyder@osceolacoia.org |
| 10 | Page | Brad Skinner | bspagecoeng@iowatelecom.net |
| 11 | Winneshiek | Lee Bjerke | lbjerke@co.winneshiek.ia.us |
| 12 | Woodbury | Mark Nahra | mnahra@sioux-city.org |
| 13 | Lyon | Jeff Williams | |
| 14 | Cerro Gordo | Mary Kelly | |
| 15 | Calhoun | Ron Haden | |
| 16 | District 3 Maintenance Manager | Dwight Rorholm | |

www.manaraa.com

# QUESTIONAIRE

1. **How many culverts are in your county? How many of them are Multi-box?**

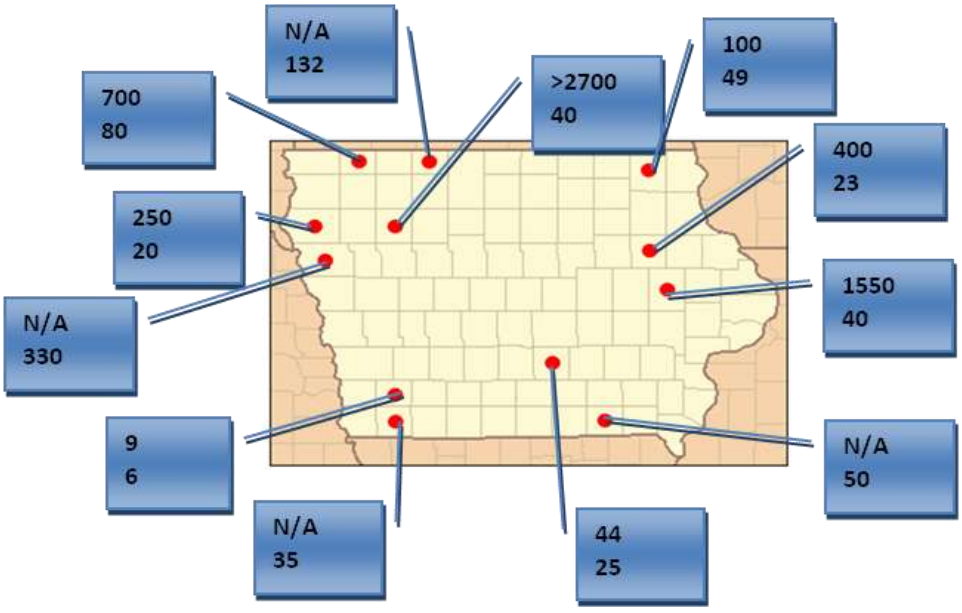


2. **How often do you inspect culverts sites and perform maintenance?**

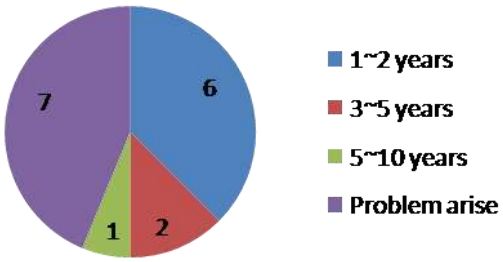


3. **Are the large storm events cleaning or aggravating culvert sedimentation?**

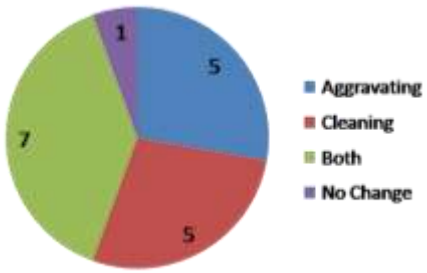


**Comment:**

- *Steve (Linn County)* provided that only 2008 flood appears to clean out culvert sedimentation, but typical high water does not (category into aggravating).

www.manaraa.com

- It should be noticed that there are 330 Multi-Box culverts in Woodbury County, and *Mark* said cleaning is true for the most.
- *Ron (Calhoun)*: Most of smaller culverts are cleaned by large storms. Larger Multi-Box silt in on barrel
- *Rorholm (District 3 Maintenance Manager):* There is much soil runoff from field in large events
- HURK underground company said if culverts are only partially silted, a large storm seems to clean out sediment unless the ditch has silted as well (category into cleaning)

4. **Please list in order (up to five) the most often encountered problems/concerns related to M-B culverts (e.g. scour, sedimentation, debris accumulation, structural, environmental)**

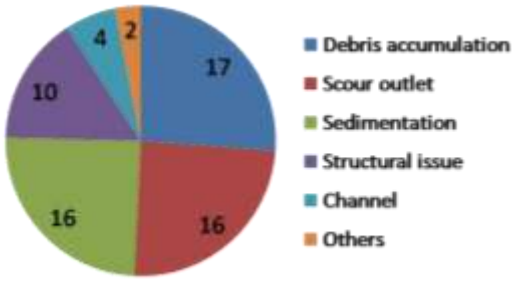


5. **Can you relate the sedimentation at M-B culvert with the season cycling?**

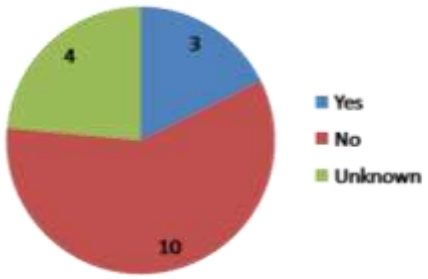


**Comment:**

- Three engineers pointed out that the sediment is prone to deposit in spring.
- Two engineers said that the process of sedimentation is too slow to relate with a

www.manaraa.com

single season.

- One engineer supposed that land use is the factor of sedimentation.

**6. Are you providing input in the design of the M-B culverts? If, yes, what input is related to sedimentation?**

| | |
|---|---|
| Yes | 6 |
| No | 6 |

**Comment:**

None of input is related to sedimentation. The inputs for design are considering the range of flows and velocities existing the barrels.

**7. Give examples of worst sedimentation situations and provide potential causes**

- 11 engineers out of 16 gave examples of sedimentation.
- Linn, Emmet, and Page Counties pointed out only one barrel can handle the flow the rest were filled.
- Woodbury and Winneshiek counties showed that they have sedimentation because of the change of upstream land use.

Steve (Linn County):

Triple barrel RCB's typically have one barrel handle the routine flow and two barrels filled. Having sediment fill inside a culvert barrel is much more difficult to correct mechanically. They also tend to collect large tree debris.

Mark (Woodbury County):

Upstream land use, lack of soil filtration from stormwater has filled barrels almost to top of barrel on up to a 6' high multi barrel. Lower barrel height culverts are more of a problem for sedimentation.

Jeff (Lyon County):

www.manaraa.com

One or two of the holes are partially close. I always thought it had to do with the main channel velocity picking one of the holes as it's favorite

Rorholm (District 3 Maintenance Manager):

Parallel barrels have a tendency to fill (partially) over time to where there is concern the design flow will not blow the partially barrels open.

**8. Do you have successful experiences regarding mitigation of sedimentation?**

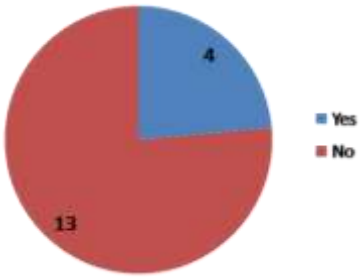


Thomas (Plymouth County): Terraces above the culvert

Jon (Buena Vista County): drop inlets

**9. What are the most difficult issues/concerns in cleaning the culvert?**

10 out of 12 answered.

Access and moving sediment are most difficult

**10. Could you provide an average cost of multi-barrel culvert cleaning ($/barrel)**

Only 4 county engineers answered. Average: $2750/barrel

HURK underground company charge: ($1×width×length×%full)/barrel

**11. Is the culvert clean-up made by your own crews or you contract out the work?**

www.manaraa.com

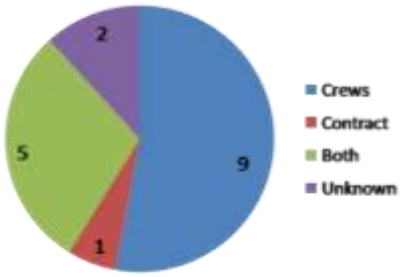


**12. Can you exemplify efficient means for culvert cleaning?**

**13. What is in your opinion the most important design objective for a culvert (please rank in order, from 1 to 7)?**

1. Stable, durable structure
2. Public/traffic safety
3. Create a stable stream and condition
4. Cost-effective maintenance
5. Control of sediment/scour/erosion
6. Flood plain management
7. Environmentally friendly

**14. List issues/problems associated with culverts that you consider that need further attention/research**

10 out of 16 answered.

Here we list issues/problems which they consider need attention/research : 1) sedimentation in barrel, 2) scour protection, 3) culvert structure design (width, numbers), 4) debris, 5) flood design.

**Comment:**

Steve (Linn County):

www.manaraa.com

RCB culverts have much of the cost associated with inlet and outlet structures on most secondary roads. Providing more cost effective inlet and outlet would make the RCB more practical. Making these structures more cheaply and easily extended would make them more practical as well. Reducing the number of barrels to one and providing design software to customize the design would provide better outcomes for most counties. Precast/prestressed barrel sections bolted together may be able to make a versatile, rapidly placed culvert.

www.manaraa.com

# APPENDIX B

## FIELD VISIT OF CULVERTS IN IOWA

Culvert is an ubiquitous structure for passing stream flowing through the highway in Iowa's secondary roads. There is a wide variety of culvert type and material used for building these culverts commensurate with the local hydrological conditions. Our research is focused on Reinforced Concrete Box (RCB) multi-barrel culverts because they are prone to buildup sediment deposits throughout the culvert areas. Table B.1 shows that most of the multi-barrel culverts in Iowa are the box shape, not circular. The field visits for documenting the culvert sedimentation were conducted in the Johnson, Marion, and Buena Vista counties (see Figure B.1). A short report for each site visit is provided below.

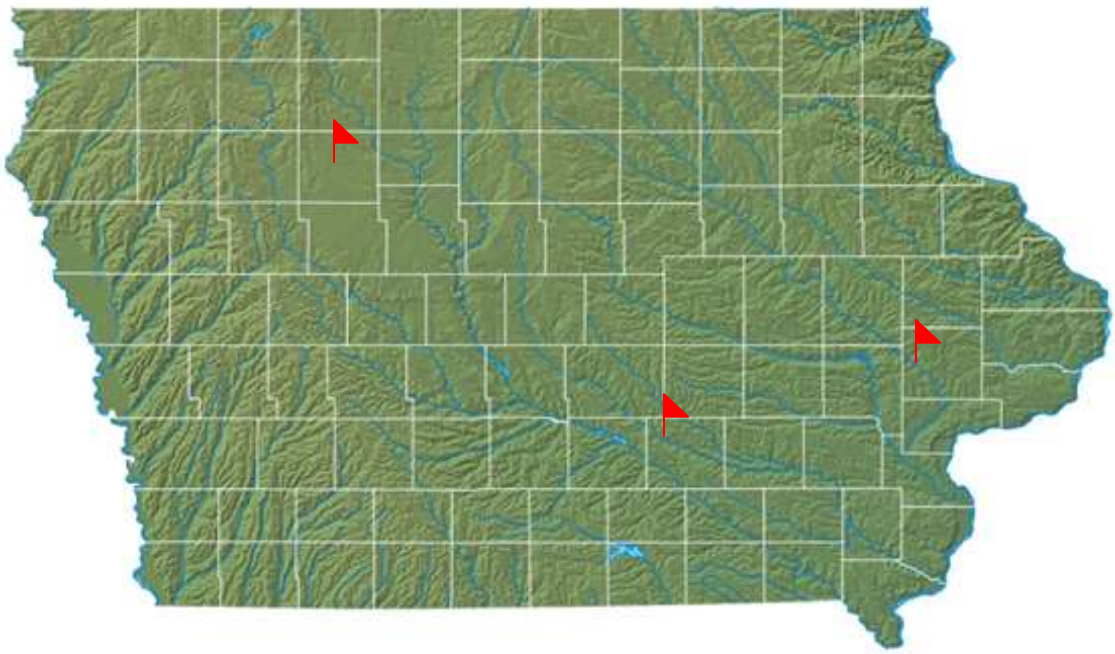

Figure B.1 Iowa Map indicate the counties we visited

www.manaraa.com

**1 Johnson County**

Statistics produced by the County engineering office regarding the multi-barrel culvert distribution (Table B.1) shows that there are 49 twin-box and 5 triple-box culverts in this county. Figure B.2 presents all triple-box culverts in Johnson County. Ten sites out of 54 were selected to visit. Site J1~J5 are three-box culverts, and Site J6~J10 are twin-box culverts. Sediment buildup problem is serious through all sites and it decreases the discharge capacity of culverts. The last maintenance for all sites is unknown. From the images took in 2007, three-box culverts is prone to trap the sediment; twin-box culverts have less sedimentation.

Table B.1. Statistics of culvert in Johnson County (Johnson county Secondary Road Department)

| RCB culvert type | Number |
|---|---|
| Twin | 49 |
| Triple | 5 |

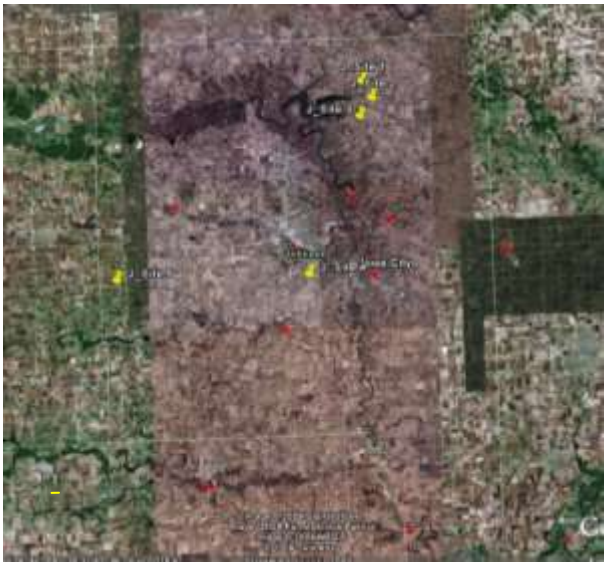

Figure B.2 Distribution of Triple-box culverts in Johnson County

www.manaraa.com

**Site J1: Mill Creek Culvert on Hwy #382**

**Site Characteristics:**

- Located on Mill Creek; built in 1962
- 10x10x53 RCB triple-box culvert
- Design drainage area is 4480 acres
- The terrain is plain
- Entrance and exit of culvert site were clean at the time of the visit, but it appeared that the culvert was recently cleaned
- Wingwall and barrels were highly skewed with respect to the main flow direction
- The site has experienced a recent flood event according to mud traces visible at the site on the flood plain.

Aerial image

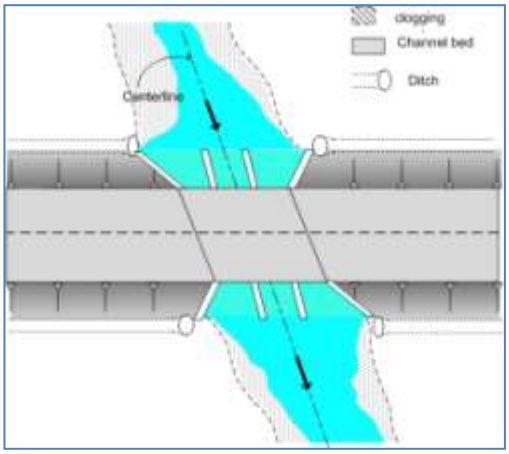


Culvert site sketch

www.manaraa.com

**Condition on March15, 2007:**

<table>
<tr><td>
</td><td>
</td></tr>
<tr><td>Flow enter culvert with a large angle. Expansion area seemed to have sedimentation before.</td><td>The barrels are clean. Based on the water mark, this site might have flood event.</td></tr>
<tr><td> </td><td> </td></tr>
<tr><td>No sour evidence was found at outlet.</td><td></td></tr>
<tr><td> </td><td>
</td></tr>
<tr><td colspan="2">Sediment transported from ditch (downstream of culvert) is considerable</td></tr>
</table>

www.manaraa.com

**Site J2: Mill Creek Culvert on Hwy #382**

**Site Characteristics:**

- Located on Mill creek; built in 1962
- 12x8x45 RCB triple-box culvert
- Design drainage area is 384 acres
- The terrain is plain
- No debris near entrance
- The entrance angle of the stream and curved flow contributed sedimentation at site

Aerial image

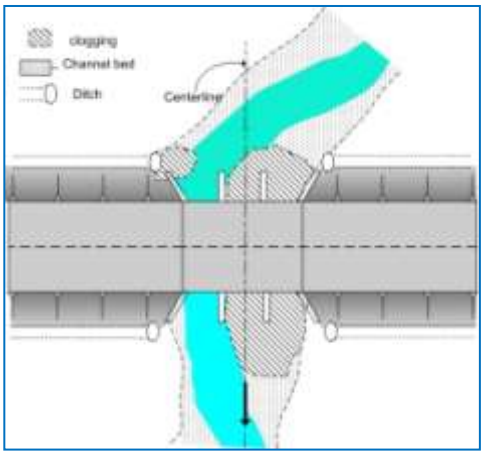


Culvert site sketch

www.manaraa.com

**Culvert condition on March15, 2007:**

<table>
<tr><td>
</td><td>
</td></tr>
<tr><td>Erosion in ditch (upstream) might provide sediment in expansion area.</td><td>Stream enters the culvert with a large angle. Wingwall and barrels were not skewed to align main flow direction.</td></tr>
<tr><td> </td><td> </td></tr>
<tr><td>Debris downstream of the culvert might trap sediment in the future</td><td>Sedimentation through the culvert on left and central barrels</td></tr>
</table>

www.manaraa.com

**Site J3: Jordan Creek Culvert (on Racine Ave)**

**Site Characteristics:**

- Located on Jordan Creek; built in 2002
- 10x8x66 RCB triple-box culvert
- Design drainage area is 2187 acres
- The terrain is plain
- Little debris near the entrance
- Sedimentation problem is serious

Aerial image

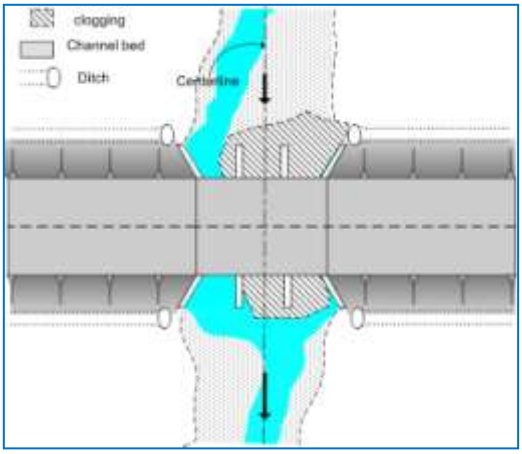


Culvert site sketch

www.manaraa.com

**Condition on March 16, 2007:**

<table>
<tr><td> </td><td>
</td></tr>
<tr><td>Serious clogging problem on the left and central parts.</td><td>The channel was shifted toward right bank because of sedimentation. Sedimentation is serious in barrels.</td></tr>
<tr><td>
</td><td>
</td></tr>
<tr><td>The flow downstream is aligned the central line of the culvert. The sedimentation on the left bank around the ditch</td><td>A small single-circle culvert was built 50ft downstream from the triple-box culvert.</td></tr>
<tr><td> </td><td> </td></tr>
<tr><td colspan="2">Rocks were placed to prevent erosion at ditches</td></tr>
</table>

www.manaraa.com

**Site J4: Deer Creek Culvert (on Hwy #218)**

**Site Characteristics:**

- Located on Dear Creek 500m downstream from a 2-box culvert (see aerial photo)
- RCB triple-box culvert
- Hilly area
- Sedimentation is serious
- No visible contribution from vegetation debris

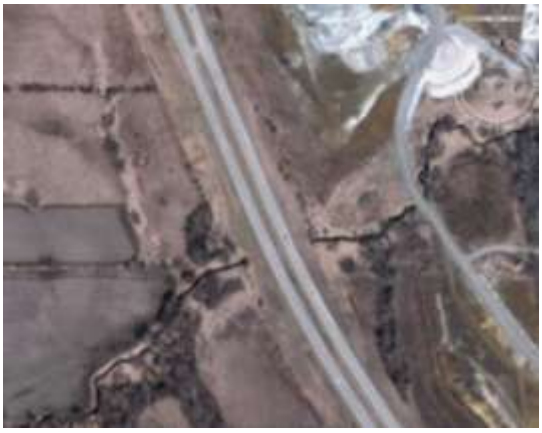

Aerial image

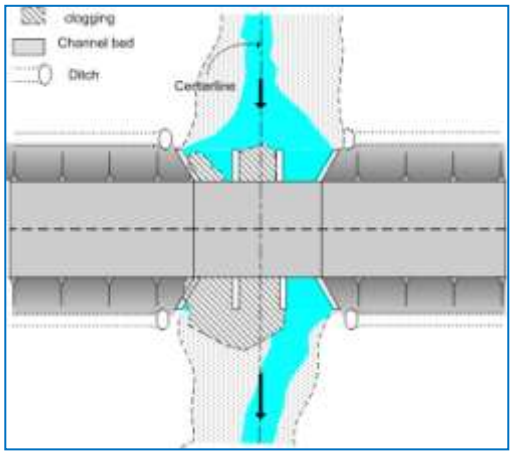


Culvert site sketch

www.manaraa.com

**Condition on April 16, 2007:**

| | |
|---|---|
| | |
| The stream is “quasi”well aligned with the culvert. Steep slopes from all the culvert sides cut strong ditches merging upstream the culvert. | Considerable clogging appears on the right and central boxes of the culvert. The left box is clean; the others are heavily sedimented (about 1 m elevation difference). |
| | |
| A very well defined stream passes through the left barrel indicating a long term sedimentation process. | Constant sedimentation level thought the more than 50m culvert length is blocking the two culvert boxes. |
| | |
| The effect of the long term sedimentation is obvious (with trees already growing on the new deposits) | Mud trapped in the grass – very recent rain event |

www.manaraa.com

**Site J5: Jordan Creek Culvert (on Black Hawks Ave)**

**Site Characteristics:**

- Located on Old Mans creek; built in 2000
- 9.8x9.8x84 RCB triple-box culvert
- Design drainage area is 3765 acres
- Entrances of right and central barrels were blocked by debris
- No sediment was deposited in barrels

Aerial photo

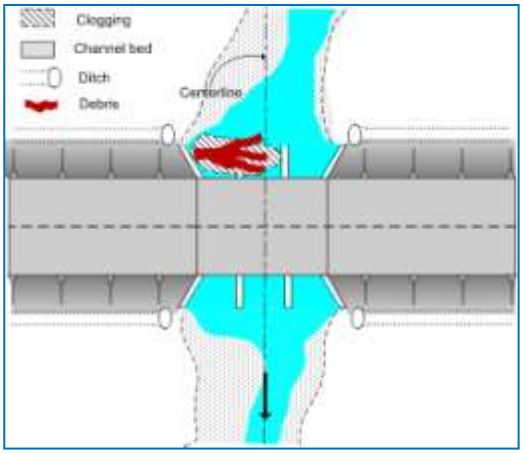


sketch of culvert

www.manaraa.com

**Condition on April 16, 2007:**

| | |
|---|---|
| | |
| Bank erosion on the right; expansion area is free of sediment. | Trees were collapsed since bank erosion and blocked the entrances of berrels |
| | |
| The flow downstream is aligned the central line of the culvert. Contraction area is free of sediment. | No sedimentation through all barrels. |
| | |
| Sediment deposited near the confluence between main stream and ditch flow | |

www.manaraa.com

**Site J6: Sand Road Culvert**

**Site Characteristics:**

- The site seems to have been subjected to cleanup recently or retrofit
- Cleanup near the bridge but far away the stream was not cleared
- Culvert with aged asymmetric deposition

www.manaraa.com

**Condition on March 15, 2007:**

| | |
|---|---|
| | |
| Upstream culvert side | The deposition upstream is asymmetric. The picture showed that culvert has been cleanup. |
| | |
| Side view (left bank) showing the new work. Curious pockets upstream the silt fences. Pockets indicated with arrows | View from downstream waterway |
| | |
| View of the downstream culvert side from the right bank | |

www.manaraa.com

**Site J7: Snyder Creek Culvert (on 480th St.)**

**Site Characteristics:**

- The culvert forces the stream to take a "S" shape while passing through the culvert
- Oblique angle to the road- quite well aligned with the stream direction – no visible problems associated with sediment deposition
- Very uniform flood plain vegetation

www.manaraa.com

**Condition on March 15, 2007:**

| | |
|---|---|
| | |
| View of upstream waterway: The right side of the culvert boxes is sedimented due to the river curvature | Side view from the upstream left bank |
| | |
| | |

www.manaraa.com

**Site 8: Dear Creek Culvert (on Kansas Ave)**

**Site Characteristics:**

- Located on Dear Creek 500m upstream from another very heavy silted 3-box culvert – see next site
- Hilly area
- Good site for monitoring sedimentation

www.manaraa.com

**Condition on March 15, 2007:**

| | |
|---|---|
| | |
| View of upstream: The stream is aligned with the left culvert barrel. Deposition is in the right barrel, and Non-symmetry of the bank is upstream the culvert | Side view of the upstream left bank: Debris plays a role in triggering and facilitating sedimentation. High erosion of the roadway drainage ditches |
| | |
| View of downstream waterway: Note the level of the high storms (indicated by the arrow) | The right bank is clogged despite that is quite free downstream (upstream control of the sedimentation process!!!) |

www.manaraa.com

**Site J9: Sander Creek Culvert (on Newport Rd)**

**Site Characteristics:**

- The terrain in the culvert vicinity is hilly
- No debris near the entrance

www.manaraa.com

**Condition on March 16, 2007:**

| | |
|---|---|
| | |
| Upstream view aligned the central line of the culvert. The stream is aligned with the right culvert barrel. | Side view from the upstream right bank. Deposition around the left barrel of the culvert |
| | |
| | |
| | |
| Downstream view along the central line of the culvert. | Water mark shows that the culvert has been through the storm event |

www.manaraa.com

**Site 10: Sander Creek Culvert (on Prairie Du Chien Rd)**

**Site Characteristics:**

- The terrain in the culvert vicinity is hilly
- No debris near the entrance
- Both Twin-box culverts are not subject to the serious sedimentation problem

www.manaraa.com

**Condition on March 16, 2007:**

| | |
|---|---|
| | |
| | Deposition is more serious in the right barrel. |
| | |
| | Downstream view aligned the central line of the culvert. The stream is passing through the left barrel |
| | |
| | The level of high water mark indicate the culvert has been through storms |

www.manaraa.com

2 Marion County

The field visit in Marion County was conducted in August 2006. Six culvert sites were visited (Figure B.3). Five are multi-barrel culverts and one is a single-barrel culvert. The vicinity of inlet and outlet was heavily vegetated. The sediment and debris deposits were considerable at all the visited sites and they obviously deteriorate the performance of structure for most culvert sites. Without a detailed investigation it could be inferred that the sedimentation processes in this county were evolving fast; for example at Site M4 a cleanup was conduce in 2004, and at the time of the visit all culvert barrels were clogged. From the USGS data it was observed that the area experienced a small flood in May 2005 which might explain the debris upstream the culvert. The stream flow was very shallow at this hydrological condition. Culvert opening invert is higher than water depth and blocks the waterway.

Figure B.3 Marion County: Yellow markers are field visit locations, and Red markers are USGS stream stations

www.manaraa.com

**Site M1: Hwy. G-76 East Culvert (on Hwy. 14)**

**Site Characteristics**

- Built in 1996
- 10'×6'×104' Triple RCB Culvert
- Logs at inlet; outlet is heavy vegetated
- Estimate remaining life at 2004: 44 yrs
- Almost no flow; dry channel
- Left and middle channels are clogged
- Last cleanup: 10 yrs ago
- The depositions at inlet and outlet are induced by the curve stream of inlet and might have confluence effect near the node of main channel and ditch flow

Aerial Photo (from Beacon)

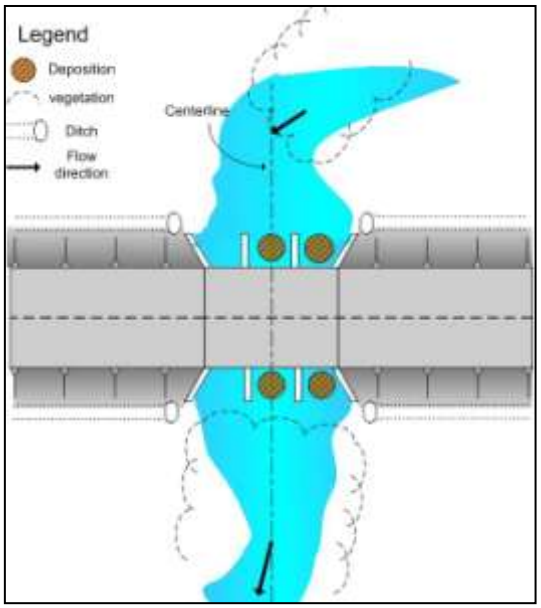


Culvert Sketch

www.manaraa.com

**Condition on August 22, 2006:**

| | |
|---|---|
| | |
| Look from left side. Arrow indicate the flow direction | Look from the center of the culvert. The channel is not well aligned with the culvert |
| | |
| Three-barrel culvert. Tow barrels were blocked by debris and sediment. | The culvert downstream was covered by the vegetation |

www.manaraa.com

**Site M2: Hwy. G-76 West Culvert (on Hwy. S-45)**

**Site Characteristics**

- Built in 1964
- 10'×10'×90' Twin RCB Culvert
- Inlet was blocked by drift; scour at outlet
- Estimate remaining life at 2004: 15 yrs
- Almost no flow; dry channel
- Removed drift 4 yrs ago

Aerial Photo (from Beacon)

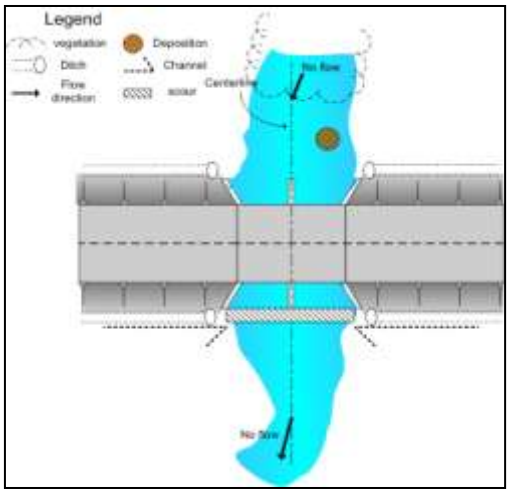


Culvert Sketch

www.manaraa.com

**Condition on August 22, 2006:**

| | |
|---|---|
| | |
| Debris was very serious which reveals that the culvert experienced a large discharge | Upstream channel thalweg is meandering |
| | |
| The downstream channel is not aligned well to the culvert | The red circle shows a serious bank erosion on the left bank downstream the culvert |
| | |
| Look at the right bank downstream the culvert. Bank erosion is also on the right bank. | Scour hole is at downstream the culvert. |

www.manaraa.com

**Site M3: Lisbon St. Culvert (on Hwy. S-45)**

**Site Characteristics**

- Built in 1982
- 12'×10'×34.5' Twin RCB Culvert
- debris at inlet; scour at outlet
- Estimate remaining life at 1996: 40 yrs

Aerial Photo (from Beacon)

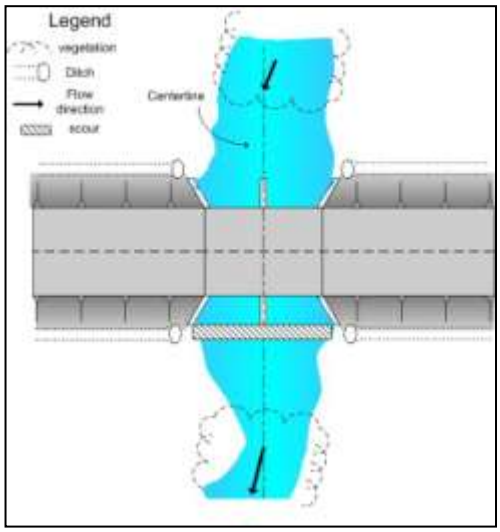


Culvert Sketch

www.manaraa.com

**Condition on August 22, 2006**

| | |
|---|---|
| | |
| Debris at inlet; no sedimentation | Inlet invert is higher than the channel bed |
| | |
| Outlet invert is higher than the channel bed. The downstream channel is not aligned well to the culvert | The barrel is clean. Water mark (white arrow) shows high discharge |

www.manaraa.com

**Site M4: 200 Ave North Culvert (on Beardsley St.)**

**Site Characteristics**

- Built in 1982
- 12'×10'×31' Ttriple RCB Culvert
- Logs at inlet; inlet and outlet are vegetated
- Estimate remaining life at 1999: 35 yrs
- Almost no flow
- Silt  in left and middle boxes
- Last cleanup: 2 yrs ago
- Sedimentation clogged all culvert boxes because stream flow into culvert with a large angle and confluence effect

Aerial Photo (from Beacon)

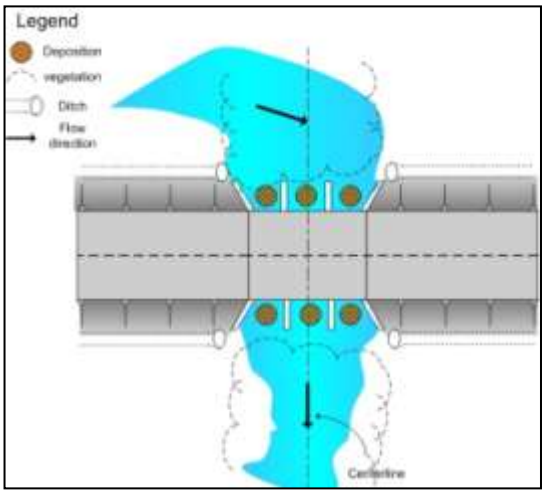


Culvert Sketch

www.manaraa.com

**Condition on August 22, 2006**

| | |
|---|---|
| | |
| The channel enters the culvert with a large angle. Red arrow indicates the thalweg of the channel. | Sedimentation and debris are very serious. Sediment built up through three barrels. |
| | |
| Flow through the right barrel. | Sedimentation is also serious downstream the culvert. |

www.manaraa.com

**Site M5: Hwy. T-15 South Culvert (on Hwy G-28)**

**Site Characteristics**

- Built in 1964
- Twin R.C.B. Culvert
- No logs at inlet
- Estimate remaining life at 2005: 25 yrs
- bend 90 degree flow at inlet
- Left channels are clogged with vegetation at both inlet and outlet
- Last cleanup: 3 yrs ago

Aerial Photo (from Beacon)

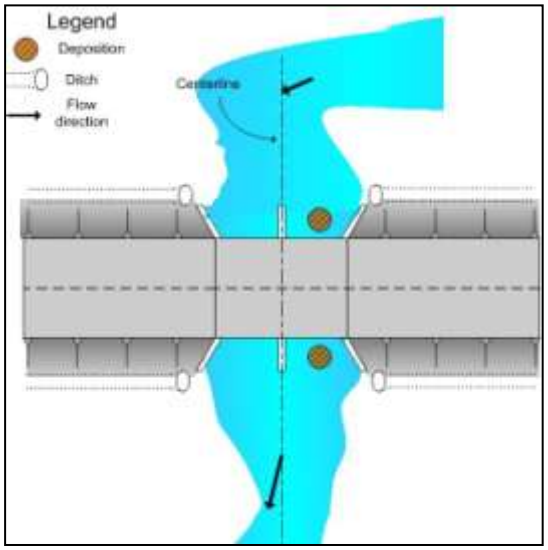


Culvert Sketch

www.manaraa.com

**Condition on August 22, 2006**

| | |
|---|---|
| | |
| The left barrel is clogged. | The stream enters the culvert with a large angle |
| | |
| The downstream channel is not aligned. | |

www.manaraa.com

**Site M6: Hwy. T-17 East Culvert (on 218th Ave)**

**Site Characteristics**

- Built in 2002
- Rigid frame culvert
- 5 ft weir at inlet
- Estimate remaining life at 2005: 50 yrs
- Although there is a weir at the inlet to reduce the amount of sedimentation into culvert, a lot of sediment deposit in the box clogging the culvert.
- Confluence effect might be important at this site

Aerial Photo (from Beacon)

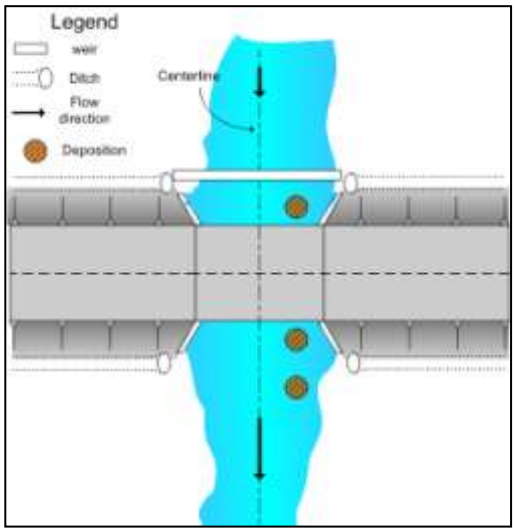


Culvert Sketch

www.manaraa.com

**Condition on August 22, 2006**

| | |
|---|---|
| | |
| 5ft weir is are the opening of the culvert | The channel upstream is aligned with the culvert |
| | |
| Rocks are left on the bank to protect from the erosion | The channel downstream is aligned with the culvert. |
| | |
| Sediment deposited through the barrel. | Sediment is prone to deposit because the velocity decrease when enter the large opening of the culvert |

www.manaraa.com

3 Buena Vista County

On June 22th 2006, we visited six culverts in Buena Vista County, out of each only four sites entail box culverts. The other culverts are of circular shape. Figure B.4 shows four locations with box culverts. Three sites displayed sediment built up, but none of the culverts were obstructed by debris. Maintenance cycle for the culverts was not tracked for us to be able to track patterns in sedimentation problems. It was reported, however, that two culvert sites have serious and continuous sedimentation problems.

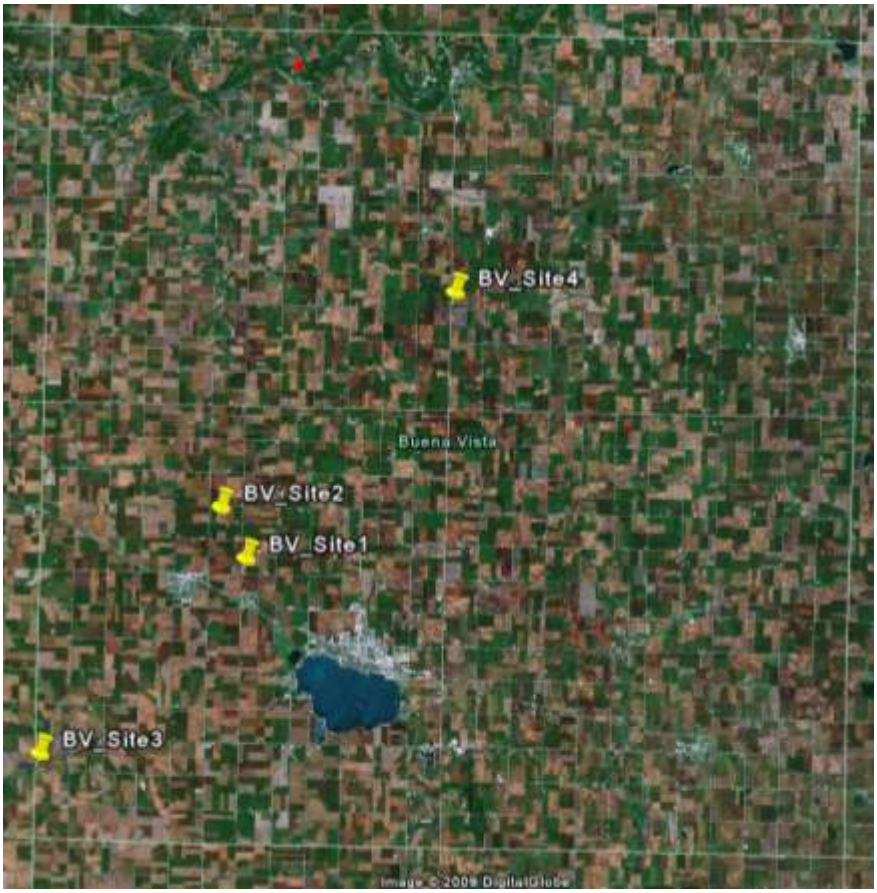


Figure B.4 Buena Vista County Map: Yellow markers are field visit locations and Red marker is USGS stream station in this county

www.manaraa.com

**Site BV1: Powell Creek Culvert**
**Site Characteristic**

- Three-box concrete culvert
- Built 20~22 years ago
- Cleaned and clogged after 2 years
- Channel was shifted toward the right bank
- Clogging problem is very serious

Aerial Photo

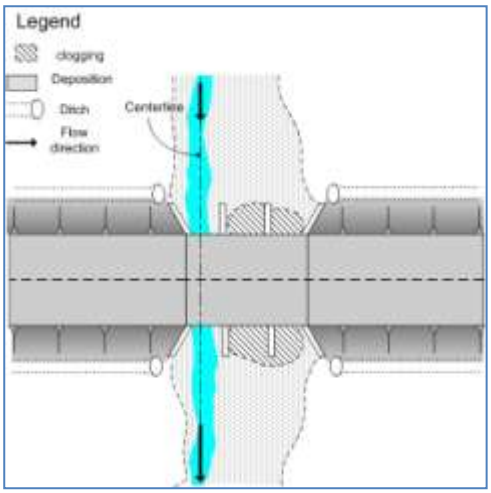


Culvert Sketch

www.manaraa.com

**Condition on June 12, 2006**

| | |
|---|---|
| | |
| The upstream channel is aligned well. | Two barrels are clogged. |
| | |
| The downstream channel is aligned well. | Sediment deposited in barrels |

www.manaraa.com

**Site BV2: 565th St. Culvert**
**Site Characteristic**

- Two-box concrete culvert
- There are long road ditches
- The upstream of the channel is dry
- Scour at the outlet of the culvert

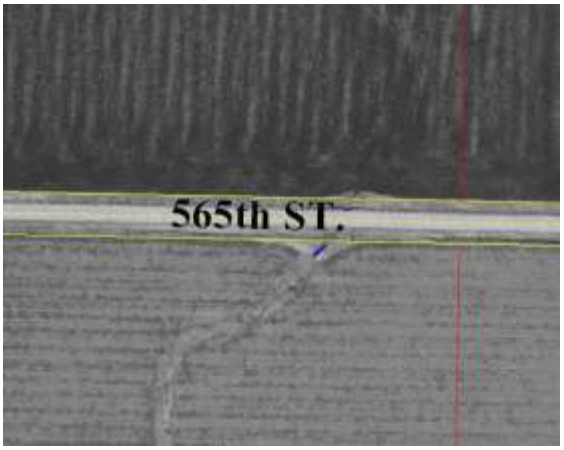


Aerial Photo

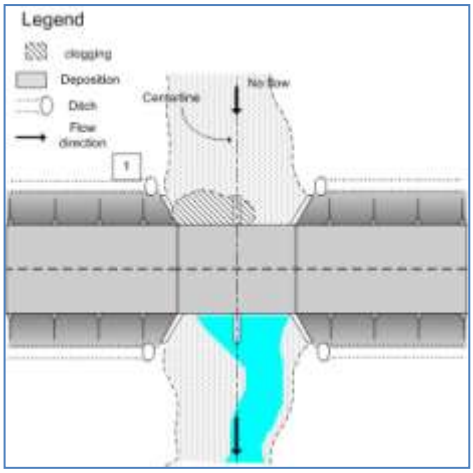


Culvert Sketch

www.manaraa.com

**Condition on June 12, 2006**

| | |
|---|---|
| | |
| Sedimentation is Upstream | The culvert is skewed. Upstream is dry. |
| | |
| Ponding area downstream the culvert | |
| | |
| Scour at the downstream. Outlet invert is higher than the channel bed. | |

www.manaraa.com

**Site BV3: 565th St. Culvert #2**
**Site Characteristic**

- Three-box concrete culvert
- It was cleaned up two years ago
- Confluence flow formed near the inlet
- There are some bars at the inlet and outlet close to the right bank of the channel

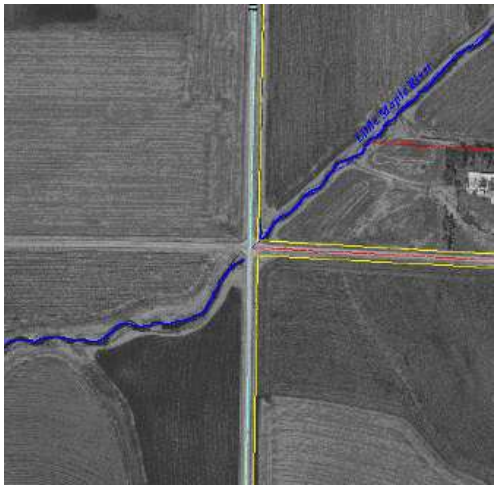

Aerial Photo

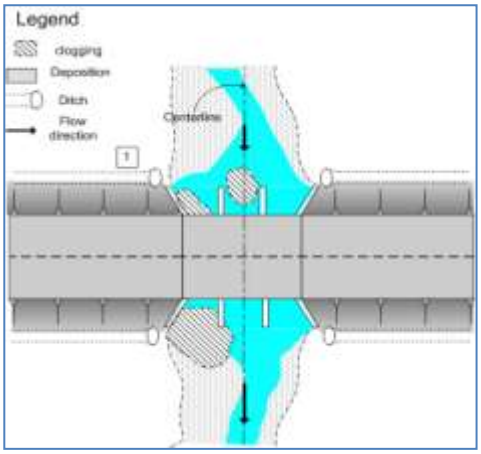


Culvert Sketch

www.manaraa.com

**Condition on June 12, 2006**

| | |
|---|---|
| | |
| Look upstream the culvert. Ditch flow from left confluences with the channel flow. | Sediment Deposited in the right and left barrels |
| | |
| Ditch upstream the culvert | The channel downstream is aligned |
| | |
| | |

www.manaraa.com

**Site BV4: 565th St. Culvert #3**
**Site Characteristic**

- Three-box concrete culvert
- It was cleaned up two years ago
- Clogging inside the culvert
- Confluence effect should be considered at this site. The bar formed near the right bank of the channel

Aerial Photo

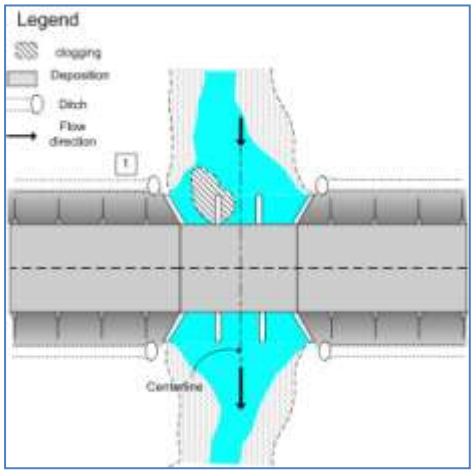


Culvert Sketch

www.manaraa.com

**Condition on June 12, 2006**

| | |
|---|---|
| | |
| A small island was built in the expansion area | No serious sedimentation in barrels |
| | |
| A small island deposited upstream the culvert | Downstream part is clean. Sedimentation is in the central barrel |

www.manaraa.com

# APPENDIX C

## MOBILE LARGE-SCALE PARTICLE IMAGE VELOCIMETERY

The Mobile Large-Scale Particle Image Velocimetry (MLSPIV) designed and constructed at IIHR – Hydroscience & Engineering (IIHR) was used for measuring free-surfaces velocities at the field. The mobile unit, illustrated in Figure C.1a, essentially comprises an imaging device set on a telescopic mast. The light weight aluminum, hydraulically operated mast allows for setting the camera from 15 ft to 50 ft above the ground level to accommodate imaging of various stream widths. Camera positioning and panning control (Figure C.1b) are remotely conducted using a notebook computer located in the truck cabin. The MLSPIV truck is equipped with a power generator, additional batteries, and an uninterrupted power supply that provides power for all equipments, a notebook computer, a pan-tilt unit, and the camera. Three guy wires are used after positioning to secure the mast against wind-induced or accidental vibrations.

Images taken from a distance at oblique angles are generally distorted, as illustrated in Figure C.2a. This type of distortion is common in LSPIV applications because the images are usually recorded from an angle that allows to cover the entire area of interest, usually large surfaces of the flow. IIHR's LSPIV team developed several algorithms for removal of the image distortion (see Figure C.2b). The most common algorithm is based on a geometrical transformation applied to the recorded images based on an in-situ topographic survey.

www.manaraa.com

Figure C.1 MLSPIV unit: a) general view; b) Camera and panning control equipment

a) Distorted image. Image recorded with digital video camera under natural light

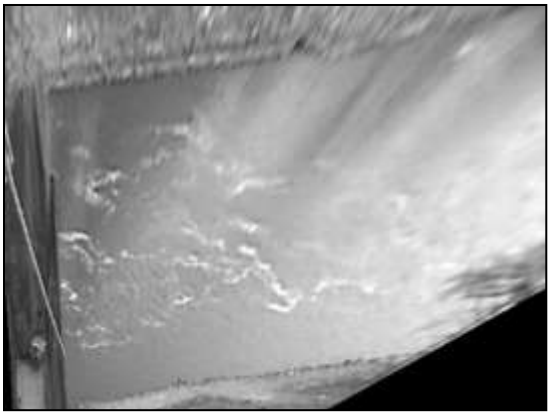

b) Undistorted image. Transformation from camera to real world coordinates obtained using 4 marker points. The software rescales flow boundaries, the size & shape of patterns in the image (note parallel river banks).

Figure C.2 Removal of image distortion due to recording with an oblique angle and reconstruction of the image in real coordinates.

www.manaraa.com

The images taken from an oblique angle have large image distortion and therefore must be geometrically corrected to use for the particle image velocimetry algorithm. Two coordinate systems are defined to create a non-distorted image, the physical coordinate system (X, Y, Z) and the CRT coordinate system (x, y), as shown in Figure C3. It should be noted that the Z-axis is vertical and must pass through the center of the camera lens and that the water surface, assumed to be horizontal, is in the XY-plane. It should also be noted that the unit in the CRT coordinate is a pixel, and that the range of the CRT coordinate is restricted to the rectangular area of hundreds of pixels when using the conventional frame-grabber for video images.

The transformation equation from the CRT coordinates ($x$, $y$) to the physical coordinates ($X$, $Y$) is assumed to be

$$X = \frac{b_1 x + b_2 y + b_3}{b_4 x + b_5 y + 1}, \qquad Y = \frac{b_6 x + b_7 y + b_8}{b_4 x + b_5 y + 1} \tag{C.1}$$

The transformation coefficients $(b_1, b_2, \cdots, b_8)$ are calculated by the least square method using the predefined coordinates of $N$ marker points on both the CRT coordinates and the physical coordinates, the value of $N$ being at least four, in both the $XY$ plane and the $xy$ plane. Thus, denoting the coordinates of the marker points for the physical plane, $(X_1, Y_1), (X_2, Y_2), \cdots, (X_N, Y_N)$ and those for the CRT coordinates, $(x_1, y_1), (x_2, y_2), \cdots, (x_N, y_N)$, the transformation coefficients are obtained by solving the following equation.

$$\mathbf{TB} = \mathbf{Z} \tag{C.2}$$

where

www.manaraa.com

$$\mathbf{T}=\begin{bmatrix} x_1 & y_1 & 1 & -x_1X_1 & -y_1X_1 & 0 & 0 & 0 \\ x_2 & y_2 & 1 & -x_2X_2 & -y_2X_2 & 0 & 0 & 0 \\ \vdots & \vdots & \vdots & \vdots & \vdots & \vdots & \vdots & \vdots \\ x_N & y_N & 1 & -x_NX_N & -y_NX_N & 0 & 0 & 0 \\ 0 & 0 & 0 & -x_1Y_1 & -y_1Y_1 & x_1 & y_1 & 1 \\ 0 & 0 & 0 & -x_2Y_2 & -y_2Y_2 & x_2 & y_2 & 1 \\ \vdots & \vdots & \vdots & \vdots & \vdots & \vdots & \vdots & \vdots \\ 0 & 0 & 0 & -x_NY_N & -y_NY_N & x_N & y_N & 1 \end{bmatrix} \tag{C.3}$$

$$\mathbf{B}=\{b_1 \quad b_2 \quad b_3 \quad b_4 \quad b_5 \quad b_6 \quad b_7 \quad b_8\}^T \tag{C.4}$$

$$\mathbf{Z}=\{X_1 \quad X_2 \quad \cdots \quad X_N \quad Y_1 \quad Y_2 \quad \cdots \quad Y_N\}^T \tag{C.5}$$

The coefficient vector $\mathbf{B}$ can be computed as

$$\mathbf{B}=\left(\mathbf{T}^T\mathbf{T}\right)^{-1}\mathbf{T}^T\mathbf{Z} \tag{C.6}$$

The reverse relationships that are the transformation equations from the physical to the CRT coordinates, are obtained from Eq. (C.1) as

$$\begin{aligned} x &= \frac{(b_5b_8-b_7)X+(b_2-b_3b_5)Y+(b_3b_7-b_2b_8)}{(b_4b_7-b_5b_6)X+(b_1b_5-b_2b_4)Y+(b_2b_6-b_1b_7)} \\ y &= \frac{(b_6-b_4b_8)X+(b_3b_4-b_1)Y+(b_1b_8-b_3b_6)}{(b_4b_7-b_5b_6)X+(b_1b_5-b_2b_4)Y+(b_2b_6-b_1b_7)} \end{aligned} \tag{C.7}$$

A non-distorted image is obtained through the following procedure as shown in Figure C4: 1) cover the physical plane with a grid having the step sizes of $\Delta X$ and $\Delta Y$, 2) calculate the CRT coordinates (x, y) for the physical coordinates (X, Y) using the inverse relation (Eq. (C.7)) of Eq. (C.1), and C.3) calculate the intensity at (X, Y) by an interpolation on the CRT plane. It is obvious that a smaller physical step size creates a larger image for the same fixed area on the CRT plane, and vice versa. The created image size should be nearly the same as or a little larger than that of the original image.

www.manaraa.com

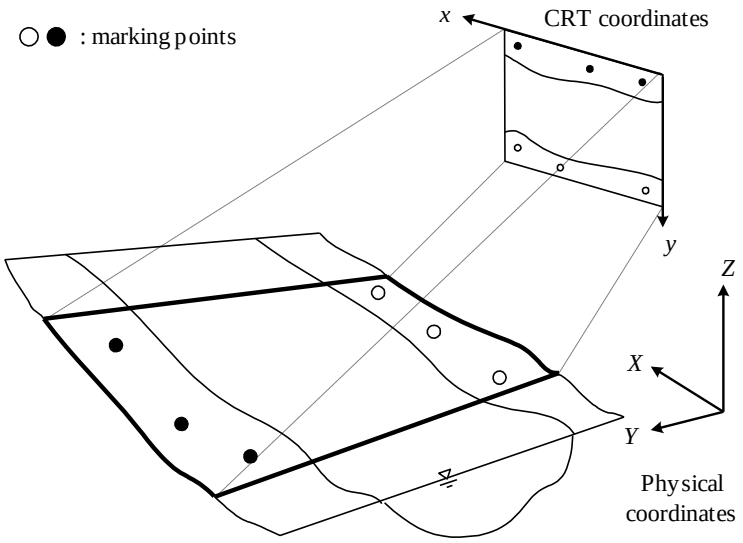


Figure C.3 Relation between CRT coordinates and physical coordinates (Fujita et al., 1998a)

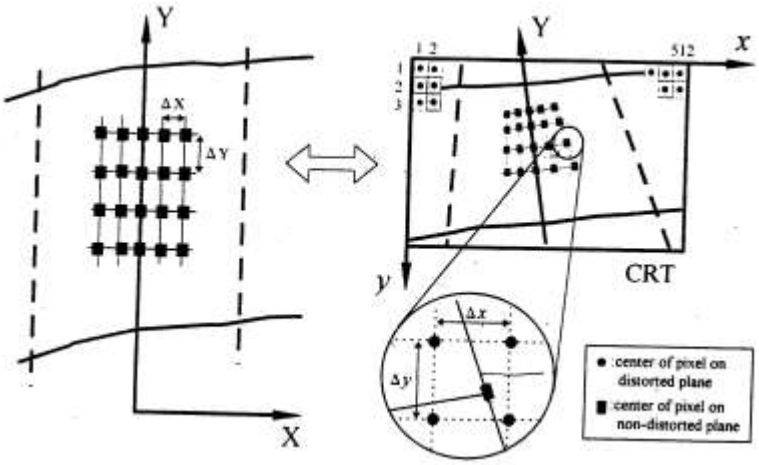


Figure C 4. Method to create non-distorted image (Fujita et al., 1998)

www.manaraa.com